UNIVERSITY OF BIRMINGHAM

Development of Autologous Macrophage-Encapsulated Gellan Fluid Gel for The Prevention of Blindness from Ocular Surface Scarring.

Mohammad Alqahtani

A thesis submitted to the University of Birmingham for the degree of

DOCTOR OF PHILOSOPHY

University of Birmingham

College of Medical and Dental Sciences

Institute of Inflammation and Ageing

March 2024

Lead Supervisor: Dr. Graham Wallace

Co-Supervisor: Prof. Saaeha Rauz

Abstract

Background: Corneal scarring is the fourth leading cause of preventable visual loss. Following infection /injury, the cornea undergoes a repair mechanism involving a strong inflammatory response, repair and degradation mechanisms. This results in an alteration of its molecular components and structure, which could potentially lead to scar formation, and ultimately cause blindness. Corneal transplantation is the standard treatment for corneal scarring, which has donors' shortage and a rejection risk. Thus, the development of a novel treatment is significantly required for maintaining the intact corneal structure. Our group using a novel gellan fluid gel to deliver a single anti-scarring molecule in a sustained manner into the effected cornea showed promising findings. Thus, we proposed using gellan fluid gel to allow sustained release of multiple molecules instead of one to limit inflammation and promote corneal tissue remodelling while minimising fibrosis, which would lead to regenerative healing of the cornea and untimely maintenance of vision. Macrophages are critical players during wound healing repones, meditating infection elimination, damaged cell clearance, resolution of inflammation, and tissue remodelling. Thus, we proposed that administration of a balance of M1 and M2 macrophages at the right time on the ocular surface using gellan fluid gel as an effective delivery system may lead to regenerative corneal wound healing and eventual preservation of sight. The present project aimed to develop autologous macrophage-encapsulated gellan fluid gel for delivering bioactive molecules that aid re-epithelialisation, while minimising fibrotic signalling cascades to aid scarless healing of the ocular surface and the preservation of sight.

Method: Human monocyte derived macrophages with pro-inflammatory (M1), anti-inflammatory (M2), and pro-healing (M2) properties were generated using GM-CSF, LPS+IFN-γ, and M-CSF, IL-4+IL-13, respectively. The viability of M1/M2 in gellan fluid

gel and its effect on macrophage phenotype at 4h were assessed by fluorescent microscopy (FM), and Flow cytometry and qPCR, respectively. To test macrophage polarisation states, M1/M2 were cultured with opposing cytokines, i.e., M1 with IL-4/13, and analysed by RNAseq and Luminex.

Result: The gellan fluid gel maintained both M1/M2 survival and polarisation states. However, the polarisation states of our generated subset of M1/M2 macrophages are not maintained in response to sequential stimulation with positing stimuli.

In conclusion: these results show that gellan fluid gel is biocompatible and can be used to deliver autologous macrophage therapy into the cornea. The instability of the M1/M2 polarisation states necessitated caution when applying them to the cornea with an unstable microenvironment.

Acknowledgment

Certainly, my PhD journey would have been impossible to navigate on my own. I owe my immense appreciation to my lead supervisor, Dr. Graham Wallace, for believing in me and for his encouragement, patience, excellent supervision, support, and guidance throughout this journey. I have to thank him for taking the time to review each section of my thesis and for his critical feedback. I also would like to extend my thanks to my co-supervisor, Prof. Saaeha Rauz, for her guidance, continuous support, and valuable advice during my PhD. Without their outstanding support, I could not have been able to finish my studies, particularly during the COVID-19 outbreak. I have to thank the Royal Embassy of Saudi Arabia Cultural Bureau, and Najran University for funding my PhD.

I would like to express my gratitude to all members of Lab 3 for their support and guidance. Special thanks go to Dr John O'Neill for teaching me the protocols of Luminex and his valuable help with cell culture. Many thanks for Dr Sally Clayton for her valuable help with qPCR and monocyte isolation. I would like to express my gratitude to my friend Abdullah Alghamdi, who has provided unlimited support during my PhD. He is also there when I need help with the processing of the blood cone and LAMB assay. Additionally, I want to thank my friend Salih Kucks for his valuable support with the flow cytometry experiments.

I am grateful to people who helped me with the generation and analysis of RNAseq data, especially the genomic centre at the University of Birmingham. I express my gratitude to Dr. Sael Alatawi for his valuable guidance and teaching me the basic of bioinformatics and his support in using the R programme. I would also like to thank Dr. Adeolu Adewoye for his valuable help with the processing of RNAseq data.

I am very grateful to my parents for their unlimited support and guidance. My sisters Hand, Eiman, and Sarah, as well as my brothers Abdullah and Saeed, have been very supportive, and I am grateful to them.

My wife Asma has been an incredible source of encouragement, support, and patience during this journey, and I am extremely grateful beyond words. I express my appreciation to my daughter Smo and my son Yahya, for their exceptional patience and understanding throughout the time I give to my studies at the university. I would like to extend my thanks to my friends, Mohammed, Mansour, Ayman, Ahmad, Khalid, Jaber and Younis for always being there for me.

COVID IMPACT STATEMENT

This project was affected by the COVID pandemic. Not only were the labs closed for several months but the blood cones that were used to obtain human macrophages were not available from the Blood Transfusion Centre. Moreover, when cones did become available again testing for COVD before use was required. The major impact of the time lost to the pandemic was that an animal model to test the effect of polarised macrophages *in vivo* was not possible to develop when the situation recovered.

Table of Contents

List of Figures

List of tables

Abbreviations

ACAID	Anterior Chamber-Associated Immune Deviation
AGM	Orta–Gonad–Mesonephros
ALOX15	Arachidonate 15-Lipoxygenase
AM	Acetoxymethyl
AP-1	Activator Protein 1
APCs	Antigen-Presenting Cells
ARG1	Arginase
BM	Basement Membrane
CCL	C-C Motif Chemokine Ligand
CCR	C-C Chemokine Receptor Type
CD	Cluster Of Differentiation
CLU	Clusterin
CMP	Common Myeloid Progenitors
CXCL	C-X-C Motif Chemokine Ligand
DCs	Dendritic Cells
DEG	Differentially Expressed Genes
DNA,	Deoxyribonucleic Acid
ds cDNAs	Double-Strand Complementary DNA
EAE	Autoimmune Encephalomyelitis
ECM,	Extracellular Matrix
EDTA	Ethylenediaminetetraacetic Acid
EGR,	Early Growth Response
EMPs	Early Erythromyeloid Progenitors
FABP4	Fatty Acid-Binding Protein 4
FACS	Fluorescence-Activated Cell Sorting
FC	Fold Change
FCS	Foetal Bovine Serum
FDA	Food And Drug Administration
FN	Fibronectin
FOLR2	Folate Receptor
G-CSF	Granulocyte Colony-Stimulating Factor
GBP	Guanylate Binding Protein
GM-CSF	Granulocyte-Macrophage Colony-Stimulating Factor
GSEA	Gene Set Enrichment Analysis
HCL	Hydrochloric Acid
HSC	Haematopoietic Stem Cells
IFI	Interferon Alpha Inducible Protein
IFIT3	Tetratricopeptide Repeats 3
IFN	Interferons
IGF	Insulin Like Growth Factor

IL	Interleukin
INHBA	Inhibin Subunit Beta A
iNOS	Inducible Nitric Oxide Synthase
IRFs	Interferon Regulatory Factor
ITSN1	Intersectin 1
KEGG	Kyoto Encyclopaedia Of Genes And Genomes
LGMN	Legumain
LIPA	Lysosomal Acid Lipase
LPS	Lipopolysaccharides
LYVE	Lymphatic Vessel Endothelial Hyaluronan Receptor
M-CSF	Macrophage Colony-Stimulating Factor
MAFB	V-Maf Musculoaponeurotic Fibrosarcoma Oncogene Homolog B
MAOA	Monoamine Oxidase A
MHC	Major Histocompatibility Complex
MK	Microbial Keratitis
MKI67	Kiel-67
MME	Macrophage Metalloelastase
MMPs	Matrix Metallopeptidase
MRC1	Mannose Receptor C Type 1
NES	Normalised Enrichment Score
NF-κB	Nuclear Factor Kappa-Light-Chain-Enhancer Of Activated B Cells
NGS	Next-Generation Sequencing
NLRP3	NOD-Like Receptor Family, Pyrin Domain Containing 3
NO	Nitric Oxide
padj	Adjusted P-Value
PAMP	Pathogen-Associated Molecular Patterns
PBMC	Peripheral Blood Mononuclear Cells
PBS	Phosphate-Buffered Saline
PCA	Principal Component Analysis
PDGF-BB	Platelet-Derived Growth Factor-Bb
PGE2	Prostaglandin E2
PI	Propidium Iodide
PRR	Pattern Recognition Receptors
PTGES	Prostaglandin E Synthase
QC	Quality Control
RANTES	Regulated On Activation, Normal T Cell Expressed And Secreted
RNA-seq	RNA Sequencing
RSAD2	Radical S-Adenosyl Methionine Domain-Containing Protein 2
SD	Standard Deviation
SERPING1	Serpin Family G Member 1
SLAMF7	Signalling Lymphocyte Activation Molecule Family Member 7
SOCS	Suppressor Of Cytokine Signalling
STAT	Signal Transducer and Activator of Transcription

TGFβ	Transforming Growth Factor
TGM2	Transglutaminase 2
Th	T-Helper Type
TLRs	Toll-Like Receptors
TNF-α	Tumour Necrosis Facto
TNFAIP6	TNF-Alpha-Induced Protein 6
TREM2	Triggering Receptor Expressed on Myeloid Cells 2
UBC	Ubiquitin C
VEGF	Vascular Endothelial Growth Factor

Chapter 1. Introduction

1.1. Human cornea

The human cornea forms the anterior portion of the eye and covers the outside of the eye, including the anterior chamber, pupil, and iris. The cornea is optically clear, as it is an avascular and well-organised layer of collagen fibrils (Sridhar, 2018). The cornea performs two major functions, because of its location. One, as a physical barrier: it protects the intraocular structure from environmental insults, which is of crucial importance, because the eye is an immunologically privileged region (Meek and Knupp, 2015). Immunologically, the eye is able to tolerate introduced antigens and eliminate the pathogenic invaders without initiating an inflammatory immune response (Niederkorn, 2011). Secondly, the transparent cornea is the major refractive part of the ocular tissue, while the remaining third of the visual power of the human eye is provided by the lens, which is able to adjust its shape to adapt to alterations in the destination of the objects. Light is passed through the cornea into the retina, where the optical nerve is situated, which converts the transmitted light into images and produces vision (Artal, 2014, Donaldson et al., 2017).

1.1.1. Anatomy of cornea

The cornea's structure is essentially separated into three cellular layers, namely, the corneal epithelium, corneal stroma, and corneal endothelium, and two acellular membranes, Bowman’s membrane and Descemet’s membrane. The acellular composite of cornea is composed of glycosaminoglycans and collagen while keratocytes, endothelial cells, and epithelial cells populate the cellular layers. The majority of the human cornea is composed of a collagen-rich layer, which is approximately 0.63 mm thick peripherally and 0.58 mm centrally **(Figure 1.1)** (Mobaraki et al., 2019, Sridhar, 2018, Bartakova et al., 2014).

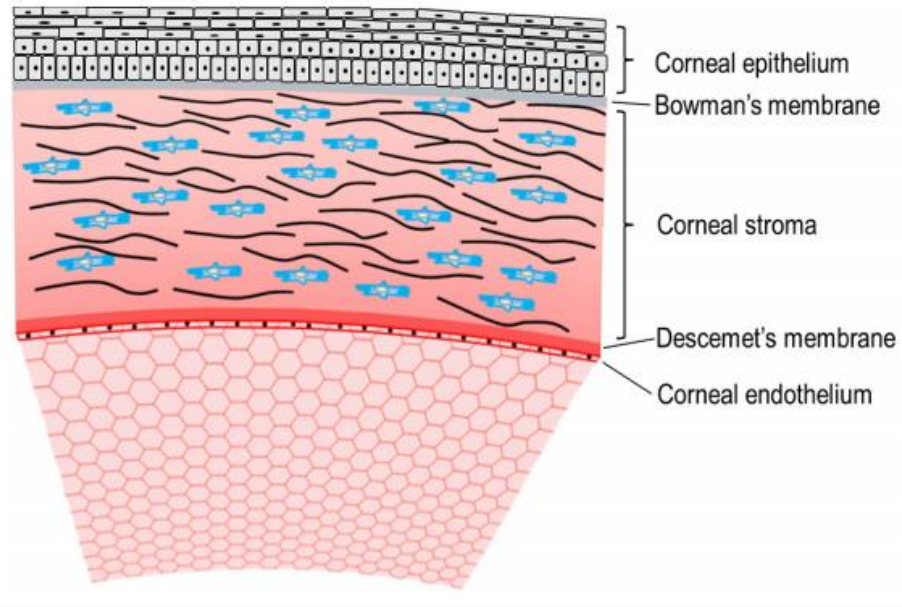

Figure 1.1Corneal structure.
The five layers of cornea from anterior to posterior. Diagram taken from Chen et al. (2018).

The epithelium of the human cornea, which is about 50 μm thick, constitutes the outermost layer of the cornea. It is composed of five to six layers of three different cell types, a stratified squamous non-keratinised epithelium with a basal layer that snaps over the front of the cornea. The corneal epithelium consists of nearly three layers of superficial cells, which overlie about three layers of wing-like epithelial cells. Posterior to the wing cells is a monolayer of mitotically active basal cells, attached to the basement membrane. Due to its location, the epithelium acts as a physical barrier to protect the influx of toxins and pathogens as well as into the epithelial layer itself and the corneal stroma. Furthermore, interaction of the epithelium with tears forms a smooth surface contributing in process of light reflection (Chen et al., 2018, Sridhar, 2018). The basement membrane (BM), which consists of matrilin-2, fibronectin (FN), nidogen, different types of collagens, perlecan, and laminin, is an important epithelial layer overlaying the Bowman's membrane. The integrity of corneal BM is essential as it plays a role in regulating cell signalling and migration between epithelial cells and

stromal layers, and abnormality of the BM is associated with the pathogenesis of scar formation (Torricelli et al., 2013).

Posterior to the corneal epithelium is the Bowman's membrane which is a smooth non-cellular layer formed of thin collagen fibrils from different types I, XII, III and V, and proteoglycans. Its thickness is approximately 10μm. its role is still uncovered. As it is nongenerative, disruption of this layer may lead to corneal scaring (Sridhar, 2018, Wilson, 2020a)

Anterior to Descemet's membrane is the corneal stroma, which occupies around 90% of the entire corneal depth. It consists of specialised cells, keratocytes, proteoglycans, and 200–250 layers of highly ordered collagen fibrils arranged in parallel primarily collagen type I with less of collagen types III, V, and VI. Keratocytes are anatomically located between the layers of the corneal stroma and have a homeostatic function in the extracellular matrix (ECM) environment of the stroma by producing molecules that are involved in the degradation and formation of ECM, such as matrix metalloproteinases (MMPs) and proteoglycans and collagen (Hassell and Birk, 2010, Sridhar, 2018, Meek and Knupp, 2015).

Anterior to the corneal endothelium, Descemet's membrane is the acellular, roughly 10 μm thick, acting as the basal lamina of the corneal endothelium and mainly consists of type IV collagen with minor amounts of collagen type VIII and type XII, perlecan, nidogens, vitronectin, laminin, and FN.

The human corneal endothelium is a monolayer of flat cells, which measures approximately 5 μm in thickness. The central function of the human corneal endothelium is to act as a barrier that modulates the transport of ions and water between corneal stroma and the aqueous humour, and it is responsible for the optical

clarity of the corneal endothelium (Schlotzer-Schrehardt et al., 2011, Sridhar, 2018). This layer is mainly composed of 4500 non-regenerative cells/mm^2 at in neonates, which are able to expand their surface to compensate for a decrease in their number with age due to cellular hypertrophy. However, the mitotically inactive nature of endothelial cells may result in dysregulation of fluid and solute balance, leading to vision defects (Chen et al., 2018).

1.1.2. Corneal transparency

Keratocytes are naturally quiescent cells, populated around 4% of stromal layer of cornea and located between paralleled collagen fibrils, and are responsible for maintaining corneal transparency by producing proteoglycans including decorin, keratocan, lumican, mimecan and collagen, type (I, V, VI, XII) as well as containing crystalline molecules within their cytoplasm. Furthermore, they produced serine protease inhibitors (serpins), including maspin which functions to inhibit the stromal cell migration in the cornea and is involved in suppression of angiogenesis, preserving avascularity of cornea (Yam et al., 2020, Pescosolido et al., 2014).

Stroma of human cornea is populated by bone marrow derived monocyte lineage cells, such as macrophages and dendritic cells, expressing CD14, CD45, CD11b, CD11c, HLA-DR and TLR4 but not CD66, CD56, CD3, and CD19. These cells are located in all the corneal stromal layers (Yamagami et al., 2006).

An early study found a dense network of resident tissue macrophages in the stroma of the rat, mouse, and human iris and ciliary body, with a density of about 600 to 800 cells/mm^2 (McMenamin et al., 1994). Initial research indicated that CD11b$^+$ macrophages are the primary immune cells residing in the cornea, constituting half of total cells (Brissette-Storkus et al., 2002). A study conducted by Hamrah et al. (2003)

revealed that corneal monocytes and macrophages were found in the posterior stroma of the normal mouse cornea. Expression of lymphatic vessel endothelial hyaluronan receptor (LYVE-1) is found on corneal macrophages situated near the corneal limbus, adjacent to the limbal lymphatics and blood vessels (Xu et al., 2007). This suggests their role in maintaining lymphatic vessel formation, to promote the resolution of inflammation and control the clinical manifestations of bacterial keratitis in an animal model (Narimatsu et al., 2019).

Single-cell RNA analysis was used to identify various subsets of myeloid cells in different ocular regions under normal conditions. The study revealed that corneal resident macrophages in mice originate from yolk sac-derived cells, as determined by fate mapping technology. Additionally, it was found that corneal macrophages have a high turnover rate, indicating a continuous replenishment from circulating blood cells (Wieghofer et al., 2021). A study by Li et al. (2022) using single-cell RNA analysis identified innate and adaptive immune cells in the periphery of the human cornea by specific markers. These results support that macrophages are the predominant innate immune cells present. Although several chemokines, such as CXCL16 and CXCL8, known for their roles in recruiting inflammatory cells, were highly expressed by macrophages and monocytes, these corneal macrophages and monocytes were also the main producers of regulatory molecules including IL-10 and TGF-β. This suggests their crucial role in the wound healing response in the human cornea.

Corneal homeostasis can be disturbed, and transparency compromised due to the abnormal formation of blood or lymphatic vessels, which can result from graft rejection, severe corneal trauma, or infection. Studies showed that resident macrophages in the mouse cornea are key contributors in both the homeostasis of lymphatic vessels in a

healthy cornea and the promotion of lymphangiogenesis in response to inflammation. For example, a significant decrease in the growth of lymphatic vessels in the peripheral cornea was observed in normal corneas, following suture placement, of mice where corneal macrophages were depleted (Maruyama et al., 2012).

A study discovered that a healthy gut microbiota is necessary for the appropriate distribution of corneal $CCR2^{-}$ macrophages, which play a critical role in normal corneogenesis in mice. Antibiotic-induced dysbiosis reduced the percentage of these macrophages, leading to abnormal alterations in the cornea, such as reduced thickness and size. Restoring the gut flora with probiotics or fecal transplants improved the abnormalities in corneal development (Wu et al., 2020).

Different levels of Ly6C expression on macrophages were used to differentiate between various subsets of macrophages with different functions. Macrophages that express a high level of Ly6C are thought to be pro-inflammatory and originate from blood monocytes, while macrophages that do not express this marker are identified as tissue resident macrophages essential for maintaining tissue and immune system homeostasis. Macrophages with low Ly6C expression levels are thought to have a pro-regenerative function, promoting the fibrosis resolution (Ramachandran et al., 2012, Lamy et al., 2022). Lamy et al. (2022) assessed the recruitment patterns of corneal macrophages in a mouse model of chemical injury at sequential time points on days 1, 3, and 6 following the injury. The percentage of $Ly6C^{-}$ recruited macrophages increased over time, with significant elevations on days 3 and 6. Conversely, the $Ly6C^{+}$ subset predominated at the beginning of the injury. The percentage of pro-regenerative $Ly6C^{low}$ expressing macrophages peaked on day 3

after injury. This indicated the recruitment of corneal macrophages and the functional roles of distinct subsets following corneal injury (Lamy et al., 2022).

A study investigated the response of corneal resident macrophages to laser-induced minor injury in the mouse cornea using *ex vivo* live imaging. As soon as the laser damage was applied, the resident macrophages in the cornea were found to extend their filopodia toward the affected area for about 40 minutes, suggesting their role in the wound healing process (Gulka et al., 2021).

The homing of monocytes and macrophages in the mouse cornea following injury was mediated by proangiogenic VEGF-A through its receptors VEGF-R1 and VEGF-R2. Depletion of monocytes and macrophages resulted in decreased formation of both lymphatic and blood vessels (Cursiefen et al., 2004).

Early studies demonstrated that the CCR5 pathway facilitates the trafficking of Langerhans cells (Yamagami et al., 2005). Monocyte-derived cells in the human corneal stroma express CCR2 constitutively and that normal epithelial cells and keratocytes express CCL2, suggesting that the CCR2/CCL2 pathway may facilitate the homing of monocyte-derived cells in human cornea (Ebihara et al., 2007).

The CX3CR1/CX3CL1 pathway, studied using $Cx3CR1^{gfp}$ transgenic mice, facilitates the migration of dendritic cells to the corneal epithelium (Chinnery et al., 2007). The replenishment rate of bone marrow-derived $CD45^{+}$ and $CD11b^{+}$ macrophages in the irradiated normal mouse cornea was assessed using $Cx3CR1^{gfp}$ transgenic mice and wild type mice. Three-fourths of corneal macrophages were replenished in the stromal cornea at 8 weeks post bone marrow transplantation. Early $eGFP^{+}$ cell migration mostly occurred in the stroma's anterior region, while by 8 weeks, the cells were evenly

dispersed throughout the stroma, This pattern may suggest infiltration of circulating monocytes from the limbus to the interior regions of the cornea (Chinnery et al., 2008).

Human monocyte recruitment was observed in patients experiencing acute corneal transplant rejection. *In vitro* experiments demonstrated that targeting the chemokine receptors CCR2 and CCR5 effectively inhibited the migration of monocytes across an endothelial barrier model (Lapp et al., 2015). The expression of adhesion molecules, such as Intercellular Adhesion Molecule-1 (ICAM-1), Platelet Endothelial Cell Adhesion Molecule-1 (PECAM-1), Vascular Cell Adhesion Molecule-1 (VCAM-1), Lymphocyte Function-associated Antigen 1 (LFA-1), and Macrophage-1 Antigen (MAC-1), was observed in human inflamed cornea. This suggests their function in aiding the migration of immune cells to the cornea (Goldberg et al., 1994).

In response to bacterial infection resident corneal cells recognise invading pathogens through their pattern recognition receptors and initiate a strong inflammatory response characterised by the secretion of a wide array of cytokines, chemokines, and adhesion molecules. These mediators, including TNF-α and lL-1 (cytokines), CCL5 and CCL2 (chemokines), and P- selection, PECAM-1 and ICAM-1 (adhesion molecules), facilitate the infiltration of immune cells, including monocytes, from blood vessels into the infected cornea (Ung and Chodosh, 2021).

Monocyte recruitment to inflamed tissues is a complex, multistep process mediated by various signalling molecules. Initially, selectins facilitate the rolling of monocytes on cytokine activated endothelial cells. This is followed by chemokine activated G protein coupled receptors on monocytes, which in turn triggers integrin activation, leading to firm adhesion through LFA-1 and very late antigen 4 binding to ICAM-1 and VCAM-1. Following adhesion, monocytes undergo polarisation and migrate towards endothelial

tight junctions, promoted by interactions between junctional adhesion molecules on endothelial cells and integrins on monocytes. Finally, interactions between PECAM-1 and CD99 facilitate endothelial cell contraction, allowing monocytes to exit the blood vassals and entry the tissue (Medrano-Bosch et al., 2023).

The concept of M1 and M2 macrophages was originally defined to parallel the Th1 and Th2 immune responses (Mills et al., 2000). However, significant studies over previous years have challenged this binary classification, suggesting instead that macrophage activation exists on a continuous spectrum of pro-inflammatory and anti-inflammatory, wound healing states (Mosser and Edwards, 2008). Thus, the binary classification of M1 and M2 macrophages may be observed in *vitro* under controlled single treatment conditions. However, *in vivo*, a diverse variety of macrophage states with overlapping phenotypes exist in response to a more complex array of signals, such as cytokines and the specific tissue microenvironment (Strizova et al., 2023, Zhao et al., 2024). The role of macrophages in fibrosis is complex with different polarisation states involved at different stages of disease progression. In early stages, the pro-inflammatory effect of M1 macrophages may dominate, clearing pathogens or responding to damaged tissue. In the latter stages anti-inflammatory and wound healing processes of M2 macrophages are more significant. Failure to resolve the situation may lead to a chronic wound healing response, epithelial-mesenchymal transition and extracellular matrix formation leading to fibrosis. M1 and M2 macrophages are part of a broader range of cells with different phenotype and markers. The balance between these subpopulations may determine the balance between inflammation, wound healing and fibrosis as seen in condition such as autoimmune diseases, idiopathic pulmonary fibrosis and scleritis (Ge et al., 2024).

1.1.2.1. Immune privilege in the cornea

Preserving the unique cellular and avascular structure of the cornea is crucial for maintaining its optical clarity and, consequently, vision. A physiological mechanism known as immune privilege is responsible for the maintenance of corneal integrity by mediating the host immune defences, preventing or minimising inflammation and immune-induced damage to the tissue microenvironment (Benhar et al., 2012). The concept of immune privilege in the eye was founded by Medawar (1948) in 1940, when allogenic skin transplanted in the anterior chamber of the eye had a prolonged survival period as compared to controls. Immune privilege in the eye is attributed to three mechanisms: (i) blood-tissue barriers to segregate the eye tissue from components of the immune response; (ii) providing a local immunosuppressive microenvironment to restrict the activity of immune cells; (iii) inducing specific immune tolerance through Anterior Chamber-Associated Immune Deviation (ACAID) (Wang et al., 2023b).

The blood retinal barriers function to isolate the internal ocular tissues from interaction with immune cells and mediators through tight conjunctions between cells in the epithelium and endothelium layers. Abundant expression and release of immune-regulatory and -suppressive mediators such as Fas ligand, alpha-melanocyte-stimulating hormone (α-MSH) and TGF-β, respectively, by the cells of the blood retinal barriers, consequently inhibiting the effects of inflammatory cells (Zhu et al., 2023).

ACAID is an unusual immune response upon exposure of allogeneic proteins or pathogens to the anterior chamber. These responses, via the spleen, lead to the production of antibodies that are able to neutralise invaders without the involvement of complement and consequential inflammation, and induction of specific immune tolerance via regulatory T cells (Niederkorn, 2011). Moreover, corneal tissue is

characterised by the low expression levels of MCH classes I and II (Niederkorn, 2011), both of which are involved in antigen presentation and the initiation of the immune response (Wieczorek et al., 2017).

The cornea itself contributes to ocular immunoprotected mechanisms by acting as an immunoregulatory site to induce the death of effector T cells and the development of T regulatory T cells. Cornea maintains its immunosuppressive property by constantly expressing immune modulatory molecules, such as programmed death-ligand 1, Fas ligand, glucocorticoid-induced TNF receptor family-related protein (GITR) ligand and cell surface TGF-β (Hori et al., 2020).

Blood and lymphatic vessels penetrate most tissues in the human body in the normal state, and are responsible for the transport of cells, nutrients and molecules. Unlike most human organs, the cornea is an avascular tissue, and its nutrients and oxygens are provided by tears, aqueous humour and limbal vessels (Hori et al., 2019). Corneal angiogenic privileged properties profoundly contribute to maintaining its immune privilege and its optical clarity. The formation of lymphatic and blood vessels in the cornea would disturb the corneal transparency and allow the infiltration of immune cells (Niederkorn, 2011). The corneal tissues maintained their avascularity by a range of mechanisms, such as the expression of anti-angiogenic angiostatin, thrombospondin and the soluble vascular endothelial growth factor receptor (VEGFR1), and α-MSH, angiogenic mediators, derived from the anterior chamber (Di Zazzo et al., 2021).

1.2. The clinical problem: Corneal scarring

Vison represents one of the most vital senses, crucial for basic survival functions for humans. A cross-sectional online questionnaire of the UK public's perceptions showed

the most valuable sense is sight (Enoch et al., 2019), while a second study in 2019 highlighted the high number of studies on visual modality as compared to other senses (Hutmacher, 2019). A recent study estimating the predominance of blindness from corneal opacification using data from surveys and worldwide publications snice 1984 to 2020 in 75 nations, found that more than five million of population aged forty and over have non-trachomatous corneal scarring blindness and moderate to severe vision loss in both eyes (Wang et al., 2023a).

Corneal scarring is one of the leading causes of the blindness globally, ranked fifth among all causes, accounting for more than 3% of global blindness incidences (Flaxman et al., 2017). Conversely, studies conducted in developing countries, such as Nepal and Saudi Arabia, showed that corneal scarring is the second or third leading cause of blindness, which may suggest that regional disparities and socioeconomic factors have an influence on the prevalence of corneal scarring blindness (Pant et al., 2022, Al-Ghamdi, 2019). The incidence of corneal opacity decreased from 1.6 million in 1990 to 1.3 million in 2015 (Wang et al. (2023a). The incidences of corneal blindness in terms of regions showed significant differences where developing countries such as the Middle East and the North Africa area have the highest rates (Kate and Basu, 2023, Mathews et al., 2018, Wang et al., 2023a). The gender-specific prevalence of corneal scarring is significantly different, as it is more dominant in men than women (Flaxman et al., 2017, Wang et al., 2023a).

Worldwide data showed that corneal blindness was a major public health issue in developing countries (Wang et al., 2014). Vision impairment does not only have adverse impacts on the life quality of blind people but also has economical, educational and employment consequences as well as an increased risk of death

(Welp et al., 2016). A study on blindness in the UK estimated that the direct cost of the health care system is more than £2.5 billion, while indirect costs, such as lost productivity, carer expenses, and others, exceeded £5.5 billion. According to World Health Organisation (WHO) (2023), blindness causes significant financial burdens, resulting in an annual loss of around $4 billion in terms of lost work and productivity.

1.2.1. Causes of corneal scarring

Corneal blindness is defined as a range of ocular disorders that affect the transparency of the cornea, causing scarring and, subsequently, sight loss (Tidke and Tidake, 2022). As the cornea is the outermost part of the eye's structure and acts as a protective barrier for interior ocular components, it tends to be frequently exposed to external insults such as infection or injury, which could lead to corneal blindness (Sridhar, 2018). A study was conducted by Mathews et al. (2018) to investigate the etiological factors of corneal blindness worldwide by examining studies from the previous decades. They found infection and trauma to the cornea were the leading causes of corneal blindness, while other factors, such as deficiency of vitamin A, inflammation, treatment-induced complications, degeneration, and genetics, can also result in corneal blindness (Burton, 2009).

Globally, significant clinical and epidemiological studies demonstrated that infectious keratitis (IK) is a significant contributor to the development of corneal blindness. at all ages in both devolving and developed nations (Tran et al., 2020, Kate and Basu, 2023, Kalaivani, 2021, Ung et al., 2019, Maharana et al., 2019). IK is a prevalent corneal disease, characterised by the invasion of pathogenic microorganisms, such as bacteria, protozoa, viruses, fungi, or combinations of which, into the cornea. This invasion and its outcome result in corneal damage associated with a higher risk of loss

of transparency. IK is considered an urgent medical condition that needs rapid intensive treatment to eradicate the infection and minimise collateral damage to highly regulated corneal components (Thomas and Geraldine, 2007).

1.2.1.1. Epidemiology of Microbial Keratitis

The prevalence of MK varies significantly with regional disparities, access to health care, socioeconomic, and climate status. Although few studies assess the recent global prevalence of MK, it is more common in low-income nations (Ting et al., 2021).

In developed countries, bacterial keratitis is the majority of microbial keratitis cases (Ting et al., 2018, Tam et al., 2017). Ocular trauma, contact lens wear, and corneal damage are the most common predisposing factors of bacterial keratitis (Farahani et al., 2017). A study conducted by Bartimote et al. (2019) to investigate the diversity of causative agents of microbial keratitis found that coagulase-negative Staphylococcal (CoNS) is the most common etiological agent of bacterial keratitis.

The pathogenicity of MK and clinical manifestations differed heavily depending on the type of infection and causative microorganism, however, a common pathophysiological process of MK was involved. Pathogenic invasion or infection is initiated by the attachment of pathogens to the outermost layer of the cornea, the epithelium, leading to penetration of the corneal surface and the development of infection. The critical factor for the development of *Pseudomonas aeruginosa* infection in the host cornea is the impairment of the outermost layer of the cornea. Wearing contact lenses is the main contributor to increasing susceptibility to the development of *P. aeruginosa* keratitis (Dempsey and Conrady, 2023).

1.2.1.2. Clinical manifestations, diagnosis and treatment of MK

Although symptoms of microbial keratitis varied depending on the aetiological microbes, acute eye pain, eye discharge, photophobia, corneal ulceration, blurred vision, sensation of foreign object, or stromal infiltrates may be common presentations. (Nguyen and Lee, 2019, Cabrera-Aguas et al., 2022, Ting et al., 2021).

Effective diagnosis of the pathogen providing appropriate and rapid therapeutic intervention, is a critical factor that significantly affects prognosis of microbial keratitis and increased risk of irreversible blindness (Lakhundi et al., 2017, Austin et al., 2017). Recent work from our group has shown that Nanopore sequencing can identify causative agents in MK and endophthalmitis within a few hours, greatly increasing potential to prescribe the correct treatment for each patient (Low et al., 2021, Low et al., 2022). The application of antibiotic eye drops to the affected cornea is the standard treatment for MK (Egrilmez and Yildirim-Theveny, 2020).

1.2.2. Overview of corneal scarring pathophysiology

Following infectious, inflammatory, chemical, or traumatic corneal injury, the corneal BM is disturbed, allowing interactions between epithelial and stromal cells, which induce corneal wound healing responses. The repair mechanism involves inflammation, formation and degradation mechanisms, and results in normal corneal matrix remodelling and the maintenance of a transparent cornea. However, regenerative corneal wound healing depends on several factors including healthy status, gender, age, and types of injury, and may not occur in all cases and lead to further alteration of the molecular components and corneal structure, damaging the transparent collagenous matrix in the cornea (scar formation) with impairment of light reflection, ultimately causing blindness. The regenerative wound healing corneal

response is more likely to occur in cases of non-extensive injuries compared to serious trauma or exposure of the wounded cornea to pathogenic invasion. In the latter case, the corneal tissues are damaged and the infection is eliminated, resulting in induction of a strong inflammatory response, recruitment of immune cells, and fibrosis (Torricelli and Wilson, 2014, Menko et al., 2019).

During corneal wound healing, epithelial cells release an array of pro-inflammatory cytokines, such as IL-1α, and IL-1β, TNF-α, and Fas ligand, which in turn triggers the apoptotic pathway in stromal keratocytes, which likely resulted in modification of its surrounding ECM, such as collagens and proteoglycans. Apoptotic keratocytes were found to be the initial alteration in stroma after corneal epithelium injury, changing their phenotype to fibroblasts, which proliferate and migrate toward the injured area. In corneal stroma, different migratory cells, including bone marrow-fibrocytes, and macrophages, have been identified. In response to the pro-inflammatory microenvironment in the ECM and platelet-derived growth factor (PDGF), TGFβ1, TGFβ2 and TGFβ 3 secreted by cells, in corneal epithelium, endothelium in paracrine or autocrine manner or tear, fibroblasts of both distinct origins transdifferentiate into myofibroblasts (Bukowiecki et al., 2017, Torricelli et al., 2016, Wilson, 2020b).

Corneal epithelial cells contribute to the formation of myofibroblasts in the context of corneal wound healing through a process known as epithelial to mesenchymal transition (Roy et al., 2015). This biological phenomenon refers to the transformation of epithelial cells, under the influence of specific mediators, into cells with mesenchymal properties. These properties are characterised by, for example, enhanced synthesis of ECM components, increased resistance to apoptosis and compromising cell-cell adhesion (Kalluri and Weinberg, 2009).

Following corneal stromal injury in mice, bone marrow-derived fibrocytes migrate to the corneal stroma and mature to myofibroblasts in parallel to keratocyte-origin myofibroblasts. When regenerative repair occurs in the epithelial BM, these myofibroblasts undergo cell death (Lassance et al., 2018). Myofibroblasts are characterised by the expression of α-smooth muscle actin (α-SMA) which is released to aid in wound contraction. In addition, myofibroblasts replicate and secrete ECM components, such as tenascin-C, FN, and collagens I, III, IV, and V, resulting in disruption in the collagen type I/type III ratio, which in turn alters the compositional structure of the stroma and ultimately leads to disorganised ECM. Moreover, myofibroblasts contribute to stabilising this disorganised ECM by producing proteoglycans, such as lumican and decorin (Shu and Lovicu, 2017).

Crystallins are an important element of ECM that contribute to optical clarity and are found to be reduced by myofibroblasts (Shu and Lovicu, 2017). Furthermore, continued secretion of epithelial cell-derived growth factors, such as TGFβ, is involved in the growth of corneal fibrosis and loss of corneal transparency. The corneal inflammatory response includes cytokines, chemokines, and other factors produced by epithelial cells, keratocytes, and recruited inflammatory cells including monocytes. This response helps in the eradication of pathogenic microorganisms and can lead to fibroblast development and generation of a disordered ECM (Torricelli and Wilson, 2014, Kamil and Mohan, 2021). All these events are involved in the pathogenesis of corneal scarring. However, the predominant mechanism of corneal wound healing with or without scarring remains poorly understood and need to be thoroughly investigated. In normal wound healing, the corneal BM is repaired, and this is possibly associated with resolution of inflammation. The influx of growth factors, such as PDGF and TGFβ, into the corneal stromal layer is undetectable, and myofibroblasts undergo cell death

as a result of the autocrine release of IL-1 in the corneal stroma. Stromal keratocytes initiate the remodelling of the compositional ECM by degradation of disorganised collagen fibrils and repopulating the corneal stroma (Ljubimov and Saghizadeh, 2015, West-Mays and Dwivedi, 2006, Medeiros et al., 2018).

1.2.2.1. Macrophage role in MK

Macrophages are a heterogeneous population of cells that produce several molecules (antimicrobial peptides, growth factors, and anti-inflammatory mediators), all of which are involved in different stage of corneal wound healing. Although the exact homing mechanism of immune cells is still poorly understood in the context of corneal injury due to its immune-privileged status, the recruitment of monocytes or macrophages to the inflamed site is postulated to be mediated by CCL2 and its receptor CCR2, as the expression level of CCL2 on corneal keratocytes and epithelial cells is enhanced following injury to the corneal epithelium (Ebihara et al., 2007). In addition to the CCL2 and CCR2 interaction, several molecules, such as neutrophil-activating peptide, granulocyte colony-stimulating factor (G-CSF), monocyte-derived neutrophil chemotactic factor, and monocyte chemotactic and activating factor, may play roles in the recruitment and activation of monocytes and macrophages in corneal injury. These chemokines have been found to be upregulated on stromal fibroblasts stimulated with TNF-α and IL1-α (Bukowiecki et al., 2017).

1.2.3. Overview of therapeutic approaches

The standard treatment for people with corneal scarring is corneal transplantation. This treatment is associated with serious problems, such as the risk of rejection, lifelong immunosuppressive drugs, and limited corneal donors (Qazi and Hamrah, 2013). In addition, the treatments that are involved in promoting tissue repair and

controlling the formation of corneal scar formation, such as tetracyclines, are found to be ineffective in preventing corneal scarring (Ralph, 2000). Limiting inflammation and promoting tissue remodelling with minimising fibrosis could lead to regenerative corneal healing and ultimately prevent sight loss.

1.3. Immune cell involvement: Macrophages

Importantly, a persistent pro-inflammatory microenvironment of stromal ECM in the cornea would promote further activation of apoptotic, inflammatory, and profibrotic cascade and eventually corneal scar formation. The eye surface has evolved and has become equipped with several mechanisms to prevent the induction of any inflammatory response associated with pathological conditions, such as keratitis (eye infection) and corneal injury, and these mechanisms are important for ocular immune privilege.

Clearance of infectious agents and damaged corneal tissue followed by resolution of the inflammation and initiation of tissue repair and remodelling without fibrosis are critical requirements of regenerative corneal wound healing. Immune cells, such as macrophages, are recruited and involved in corneal wound healing. Macrophages play an important role in the killing of pathogenic microorganisms, clearance of apoptotic cells, resolution of inflammation, and the formation and degradation of disorganised ECM (Kim and Nair, 2019, Smigiel and Parks, 2018).

Macrophages are phagocytes that are equipped to perform efferocytosis, a process by which macrophages contribute to tissue homeostasis by removing debris and dead cells without initiating inflammation (Mosser and Edwards, 2008, Boada-Romero et al., 2020). Metchnikoff was the first person to describe macrophages as phagocytic cells, and he won the Nobel Prize for this discovery (Gordon, 2008). Immunologically,

the macrophages' function is to ingest invading pathogens by recognising pathogenic products, e.g., pathogen-associated molecular patterns (PAMP), such as lipopolysaccharides (LPS), through their pattern recognition receptors (PRR) like toll-like receptors (TLR). Resident macrophages release cytokines such as IL-6 and TNF in the tissue to activate endothelium which allows to recruitment of inflammatory cells. To trigger an adaptive response, macrophages present engulfed antigens to immune cells (CD4 and CD8 T lymphocytes) via their major histocompatibility complex (MHC) molecules and initiate an immune response (Watts, 1997, Arango Duque and Descoteaux, 2014). In addition, macrophages continue to clear necrotic cell debris. Furthermore, macrophages resolve inflammation and repair damaged tissue in response to local environmental and physiological alterations (Mosser and Edwards, 2008).

1.3.1. Macrophage ontology

The previous concept of the origin of macrophages, that adult bone marrow-derived circulating monocytes infiltrate peripheral tissue and differentiate into tissue-resident macrophages, has been challenged in recent years. Fate mapping analyses have shown that tissue-resident macrophages including those in the brain, skin, and heart are seeded in embryonic tissue before birth and have descended from embryonic precursors. Moreover, it was found that these embryo-derived macrophages are capable of renewing themselves in situ without monocytic contribution, while macrophages that originated from adult monocytes have been identified to be either long or short-lived and their maintenance depends on infiltrated monocytes (Fan et al., 2016, Mass et al., 2023). Some infiltrated monocytes have found to act as antigen-presenting cells APCs in tissue, and do not develop into macrophages (Jakubzick et al., 2013). Based on the developmental period of macrophages, there are three

sources of tissue-resident macrophages, yolk sac progenitor- and foetal liver progenitor-derived cells generated prenatally, and bone marrow progenitor-derived cells developed postnatally (**Figure 1.1** taken from Fan et al. (2016).

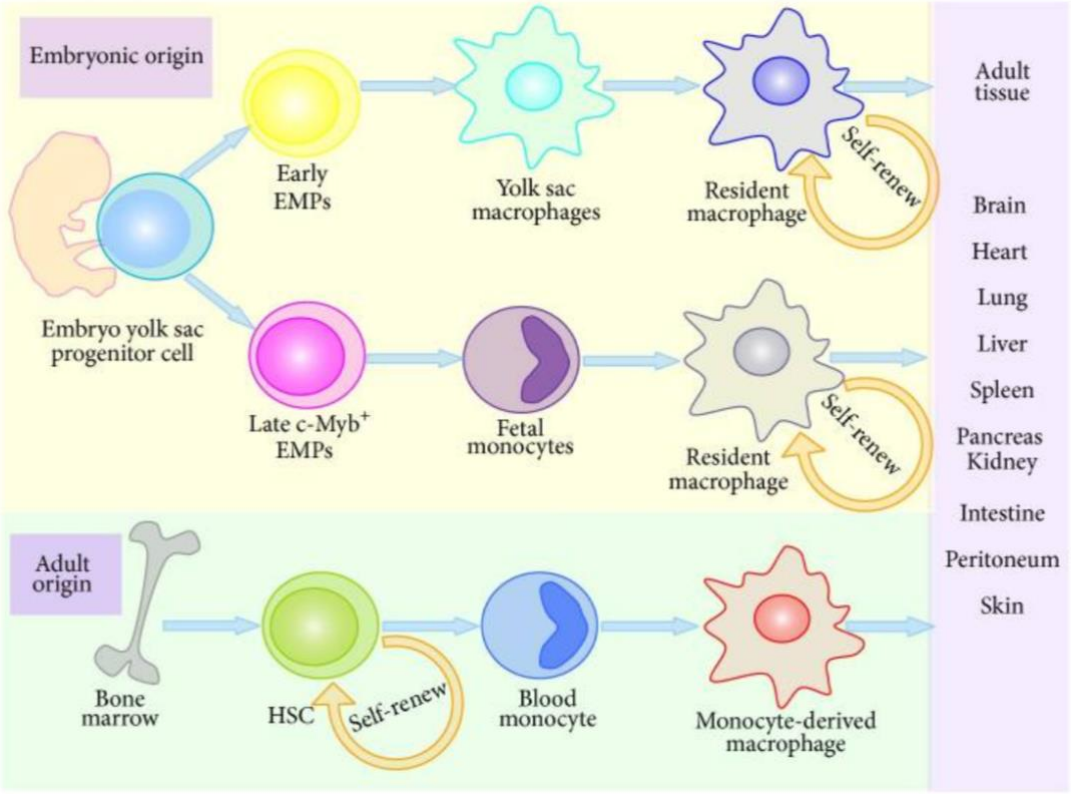

Figure 1.2 Three sources of tissue-resident macrophages.
During embryonic development, yolk sac macrophages and foetal monocytes are generated, which give rise to long-lived macrophages with self-renewal ability. These resident macrophages populate peripheral tissue such as the brain. After birth, blood monocytes are generated from BM-derived haematopoietic stem cells (HSCs), which infiltrate peripheral tissue in response to infection, inflammation, and injury. These monocyte-derived macrophages have a long or short lifespan. Figure taken from Fan et al. (2016).

Early or primitive haematopoiesis occurs in the yolk sac approximately at the beginning of day 7 of embryonic development (E7.0) in mice and at around gestational age of 3 weeks in humans. At this stage, yolk sac derived macrophages and erythrocytes are generated from early erythromyeloid progenitors (EMPs)

independent of the transcription factor Myb, which is crucial for the development of all lineages of the haematopoietic system. These prenatally derived macrophages populate the brain tissue and are maintained by self-renewal through adulthood. At approximately E9.5 in mice and at a gestational age of 5 weeks in humans, late EMPs give rise to monocytes in the foetal liver in the presence of Myb expression. These foetal liver-derived monocytes populate most of the embryonic tissue except for the brain and are capable of proliferation to maintain their presence (Wang et al., 2019b, Ginhoux and Guilliams, 2016).

Definitive haematopoiesis occurs when foetal liver-derived haematopoietic stem cells (HSCs) are generated by the aorta–gonad–mesonephros (AGM) region of the embryo between E10 to E11 in mice (Ginhoux and Guilliams, 2016). These foetal liver-derived HSCs give rise to several haematopoietic progenitors including foetal liver-derived monocytes, which precipitate in the tissue-resident macrophage pool until haematopoiesis begins in the bone marrow after birth (Hoeffel and Ginhoux, 2018). Therefore, tissue-resident macrophages are generated from both yolk sac-derived and foetal liver-derived monocytes and HSCs during embryonic development.

After birth, haematopoiesis mainly occurs in the bone marrow, where HSCs undergo highly restricted differentiation steps, which results in various haematopoietic progenitors, including common myeloid progenitors (CMP). CMP gives rise to all myeloid lineage cells and differentiate into granulocyte-macrophage progenitor, which gives rise to the monocyte and dendritic cell progenitor. Monocytes arise from the common monocyte cell progenitor, while DCs arise from common dendritic cell progenitor (Udalova et al., 2016).

Monocytes are innate immune cells that are released from the bone marrow to the blood circulation and comprise almost 10% of peripheral white blood cells. Based on the combination of CD14 and CD16 expression, human monocytes are classified into three subpopulations. Monocytes that express both proteins are called intermediate monocytes, those that expresses $CD14^{Low}$ and CD16 are non-classical monocytes, and those that express CD14 only are classical monocytes. In mice, classical monocytes are those that express $Ly6C^{hi}$ $CD43^{-}$ whereas non-classical monocytes are those that express $Ly6C^{lo}$ $CD43^{+}$. Intermediate monocytes express both proteins (Wolf et al., 2019a, Guilliams et al., 2018). Classical and non-classical monocytes were found to be similar in humans and mice; however, they are distinct in terms of their gene profiles where only monocytes in mice carried the signature of the transcription factor, peroxisome proliferator-activated receptor γ (PPARγ) (Ingersoll et al., 2010). Monocytes in the circulation infiltrate the peripheral tissues under the influence of several stimuli, such as macrophage depletion, inflammatory conditions, and physiological stress, and differentiate into short-lived macrophages (Udalova et al., 2016).

HSC and yolk sac-derived resident macrophages coexist in the same tissue, such as in the pancreas. The pancreas has two sites: islets of Langerhans, where the macrophages originate from the HSC, and inter-acinar stroma, which contains two populations derived from primitive or definitive haematopoiesis. When all the macrophages are replaced after lethal radiation by donor stem cells, these replaced cells acquire the original phenotype macrophages from different anatomical locations (Calderon et al., 2015). It seems that the local microenvironment plays a crucial role in the development and polarisation of macrophages.

1.3.2. Functional heterogeneity of macrophages in different resting tissues

Macrophages are present in all organ tissues in the body, including microglia and Kupffer cells in the brain and liver, respectively. Macrophages play crucially homeostatic and immunological functions in various tissues, and this may be because of their heterogeneity. In the spleen, there are different types of macrophages located in various areas, including metallophilic macrophages, white and red pulp macrophages, and marginal zone macrophages (da Silva et al., 2015). An example of homeostatic function of macrophages is in the liver where Kupffer cells are involved in the regulation of iron metabolism (Scott and Guilliams, 2018).

Macrophages express pathogen recognition receptors, such as TLRs and the cytosolic nucleotide-binding domain leucine-rich repeat-containing proteins. The binding of these receptors to their ligands results in a significant inflammatory response to eliminate the pathogen (Price and Vance, 2014). Tissue macrophages differ depending upon the organs in which they reside. For example, different C-type lectin receptors are expressed in alveolar macrophages, which are important for the recognition of microorganisms, while lamina propria macrophages, which might be involved in tolerance, do not express C-type lectins (Hume, 2015).

Macrophage populations share core features in terms of transcription, but each tissue-specific macrophage has distinct genomic signatures which possess unique functions in specific tissues. It appears that the tissue microenvironment plays a critical role in macrophage development and function. For instance, splenic macrophages have been found to be controlled by transcription factor Spi-C, which is involved in the haem concentration and, sequentially, in the phagocytosis of red blood cells. Spic-knockout

mice suffer from dysregulated phagocytosis, which results in iron accumulation (Kohyama et al., 2009). There are differences in the signature of the genes involved in metabolism analysis of intestinal and peritoneal (small and large) macrophages; however, the metabolic signature between the two populations of peritoneal macrophages is similar, indicating the influence of tissue cues (Stunault et al., 2018).

1.3.3. Macrophage activation

Macrophages have the ability to change their phenotype, function, and cytokine secretion in response to external environment stimuli and tissue-specific signals via a process called macrophage polarisation. Based on the macrophage response to these various cues, there is a spectrum of macrophage activation states ranging from M1 subsets (classical activation), which promote inflammation, to M2 subsets (alternative activation), where macrophages are involved in the resolution of inflammation and promotion of wound healing. Both populations exhibit differences in surface markers and gene expression profiles. Culture of blood monocytes in the presence of macrophage colony-stimulating factor (M-CSF) *in vitro* produces M2 macrophages, but treating the same monocytes with granulocyte-macrophage colony-stimulating factor (GM-CSF) results in M1 macrophages (Verreck et al., 2004, Murray, 2017). In addition, macrophages activated with interferon-gamma (IFN-γ) and LPS generates pro-inflammatory macrophages, whereas interleukin-13 (IL-13)and (IL-4) stimulation and parasitic infections results in wound healing macrophages (Martinez et al., 2013, Gordon and Martinez, 2010). Therefore, the plasticity of macrophages seems to depend on the type of stimuli.

1.3.4. M1 macrophages

M1 macrophages are induced via PAMP such as LPS binding TLR4 or by exposing them to cytokines of T lymphocyte type 1. Macrophages stimulated with LPS induced signalling pathways through activator protein 1 (AP-1), STAT1, EGR, NF-κB, and IRFs (Martinez and Gordon, 2014). In addition to LPS, IFN-γ and TNF released by different innate and adaptive cells such as natural killer cells and type 1 T lymphocyte were shown to generate M1 macrophages, which have microbicidal or tumoricidal activity by producing a variety of pro-inflammatory cytokines (Mosser and Edwards, 2008). GM-CSF, a crucial element in regulation of haematopoiesis, is another growth factor that has been identified to be involved in the maturation of M1 macrophages (Verreck et al., 2004).

The inflammatory response of M1 macrophages is characterised by the upregulated expression of functional surface markers on macrophages, such as MHC II, CD80, and CD86, inducible nitric oxide synthase (iNOS), TLRs 1 and 4, and IL-1R, all of which are important in the clearance of pathogens and antigen presentation to induce adaptive immunity. Moreover, M1 macrophages produce a diversity of pro-inflammatory mediators, such as GM-CSF, M-CSF, IL-8, IFNβ, IL-12, TNF-α, IL-6, IL-1α and β, IL-23, and reactive oxygen species (ROS), to promote microbicidal or tumoricidal activity. In addition, M1 macrophages produce an array of chemokines, including CCL2, CCL5, CXCL9, and CXCL10, some of which are involved in the induction of immune cell recruitment (Martinez and Gordon, 2014, Shapouri-Moghaddam et al., 2018).

A crucial role of macrophages in directly eradicating invading pathogens is through phagocytosis. Macrophages express a variety of PRR such as TLRs, complement

receptors, and Fc receptors to detect microbial products, complement and antibody-bound microorganisms. This interaction initiates an immune response against the invading pathogens, including inflammation and phagocytosis (Hirayama et al., 2018, van Lookeren Campagne et al., 2007). Activated macrophages form a phagocytic cup to engulf the microbes into phagosomes. Within these phagosomes, macrophages import toxic elements, such as copper and zinc, and limit the availability of essential nutrients like iron, both of which contribute to the destruction of the engulfed microbes. The phagosomes then mature and fuse with lysosomes, creating an acidic environment known as a phagolysosome. In the phagolysosome, the ingested microbes are digested and killed and by a combination of antimicrobial agents, including ROS, NO, microbicidal peptides, and proteases (Leseigneur et al., 2020). ROS, such as superoxide anions , hydrogen peroxide , and hydroxyl radicals , are primarily generated by the mitochondrial electron transport chain and the nicotinamide adenine dinucleotide phosphate hydrogen oxidase enzyme family within activated macrophages (Herb and Schramm, 2021).

The strong inflammatory response generated by M1 macrophages has been found to be associated with pathological conditions, including host tissue damage, disruption of wound healing, and tissue regeneration, which may result in the loss of tissue function, such as corneal scarring (Smigiel and Parks, 2018). To control these conditions, regulatory macrophages are generated to resolve the inflammation and to contribute to the regenerative repair of damaged tissue.

1.3.5. M2 macrophages

In response to inducers like IL-4, IL-10, IL-13, glucocorticoids, and M-CSF, M2 macrophages form three subpopulations with functional diversity: M2a, M2b, and M2c.

Although M2 macrophages play a crucial role in wound healing, these M2-like macrophages have different functions (Martinez and Gordon, 2014).

Both IL-4 and IL-13 can produce M2a macrophages, which have a wound healing behaviour and express the scavenger receptor (CD163), the decoy receptor IL-1R, MMPs, arginase 1 (ARG1), mannose receptor (CD206), and the IL-1R antagonist. This subset of M2 macrophages stimulate the formation of new blood vessels by secreting vascular endothelial growth factor A (VEGF-A). Other pro-healing roles of IL-4-induced macrophages include induction of myofibroblast differentiation and cellular proliferation, which are mediated by the release of growth factors such as (TGF-β), PDGF, endothelial growth factor, and insulin-like growth factor 1 (IGF-1). IL-4 and IL-13 signalling are induced via activation of IRF4, STAT6. SOCS1, and Mannose Receptor C type 1 (MRC1). Enhanced expression of CCL22, TGF-β, CCL18, CCL17 and IL-10 are liked with IL-4 induced macrophages. IL-4 has been shown to increase the endocytosis in macrophages and induce and production of ECM components such as collagen and polyamines, which are vital for tissue repair and regeneration. Excessive secretion of these molecules can, however, lead to fibrosis; therefore, the function of M2a macrophages needs to be controlled (Mosser and Edwards, 2008, Viola et al., 2019, Wynn and Vannella, 2016, Yao et al., 2019).

M2b macrophages are an immunosuppressive population induced by the combination of immune complexes with LPS or IL-1R Ligands. These macrophages exhibit anti-inflammatory and pro-inflammatory phenotypes by producing cytokines, such as low levels of IL-12, IL-6, and IL-1β, as well as CCL1, which facilitates the recruitment of regulatory T cells. These macrophages found to enhance the healing progression

upon cardiac ischemia and spinal cord injuries (Roszer, 2015, Martinez and Gordon, 2014, Wang et al., 2019a).

Another immunoregulatory population of M2 macrophages, is IL-10, glucocorticoid, or TGF-β -induced macrophages namely, M2c macrophages. These macrophages showed anti-inflammatory function by producing cytokines such as IL-10 and TGFβ. These macrophages were found to promote the removal of dead cells, and expressed CCL18, TLR1, CCL16, TLR8, CXL13, CXCL4, and CD206 (Roszer, 2015, Yao et al., 2019, Viola et al., 2019). In addition, M-CSF, which is consistently generated by endothelial cells, macrophages, fibroblasts, stromal cells, osteoblasts and smooth muscle cells, and, has been shown to induce M2 macrophages (Martinez et al., 2006, Verreck et al., 2004).

1.3.6. Metabolism of macrophages

Macrophages undergo metabolic rewiring in response to different stimuli from either extrinsic or tissue microenvironments, which is crucial for maintaining their specific function and continuing their polarisation under specific conditions (Viola et al., 2019).

M1 macrophages have been found to be associated with glycolysis. During the infection, macrophages need to induce strong inflammatory responses to control invading pathogen and thus they require a source of energy. Glycolysis is involved in the production of inflammatory cytokines such as IL-6 and TNFα as well as ROS secretion and inflammasome activation. When macrophages were stimulated with LPS and IFN-γ, glucose transporter 1 (GLUT1) was upregulated on the macrophage surface as a result of the quick need for glucose by the macrophages (Fukuzumi et al., 1996). Hypoxia-inducible factor alpha (HIF-1α) is a transcriptional factor that is responsible for the regulation of the glycolytic genes, including GLUT1, in

macrophages. It has been found to be induced following stimulation of macrophages with LPS, as a result of disruption of the Krebs cycle, leads to succinate accumulation and increased itaconate, an important antimicrobial element (Viola et al., 2019). However, its deletion leads to impaired antimicrobial and inflammatory activity of macrophages in response to fungal and bacterial infection *in vitro* and *in vivo* (Li et al., 2018a).

The significance of glycolysis for macrophage function can be noted in insufficient phagocytosis; for example, in *C. albicans* infection, where the yeast cells compete with immune cells, particularly macrophages, for glucose uptake (Tucey et al., 2018).

Arginine is a good example of how metabolic reprogramming regulates phenotypic macrophages. In LPS or IFN-γ-induced macrophages, iNOS is upregulated, leading to the conversion of arginine to nitric oxide (NO) and the subsequent production of NO, which has antimicrobial properties, particularly in intercellular infection. Conversely, M2 macrophages upregulate Arg1, which converts arginine to ornithine and urea, resulting in the formation of polyamines and proline, which are involved in cell proliferation and collagen synthesis, critical for tissue repair (Shapouri-Moghaddam et al., 2018, Stunault et al., 2018).

Metabolism of iron is another example of metabolic differences among M2 and M1 macrophages. M1 macrophages are characterised by elevated expression of ferritin, responsible for storing iron, which in turn limits its consumption by infective agents, and consequently inhibits infection development. However, increased expression of an iron-carrying protein, ferroportin, was associated with M2 macrophages, leading to increased production of iron that is involved in tissue repair (Shapouri-Moghaddam et al., 2018).

Efferocytosis is the clearance of dead lipid-containing cells performed effectively by M2. Increased fatty acid oxidation is involved in efferocytosis, whereas enhanced glycolysis leads to the impairment of efferocytosis. Macrophages consume fatty acid by CD36, and its ablation leads to the failure of M2 activation (Stunault et al., 2018).

1.3.7. Role of macrophages in corneal wound healing

The result of the wound healing response in most species and different organs can be ranked from regenerative healing, in which the function of all injured areas of tissue are restored to normal, to no regenerative repair, in which all wounded tissues are substituted with scar tissue, disturbing the organ function. The wound healing mechanism includes several phases, starting from stopping of bleeding (haemostasis phase), followed by clearing of pathogenic microorganisms and damaged tissue from the wound by phagocytic cells such as macrophages (inflammation phase). In response to secreted growth factors and cytokines, the cells begin to proliferate and migrate to precipitate wound closure by depositing of ECM (proliferative phase). The final phase is the remodelling phase where the deposited EMC is reorganised to restore the tissue-specific function to that before injury (Bouchery and Harris, 2019). However, as cornea is known to be an avascular tissue, the coagulation phase is not involved in the wound healing response of the cornea (Bukowiecki et al., 2017).

Weng et al. (2018) used a model of spontaneous regression of liver fibrosis to demonstrate that deletion of IL-4Rα, which is the receptor for IL-4 and IL-13 expressed on macrophages, delays the resolution of liver fibrosis. They found that IL-4Rα regulates the polarisation of macrophages and also induces the production of the fibrolytic macrophage metalloelastase (MME), which contributes to the reversal of

fibrosis (Weng et al., 2018). This highlights the significance of macrophages in fibrosis regression.

Liu et al. (2017) showed that two different subsets of macrophages coexist in murine corneas $CCR2^{-}$ and $CCR2^{+}$ corneal macrophages. Each subset appears at certain days during embryonic development and exhibits functional, phenotypic, and gene expression differences. On day 12.5, $CCR2^{-}$ macrophages are found to be present and exhibit gene expression and phenotypes similar to macrophages originated from umbilical vesicles, such as macrophages in the brain. This subset has self-renewal capacity in the resting cornea, but it promotes an anti-inflammatory environment in the late phase of the wound healing response in an injured corneal epithelium and can be repopulated by circulating monocytes.

$CCR2^{+}$ macrophages present on embryonic day 17.5 either in normal or wounded epithelial cornea are maintained by blood circulation-derived monocytes. These subsets demonstrate pro-inflammatory properties at the beginning of the wound healing process. Ablation of $CCR2^{-}$ and/or $CCR2^{+}$ corneal macrophages by anti-CSF1R antibodies and CCR2 antagonists respectively leads to delays in the wound healing process of the corneal epithelium. Depletion of $CCR2^{-}$ macrophages only in the corneas of mice following epithelium wounding resulted in a significant increase in the influx of neutrophils at the injured site and enhanced expression of inflammatory cytokines including TNF-α and IL-1β. In contrast, deletion of $CCR2^{+}$ macrophages weaken the inflammatory response by a reduction in the expression of inflammatory cytokines and recruited neutrophils (Liu et al., 2017). This study significantly supports the important contribution of different types of corneal macrophages in regenerative repair and remodelling of corneal wound healing by regulation of inflammation and

possibly the fibrosis during the healing response. $CCR2^-$ corneal tissue resident macrophages are essential for the restoration of nerve function and density in the cornea following injury in mice (Liu et al., 2018). Macrophage-expressed molecules are essential for infection elimination and subsequently maintaining corneal clarity. In a mouse model of microbial keratitis, a deficiency in lumican expression on macrophages, which is involved in mediating the TLR4 response to bacterial infection, led to insufficient initial immune response during the early phase of infection and a persistent inflammatory reaction. Consequently, this resulted in increased bacterial concentration and inadequate restoration of corneal transparency (Shao et al., 2013). A recent study by found the coexistence of tissue-resident corneal macrophages and monocyte-derived macrophages in the normal human cornea (Downie et al., 2023).

In a recent study, a skin wound healing model was used to investigate the role of hydrogel combined with prostaglandin E2 (PGE2) in wound healing and regeneration (Zhang et al., 2018). They showed that PGE2 hydrogel enhanced the wound healing process with a significant reduction in fibrosis following injury. They further examined the beneficial effect of PGE2 hydrogel and demonstrated that PGE2 secretion induced polarisation of macrophages toward M2 at the injured area.

Corneal macrophages are located between keratocytes and collagen fibrils in the posterior and anterior parts of normal mouse stroma. Corneal macrophages are involved in maintaining homeostasis of the lymphatic vessel, which is essential for the resolution of physiological inflammation. Hos et al. (2016) investigated the role of IL-10 on corneal lymphangiogenesis following sterile inflammation and reported increased the formation of lymphatic vessels, reduced inflammation in the cornea, and concluded that the resolution of corneal inflammation is attributed to infiltrated

corneal macrophages, which exhibit increased expression of IL-10 and prolymphangiogenic factors like lymphatic vessel endothelial hyaluronan receptor (LYVE-)1 and VEGF-c .They assumed that these anti-inflammatory and prolymphangiogenic macrophages facilitate the removal of inflammatory cells (Hos et al., 2016). This study provides evidence for the therapeutic effect of polarised macrophages in termination of corneal inflammation, which if continued without control may lead to further ocular damage and the ultimately initiation of pro-fibrotic pathways and corneal scarring.

A recent study by Wolf et al. (2019b) investigated the role of macrophage releasing proteinases (MMP12) on the interaction of CCL2 and CCR2 in a chemical injury model of epithelial and stromal cornea. CCL2 and CCR2 signalling was found to increase the recruitment of inflammatory macrophages, neovascularisation, and corneal scarring in the injured corneas of MMP12-deficient mice. They further investigated how MMP12 controls the CCL2-CCR2 interaction, and assumed that following corneal injury, keratocytes and corneal macrophages produce CCL2 to recruit monocytes, which in turn promotes angiogenesis. To regulate this process, corneal macrophages also release MMP12, which is known to deactivate CCL2, disrupting the interaction between CCL2 and CCR2. Consequently, homing macrophages and angiogenesis are inhibited, ultimately preventing scar formation (Wolf et al., 2019b). This study may support the critically reparative response of macrophages in corneal injury and also indicate the significance of the balance of M1 and M2 macrophages.

Tissue resident macrophages are major contributors to organ homeostasis including in the eye (Wang et al., 2019b). The nerves in the cornea significantly contribute to the physical barrier function of the cornea by instructing the eyelid to close in response to

external insults (Yang et al., 2018). Seyed-Razavi et al. (2014) investigated the interplay between corneal macrophages and sensory nerves of normal or injured cornea and found corneal macrophages situated closely with corneal nerve branches; however, these macrophages dissociated from the sensory nerves and migrated to the central cornea two hours following an injury (Seyed-Razavi et al., 2014). This finding may indicate the reparative role of corneal macrophages in corneal wound healing (Chinnery et al., 2017)**.**

The polarisation state of macrophages is essential for proper wound healing (Wynn and Vannella, 2016). Researchers investigated the inflammatory, angiogenetic and fibrotic effect of pioglitazone hydrochloride, a peroxisome proliferator-activated receptor gamma (PPARγ) agonist, on the cornea of rat alkali burn model. PPARγ is a critical transcription factor that can negatively regulates the proinflammatory gene expression of macrophages. The corneas of rats treated with PPARγ agonist had lesser inflammatory response, as the infiltration of both neutrophils and macrophages was decreased compared to the control group. Further, the corneas of the PPARγ group had decreased neovascular and profibrotic responses, which resulted in a reduced opacity of the cornea, as compared with the controls. Importantly, although the number of recruited macrophages in the inflamed cornea was inhibited in the PPARγ group, M2 macrophages were more prominent in the same group, which indicate the significant role of the infiltration rate of macrophages and their polarisation state in corneal wound healing (Uchiyama et al., 2013).

Recently, Weng et al. (2020) examined the regenerative effect of the human stromal stem cell transplantation on mouse injured cornea. Stromal stem cells cocultured with mouse LPS+IFN-γ induced M1 and IL-4 induced M2 macrophages. qPCR analysis

revealed that LPS+IFN-γ induced M1 induced expression of TGFβ3, which mediated the anti-fibrotic effect of transplantation to an injured cornea, while M2 macrophages have no effect on (TGFβ 3) expression (Weng et al., 2020). This study indicated the critical effect of macrophage polarisation state on corneal wound healing process and fibrosis.

Therefore, it seems that macrophages are a critical player during corneal wound healing, where they meditate elimination of infection, clearance of damaged cells, resolution of inflammation, and tissue remodelling. Using macrophages as cell-based therapy to promote regenerative corneal wound healing and preserve its transparency would be a promising intervention.

As stated above the outcome of a challenge to tissue is dependent on the contribution of different cell types over the course of the event. An early response by resident cells including macrophages signals the challenge leading to movement to the site and activation of endothelium to attract new cells from the blood. There is a structure to this response with an initial influx of pro-inflammatory cells to deal with the situation which is followed by a more resolving response to drive tissue homeostasis. Monocytes can sense the microenvironment to which they enter and alter their phenotype accordingly to aid inflammation, immune regulation and tissue maintenance. An imbalance between macrophage subpopulations can contribute to a failure to clear the challenge or for resolution of immune response.

Our hypothesis is that by generating macrophage populations *in vitro* for delivery to the challenge site, in this case the cornea, the pathway can be influenced. For example, aiding the initial inflammatory response, can lead to increased, more rapid clearance of pathogens, or increasing wound healing response to aid resolution. The

lab-polarised macrophage populations could be delivered separately or in combination at different stages of the response. For example, M2 macrophages produce IL-10 which will inhibit the inflammatory response and TGFβ is involved in ECM production and wound healing. An ability to manipulate the ongoing response in the cornea would have the potential to achieve the best outcome i.e. repair without fibrosis.
It is envisaged that as the macrophages will be polarised *in vitro* they will maintain the same phenotype in tissue whether inflamed or healing.

To facilitate the delivery of these lab-polarised cells a gellan fluid gel has been developed in the group and has previously been used to deliver decorin, an antifibrotic molecules to the damaged cornea of mice with a positive effect (Hill et al., 2018). Delivery of lab-polarised macrophages in such fluid gel will allow for their slow release on the damaged corneal surface and protect from blinking and tear washing from the surface.

1.4. Delivery platform: Gellan Fluid gel

Gellan gum is an anionic polysaccharide produced by bacterial fermentation and consists of repeated units of tetrasaccharide (Morris et al., 2012). There are two different forms of gellan gum, deacetylate and acetylate. Ionic salt, pH, and temperature can modify the physical properties of gellan gum. Gellan gum is an optically clear and nontoxic substance that has been approved by the Food and Drug Administration (FDA). It is broadly used in biomedical applications, e.g., as a thickener in eye drop formulations (Chouhan et al., 2019, Hill et al., 2018).

Gellan fluid gel can exhibit solid–liquid–solid transitions. When shear force is applied during gelation, it prevents the formation of a continuous gel structure, instead producing microparticles with ribbon and round morphology (Norton et al., 1999,

Cooke et al., 2018). The gel particles exhibit solid properties at rest, and the application of shear force disrupts these particles into solution and formation of liquid properties. This process can prevent changes in the chemical structure of the gellan fluid gel component, whereas the physical properties are manipulated (Cooke et al., 2018). Exploiting shifts between solid, liquid, and solid phases would increases the retention of therapeutic molecules on the ocular surface, which are removed in minutes by blinking (Snibson et al., 1992).

Gellan fluid gel enables the entrapment of molecules and cells to facilitate a sustained localised therapeutic agent delivery from optically transparent dressings. It can also cover curved surfaces of any size and has shown effective outcomes when used experimentally. Recently, Hill et al. (2018) investigated the use of gellan fluid gel as a continuing delivery system for decorin, which is an anti-fibrotic molecule, was used to prevent corneal scarring in a bacterial keratitis model. They reported that the gellan-based eye drop system enhanced corneal opacity on its own, improved the sustained release of decorin on the ocular surface, and did not interact with decorin (Hill et al., 2018). Therefore, the use of gellan fluid gel as a delivery technology for polarised macrophage-based therapy would be a promising intervention to prevent corneal scarring.

1.5. RNA sequencing (RNA-seq)

Genes in DNA encode all the information required to specify the phenotype and function of cells. The information contained in individual genes can be transcribed into RNA and then translated into proteins (Crick, 1970), via a cellular process known as gene expression (Finotello and Di Camillo, 2015). RNAs that are transcribed when a disease or other condition is present may elucidate unique alterations that these cells

experience. Indeed, the relative abundances of these RNAs could indicate the expression levels of relevant gene (Finotello and Di Camillo, 2015). Thus, we employed a next-generation sequencing (NGS) technology called RNA sequencing (RNA-seq) for transcriptional profiling our generated subset of macrophages.

RNA-seq is an NGS technology used to comprehensively investigate the transcriptome of a cell to identify variations between normal and pathological conditions (Wang et al., 2009). The fundamental concept of RNAseq technology involves sequencing complementary (cDNA) derived from the original RNA using a sequencer platform such as Illumine and computationally quantifying the number of sequence reads that align to a reference genome, thereby indicating the level of gene expression as well as preformed the downstream analysis such as pathway analysis (Oshlack et al., 2010, Deshpande et al., 2023, Wolf, 2013). RNAseq quantifies the gene expression level to identify the differentially expressed gene among different conditions, consequently drawing the biological significance of the corresponding genes that are differentially expressed.

Importantly, it enables researchers to accurately quantify the gene expression level as well as recognise de novo transcripts using low-concentration total RNA in a very high-throughput manner. It has the capacity to detect genes with low and high expression levels (Wang et al., 2009). The prevalent use of RNA-seq significantly decreased its cost when compared to microarray technology because microarrays only measure certain or target genes (Negi et al., 2022).

1.6. Hypothesis

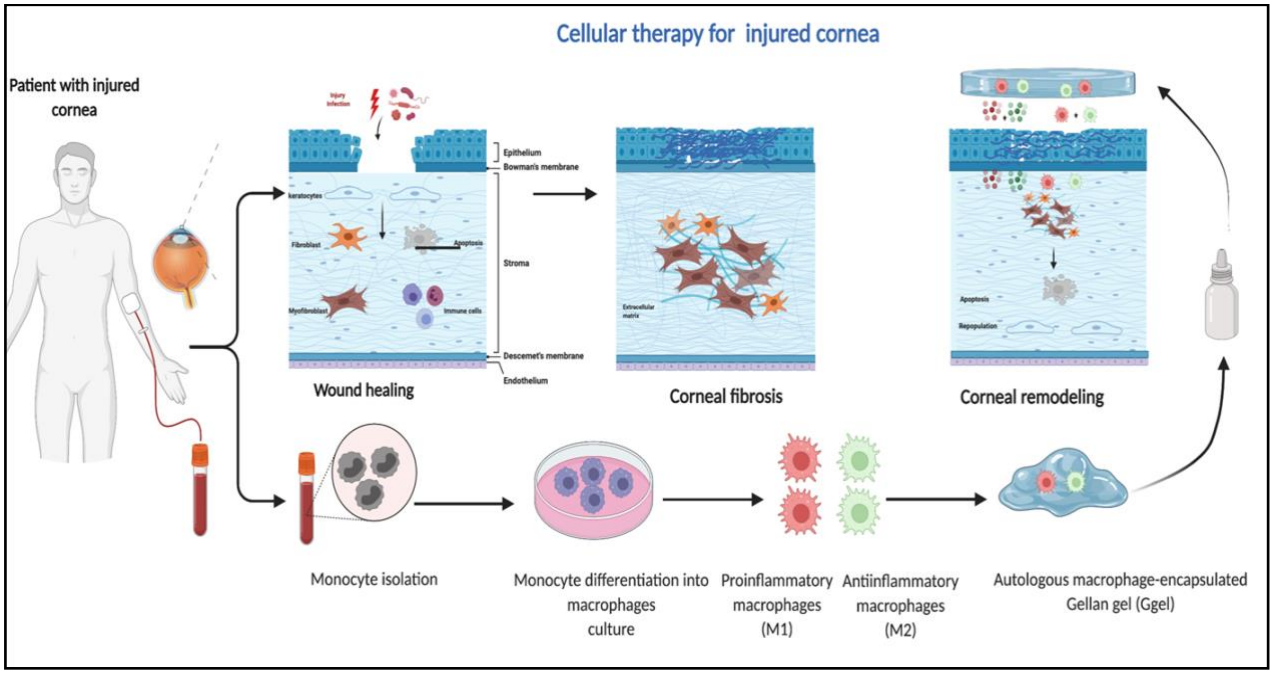

Figure 1.3 Schematic description of Hypothesis.

That critical therapeutic intervention should rapidly restrain or minimise the corneal infection and inflammation associated damage by immediate eradication of pathological agents and promote the regenerative repaired of damaged tissue of cornea. Using bioactive membrane, a mixture of macrophages with anti-microbial and pro-generative healing properties could achieved this. We hypothesise that the Gellan fluid gel will provide protective layer that can deliver macrophages derived antimicrobial and pro-healing agents and increased their retention on ocular surface.

1.6.1. Aims

- To generate M1 and M2 polarisation macrophages from human blood monocytes
- To assess biocompatibility of macrophage subpopulations in gellan gel for delivery to ocular surface

- To determine the maintenance of polarisation of human macrophage subpopulations in response to different cytokine environment.

Chapter 2. Materials and Methods Method

2.1. Materials

Table 2.1Products for cell culture, monocyte isolation and macrophages stimulation

Products	Company	Product Number
Ethylenediaminetetraacetic acid disodium salt (EDTA)	Sigma Aldrich	E7889
RosetteSep™ Human Monocyte Enrichment Cocktail	STEMCELL Technologies Inc	15068
Phosphate-buffered saline (PBS)	Thermo Fisher scientific	18912014
Foetal Bovine Serum	Labtech	FCS-SA
Ficoll Paque Plus	Sigma Aldrich	GE17144003
Trypan blue	Sigma Aldrich	T8154
RPMI1640 medium 1X with L-Glutamine	Thermo Fisher scientific	21875034
Cell scraper	Thermo Fisher scientific	10508292
24 well culture plate	Corning	3337
Cell Dissociation Buffer, enzyme-free, PBS	Thermo Fisher scientific	13151014
RNA isolation		
iScript cDNA Synthesis Kit 25x20ul reactions	BIO RAD	1708891
TB Green® Premix Ex Taq™ II (Tli RNase H Plus)	TAKARA	RR820B
RNase-Free DNase Set	Qiagen	79254
RNeasy Mini Kit	Qiagen	74104
RiboPure™ Kit	Invitrogen	AM1924
Viability Test		
Calcein, AM	Thermo Fisher scientific	C3099
Propidium Iodide	Thermo Fisher scientific	P3566
Gellan fluid gel		
NaCl	Sigma Aldrich	S3014
Kelcogel Gellan CG-LA (powder)	CP Kelco	
RNAseq		
Lexogen - QuantSeq 3’ mRNA-Seq Library Prep Kit FWD (Forward)	Lexogen	015.96
Unique Molecular Identifier (UMI) Second Strand Synthesis Module for QuantSeq FWD	Lexogen	81.96
NextSeq High 75 v2.5	Illlumina	20024906

Table 2.2 Products macrophages stimulation

Products	Company	Working concentration/C	Product Number
Recombinant Human(rh) GM-CSF	PeproTech	10 ng/mL	300-03
rh M-CSF	PeproTech	50 ng/mL	300-25
rh IFNγ	PeproTech	20 ng/mL	300-02
rh IL- 4	PeproTech	20 ng/mL	200-04
IL-13	PeproTech	20 ng/mL	200-13
LPS from Escherichia coli O128:B12	Sigma Aldrich	20 ng/mL	L2887-5MG

Table 2.3 Products for flow cytometry

Products	Clone	Company	Product Number	Dilution
Anti-Human, CD80 PE	2D10.4	eBioscience	12-0809-41	1:20
Anti-Human CD14 FITC	61D3	Invitrogen	11-0149-42	1:20
Anti-Human CD163 PerCP-eFlour	GHI61	Invitrogen	46-1639-42	1:20
Anti-Human CD206 APC	19.2	Invitrogen	17-2069-42	1:20
Mouse IgG1 kappa Isotype Control PE	MOPC-21	Biolegend	400112	1:20
Mouse IgG1 kappa Isotype Control FITC	MOPC-21	Biolegend	400108	1:20
Mouse IgG1 kappa Isotype Control APC	MOPC-21	Biolegend	400120	1:20
Mouse IgG1 kappa Isotype Control PerCP-eFluor 710	P3.6.2.8.1	Invitrogen	46-4714-80	1:20
Fixable viability dye eFlour™ 450	-	Invitrogen	65-863-14	1:1000
Fc Blocking Reagent, human	-	Miltenyi Biotec	130-059-901	1:50
Ultra Compensation eBeads	-	Invitrogen	01-2222-42	
Zombie Aqua Fixable Viability	-	Biolegend	423101	1:1000

Table 2.4 Products for Luminex assay

Products	Company	Product Number
Bio-Plex Pro Human Cytokine IL-1b	Bio-Rad	171B5001M
Bio-Plex Pro Human Cytokine IL-4	Bio-Rad	171B5004M
Bio-Plex Pro Human Cytokine IL-8	Bio-Rad	171B5008M
Bio-Plex Pro Human Cytokine IL-10	Bio-Rad	171B5010M
Bio-Plex Pro Human Cytokine IL-12 (p70)	Bio-Rad	171B5011M
Bio-Plex Pro Human Cytokine IL-13	Bio-Rad	171B5012M
Bio-Plex Pro Human Cytokine PDGF-BB	Bio-Rad	171B5024M
Bio-Plex Pro Human Cytokine RANTES	Bio-Rad	171B5025M
Bio-Plex Pro Human Cytokine TNF-a	Bio-Rad	171B5026M
Bio-Plex Pro Human Cytokine VEGF	Bio-Rad	171B5027M
Bio-Plex Pro Reagent Kit 3 Flat Plate	Bio-Rad	171304090M
Bio-Plex Pro HuCSP, Standards	Bio-Rad	12007919
Human MMP Premixed Magnetic Luminex Performance Assay	Bio-Techne	FCSTM07-01
TGF-beta Premixed Magnetic Luminex Performance Assay	Bio-Techne	FCSTM17-01

2.2. Method

2.2.1. Isolation of primary human monocytes

A fresh leukapheresis cone, obtained from the National Blood Transfusion Service, was processed for monocyte isolation. Cells were collected under ethical approval in accordance with the Declaration of Helsinki (Birmingham East, North and Solihull Ethics Committee: Inflammation in Ocular Surface Disease IOSD 08/H1206/165, UKCRN 7448). Whole blood was transferred into a 50-mL flacon tube, treated with 1 mM ethylenediaminetetraacetic acid (EDTA), and gently mixed. 75 µL/mL of (StemCell RosetteSep™) Human Monocyte Enrichment Cocktail was added to the tube. The contents were gently mixed, and the tube was incubated for 20 min at room temperature. Phosphate-buffered saline (PBS) with 2% heat-inactivated foetal bovine serum (FCS) + 1 mM EDTA was added to the blood-containing tube and gently mixed. The diluted blood was slowly layered on a Ficoll gradient and centrifuged at 1200 × *g*

with the lowest acceleration and zero deceleration for 30 min. The buffy coat or monocytic layer trapped between the Ficoll gradient and plasma (**Figure 2.1**) were collected by a Pasteur pipette and transferred into a new 50-mL tube, washed four times with PBS with 2% FCS + 1 mM EDTA, and centrifuged at 300 × *g* for 10 min. Monocytes were resuspended in 50 mL of PBS with 2% FCS + 1 mM EDTA and counted following Trypan blue staining in a haemocytometer.

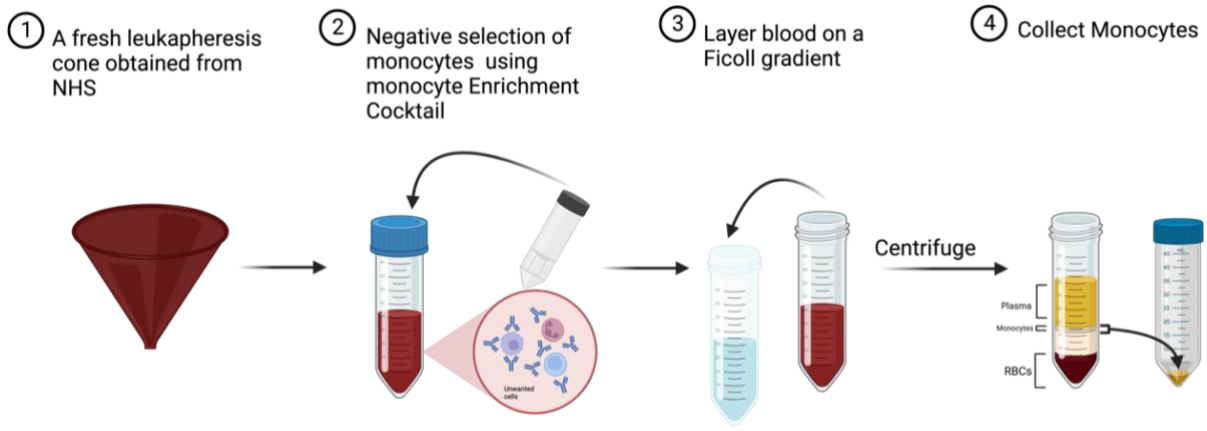

Figure 2.1 Schematic description of monocyte isolation process.
The figure was drawn by BioRender.com.

2.2.2. Differentiation and polarisation of M1 and M2 macrophages

Monocytes were resuspended in RPMI media with 5% FCS and seeded in 10 cm dishes at a density of 10–15 × 10^6/10 mL. To generate M1 macrophages, 10 ng/mL of recombinant human GM-CSF was added to the media, while 50 ng/mL of M-CSF was added to produce M2 macrophages (day 0). The cells were incubated in a 5% CO_2 incubator at 37°C for 6 days. On day 3, the medium was replaced with fresh GM-CSF or M-CSF. On day 6, the cells were harvested for further experiments (**Figure 2.2**).

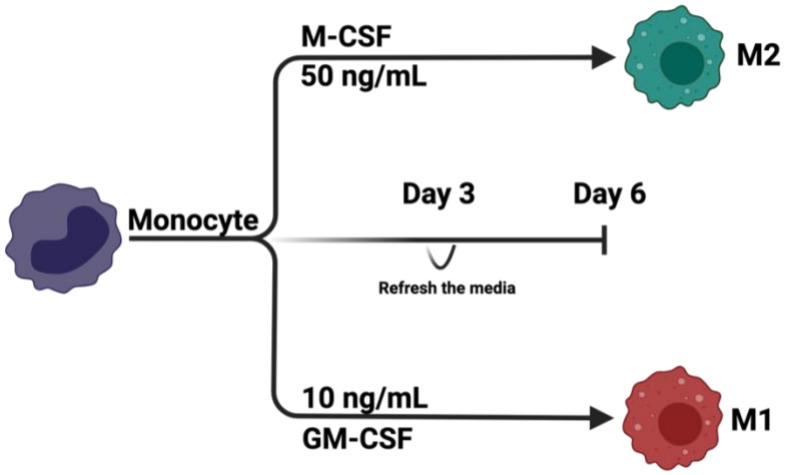

Figure 2.2 Schematic description of M1 and M2 macrophages.

On day 0**,** isolated monocytes were seeded in 10 cm dishes at a density of 10–15 × 10^6/10 mL-containing 10 ng/mL GM-CSF or 50 ng/mL of M-CSF produce M1 and M2, respectively. The cells were incubated in a 5% CO_2 incubator at 37°C for 6 days. The medium was replaced with fresh GM-CSF or M-CSF on day 3. Monocyte derived macrophages were harvested on day 6. The figure was drawn by BioRender.com.

2.2.3. Macrophage stimulation for RNAseq experiment

On day 6, M1 and M2, labelled as M1 (I) and M2 (I), were either harvested or stimulated with LPS and IFNγ or IL-4 and IL-13 (20ng/ml) and incubated for 2 days in a 5% CO2 incubator at 37°C to generate M1 (II) and M2 (II), respectively.

To identifying the persistence of their polarisation states, M1 (II) and M2 (II) were either harvested or maintained in cytokines-free media for 6 days in a 5% CO2 incubator at 37°C. Thereafter, stimulation with contrasting cytokines was performed, where M1 (II) received 20 ng/mL of IL-4 and IL-13, while M2 (II) received 20 ng/mL of LPS and IFNγ and incubated for 2 days in a 5% CO2 incubator at 37°C to produce M1 (III) and M2 (III) (**Figure 2.3**). On day 16, human cells were harvested. The supernatants from all subsets were collected each time human cells were harvested and stored at -80°C for validation assays of RNAseq results. We designed this model based on Tarique et al.

(2015), Verreck et al. (2006) with modifications to simultaneously characterise our generated cells and assess the persistence and/or reversibility of their polarisation states in response to subsequent stimuli with opposing effects **(Figure 4.1).**

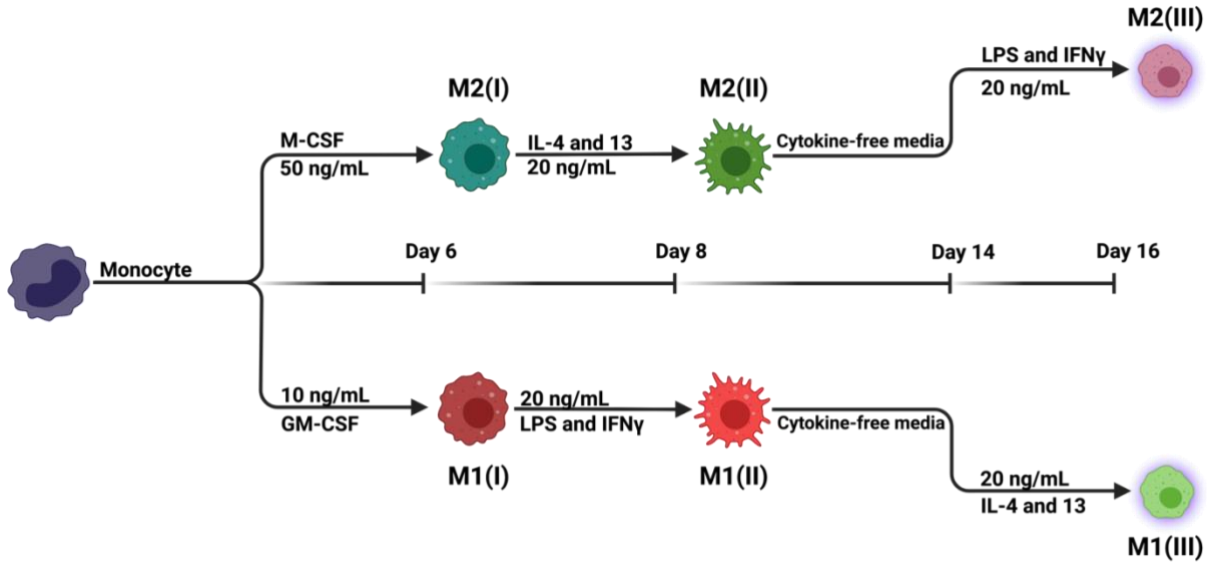

Figure 2.3 Schematic description of the polarisation model to generate subset of monocyte-derived macrophages.
Primary human monocytes were isolated and matured into both M1 (I) and M2 (I) macrophages using 10 ng/mL of GM-CSF and 50 ng/mL of M-CSF growth factors, respectively. On day 6, M1 (I) and M2 (I) were either harvested or stimulated with 20 ng/mL LPS and IFN-γ and IL-4 and IL-13 for 2 days to generate M1 (II) and M2 (II), respectively. M1 (II) and M2 (II) were either harvested or maintained in cytokine-free media for 6 days, followed by stimulation with contrasting cytokines (20 ng/mL IL-4 and IL-13 and LPS and IFNγ for 2 days) to produce M1 (III) and M2 (III), respectively. The figure was drawn by BioRender.com.

2.2.4. Harvesting of macrophages

The medium was removed, and the cells were washed with PBS. As macrophages are adherent cells, non-enzymatic disassociation solution (4 mL/dish) was used to detach the cells from the bottom of the plate or petri dish. The plates were incubated for 15 min in a 5% CO_2 incubator at 37°C and a cell scraper to remove strong adherent

cells, which were washed three times and resuspended in medium to perform further experiments.

2.2.5. Viability test

To assess the biocompatibility of gellan fluid gel on different type of macrophages, Calcein-AM and Propidium Iodide (AM/PI stain) were used. Calcein AM is nonfluorescent calcein with an acetoxymethyl group ester that can pass across cell membranes and label living cells. This acetoxymethyl (AM) ester group is cleaved by Intracellular esterase as soon as the molecule enters the cell, resulting in the production of the green dye. However, dead cells, which exhibited damaged cell membranes, are not able to maintain Calcein and lost the emitted green light (Neri et al., 2001). In contrast, PI is membrane impermeable red dye that enter the compromised membrane of dead cells, staining them. Fluorescence microscope (Leica DM6000 Fluorescence Microscope) was used to observe the fluorescence emitted from live and dead cells.

2.2.6. Preparation of 0.9 % Gellan fluid gel

To a spinner flask, 21 mL of deionised water was added, and the flask was then placed on magnetic stirrer at speed 3 and 150°C. 0.3 g of gellan powder was added to deionised water at 90°C and stirred at speed 3. Thereafter, 1.5 mL of PBS was added to bring the pH to 7.4 (neutral), followed by the addition of 1.5 mL 0.2 M NaCl to promote the cross-linking process of gel. The temperature and speed of the magnetic stirrer plate were reduced to 38°C and 1.5, respectively, and 6-mL serum-free medium was added to the flask. The resultant gellan fluid gel was collected in 15 mL tube and stored in the fridge for experiments.

To prepare cells in gellan gel, on day 6, the polarised cells were harvested by centrifugation at 300 × *g* for 10 min, and the obtained pellets were suspended in serum-free medium. AM/PI stain solution was made by combining10µL of Calcein-AM and 5µL of PI stain with 5µL of PBS and then kept in a dark fridge until it was used. Subsequently, M1 and M2 macrophages (10 µL/3 × 10^5) were added and mixed with 200 µL of gellan fluid gel or with 200 µL of serum-free medium as the control, and then plated in a 24-well plate. Cells were incubated for 4 h in a 5% CO_2 incubator at 37°C. The medium was then aspirated from the control groups. We selected the 4 h incubation period based on our previous experiment, where the gellan fluid gel remained on the ocular surface of a mouse model for 4 h before being removed by blinking. The cells were then stained by AM/PI stain and incubated for 15 min in a 5% CO_2 incubator at 37°C. Following staining, a viability test was performed using a fluorescence microscope to assess live and dead cells at wavelengths of 490 nm and 535 nm, respectively. Earlier attempts to mix the cells directly with gellan fluid gel in the plate resulted in inconsistent cell distribution. To address this, the cells were first mixed with the gellan fluid gel in an Eppendorf tube to ensure uniform distribution, and the mixture was then plated into the wells.

To calculate the percentage of live we use cell ImageJ software to count the live and dead cells, and we use the below formulate to find the live cell percentage.

$$\text{Live cell percentage} = \frac{Live\ cell\ number}{Total\ cell\ number} x100$$

2.2.7. Staining for flow cytometry analysis

To phenotype our generated M1 and M2 macrophages, the cells were harvested on day 6 and prepared for flow cytometry staining. On day 6, harvested cells were

replated in a 6-well plate (1-1.6 × 10^6) in RPMI media with 5% FCS and 10 ng/mL of GM-CSF or 50 ng/mL of M-CSF respectively, then incubated for 24 h in a 5% CO2 incubator at 37°C. On day 7, the medium was removed, and the cells were washed three times with PBS. Subsequently, 1.5 mL of gellan fluid gel or serum-free medium (controls) were added to the cells in a 6-well plate and then incubated for 4 h in a 5% CO2 incubator at 37°C, when the cells were harvested and prepared for flow cytometry staining.

Harvested cells were counted and placed in a fluorescence-activated cell sorting (FACS) tube (0.3-1.5 × $10^{6)}$, followed by washing them three times with PBS at 300 × *g* for 5 min each time. The cells were stained with diluted fixable viability dye eFlour 450 or diluted Zombie Aqua dye and incubated for 20 min at 4°C. The stained cells were washed using cold FACS buffer (PBS + 2% FCS and 0.009% sodium azide) and the pellet resuspended in 50 µL of diluted Fc block and incubated for 10 min at 4°C. After washing, the pellet was resuspended in 50 µL of master mix of antibodies (CD80-PE, CD14-FITC, CD163 PerCP-eFluor-710, and CD206-APC) and incubated for 30 min at 4°C. For isotype control tubes, the pellet was resuspended in 50 µL of master mix of isotype control antibodies (mouse IgG1 kappa Isotype Control for FITC, PE, PerCP-eFluor 710, or APC) and incubated for 30 min at 4°Cthen washed three times. The pellet was resuspended in 200 µL of FACS buffer for analysis by BD LSRFortessa™ X-20. FlowJo software was used for the analysis of data.

For compensation, the pellet cells or beads were stained in a single colour by adding 50 µL of diluted antibody (CD80-PE, CD14-FITC, CD163-PerCP-eFluor-710, or CD206-APC), or resuspended in FACS buffer (unstained cell tube) and incubated for 30 min or 10 min for beads. The stained cells or beads and non-stained cells were

washed and resuspended in 200 µL of FACS buffer for analysis by BD LSRFortessa™ X-20. The gating strategy is explained in (**Figure 2.4**).

To measure the expression level of stained surface markers (CD14, CD80, CD206, and CD163) on both M1 and M2, histogram plots of isotype controls of each marker were used. These isotype controls set the gate for the positive population of their respective markers to determine the parentage of expression level.

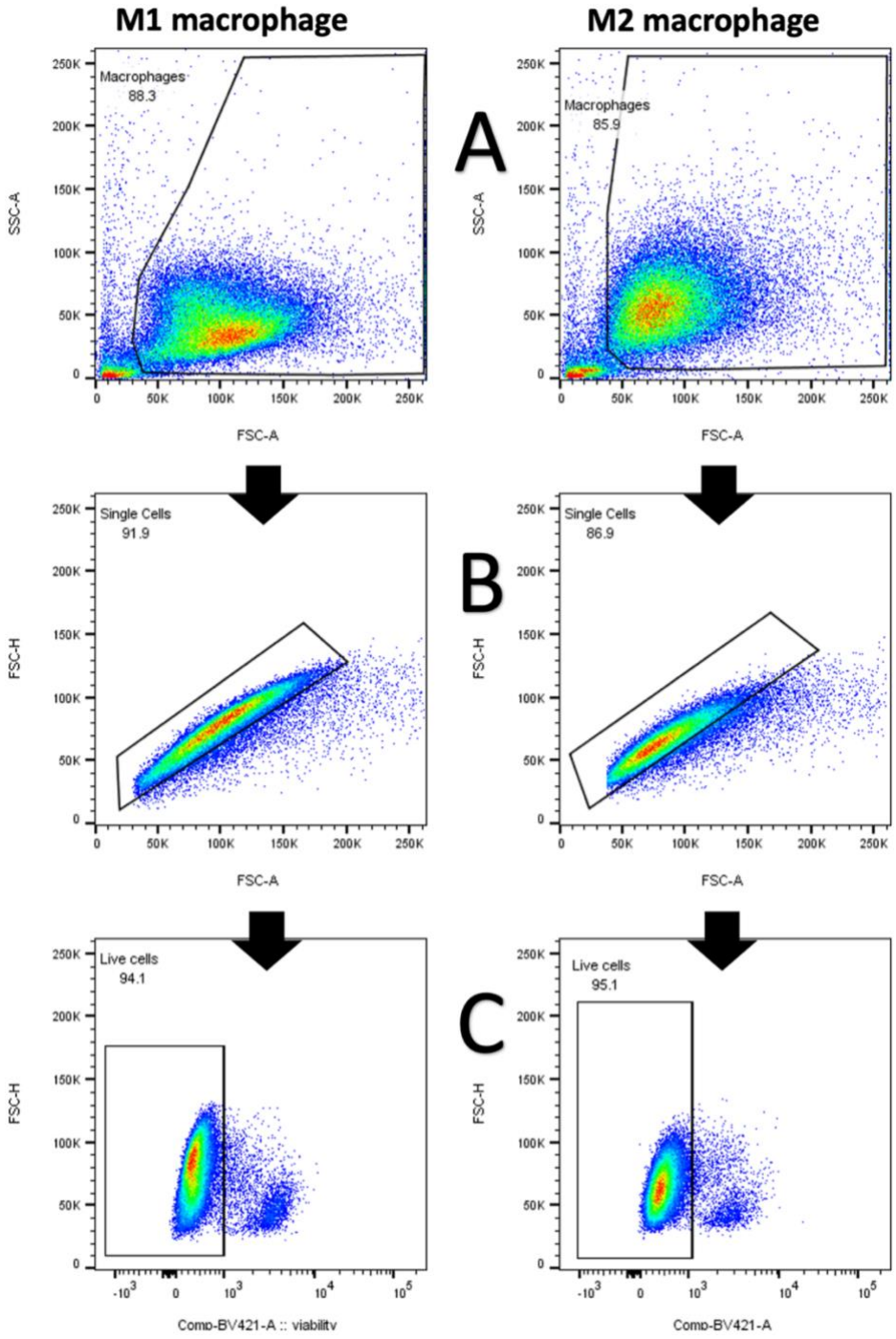

Figure 2.4 The gating strategy of flow cytometry for analysing our generated M1 and M2 macrophages.

M1 macrophages (right) and M2 macrophages (left). **A)** showed the total of Macrophage without derby cells. **B)** showed single cells of total macrophages**. C)** represented exclusion of dead cells**.**

2.2.8. RNAseq and qPCR experiment

For RNAseq or qPCR experiments, the process began by removing the medium from the cells, followed by washing the cells three times. Afterward, the appropriate volume of lysis solution was added to the cells and the cell lysate was stored at -80°C for RNAseq or qPCR experiments (**Table 2.3)**.

Table 2.5 An appropriate volume of lysis solution

Type of kit	**Plate**	**lysis solution volume**
RiboPure™ Kit	Petri dish	1 mL
RNeasy Mini Kit	Petri dish	600 µL
RNeasy Mini Kit	6 well plate	350 µL

2.2.9. RNA extraction

Following medium removal from the cells and washing the cells, two type of RNA isolation kits, including RiboPure Kit and RNeasy Mini Kit, were used to isolate the RNA from cultured cells.

RiboPure™ Kit was used to isolate the RNA from the cultured cells for phenotype of M1 and M1 macrophage experiments. A total of 1 mL of TRI Reagent® per 10 cm^2 was added to cultured cells and mixed well. The cell lysate was incubated at room temperature for 5 min and then collected in a new 1.5 mL microcentrifuge tube. Chloroform (200 µL) was added to the lysate and which was vortexed immediately for 12 seconds at the highest speed, and incubated for 5 min at room temperature, and centrifugated at 12000 ×g at 8°C for 10 min. Up to 400 µl of the aqueous phase was transferred to a new 1.5 mL microcentrifuge tube and 200 µL of ethanol (100%) was added to the tube and vortexed at highest speed for 5 seconds. The mixture was then

transferred onto a new collection tube through a filter cartridge and washed with 500 µL of wash solution twice at 12000 ×g at room temperature for 30 seconds. The third wash was performed without using the wash solution. The filter cartridge was placed in a new collection tube and 100 µL of elution buffer was added and incubated for 2 min. The tube was then centrifugated at room temperature for 30 seconds.

RNeasy Mini Kit was used to isolate RNA from the cultured cells for evaluating Gellan fluid gel impacts on activation states of M1 and M2, RNAseq and validation experiments. Fresh lysis buffer was prepared by adding 10µl/ml of 2-mercaptoethanol into lysis buffer RLT, enhancing the stability of RNA during isolation process. An appropriate volume of lysis buffer RLT **(table 2.3)** was added to cultured cells and mixed well to homogenised and then collected in a new 1.5 mL microcentrifuge tube. The cell lysate was immediately processed or stored at -80°C. To process frozen cell lysates, they were incubated in a water bath at 37°C until defrosted.

Equal volume of 70% ethanol was then added to the lysate and mixed well. Up to 700µl of mixture was transferred onto 2 mL collection tube through a filter cartridge and centrifugated at 12000 ×g at room temperature for 15 seconds. After removing the flow-through, 700 or 350 µL, for DNase treatment (RNASeq preparation), of initial wash solution (RW1) was added to a filter cartridge and centrifugated at 12000 ×g at room temperature for 15 seconds.

For DNase treatment, 80 µL/sample of mixture containing 70 µl Buffer RDD and 10 µl DNase I stock solution, deoxyribonuclease I, was added to the centre of a filter cartridge and incubated at room temperature for 15 min. After incubation, 350 µL of initial wash solution (RW1) was added to a filter cartridge and centrifugated at 12000 ×g at room temperature for 15 seconds.

The next wash was performed with 500 µl Buffer RPE for both methods and centrifugated at 12000 ×g at room temperature for 2 min, following by placing the filter cartridge in a new collection tube and centrifugating at full speed at room temperature for 1 min. The filter cartridge was placed in a new 1.5 mL collection tube and 40-50 µL of RNAse-free water was directly added to the filter cartridge centrifugated at 12000 ×g at room temperature for 1 min.

The recovered RNA was used for RNA library preparation, cDNA synthesis or stored immediately at -80°C. The quality of the purified RNA was within the recommended range >1.6 at 260/280 ratio, measured using a NanoDrop 1000A spectrophotometer.

2.2.10. cDNA synthesis and quantitative polymerase chain reaction (qPCR)

iScript cDNA Synthesis Kit was used to generate complementary DNA (cDNA) from 400-500 ng of the total extracted RNA as instructed by the manufacturer's protocol. A total of 4 µL of 5x iScript Reaction Mix, 1 µL of iScript reverse transcriptase and an appropriate volume of nuclease-free water were added to 400-500 ng of total RNA to make up to 20µL. The mixture was then exposed to thermal cycling using the following settings: 25ºC for 5 min(annealing), 46ºC for 20 min (reverse transcription), and 95ºC for 1 min(inactivation). The cDNA was diluted with nuclease-free water before use in the qPCR experiments.

qPCR was preformed using the following Eurofins primers (*UBC, SERPING1, CXCL9, CXCL10, GBP5, MRC1, CCL17, TGM2, IL12B, PTGES, CCL22, CCL26, MKI67 and IGF1, and CD163*) and TB Green Premix Ex Taq II (Tli RNase H Plus) on Bio-Rad CFX384 systems. The master mix for each primer contained 0.3 µL of reverse primer, 0.3 µL of forward primer and 3 µL of TB Green, per well. 2.4 µL of the diluted cDNA

samples or nuclease-free water (controls) was added to make the total volume of reaction 6uL/well. The PCR plate (384 well) was sealed and centrifugated at 300 × g for 1 min and incubated in the thermal cycler using the following conditions: 95ºC for 30 seconds, 39 cycles (at 95ºC for 10 seconds, at 59ºC for 30 seconds and at 78ºC for 20 seconds) and then at 65ºC for 31 seconds. Bio-Rad CFX Manager software was used for data analysis. The delta cycle thresholds (dCT) (CT for gene – CT for *UBC*, a reference gene) or negative of dCT (-dCT) was measured to determine the expression level of gene as mentioned in the legend of figure.

2.2.11. RNAseq experiment

RNA from different subsets of M1 and M2 macrophages was isolated using RNeasy Mini and the RNase-Free DNase Set, as demonstrated above. Following isolation, RNAs were submitted to the University of Birmingham Genome Centre to perform single-end sequencing using NextSeq High 75 v2.5 kit on illumine NextSeq 500 System.

Briefly, submitted RNAs were initially subjected to quality control (QC) assessment to determine the integrity and concentration of RNA using a Qubit High Sensitivity RNA assay and an RNA tape on the Agilent Tape Station, receptively. The samples with an RNA Integrity Number (RIN) >7 were used for RNAseq library preparation, as shown in **Figure 2.5**. 10 ng of RNA was the input concentration for RNAseq library preparation. Unique Molecular Identifiers (UMIs) were used to uniquely distinguish each single RNA for library preparation, which helped to exclude any bias of replication. Lexogen QuantSeq 3' mRNA-Seq Library Prep Kit FWD was used for library preparation. The libraries were then subjected to QC assessment and normalised to 4 nanomolar (nM). The single-end sequencing was performed using the

NextSeq High 75 v2.5 kit on the iIlumine NextSeq 500 System. Following QC assessment by the Genomic Centre, we performed pre-processing steps, from trimming adaptors and reads with low-quality alignment and mapping on the human genome (GRCh38) to gaining metrics for the gene expression level (count table) using the LEXOGEN Pipeline on the BlueBee® Genomics Platform. Raw counts of gene expression were used as input for differential gene expression analysis and pathway analysis using R software. An overview of RNAseq and data processing workflows is described in **Figure 2.6**.

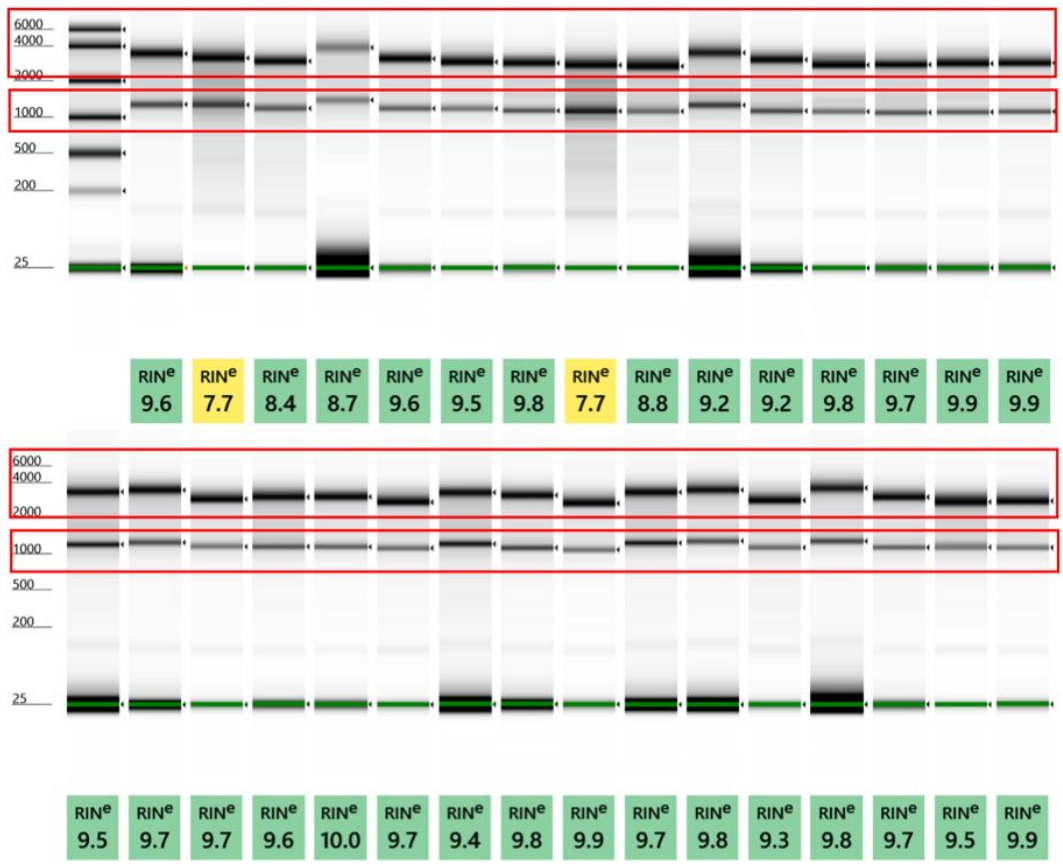

Figure 2.5 Representative results for the integrity of extracted RNAs before RNAseq.

Tape Station results showed a heavy band of 28S subunit of ribosomal RNA (28S) at the top and a light band of 18s below to indicate the integrity of RNA.

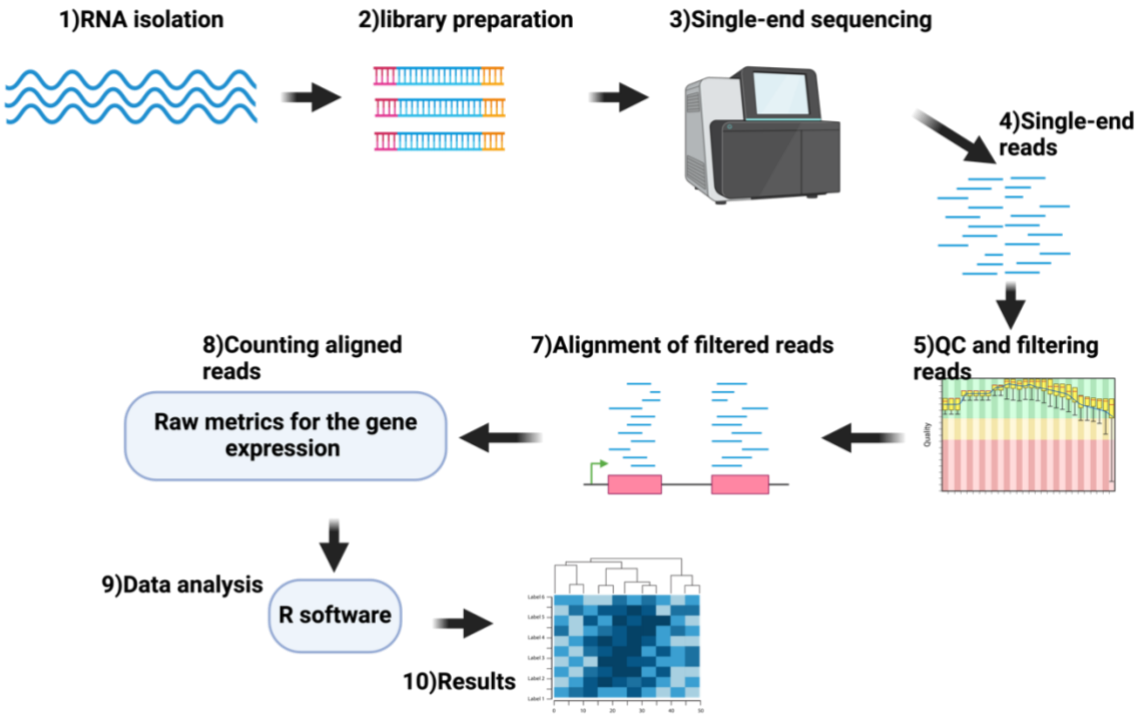

Figure 2.6 An overview of RNAseq and data processing workflows.
Initially, RNA was isolated, followed by library preparation, including double-strand complementary DNA (ds cDNAs) synthesis, adaptor and index ligation to the end of cDNA, and PCR amplification. Next, libraries were pooled prior to sequencing. Following read generation and QC assessment, sequencing data were uploaded to the BlueBee® Genomics Platform for data processing. Quantesq 2.3.6 FWD UMI pipeline was used for data processing steps from trimming adaptors and reads with low quality, alignment, and mapping on the human genome (GRCh38), to gaining raw metrics for the gene expression level. Thereafter, raw metrics were exported and used for data analysis using R software. The figure was drawn by BioRender.com.

2.2.12. Bioinformatic analysis

Raw metrics or counts were used for differential gene expression analysis using the DESeq2 package (Love et al., 2014). For QC of data using Principal component analysis (PCA) and Pearson's correlation analysis and Log2 of normalised count+1 was used for Pearson correlation analysis, which was represented as a heatmap using Circlize and Complex Heatmap packages (Gu et al., 2016, Gu et al., 2014). Regularised logarithm transformation (rlog) of raw counts using the DESeq2 package

was used for PCA, which was plotted as a PCA plot using the DESeq2 package (Love et al., 2014).

For top variable gene analysis, (rlog) of raw counts were used to calculate the variance of gene expression among samples, followed by identifying the top variable gene, which was represented as a heatmap using Complex Heatmap package(Gu et al., 2016). Gene IDs were changed from ensembl ID to gene symbol using AnnotationDbi and org.Hs.eg.db package (Carlson, 2021, Pagès et al., 2021).

Differentially expressed genes (DEG) between subsets of macrophages were identified as genes with an adjusted p-value (padj) less than 0.05 and a log2 Fold Change (log2 FC) equal to or higher than 1.5, indicating upregulation, or -1.5 or less, indicating downregulation. These DEGs between two subsets of macrophages were plotted as a volcano plot using ggplot2 and ggrepel packages (Wickham et al., 2016, Slowikowski, 2020).

For Gene Set Enrichment Analysis (GSEA), the DEGs were ranked and used as input for enrichment analysis of Hallmark pathways using the fgsea and msigdbr packages (Dolgalev, 2022, Korotkevich et al., 2016). Significantly enriched pathways (padj <0.05) were plotted. For KEGG analysis, upregulated or downregulated DEGs were used as input for the enrichment analysis (Wu et al., 2021). Significantly enriched pathways (padj <0.05) were then plotted.

2.2.13. Luminex

Luminex was carried out on supernatants from different subsets of macrophages (**Figure** 2.3), which were collected during the cell harvest and stored at -80 until usage. To process frozen supernatants, they were incubated in a water bath at 37°C until

defrosted and then centrifuged at 10000 × *g* for 10 min 4°C before dilution. The manufacturer's instructions were followed for the preparation of all reagents, with the exclusion that volumes were cut in half to allow for the running of two plates.

2.2.13.1. Cytokine analysis using Bio-Rad kit

Serial dilutions using RPMI media were performed to prepare the standards. 25 µL of diluted beads were added to a 96-well plate, followed by sealing the plate. The plate was washed twice with wash buffer using a magnetic device. 25 µL of supernatant, standards and blank (RPMI media) were added in duplicate to wells. The plate was placed on a shaker set at 850 rpm for 30 min at room temperature, followed by an overnight incubation in a fridge. The plate was incubated on a shaker at 850 rpm for 5 min at room temperature, followed by three times of washes with wash buffer using a magnetic device. 12.5 µL of diluted detection antibody were then added to a 96-well plate and then incubated at room temperature on a shaker at 850 rpm for 30 min. Following three times of washing, 25 µL of diluted Streptavidin-PE was then added to a 96-well plate and then incubated at room temperature on a shaker at 850 rpm for 10 min, followed by three times of washing. Then, beads in the plate were resuspended in 62.2 µL of assay buffer and then incubated at room temperature on a shaker at 850 rpm for 30 second. Thereafter, the plate was run and analysed by the Bio-Plex 200 system.

2.2.13.2. TGFβ1 and MMP7 analysis using Bio-Techne

For TGFβ1 measurement, supernatants were activated to convert latent TGFβ1 to its active form with 20 µL of Hydrochloric acid (HCL) added to 100 µL of supernatant and incubated at room temperature for 15 min, followed by 20 µL of 1.2N NaOH plus 0.5M HEPES to neutralise the pH of the supernatants. For MMP7 and TGFβ1, supernatants were diluted 1:5 with calibrator diluent. Serial dilutions using calibrator diluent were performed to prepare the standards for MMP7 and TGFβ1. 25 µL of diluted supernatant, diluted microparticles, and standards were added in duplicate to a 96-well plate (Luminex), followed by sealing the plate. The plates were then placed on a shaker set at 850 rpm for 2 h at room temperature, followed by an overnight incubation in a fridge. The plates were incubated on a shaker at 850 rpm for 5 min at room temperature, followed by three washes with wash buffer using a magnetic device. 25 µL of diluted Biotin antibody was then added to a 96-well plate and incubated at room temperature on a shaker at 850 rpm for 1h. Following three washes, 25 µL of diluted Streptavidin-PE was added to a 96-well plate and incubated at room temperature on a shaker at 850 rpm for 30 min, followed by three washes. Microparticles in the plate were resuspended in 100 µL of wash buffer and incubated at room temperature on a shaker at 850 rpm for 2 min. Finally, the plate was run and analysed by the Bio-Plex 200 system.

2.2.14. Statistics

GraphPad Prism version 7 or 10 was used to perform statistical analysis and generate graphs. The type of statistical test used and the p-value (* $p < 0.05$, ** $p < 0.01$, *** $p < 0.005$) were indicated in the legend. To compare phenotypic differences of four markers between M1 and M2 macrophages, a repeated measures two-way ANOVA

with Šídák's multiple comparisons test was applied (Figures 3.2, 6, and 7). The statistical significance of individual gene expression was assessed using multiple Mann-Whitney tests (Figures 3.4 and 6). The proportion of live macrophages under different conditions was compared using the Wilcoxon test (Figure 3.5). An ordinary two-way ANOVA with Šídák's multiple comparisons test was used to assess the expression of four genes across two different conditions (Figures 3.8 and 9). The concentration of individual molecules among three different conditions was evaluated using one-way ANOVA with Dunn's multiple comparisons test (Figures 5.3- 6).

Chapter 3. Macrophage phenotype and Gellan Fluid Gel

3.1. Background

The delivery of therapeutic agents to the complex structure of the ocular surface is still a considerable limitation that hinders treatment efficacy (Wels et al., 2021). To this end, gellan fluid gel is proposed as an ocular topical delivery platform, which will enhance the effectiveness of treatment by increasing treatment retention and decreasing dosage, consequently boosting patient compliance (Gote et al., 2019). Such opinion supports our hypothesis that gellan fluid gel could be utilised as a delivery system to apply polarised macrophages on the ocular surface for delivering bioactive molecules (antimicrobial peptides, growth factors, and anti-inflammatory mediators) to promote scar-free corneal healing and preservation of vision.

To ensure the maturation of isolated monocytes into GM-CSF-stimulated macrophages (M1) and M-CSF-stimulated macrophages (M2), flow cytometric analysis was conducted to investigate the expression of CD14, CD80, CD163, and CD206 on both populations. Briefly, CD14 has been identified as a Pattern Recognition Receptor (PRR) and also a co-receptor for many Toll-like Receptors (TLRs) that specifically recognises LPS and is involved in the signalling cascade to induce the inflammatory response (Wu et al., 2019, Zanoni and Granucci, 2013). Expression of CD14 was found to be higher on M-CSF derived M2 than GM-CSF derived M1 in vitro (Akagawa et al., 2006, Bender et al., 2004, Lukic et al., 2017).

CD80 is a co-stimulation protein that activates T-cells. It was found that GM-CSF significantly induced the CD80 expression on M1 as compared with M2 (Ambarus et al., 2012).

CD163 and **CD206** are influential anti-inflammatory molecules that are expressed mainly on the macrophage or monocyte lineage. **CD163**, a scavenger receptor for the

haptoglobin-haemoglobin complex, resolves inflammation by clearing haemoglobin and stimulating the production of anti-inflammatory cytokines. **CD206** is the macrophage mannose receptor that is involved in scavenging endogenous glycoproteins, recognising pathogens, and presenting antigens (Yilmaz et al., 2022). Efferocytosis is a homeostatic process carried out by both immune and non-immune cells, including macrophages, to clear dying cells in an inflammation free manner, thereby maintaining tissue homeostasis (Doran et al., 2020). Efferocytosis consists of sequential phases, starting with the sensing of surrounding tissues to recognize the 'find me' signals released by dying cells. The identification of these signals by phagocytes results in the upregulation of phagocytic receptors, engulfment and digestion of the apoptotic cells and switching phenotype to an anti-inflammatory, pro-healing state and enhancing their trafficking capacity. (Mehrotra and Ravichandran, 2022). Pro-resolving macrophage induction, including increased IL-10 secretion, was observed following the efferocytosis of dying neutrophils (Filardy et al., 2010). CD163 and CD206, which are typically involved in efferocytosis, were found to be upregulated in alveolar macrophages in an in *vitro* model of acute respiratory distress syndrome, which is linked with dysfunctional efferocytosis (Mahida et al., 2021).

Previous studies identified CD163 as an M2 marker whereas CD206 was expressed on both M1 and M2 (Ambarus et al., 2012, Arango Duque and Descoteaux, 2014, Bender et al., 2004). Thus, the expression of these surface membranes was selected to confirm the maturation of both M1 and M2 before seeding them within gellan fluid.

Thus, the first objective of the current chapter is to effectively isolate human monocytes from blood cones and confirm their maturation into macrophages with the M1 or M2 phenotype. The second objective is to assesses the viability of the M1 and

M2 macrophages after seeding them within gellan fluid gel for 4 h. Finally, to investigate the polarisation status of M1 and M2 macrophages after seeding them within gellan fluid gel for 4 h.

3.2. Results

At the beginning of the project, we used a plastic adherence method where monocytes were isolated from peripheral blood mononuclear cells (PBMCs) by allowing them to adhere to the plastic flask, followed by the removal of non-adherent cells. However, this technique resulted in insufficient cell yield to be processed for further experiments. This observation is similar to those reported by Nielsen et al. (2019). Other methods used to segregate monocytes from peripheral blood mononuclear cells (PBMCs) for human macrophage studies *in vitro* are negative selection and positive $CD14^+$ monocyte selection. However, previous studies comparing the impacts of these two approaches on cell number and function of either isolated monocyte or derived macrophage concluded that although high purity and cell number were associated with positive selection, negative selection does not result in impaired function of isolated cells. (Neu et al., 2013, Hornschuh et al., 2022, Bhattacharjee et al., 2017). Therefore, we employed negative selection to generate our M1 and M2 macrophage model.

Following monocyte isolation, monocytes were cultured with media containing growth factors 10 ng/mL GM-CSF or 50 ng/mL M-CSF for 6 days to produce M1 and M2 macrophages, respectively, as designated in **Figure 3.1, A.** M1 and M2 macrophages displayed different morphology, where M1exhbtied a rounded shape while M2 have an elongated shape **(Figure 3.1, B and C)**

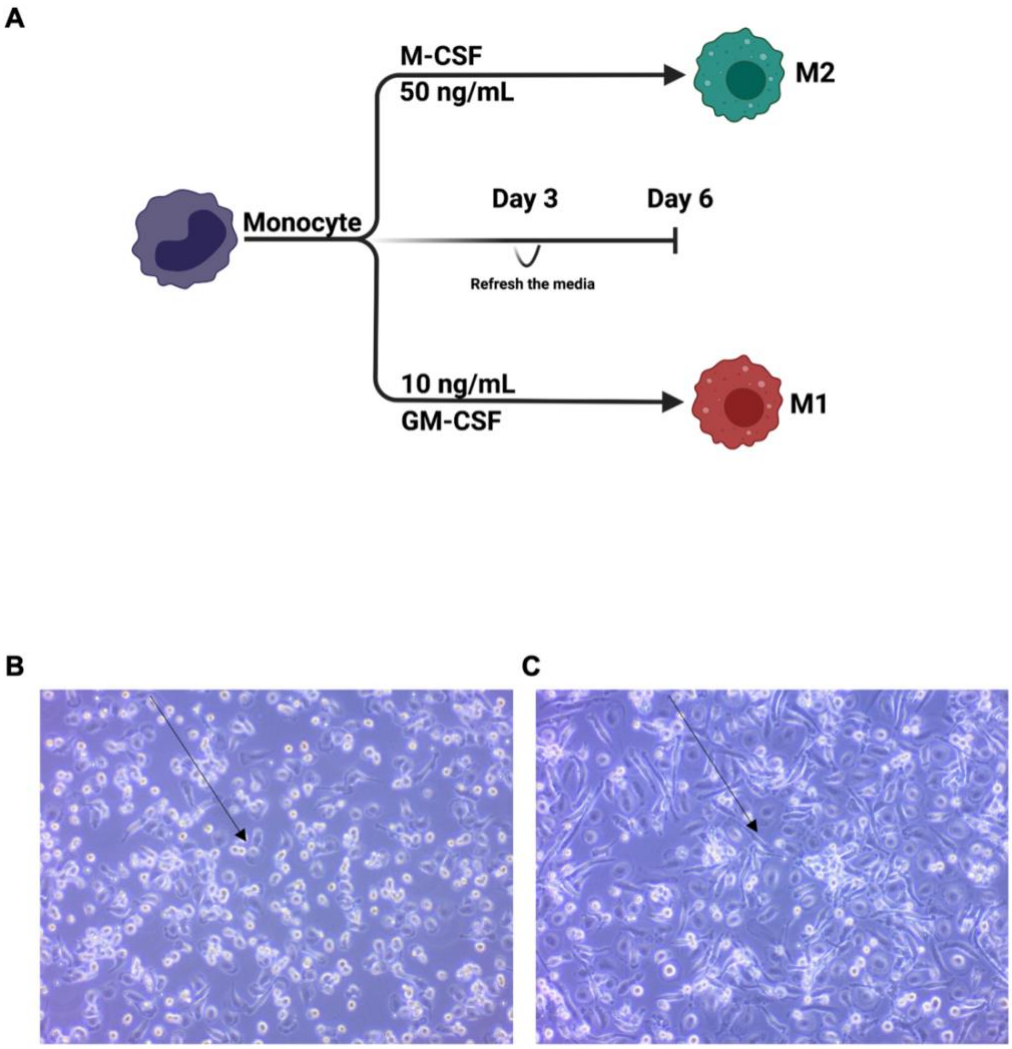

Figure 3.1 Differentiation model of monocyte derived M1 and M2 macrophages and distinct morphology between them.

Primary human monocytes were isolated and matured to both M1 and M2 macrophages using 10 ng/mL of GM-CSF and 50 ng/mL of M-CSF growth factors, respectively. **(A)** presents the polarisation model to generate monocyte-derived macrophages. (**B)** Representative image for M1 (a rounded shape) and **(C)** M2 (an elongated shape) within the medium using the inverted Microscope(10x). The figure was drawn by BioRender.com.

3.2.1. Phenotypic differences between M1 and M2 macrophages confirmed the effective maturation and polarisation of human monocytes.

Results of the flow cytometry revealed that M1 expressed a high level of CD80, and CD206 but not CD163. On the other hand, CD14, CD163 and CD206 expression were highly upregulated on M2 (**Figure 3.2, A-D**). A comparison of the expression levels of these surface markers on the two populations indicated that CD14 upregulation was significantly higher on M2 than on M1. This high expression of CD14 on M2 macrophages could be attributed to its role in the clearance of apoptotic cells, which is typically associated with M2 macrophages (Gregory, 2000). Importantly, CD80 and CD163 expression levels significantly differed between the two populations. CD80 was highly expressed on M1 but not on M2, while CD163 expression was significantly higher on M2 than on M1 (**Figure 3.2, E**). No statistical distinction was seen in CD206 expression among M1 and M2.

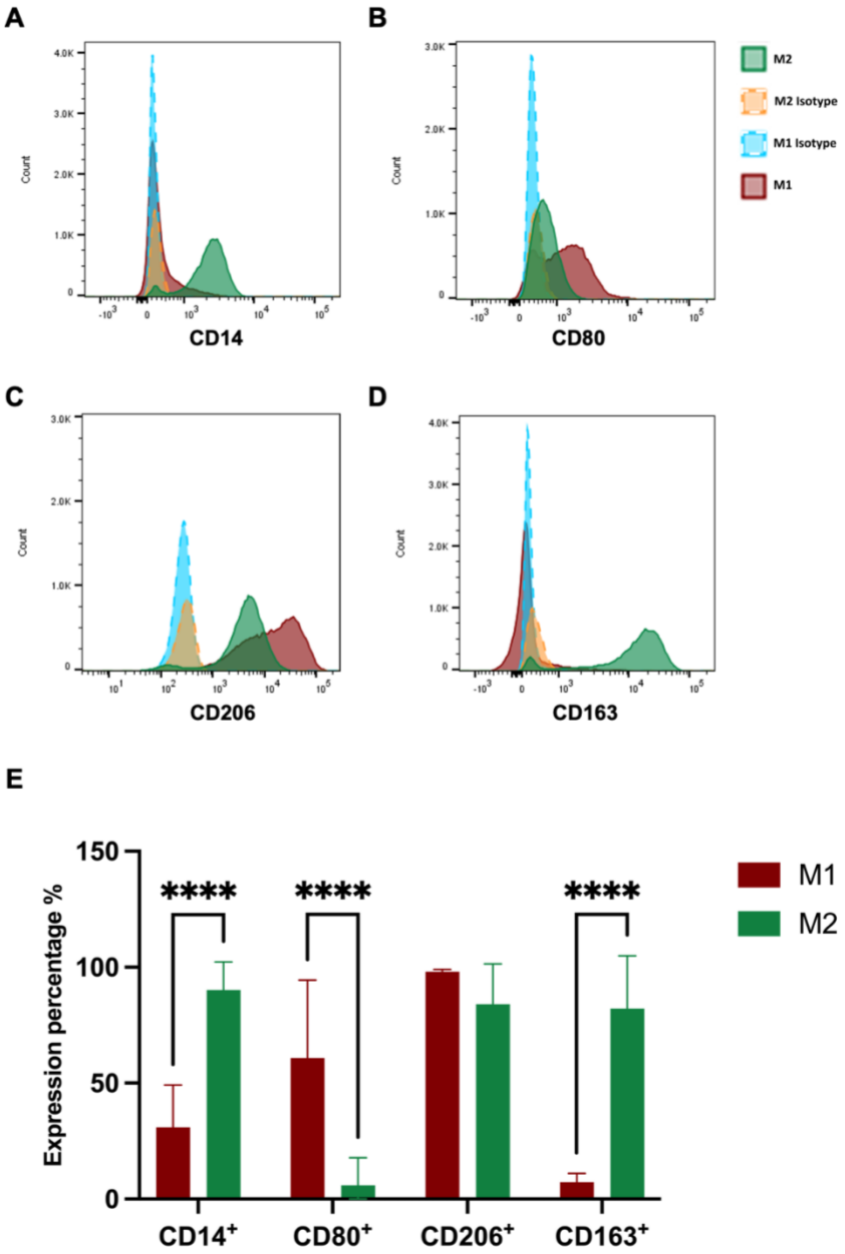

Figure 3.2 Phenotypic differences between M1 and M2 macrophages.
Primary human monocytes were isolated and matured to both M1 and M2 macrophages using 10 ng/mL of GM-CSF and 50 ng/mL of M-CSF growth factors, respectively. On day 6, cells were harvested and resuspended in 50 µL of master mix of antibodies or 50 µL of master mix of isotype control antibodies (mouse IgG1 kappa Isotype Control for FITC, PE, PerCP-eFluor 710, or APC). **(A)** Representative histogram for CD14 expression. **(B)** CD80 **(C)** CD206 and **(D)** CD163. **(E)** presents a comparison of phenotypic differences between M1 and M2 macrophages using repeated measures *two-way ANOVA* with Šídák's multiple comparisons test (n = 4 experiments). **** p <0.0001.

3.2.2. *CCL17* is significantly expressed in M1 macrophages, whereas M2 macrophages express *CD163*

The above results are as expected and can confirm that the monocytes gave rise to polarised macrophages. However, it is important to conduct further experiments to characterise these populations at molecular level before seeding them within gellan fluid to inspect transcriptional alterations.

Monocytes are highly plastic cells because of their capacity to change their activation states and phenotype in response to environmental cues (Yang et al., 2014, Das et al., 2015). Furthermore, the activation state of macrophages is a crucial factor in corneal wound healing and scarring (Hadrian et al., 2021, Liu and Li, 2021). Thus, it is critical to characterise our differentiated M1 and M2 to identify their activation states before seeding them within gellan fluid gel. To perform this experiment, we selected several genes specific for M1 or M2 macrophages based on studies using the immortalised monocyte cell line, THP-1. It was demonstrated that the generation of M1 and M2 macrophages from THP-1 resulted in macrophages that shared the similar phenotype of primary human M1 and M2, with *GBP5, SERPING1, CXCL9, and CXCL10* being specific markers of THP-1-derived M1 macrophages, whereas THP-1 derived M2 macrophages express*, MRC1, CCL17, TGM2 and CD163* (Baxter et al., 2020, Huwait et al., 2022). Therefore, we selected these genes to determine the genetic characteristics of our M1 and M2 macrophages, by assessing these genes prior to mixing them with gellan fluid gel **Table 1**.

Table 3.1 Description of selected gene functions and rationale for choosing.

Gene name	Symbol	Gene role in macrophages	Rationale for choosing (gene expression)
C-X-C motif chemokine ligand 9	*CXCL9*	Encodes CXCL9 chemokine, CXCR3 ligands and IFN-γ inducer, involved in T cell recruitment (Farber, 1990, Metzemaekers et al., 2018)	Highly expressed on M1 macrophages (Beyer et al., 2012)
C-C motif chemokine ligand 17	*CCL17*	Encodes CCL17 chemokine, CCR4 ligands and IL-4 inducer, involved in T cell recruitment (Mantovani et al., 2004, Mosser and Edwards, 2008)	Highly expressed on human M2 macrophages (Beyer et al., 2012)
C-X-C motif chemokine ligand 10	*CXCL10*	Encodes CXCL10 chemokine, CXCR3 ligands and IFN-γ inducer, involved in T, NK cell and monocyte trafficking (Lee et al., 2009).	Highly expressed on human M1 macrophages (Jaguin et al., 2013)
Guanylate Binding Protein 5	*GBP5*	Involved in the activation of NOD-like receptor family, pyrin domain containing 3 (NLRP3) inflammasome(He et al., 2016)	Highly expressed on human M1 macrophages (Baxter et al., 2020, Huwait et al., 2022, Fujiwara et al., 2016)
Mannose receptor C type 1	*MRC1*	Encodes CD206, a mannose receptor, involved in scavenging endogenous glycoproteins, recognising pathogens, and presenting antigens. ((Yilmaz et al., 2022)	Highly expressed on human M2 macrophages(Baxter et al., 2020)
Transglutaminase 2	*TGM2*	Encodes TGM2 protein involved in inducing efferocytosis, recruitment of eosinophil and cell adhesion and fibrosis (Eligini et al., 2016, Rebe et al., 2009, Abdelaziz et al., 2020, Lai and Greenberg, 2013)	Highly expressed on human M2 macrophages(Baxter et al., 2020)
Serpin Family G Member 1	*SERPING1*	Encodes a C1 inhibitor, involved in the regulation of complement activation(Luo et al., 2018)	Highly expressed on human M1 macrophages (Baxter et al., 2020, Huwait et al., 2022)
Cluster of differentiation 163	*CD163*	Encodes CD163, a scavenger receptor for the haptoglobin-haemoglobin complex, resolve inflammation by clearing haemoglobin and stimulating the production of anti-inflammatory cytokines(Yilmaz et al., 2022)	Highly expressed on human M2 macrophages(Brocheriou et al., 2011, Fujiwara et al., 2016)

As our designed experiment (M1 and M2 macrophages) that were used in qPCR analysis did not contain an untreated sample (a calibrator), delta CT (dCT) measurements were used to indicate the gene expression level of M1 and M2 macrophages; higher CT values indicate a low level of gene expression.

A comparison of the dCT values (gene – UBC) of these selected M1 genetic markers in the two macrophage populations revealed that although *GBP5* and *SERPING1* have higher dCT values on M1 than on M2, no statistical differences were observed in the gene expression level of *CXCL9, CXCL10, GBP5, and SERPING1* between M1 and M2 macrophages **(Figure 3.3)**. Indeed, our findings indicate that similar levels of gene expression were found for *CXCL9* and *10 on* M1 and M2 macrophages **(Figure 3.3, C and D).** Taken together, these findings are inconsistent with studies reviewed in **Table 3.1** and also indicate that *CXCL9, CXCL10, GBP5,* and *SERPING1* genes are not specifically expressed on our GM-CSF derived M1 as some of these genes are induced by pro-inflammatory cytokines such as IFN-γ, as mentioned **Table 3.1**.

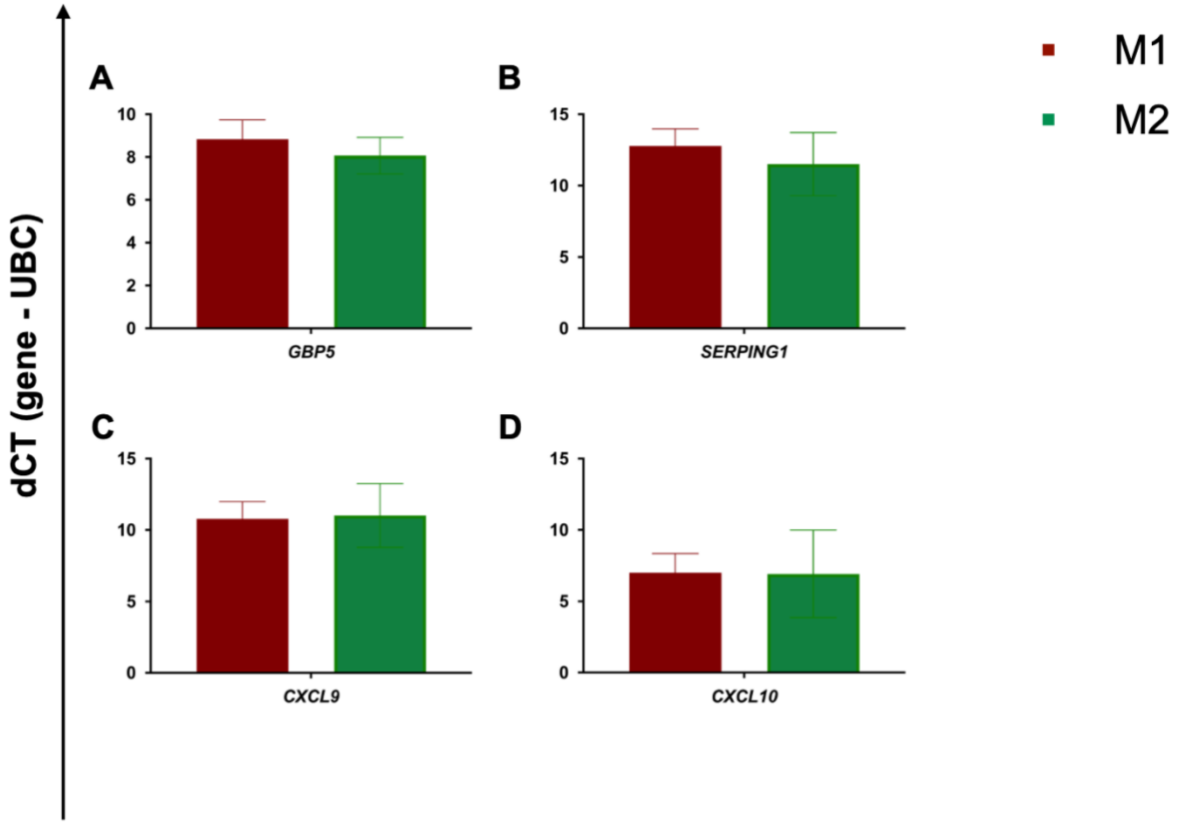

Figure 3.3 qPCR analysis of dCT value differences of selected M1 makers between M1 and M2 macrophages.

Isolated peripheral blood monocytes were treated with GM-CSF and M-CSF to produce human M1 and M2 macrophages, respectively. The cDNA from M1 and M2 macrophages was used to perform qPCR analysis. The difference in dCT values (gene – a normaliser (UBC)) of each gene between M1 and M2 macrophages were assessed. the comparison of dCT values for the different genes between M1 and M2 macrophages. **(A)** presents *GBP5*, **(B)** *SERPING1 CCL17*, (**C)** *CXCL9* and **(D)** *CXCL10.* Statistical significance was determined using multiple Mann-Whitney tests; n = 9 experimental replicates.

However, the comparison of selected marker expression for M2, including *MRC1, CCL17, TGM2 and CD163* in our M1 and M2 macrophages showed that dCT measurements of *CCL17* was significantly lower in M1 than in M2 macrophages **(Figure 3.4, B).** Lower dCT values of *CCL17* on M1 macrophages indicated that it is a potential M1 marker. Unlike *CCL17,* dCT values of *CD163* tended to show that mRNA levels of *CD163* in M2 macrophages were statistically increased relative to M1 macrophages (**Figure 3.4, C)**. When dCT values of *MCR1 and TGM2* were compared, M1 macrophages had higher mRNA levels of these molecules; however, there were

no statistical distinctions, as shown in **(Figure 3.4, A and D)**. Taken together, these results indicate that *CCL17* and *CD163* may be specific markers for M1 and M2 macrophages, respectively. The specific expression of the CD163 gene on M2 macrophages is in line with our flow cytometric results, where we showed CD163 as a surface marker for M2 macrophages (**Figure 3.2)**.

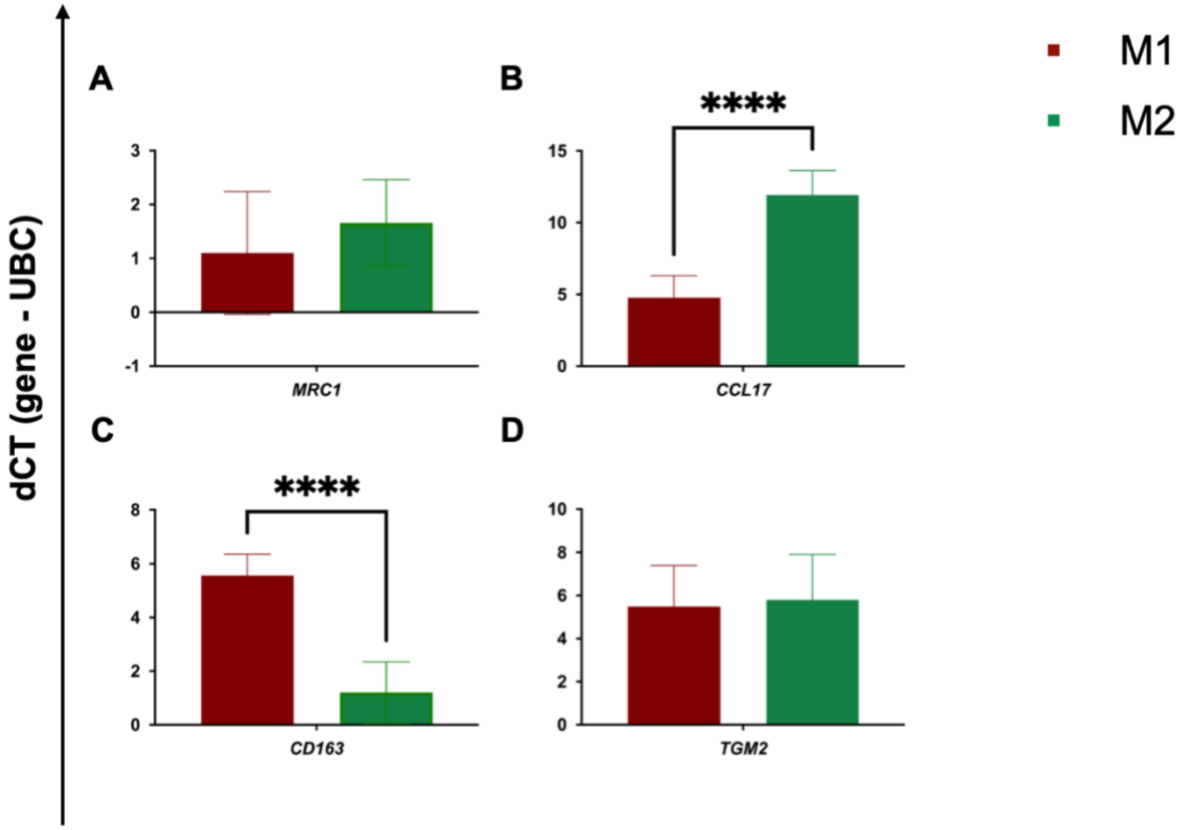

Figure 3.4 qPCR analysis of dCT value differences of selected M2 makers between M1 and M2 macrophages.

Isolated peripheral blood monocytes were treated with GM-CSF and M-CSF to produce human M1 and M2 macrophages, respectively. The cDNA from M1 and M2 macrophages was used to perform qPCR analysis. The difference in dCT values (gene – a normaliser (UBC)) of each gene between M1 and M2 macrophages were assessed. the comparison of dCT values for the different genes between M1 and M2 macrophages. (A) presents *MRC1*, (B) *CCL17*, (C) *CD163* and (D) *TGM2*. Statistical significance was determined using multiple Mann-Whitney tests. **** $p < 0.0001$; n = 9 independent experiments.

Overall, these findings are not consistent with previous studies mentioned in **Table 3.1**, which may emphasise the impact of the cytokine type and macrophage origin on the phenotypic features of differentiated macrophages *in vitro*. Thus, these findings revealed that the identification of the activation status of our macrophages cannot exclusively rely on a limited number of markers at the mRNA and protein level, but rather should be accommodated by a global characterisation.

3.2.3. Gellan fluid gel is a biocompatible delivering system.

We proposed that applying M1 and M2 macrophages on the injured ocular surface via a gellan fluid gel delivery system may promote scarless corneal wound repair and consequently preserve sight. Therefore, the effects of the biocompatibility of gellan fluid gel on M1/M2 macrophages *in vitro* was assessed using cellular viability staining called Calcein-AM and Propidium Iodide (AM/PI stain). AM/PI stain simultaneously stains live and dead cells.

Fluorescence microscopic analysis for triplicate experiments showed that the majority (~more than 70%) of the M1 and M2 macrophages with or without the gellan fluid gel were alive after incubation for 4 h, as shown in **(Figure 3.5, A and B)**. Importantly, when comparing the proportion of viable M1/M2 macrophages in gellan fluid gel to those in serum-free medium (controls), no statistically significant difference was found, as shown in **(Figure 3.5, C)**.

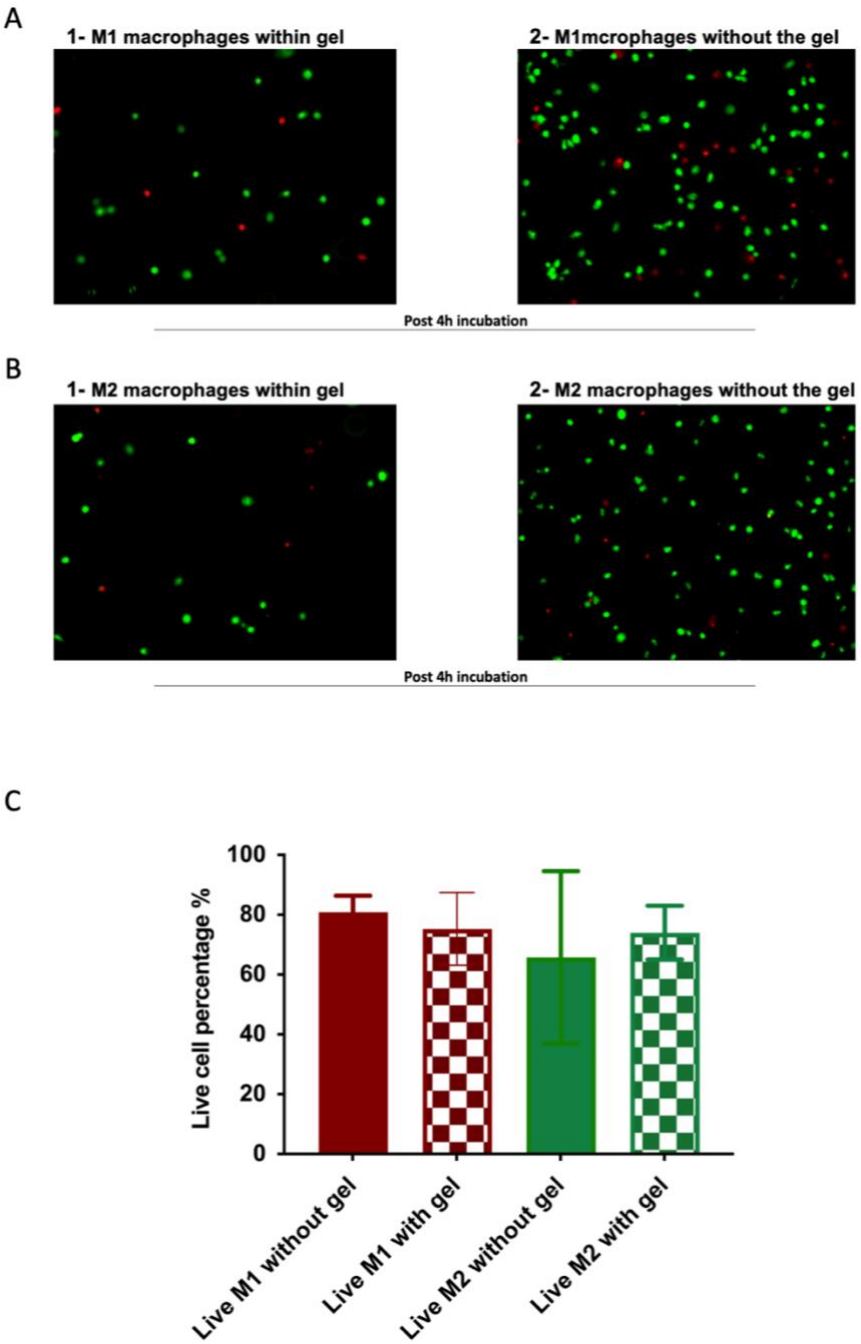

Figure 3.5 Florescence microscopic analysis of the viability of polarised macrophages with or without gellan fluid gel.

Primary human monocytes were isolated and matured to both M1 and M2 macrophages using GM-CSF and M-CSF cytokines, respectively. Harvested M1 and M2 macrophages (3×10^5/10 µL) were mixed with 200 µL of gellan fluid gel or serum-free medium (controls) and plated in 24-well plates. After incubation for 4 h, all the cells were stained with (MA/PI) (live: green and dead: red) stain. Viability test was performed using florescence microscopy (20×). **(A,1)** Representative image of M1 in gellan gel and **(A,2)** in serum. **(B,1)** Representative image for M2 in gellan gel and **(B,2)** in serum). **(C)** presents a comparison of the proportion of live macrophages among the different conditions using *Wilcoxon* test. (Six technical replicates per experiment; n = 3 biological replicates).

3.2.4. Expression of surface markers on M1 macrophages treated with gellan fluid gel.

Following confirmation of the biocompatibility of gellan fluid gel, we sought to investigate whether our delivery platform interfered with our differentiated M1 and M2 macrophages and alter their polarisation states. Expression of surface markers, CD14, CD80, CD206, and CD163 on our generated M1 and M2 macrophages post seeding in gellan gel for 4 hours was assessed by flow cytometry.

When M1 and M2 macrophages were mixed with gellan fluid gel or serum-free medium (controls), we were unable to recover M1 and M2 from the gel for use in a flow cytometry study, despite many attempts, such as diluting the gellan fluid gel and centrifuging it at high speeds **(Figure S1)**. To address this issue, M1 and M2 macrophages were cultured as monolayers. Subsequently, either gellan fluid gel or serum-free media was added to each culture, and the mixtures were incubated for 4 hours before assessing M1 and M2 surface markers. Both M1 macrophages mixed with or without gellan fluid gel showed similar expression levels of CD14, CD80, CD206 and CD163, and no statistical differences were found between the two conditions, as shown in **(Figure 3.6).** These results indicate that our proposed delivery platform for polarised macrophage-based therapy for the prevention of corneal fibrosis does not interact with our generated M1 macrophages, consequently maintaining their polarisation states at protein levels. Although the retention time for gellan fluid gel was 4 h in the mouse model, it is worth mentioning that this incubation period may not be sufficient to capture potential alterations in the expression of all proteins, which could require a longer time to appear. Therefore, a longer incubation period may strengthen

our findings. Although macrophage viability was not assessed using fluorescence microscopy with this monolayer method of mixing, which could potentially affect the results of surface marker expression, dead cells were excluded from the flow cytometric analysis.

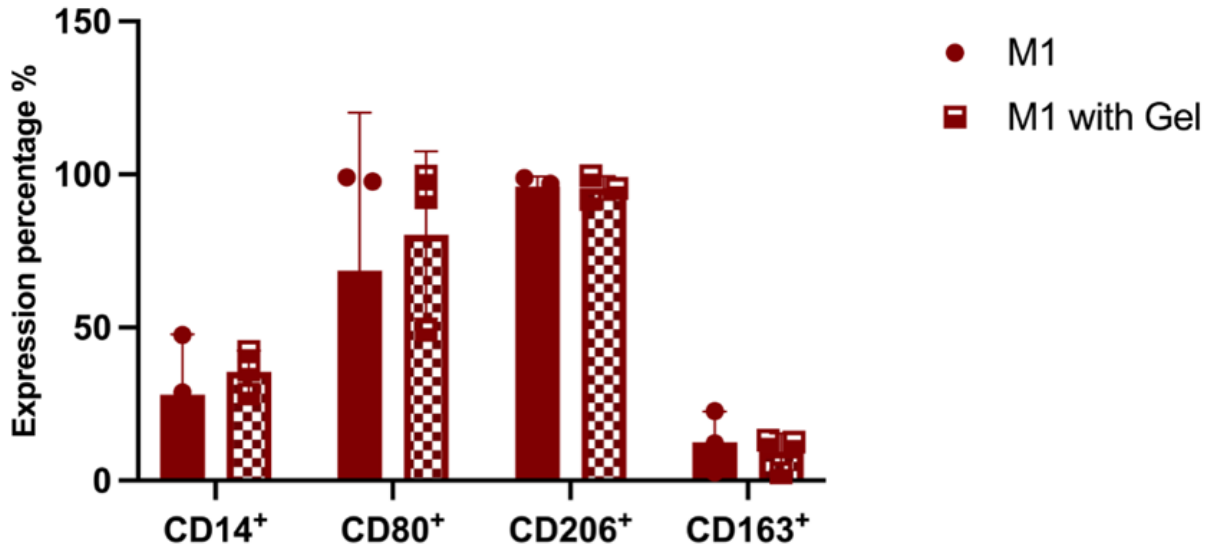

Figure 3.6 Flow cytometric analysis of phenotypic differences between M1 macrophages with or without gellan fluid gel.
Primary human monocytes were isolated and matured into both M1 and M2 macrophages using 10 ng/mL of GM-CSF and 50 ng/mL of M-CSF growth factors, respectively. On day 6, the cells were seeded in 6 well plates and incubated for 24 h. On day 7, M1 and M2 macrophages were mixed with 2mL of gellan fluid gel or serum-free medium (controls). After incubation for 4 h, all the cells were harvested and resuspended in 50 µL of a master mix of antibodies or 50 µL of a master mix of isotype control antibodies. Flow cytometric analysis of phenotypic differences between polarised macrophages was performed using BD LSRFortessa™ X-20. (Graph) presents a comparison of phenotypic differences between M1 with and without gellan fluid gel using repeated measures *two-way ANOVA* with Šídák's multiple comparisons test (n = 3 biological replicates).

3.2.5. Expression of surface markers on M2 macrophages treated with gellan fluid gel.

Unlike M1, M2 macrophages seeded with gellan fluid gel had a significant decline in CD163 expression (~45%) when compared with M2 without gellan fluid gel (~90%) **(Figure 3.7)**. Comparison of expression levels for CD14, CD80, and CD206 on M2 macrophages with and without gellan fluid gel application showed no significant difference **(Figure 3.7)**.

These findings led us to further investigate the effects of gellan fluid gel on the polarisation states of our M1 and M2 macrophages by assessing alterations in their genes that are either involved with pro- or anti-inflammatory response (Murray and Wynn, 2011).

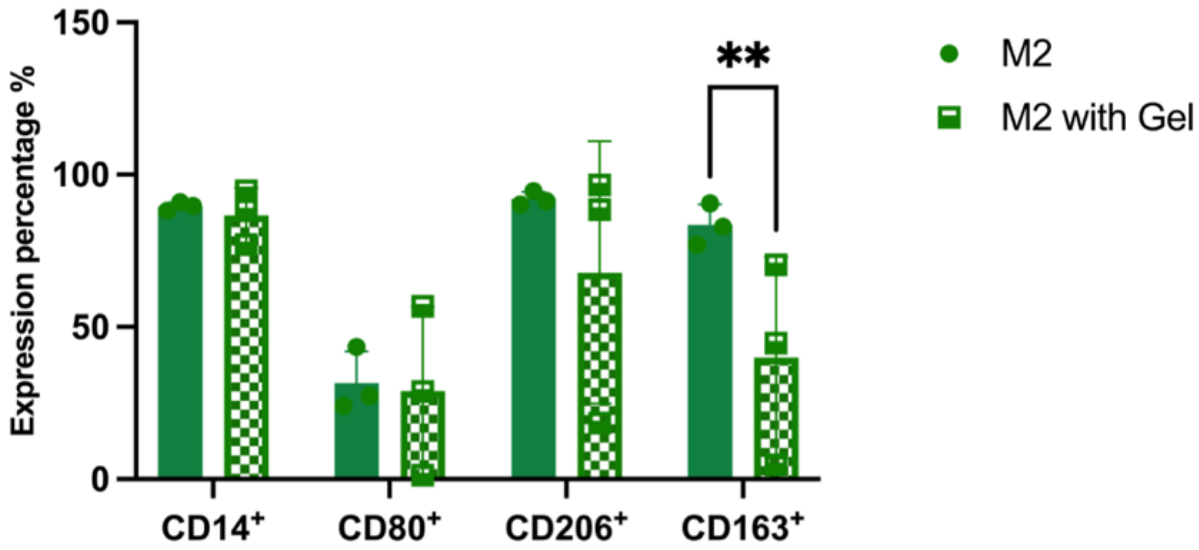

Figure 3.7 Flow cytometric analysis of phenotypic differences between M2 macrophages with or without gellan fluid gel.
Primary human monocytes were isolated and matured to M2 macrophages using 50 ng/mL of M-CSF. On day 6, the cells were seeded in 6 wells plate and incubated for 24 h. On day 7, 2mL of gellan fluid gel or serum-free medium was added. After incubation for 4 h, all the cells were harvested cells and resuspended in 50 µL of a master mix of antibodies or 50 µL of a master mix of isotype control antibodies. Flow cytometric analysis of phenotypic differences between polarised macrophages was preformed using BD LSRFortessa™ X-20. (Graph) presents a comparison of phenotypic differences between M2 with and without gellan fluid gel using repeated measures *two-way ANOVA* with Šídák's multiple comparisons test (n = 3 biological replicates). (** $p<0.01$).

3.2.6. Pro- and anti-inflammatory properties of M1 macrophages with gellan fluid gel at selected molecular levels have not significantly changed.

To determine whether our delivery platform changes the phenotype of M1 and M2 macrophages, expression levels of pro- and anti-inflammatory genes on both our M1 and M2 macrophages upon 4-hour incubation with gellan fluid gel were assessed using qPCR. Using our RNA sequencing data (discussed in detail in chapter four), it was found that *IL12β, PTGES,* and *CXCL10* genes were significantly more highly

expressed on macrophages stimulated with LPS and IFN-γ, whereas IL-4 and IL-13 stimulated macrophages appreciably upregulated *CD163, IGF and CCL22 genes*. MKI67 gene had a similar expression level in both GM-CSF derived M1 and M-CSF derived M2. The relevant functions of these genes are detailed in T**able 3.2**.

The qPCR analysis of pro-inflammatory gene expression, including *IL12β, PTGES, and CXCL10*, in M1 macrophages with and without gellan fluid gel showed no statistical differences (**Figure 3.8, A)**. Similarly, expression levels of anti-inflammatory genes, *CD163, IGF and CCL22,* in M1 macrophages with and without gellan fluid gel were similar, and no significant changes were observed between both conditions **(Figure 3.8, B)**. Taken together, these molecular findings may indicate that the gellan fluid gel does not alter the polarisation states of M1 at the mRNA level.

Table 3.2 Description of selected gene functions

Gene name	**Symbol**	**Gene role in macrophages**
Interleukin-12beta	*IL12β*	Encodes p40, a subunit of IL12 cytokine, IL12Rβ1 ligand, involved in activation of NK cells and Th1 cells responses (Zundler and Neurath, 2015, Sieburth et al., 1992).
Prostaglandin E synthase	*PTGES*	Encodes an enzyme called microsomal prostaglandin E synthase 1 (MPGES1), involved in production of prostaglandin E2 (Jegerschold et al., 2008)
Insulin like growth factor 1	*IGF1*	Encodes Insulin like growth factor 1, IGF1R ligands, involved in muscle regeneration and inhibition of inflammation(Zundler and Neurath, 2015)
C-C motif chemokine ligand 22	*CCL22*	Encodes CCL22 chemokine, CCR4 ligand, involved in CCR4+ cell, T, monocyte and NK cell trafficking.(Mantovani et al., 2004).

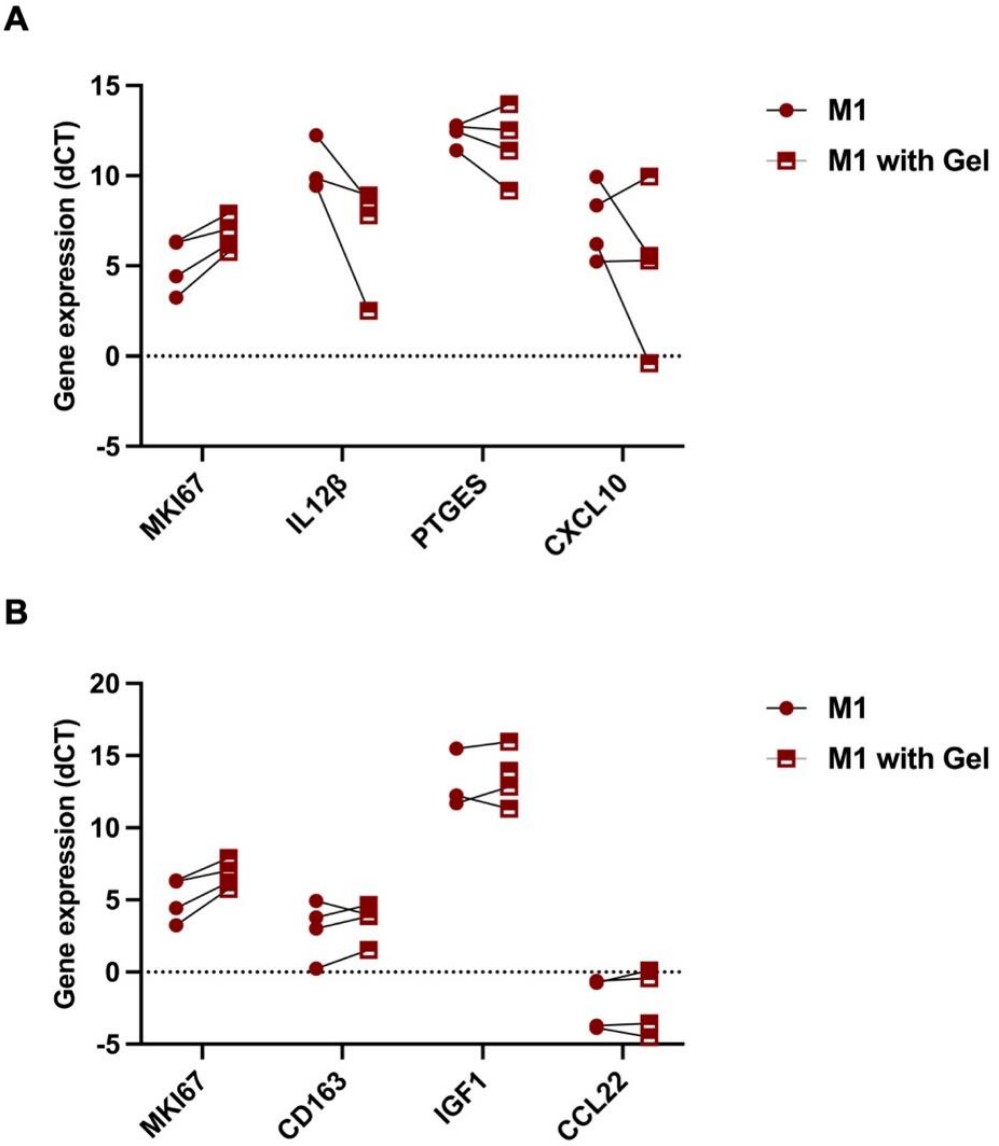

Figure 3.8 qPCR analysis of dCT value differences of pro- and anti-inflammatory genes between M1 macrophages with or without gellan fluid gel. Primary human monocytes were isolated and matured into M1 macrophages using 10 ng/mL of GM-CSF and 50 ng/mL of M-CSF growth factors, respectively. On day 6, the cells were seeded in 6 well plates and incubated for 24 h. On day 7, macrophages were mixed with 2mL of gellan fluid gel or serum-free medium (controls) and incubated for 4 h. The cDNA from macrophages was used to perform qPCR analysis. The difference in dCT values (gene – a normaliser (UBC)) of each gene between macrophages with or without gellan fluid gel were assessed. **(A)** the comparison of dCT values for the pro-inflammatory genes between both conditions. **(B)** the comparison of dCT values for the anti-inflammatory genes of both conditions using ordinary *two-way ANOVA* with Šídák's multiple comparisons test (n = 3 biological replicates).

3.2.7. Gellan fluid gel does not alter the polarisation state of M2 macrophages.

We investigate the expression level of the same selected genes in M2 macrophages with and without gellan fluid gel to determine the impact of this platform on our polarisation model. Our findings showed that *IL12β, PTGES, and CXCL10* genes in M2 macrophages with and without gellan fluid gel have similar dCT values, and no statistical differences were observed, as shown in (**Figure 3.9, A)**. No significant changes in expression of *CD163, IGF1 and CCL22* in M2 macrophages with and without gellan fluid gel were observed, **(Figure3.9, B)**. In contrast with our flow cytometric results **(Figure3.7)**, *CD163* expression levels in M2 macrophages with and without gellan had comparable dCT values. Overall, although these findings may suggest that the gellan fluid gel does not significantly affect the gene expression profiles of M1 and M2 macrophages, the observed reduction in CD163 protein levels may be attributed to CD163 shedding. It is worth mentioning that an increase in gene expression does not always result in corresponding protein expression.

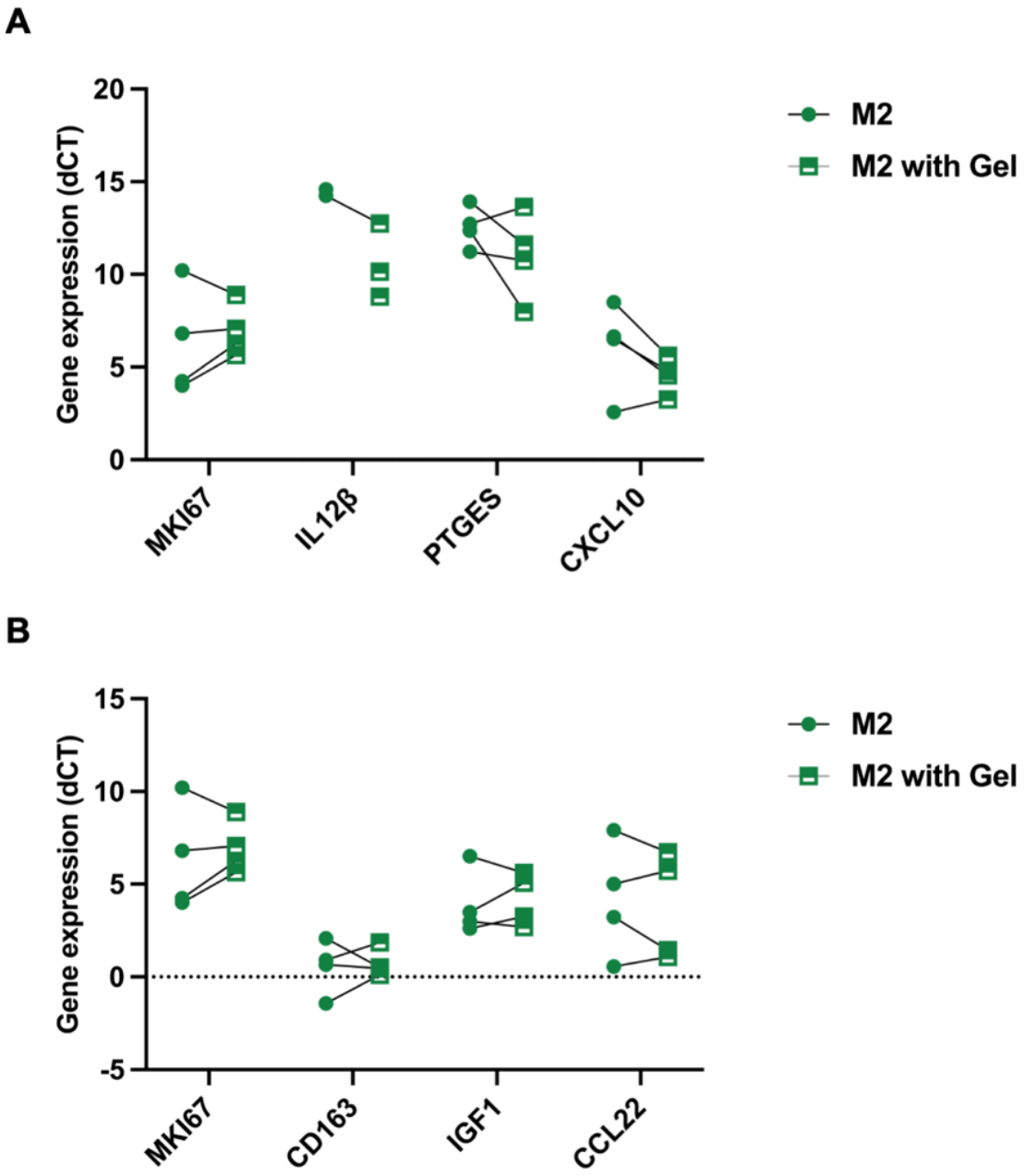

Figure 3.9 qPCR analysis of dCT value differences of pro- and anti-inflammatory genes on M2 macrophages with or without gellan fluid gel.
Primary human monocytes were isolated and matured into M2 macrophages using 10 ng/mL of GM-CSF and 50 ng/mL of M-CSF growth factors, respectively. On day 6, the cells were seeded in 6 well plates and incubated for 24 h. On day 7, macrophages were mixed with 2mL of gellan fluid gel or serum-free medium (controls) and incubated for 4 h. The cDNA from macrophages was used to perform qPCR analysis. The difference in dCT values (gene – a normaliser (UBC)) of each gene between macrophages with or without gellan fluid gel were assessed. **(A)** the comparison of dCT values for the pro-inflammatory genes between both conditions. **(B)** the comparison of dCT values for the anti-inflammatory genes of both conditions using ordinary *two-way ANOVA* with Šídák's multiple comparisons test (n = 3 biological replicates).

3.3. Discussion

Wound healing mechanisms are complex processes involving a series of stages, finally ending in the recovery of the injured area associated with scar formation (Wilkinson and Hardman, 2020). In certain tissues, the presence of a scar after wound healing is not problematic; however, in the cornea, it may lead to loss of its transparency and consequently vision impairment (Wilson et al., 2022, Bender et al., 2004). It is well known that macrophages, their polarisation state, and secreted mediators are critical players in all phases of wound healing (Snyder et al., 2016, Lis-Lopez et al., 2021, Willenborg et al., 2022); thus, we proposed that administration of M1 or M2 macrophages at the right time may lead to regenerative corneal wound healing and eventual preservation of sight. The ocular surface experiences a blinking process by which directly administered treatments are removed rapidly. Thus, we proposed that gellan fluid gel could function as an effective platform for delivering such a cell-based therapy on the ocular surface.

In the present study, isolated human monocytes were cultured with GM-CSF and M-CSF to generate M1 and M2 macrophages, respectively. To confirm monocyte maturation into M1 and M2 macrophages, the cell morphology and the expression of CD14, CD80, CD163, and CD206 on the surface of our polarised macrophages were assessed using an inverted microscope and flow cytometry.

According to the literature**,** it is expected that GM-CSF derived M1 macrophages would significantly express CD80, whereas CD14 and CD163 expression are induced on M-CSF derived M2 macrophages. Although CD206 surface protein was identified as an IL-4 induced M2 marker in mice (Stein et al., 1992), its expression was induced on

both GM-CSF derived M1 and M-CSF-derived M2. Our results were consistent with our expectations and the literature.

In accordance with our findings on morphological characteristics, we found that the GM-CSF derived M1 was rounded, while the M-CSF derived M1 was elongated (Brocheriou et al., 2011, Waldo et al., 2008). Consistent with our findings about the phenotype of our M1 and M2 macrophages, Bender et al. (2004) found that macrophages cultured with M-CSF and IL10 have increased CD14 expression. In contrast to CD14, Verreck et al. (2004) found M-CSF derived M2 to have a high level of CD80 expression, consistent with our findings (Verreck et al., 2004).

Unlike human macrophages, Lari et al. (2007) showed no significant differences in CD80 expression between mouse GM-CSF and M-CSF derived M1 and M2 macrophages, respectively (Lari et al., 2007). This difference highlights the fact that human and mouse macrophages exhibit distinctive phenotypes. Ambarus et al. (2012) validated the phenotypic markers expressed on GM-CSF and M-CSF derived human M1 and M2, respectively, in vitro. Despite differences in concentrations of GM-CSF (50 ng/mL) and incubation duration (4 days), their findings agreed with our results regarding distinctive expressions of CD14, 80, and 163 among our M1 and M2 macrophages.

However, an interesting study by Boyette et al. (2017) demonstrated that although human classical, intermediate, and non-classical monocytes differentiated into macrophages and acquired the shape of M1 and M2 macrophages in the presence of GM-CSF and M-CSF, respectively, each subtype of monocyte produced macrophages that have distinctive cell surface markers, including CD14, 80, and 163, as well as a cytokine production profile. Different methods of monocyte isolation, including

negative, positive, and plastic adherent, produce different percentages of the three types of monocytes. These subtypes of monocytes differentiated into M1 and M2 macrophages that exhibit differential phenotype and function (Nielsen et al., 2019), consistent with Boyette et al. (2017). As we used a negative selection method in our experiments, most cells obtained would be classical monocytes.

In line with our findings, M-CSF derived M2 macrophages displayed significantly higher expression of CD163 and CD14 as compared to M1 macrophages derived from GM-CSF. The high expression levels of CD14, and CD206 and CD163 on our M2 macrophages may indicate their potent phagocytic function, as reported by Schulz et al. (2019). In contrast to our findings, CD80 expression was not detected on M1 and M2 macrophages, as reported by Samaniego et al. (2014).

Overall, our findings would confirm maturation of generated M1 and M2 from blood monocytes cultured with GM-CSF and M-CSF, respectively. Furthermore, we could identify CD80 as an M1 marker, while CD14 and CD163 are exclusively M2 makers for our polarisation model. This is because the expression levels of these surface makers could be altered by several factors, including secondary stimulation, stimulation duration, type of isolation method, and concertation stimuli (Ambarus et al., 2012, Vogel et al., 2014, Unuvar Purcu et al., 2022, Boyette et al., 2017, Nielsen et al., 2020).

Therefore, it is worth conducting further studies to determine the transcriptional signature, cytokine profile, and function of M1 and M2 macrophages. All these differences in the phenotype of monocyte differentiated M1 and M2 macrophages emphasised the importance of characterising our polarisation systems.

We investigated the expression of *SERPING1, CXCL9, CXCL10, GBP5 as M1* markers and *MRC1, CCL17, TGM2* and *CD163* as M2 markers using qPCR analysis. We showed that expression levels of most of these genes, have no specificity in the two populations except for CCL17, specific for M1 macrophages, and CD163, specific for M2 macrophages. As mentioned in **Table 3.1**, many studies identified *SERPING1*, *CXCL9*, *CXCL10* and *GBP5* as specific markers of monocytic THP-1-derived M1, and *MRC1, CCL17, TGM2*, and *CD163* for M2 macrophages, which are only partially consistent with our findings. The observed differences may be attributed to that THP-1 derived macrophages were polarised by using LPS and IFN-γ, IL-4 and IL-13, or IL10 cytokines to induce M1, M2a and M2c macrophages, respectively, in the previous studies. By comparison, we used GM-CSF and M-CSF cytokines to generate our M1 and M2 macrophages, which may explain these conflicting findings. Another explanation for these conflicting results is that monocytic THP-1 cells are immortalised cells originated from human acute monocytic leukaemia, and their genetic background may contribute to the observed distinction in transcriptional expression compared with human primary macrophages. Tedesco et al. (2018) found that THP-1 derived M1 and M2 macrophages have distinctive cytokine and mRNA expression profiles upon activation by LPS and IFN-γ and IL-4 and IL-13 as compared to primary human M1 and M2 under the same conditions. (Tedesco et al., 2018).

Differentiation of macrophages using GM-CSF and M-CSF growth factors lead to M1 and M2 macrophage-like phenotypes. Furthermore, these two subsets responded differentially when stimulated with the same cytokines such as LPS or IFN-γ, in which M1 macrophages were found to produce proinflammatory cytokines, such as IL12, whereas M2 macrophages released a high level of IL10 (Verreck et al., 2004, Verreck et al., 2006). In addition, GM-CSF- and M-CSF-stimulated M1 and M2 exhibited

distinctive transcriptional features and markers compared with macrophages induced using IFN-γ, IL-4, or others. GM-CSF and M-CSF seem to prime or mature macrophages before fully activated M1 and M2 with pro-or anti-inflammatory stimuli (Lukic et al., 2017, Hamilton et al., 2014).

Although CCL17 chemokine is typically upregulated in IL-4-induced human M2 macrophages (Abdelfattah et al., 2016), studies showed that human monocyte derived macrophages stimulated with the GM-CSF cytokine upregulated CCL17 at RNA and protein levels as compared to M2 derived from M-CSF (Achuthan et al., 2016) or M-CSF with IL10 at mRNA levels (Waldo et al., 2008). M1 markers, CXCL10 and CXCL9, have a similar expression level on M-CSF, however, IL-4 stimulation significantly decreases their expression as compared to these macrophages with or without LPS and IFN-γ stimulation (Martinez et al., 2006). This would confirm GM-CSF and M-CSF differentiated and matured monocytes into macrophages with pro-inflammatory and anti-inflammatory features, respectively, rather than fully activating them. This led us to use LPS with IFN-γ or IL-4 with IL-13 for activation of our primed M1 and M2 macrophages in future experiments. A significant upregulation of *CD163* expression on M-CSF derived M2 as compared to GM-CSF derived M1 is supported by previous studies (Lescoat et al., 2018, Waldo et al., 2008).

Together, our results showed that CCL17 is significantly expressed on GM-CSF-stimulated M1 macrophages, whereas CD163 is a specific marker for M-CSF-stimulated M2 macrophages.

Gellan fluid gel has a broad range of biomedical applications as a delivery system for bioactive factors, such as topical applications to improve wound healing and cartilage regeneration (Cooke et al., 2018). Due to its biocompatibility and its solid–liquid–solid

transition properties, it is a potent candidate to be applied on curved surface and a weakly bioavailable organ (eye) to increase retention of therapeutic agents. Thus, the biocompatibility of this delivery system was examined in the present study, and gellan fluid gel was found to be biocompatible and did not exert any toxic effects on M1 and M2 macrophages. This finding agrees with the results of a study by Chouhan et al. (2019) investigating the toxicity of gellan fluid gel on human corneal fibroblast culture. Consistent with these results, Ter Horst et al. (2019) examined the potential use of gellan fluid gel for delivering autologous keratinocytes to the surface of the burned skin of patients to aid the healing process while minimising scar formation. Gellan fluid gel was found to preserve elevated levels of live human dermal fibroblasts until 7 days following seeding.

Maintaining the polarisation states of our M1 and M2 macrophages while applying them to the ocular surface is critical. Thus, we evaluated the effect of gellan fluid gel on our polarised M1 and M2 macrophages. Only CD163 on M2 macrophages showed a significant decrease in surface expression upon gellan fluid gel treatment. An explanation of this observed effect is the morphological differences of our generated M1 and M2 macrophages, where M1 macrophages exhibit a rounded shape with pro-inflammatory properties and M2 macrophages exhibit an elongated shape with anti-inflammatory features. A study by McWhorter et al. (2013) investigated the effect of the physical alteration of macrophage morphology on their activation states. The morphology of M-CSF-stimulated derived mouse macrophages was altered to be elongated using the micropattern method in the absence of anti-inflammatory IL-13 and IL-4. This alteration promoted macrophages towards upregulation of the M2 surface markers, including CD206, arginase-1 and YM-1 and the potent secretion of anti-inflammatory cytokines. Simultaneously, this elongation prevents macrophages

from switching towards M1 in the presence of pro-inflammatory stimuli like LPS and IFN-γ (Jain et al., 2019). This would explain the changes in the phenotype of M2 macrophages, especially the lower expression of CD163, an M2-specific marker, after gellan fluid gel application. Layering gellan fluid gel on the top monolayer may alter the M2 macrophage shape to become more M1-like macrophages. This observation could suggest using the GM-CSF derived macrophages only to produce M1 and M2 macrophages, as they are able to polarise to M1 and M2 phenotypes. In line with this idea, Ambarus et al. (2012) suggested M-CSF derived M2 macrophages exhibited a higher level of plasticity as compared to GM-CSF derived M1 macrophages. Moreover, a comprehensive review by Jain et al. (2019), focusing on the implications of physical factors and stress, such as substrate and interstitial flow of tumour tissue, on macrophage polarisation states, emphasised the significance of considering the physical factor role within the environment surrounding macrophages in architecting their activation states (Jain et al., 2019). For example, it was found that tumours with low regression are characterised by an increase in the inflex of interstitial flow, and this elevation acts as physical stress to polarise macrophages to the M2 phenotype (Li et al., 2018b). This is a potential explanation for the reduction of CD163 on the surface of M2 macrophages cultured with gellan fluid gel, where CD163 shedding occurred as a result of macrophage activation in response to the physical force of gellan fluid gel.

CD163 shedding on macrophages is a well-known mechanism for releasing soluble CD163 (sCD163) into the circulation upon activation through TLR (Nielsen et al., 2020). sCD163 is classified as a biomarker for several diseases, including infection and inflammation (Moller, 2012).

However, qPCR results for expression levels of pro- and anti-inflammatory genes, including *CD163*, showed that the gellan fluid gel does not affect the gene expression profiles of M1 and M2 macrophages. Nevertheless, various mechanisms, such as post-transcriptional and translational regulation, can influence protein levels, leading to inconsistencies between gene and protein expression (Istomine et al., 2016).

Moreover, the gellan fluid gel, as proposed, should be mixed with M1 and M2 macrophages but not layered on top of cultured M1 and M2 macrophages. Mixing M1 and M2 macrophages within the gellan fluid gel may result in the maintenance of the specific expression of CD163 on the surface of M2 macrophages.

Alginate fluid gel, which was used as a device to deliver chondrocytes to promote cartilage regeneration (Cooke et al., 2018), was found to change the phenotype of these cells and dedifferentiate them to fibroblasts following seeding the cells within the gel for the long period. However, the gellan fluid gel has been found to be removed within four hours from corneal surface by mechanical shear stress caused by blinking of eyelid and tear production. Although blinking process is associated the poor retention of eye drop, it could boost the release of seeding macrophages *in vivo*.

In conclusion, we effectively produced two subsets of macrophages. We showed that gellan fluid gel is a biocompatible material and has potential applicability as a delivery system for M1 and M2 macrophages onto the cornea. Thus, further experiments are required to generate different subsets of M1 and M2 macrophages and phenotype them with the aim of assessing their polarisation states.

Chapter 4. The gene expression profiling of different subset of macrophages

4.1. Introduction

In the previous chapter, we concluded that gellan fluid gel is biocompatible and an applicable platform to deliver our macrophage-based therapy onto the ocular surface to prevent corneal fibrosis. We showed that gellan fluid gel has no effect on the percentage of macrophage viability and the phenotype of our M1 and M2 macrophages, with the exception of a reduction in the expression of CD163 in our M2 macrophages. In addition, we discriminated between GM-CSF-derived M1 and M-CSF-derived M2 macrophages. We investigated the expression of well-known M1 and M2 markers, GBP*5*, *SERPING1*, *CXCL9*, and *CXCL10* genes for M1 and *MRC1*, *CCL17*, *TGM2*, and *CD163* genes for M2. We found that both M1 and M2 macrophages expressed a similar level of these markers, with the exception of CD163 and CCL17. Only CD163 was identified as a marker for our M2 macrophages, while CCL17, was significantly expressed in our M1macrophages. This may suggest that our GM-CSF-derived M1 and M-CSF-derived M2 macrophages may differ from M1 and M2 macrophages that were differentiated by strong pro- or anti-inflammatory stimuli, such as LPS, IFN-γ, IL-4, or IL-13. Studies showed that GM-CSF and M-CSF growth factors seem to only mature these CSF-derived macrophages but not fully stimulate them (Hamilton et al., 2014, Lukic et al., 2017). To address this concept the pro-inflammatory and pro-healing properties of our M1 and M2 macrophages were boosted by stimulating M1 and M2 with LPS and IFN-γ, or IL-4 and IL-13, respectively.

Macrophage polarisation states or phenotype are crucial in regulation of wound healing response in cornea (Liu and Li, 2021, Liu et al., 2017, Xu et al., 2022). During corneal healing process and potential fibrosis, corneal microenvironments would contain bacterial components, pro- and anti-inflammatory and other molecules. These

microenvironment derived molecules have opposing roles in macrophage polarisation (de Oliveira and Wilson, 2020, McDermott et al., 2005). Thus, the persistence of our functionally polarised macrophage states in response to corneal microenvironment signals are crucial in our macrophages-based therapy. The findings of the stability of macrophage polarisation states are controversial. For example, it was shown when GM-CSF differentiated M1 and M-CSF differentiated M2 macrophages stimulated with LPS or LPS and IFN-γ, M-CSF differentiated M2 exhibited slightly similar expression level of some of M1 markers, but they failed to produce pro-inflammatory cytokines, such as IL24 and IL12p40 (Verreck et al., 2004, Verreck et al., 2006), or released a lower level as compared to GM-CSF differentiated M1 (Jaguin et al., 2013). Furthermore, a study found that macrophages activated by LPS and IFN-γ did not switch to M2 when treated with IL-4 in vitro (Van den Bossche et al., 2016).

However, other studies found that M1 and M2 undergo phenotypic and functional repolarisation in response to opposing stimulatory cytokines. For instance, M2 macrophages stimulated with LPS and IFN-γ can repolarise towards an M1-like phenotype (Tarique et al., 2015, Xu et al., 2013). These controversial findings could be attributed to several factors related to the methods of macrophage differentiation from human monocytes, as mentioned in the previous chapter. For example, Chen et al. (2015) examined the effects of cell detachment techniques, including enzymatic and enzymatic-free solutions, on macrophage surface markers and function using human monocyte-derived M1 and M2 macrophages in vitro. Enzymatic approaches influence CD14, CD206, and CD163 expression levels and the function of CD206 and CD163 when compared with non-enzymatic methods (Chen et al., 2015).

Thus, characterisation of our macrophage phenotype and assessment of the stability of their polarisation states are essential before their application as cell therapy for the prevention of corneal scarring.

The aim of this chapter is to determine the persistence and reversibility of M1 and M2 polarisation states when they are subjected to subsequent stimuli with opposing effects in an attempt to mimic the sequential phases of the corneal healing mechanism.

We employed a next-generation sequencing (NGS) technology called RNA-seq to transcriptionally profile our generated subsets of macrophages and assess their polarisation states. To our knowledge, there was no study assessing the stability of polarisation states using RNA-seq.

From the human monocytes of seven healthy donors, we derived both M1 (I, II, and III) and M2 (I, II, and III) macrophages **(Figure 4.1)** to minimise the variability and enhance the reliability of our differential gene expression analysis and consequently downstream analysis (Lamarre et al., 2018, Conesa et al., 2016). Following RNA isolation, purified RNAs were submitted to the Genomics Birmingham Service at the University of Birmingham for library preparation and generation of the sequencing data.

Briefly, the region close to the 3' end of mature mRNA was captured and processed for library preparation and single-end sequencing (Moll et al., 2014). Following QC assessment by the Genomic Centre, we performed pre-processing steps, including from trimming adaptors and reads with low-quality alignment and mapping on the human genome (GRCh38) to gaining metrics for the gene expression level (count table) using the LEXOGEN Pipeline on the BlueBee® Genomics Platform. These raw

reads of gene expression levels were used as input for differential gene expression and pathway analysis using R software.

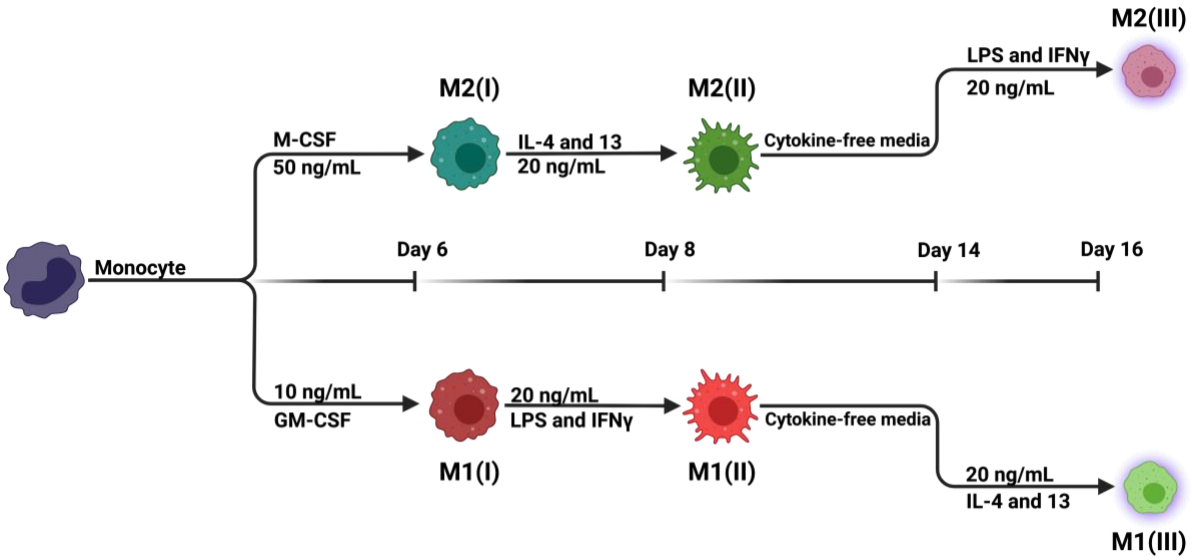

Figure 4.1 Schematic description of the polarisation model to generate subset of monocyte-derived macrophages.
Primary human monocytes were isolated and matured into both M1 (I) and M2 (I) macrophages using 10 ng/mL of GM-CSF and 50 ng/mL of M-CSF growth factors, respectively. On day 6, M1 (I) and M2 (I) were either harvested or stimulated with 20 ng/mL LPS and IFN-γ and IL-4 and IL-13 for 2 days to generate M1 (II) and M2 (II), respectively. M1 (II) and M2 (II) were either harvested or maintained in cytokines-free media for 6 days, followed by stimulation with contrasting cytokines (20 ng/mL IL-4 and IL-13 and LPS and IFN-γ for 2 days) to produce M1 (III) and M2 (III), respectively. The figure was drawn using BioRender.com.

4.2. Results

4.2.1. An overview of gene expression variability across six subsets of M1 and M2 macrophages

Before proceeding with downstream analysis, we assessed the quality of our data at a global level. This includes evaluating variances and correlations among samples from either the same or different populations of macrophages to identify the outliers. We performed principal component analysis (PCA), which is an approach to represent the expression values of individual genes for each sample in a single plot to facilitate the capture of the entire variation of gene expression values among samples and different conditions (Koch et al., 2018, Steinbaugh et al., 2017). Regularised logarithm transformation of the expression values of individual genes for each sample are used as input for PCA.

Pearson's correlation was used to determine the similarity and dissimilarity among all samples from either the same or different populations of macrophages by clustering them according to their similarity to each other. This method used the transformation of normalised expression values as input for the analysis to produce a range from -1 to 1, where one indicated the high similarity, that were presented as a heatmap (Koch et al., 2018, Steinbaugh et al., 2017). These analyses significantly enhance statistical power and consequently the reliability and reproducibility of our findings (Koch et al., 2018, Steinbaugh et al., 2017).

PCA showed how each subset of M1 and M2 macrophages separated and clustered together, demonstrating overall similarity and variation across M1 and M2 macrophages **(Figure 4.2).** This showed a difference in the gene expression profiles among the six populations of M1 and M2 macrophages, which is attributed to the type

of growth factor and pro-and anti-inflammatory stimuli. While PC1 explained 52% of the total variance among the six populations, which separated M1 (II) and M2 (III) from the remaining populations, PC2 showed 15%, particularly separating M2 (I) from M1 (III). M1 (I) and M2 (I) clustered independently of each other, while M1 (II) and M2 (III) clustered together, illustrating the impact of LPS and IFN-γ stimulation on their gene expression profiles. Similarly, the effect of IL-4 and IL-13 stimulation was observed in the M1 (III) and M2 (II) subsets, where they clustered on the same side of the PCA plot, indicating similarity of their transcriptional expression.

Consistent with PCA, Pearson's correlation analysis showed that most of the samples that were treated with the same stimuli clustered together, suggesting the effect of the type of stimuli on their gene expression profile, as shown in **Figure 4.3**. The high similarity between M1 (II) and M2 (III) suggests the significant impact of LPS and IFN-γ stimulation on their polarisation states.

To visualise the variation in gene expression across individual genes, we determined the top 100 highly variable genes across the six subsets of macrophages and presented them as a heatmap, as shown in **Figure 4.4.** Stimulation of both M1 (II) and M2 (III) with LPS and IFN-γ leads to the upregulation of considerable numbers of genes in both subsets and ultimately their clustering together, as suggested by the PCA plot (**Figure 4.2**). These upregulated genes in M1 (II) and M2 (III) subsets are encoded for pro-inflammatory cytokines, chemokines, or transcription factors such as *IL12β*, *CXCL9,10, CCL5*, or Interferon Regulatory Factor 1 (*IRF1*), respectively, suggesting a higher level of similarity in their transcriptional profiles. In contrast, stimulation of both M2 (II) and M1 (III) with IL-4 and IL-13 cytokines resulted in upregulation of genes related to the M2 macrophage phenotype, such as monoamine oxidase A (MAOA)

(Cathcart and Bhattacharjee, 2014), CCL22, and arachidonate 15-Lipoxygenase (ALOX15*)*, and a reduction in expression of pro-inflammatory-related genes, leading to their clustering away for LPS and IFN-γ-stimulated subsets.

Together, these results show that the variance in gene expression profiles across both M1 and M2 subsets was, to some extent, driven by the type of stimuli, indicating the good quality of the data. However, the effect of the type of stimuli on the macrophages polarisation states needs to be confirmed by assessing differentially expressed genes (DEG) among the M1 and M2 subsets and their associated biological functions.

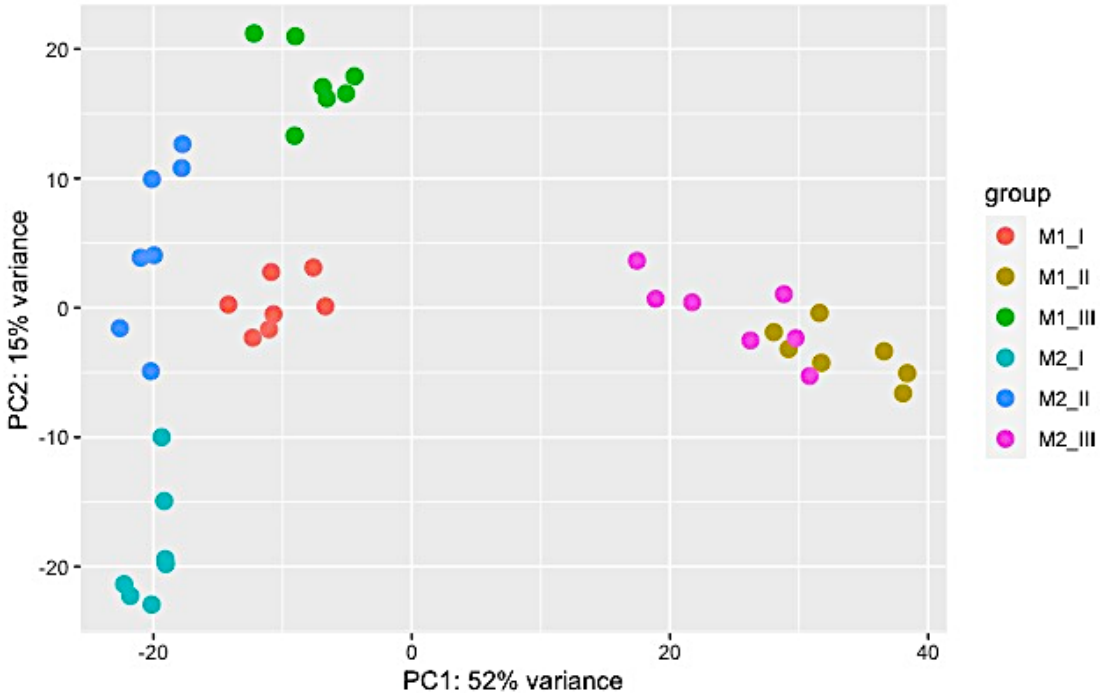

Figure 4.2 An overview of the variation in gene expression profiles across samples from the M1 and M2 subsets.
Macrophage subpopulations were generated from primary human monocytes. The mRNA of these subpopulations was captured and sequenced on the Illumina platform, followed by mapping sequencing reads on the human genome to finally obtain expression values. Regularised logarithm transformation(rlog) of raw data was calculated using DESeq2 analysis to perform PCA. A two-dimensional plot of PC1 and PC2 showed the gene expression variation among all seven biological replicates across six subsets of macrophages. (n = 7).

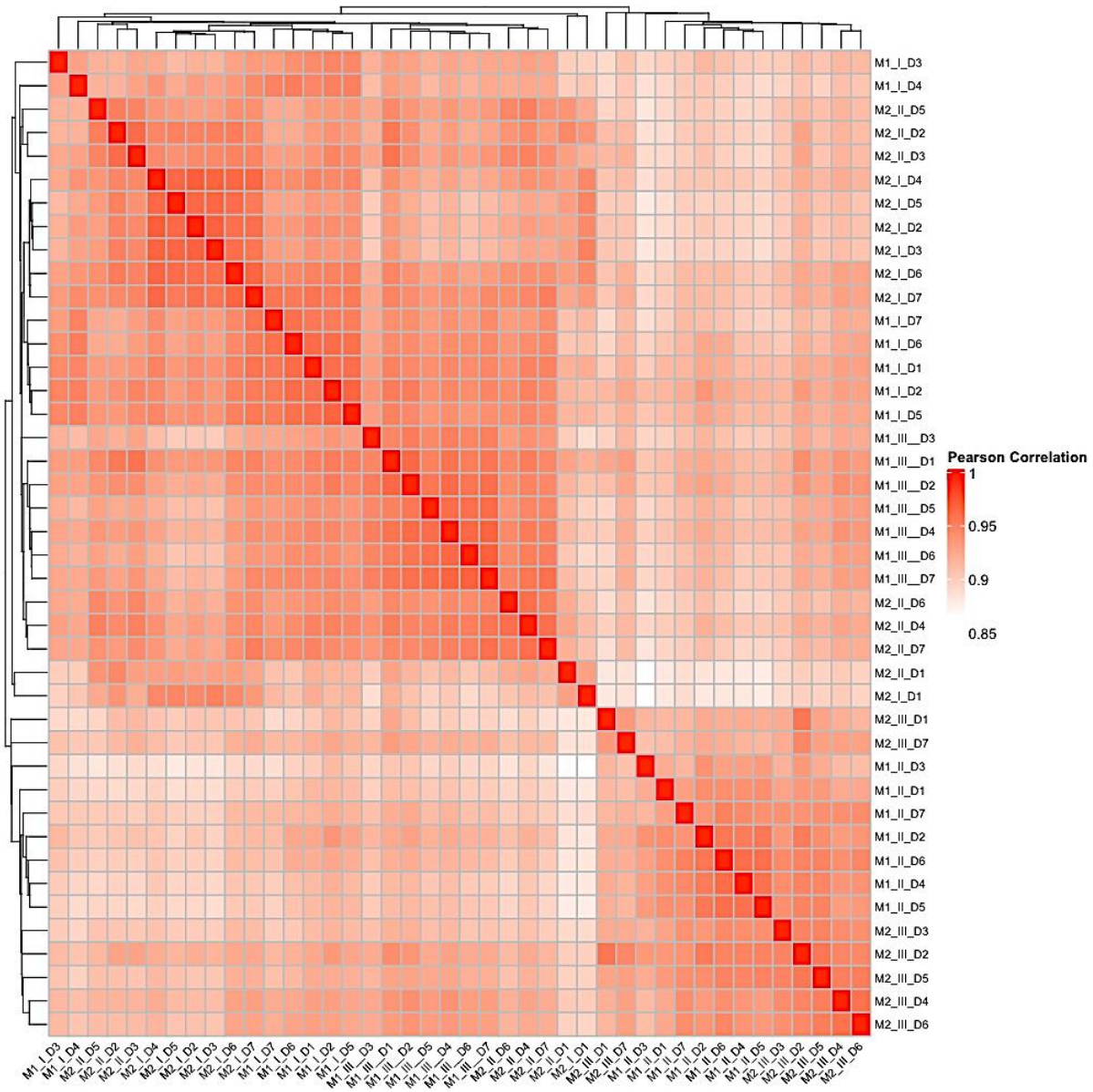

Figure 4.3 An overview of the similarities in gene expression profiles across samples from the M1 and M2 subsets.

Macrophage subpopulations were generated from primary human monocytes. The mRNA of these subpopulations was captured and sequenced on the Illumina platform, followed by mapping sequencing reads on the human genome to finally obtain expression values. Log2 of normalised counts+1 was calculated using DESeq2 analysis to perform Pearson's correlation analysis. The heatmap displayed a correlation (r) among all seven biological replicates across six subsets of macrophages. The colour intensity of the heatmap reflects the level of correlation (r), with darker red indicating a higher level of similarity. (n = 7).

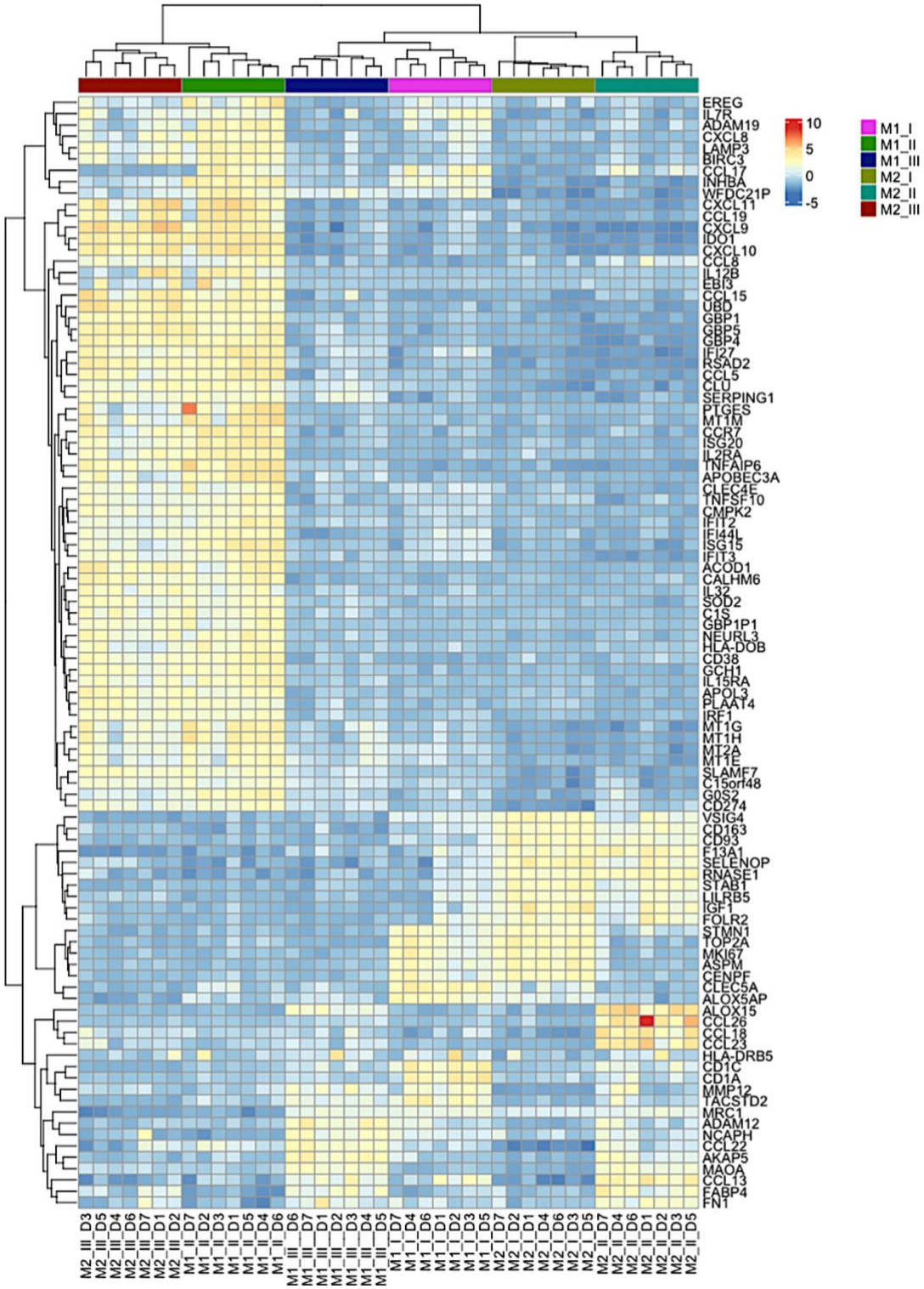

Figure 4.4 Top 100 highly variable genes across M1 and M2 subpopulations.
Macrophage subpopulations were generated from primary human monocytes. The mRNA of these subpopulations was captured and sequenced on the Illumina platform, followed by mapping sequencing reads on the human genome to finally obtain expression values. Rlog of raw data was calculated using DESeq2 analysis to identify the top variable genes across all subpopulations of macrophages. Heatmap with hierarchical clustering of the 100 highly variable genes across subpopulations (n = 7).

4.2.2. Transcriptional differences between the M1 and M2 subpopulations.

As M1 (I) and M2 (I) were previously used to investigate the biocompatibility of gellan fluid gel, we aim to transcriptionally characterise them by investigating variation in their gene expression. Additionally, we explored transcriptional variation between M1 (II) and M2 (II).

4.2.2.1. Comparative analysis of differentially expressed genes and enrichment analysis between M1 (I) and M2 (I) subsets, as well as between M1 (II) and M2 (II) subsets.

We visualised the global differences between the four populations, including M1 (I), M2 (I), M1 (II) and M2 (II), by identifying the top 100 variable genes, as described in **Figure 4.5.** As expected, the expression level of LPS and IFN-γ-induced genes, such as *CXCL9*, *CXCL10*, *CXCL11*, and guanylate-binding protein (*GBP*) (1,4,5), and *IL12β*, was higher in M1 (II), indicating the enhancement of their pro-inflammatory phenotype. Conversely, higher expression levels of IL-4 and IL-13-induced genes, such as *CCL26*, *ALOX15*, *CCL18*, and *CCL23*, were observed in M2 (II), similarly showing their anti-inflammatory features **(Figure 4.5).**

M2 marker gene expression, including *CD163*, *CD209*, and Insulin-Like Growth Factor 1 (*IGF1*), was increased in both M2 (I) and M2 (II), leading to their clustering together. In contrast, genes related to M1 macrophages, *IL7R* and (Inhibin Subunit Beta A (*INHBA*) (Martinez et al., 2006), exhibited a higher level of induction in M1 (I) and M1 (II) **(Figure 4.5).**

Next, we performed the differential expression analysis between M1 (I) and M2 (I). A total of 747 DEGs were identified, of which 384, *INHBA*, *CCL17* and *MMP12* were upregulated in M1 (I), while 363, such as Legumain (*LGMN*), Intersectin-1 (*ITSN1*), the v-Maf Avian Musculoaponeurotic Fibrosarcoma Oncogene Homolog B (*MAFB*), and *CD93*, were upregulated in M2 (I) **(Figure 4.6a**). Like M1 (I) and M2 (I), 1966 DEGs between M1 (II) and M2 (II) were identified, indicating the significant transcriptional distinction between M1 (II) and M2 (II), as shown in **Figure 4.6b.**

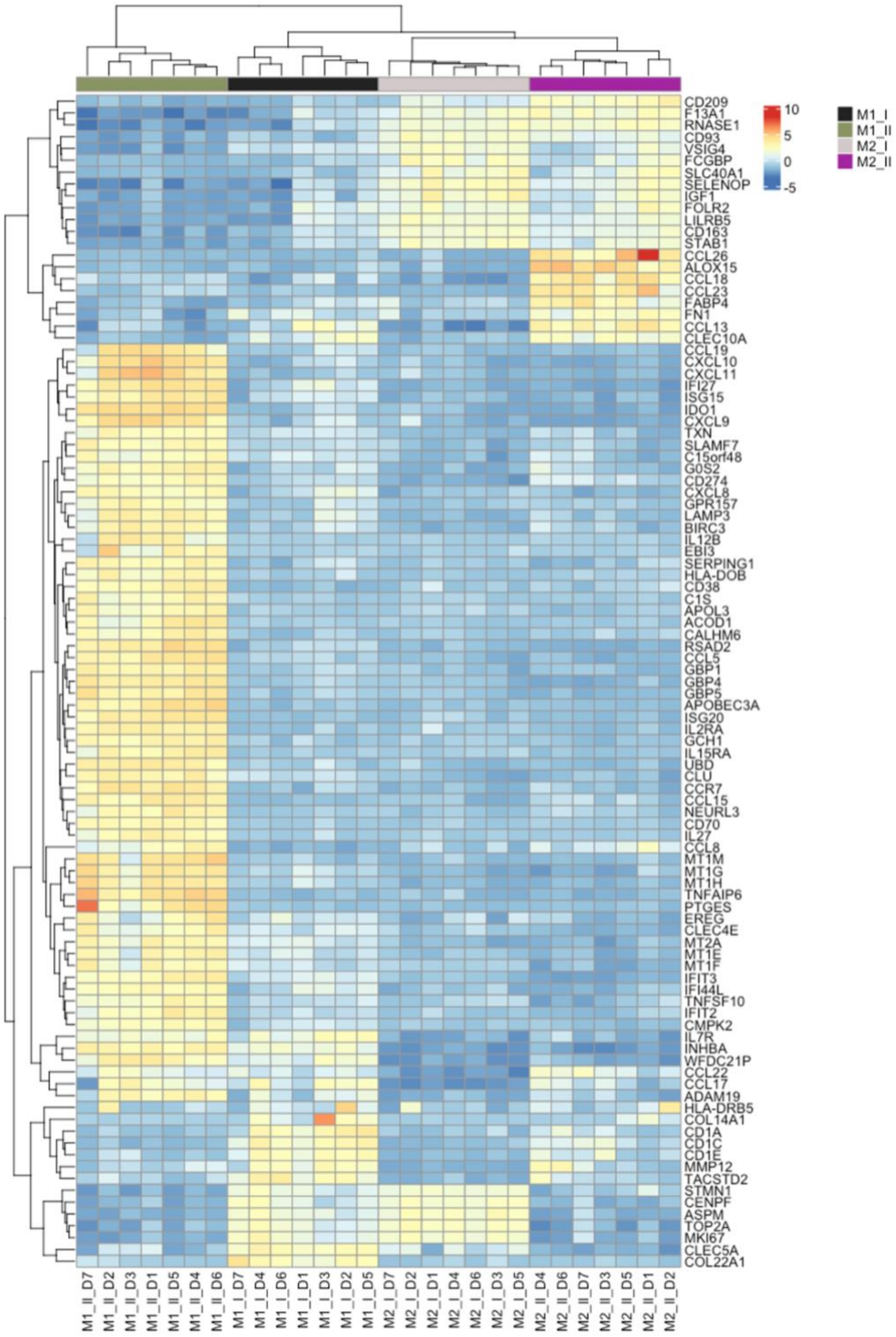

Figure 4.5 Top 100 highly variable genes between M1 (I), M1 (II), M2 (I) and M2 (II).

Rlog of raw data was calculated using DESeq2 analysis to identify the top variable genes across M1 (I), M1 (II), M2 (I) and M2 (II) subsets. Heatmap with hierarchical clustering of the 100 highly variable genes across subpopulations (n = 7).

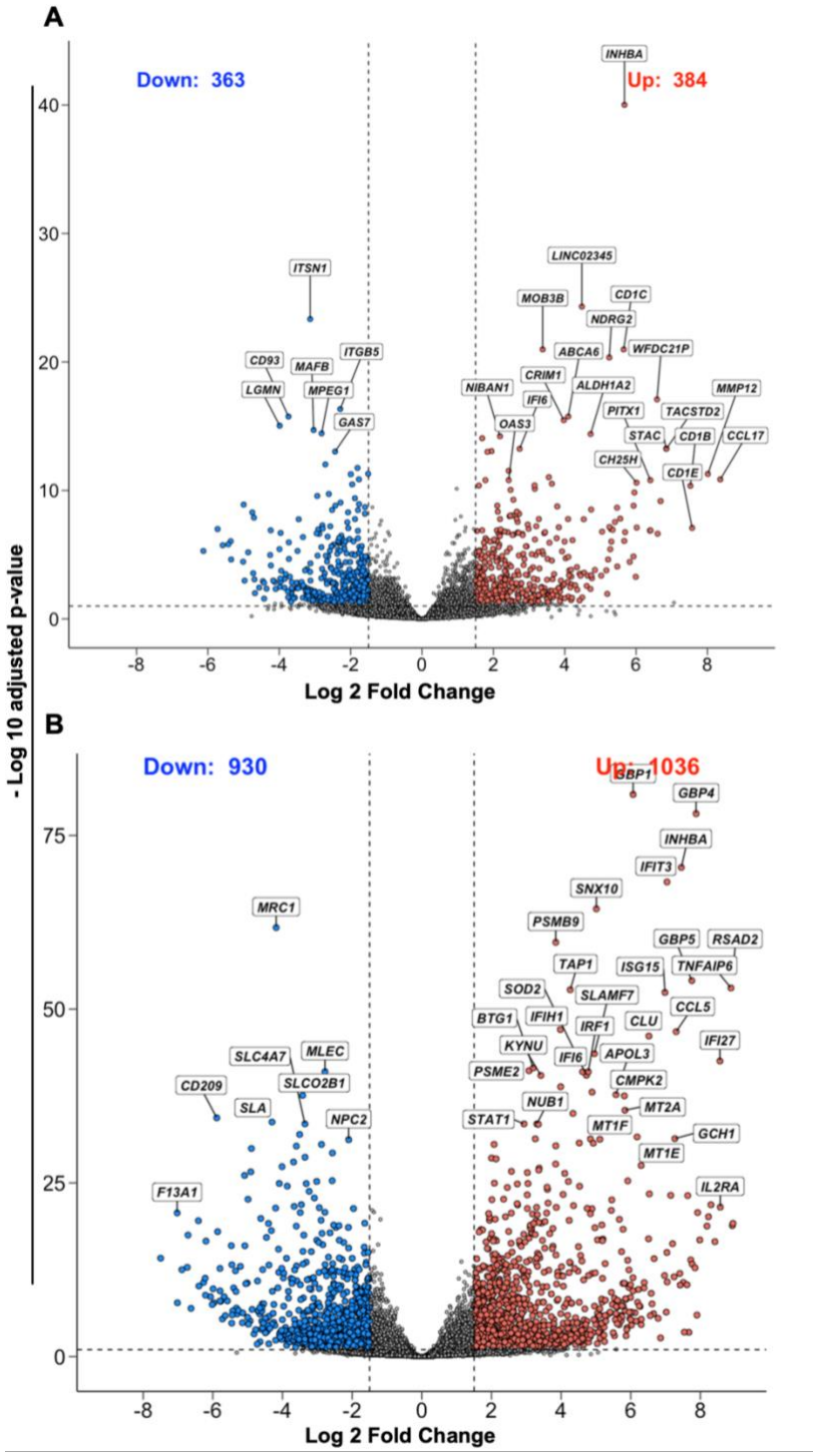

Figure 4.6 Differentially expressed genes between M1 (I) and (II) as well as between M1 (II) and M2 (II).

The normalised expression values were used to perform the differential gene expression analysis using DESeq2 analysis. Significantly up or downregulated genes were defined based on the following: (padj <0.05) and (log2 FC=>1.5 or =<-1.5), respectively. **(A)** Volcano plot of upregulated genes in M1 (I) versus M2 (I), depicted in red (**384)**, and downregulated genes in M1 (I), depicted in blue (**363)**. (**B)** volcano plot of upregulated genes in M1 (II) versus M2 (II), depicted in red (**1036)**, and downregulated genes in M1 (II), depicted in blue (**930)**. (n = 7).

Following the identification of DEGs, these genes were subjected to gene set enrichment analysis (GSEA) for hallmark pathways to determine the associated biological phenotype linked with these genes. Comparative analysis of hallmark pathway analyses between M1 (I) and M2 (I) showed that DEGs in M1 (I) were associated with significant upregulation of inflammatory pathways, including interferon gamma response and allograft rejection pathways, as shown in **Figure 4.7a.** No significant downregulated hallmark pathways were detected in M1 (I) compared to M2 (I) (**Figure 4.7a)**. Regarding enrichment of the upregulated genes in the Kyoto Encyclopaedia of Genes and Genomes (KEGG) pathway analysis, hematopoietic cell lineage, rheumatoid arthritis, and cytokine-cytokine receptor interaction pathways were significantly upregulated in M1 (I) as compared to M2 (I) **(Figure 4.8a)**. However, significant downregulation of the complement and coagulation cascade pathways was associated with downregulated genes in M1 (I) **(Figure 4.8b)**.

Interferon gamma and alpha, inflammatory response, TNFA signalling via NF-$_K$B, NOD-like receptor signalling and viral infection response in Hallmark and KEGG analyses were significantly upregulated in M1 (II) as compared to M2 (II), demonstrating the enhancement of their pro-inflammatory properties **(Figure 4.7b; Figure 4.8c)**. Similarly, significantly downregulated genes in M1 (II), which are upregulated in M2 (II), are associated with upregulated pathways such as hematopoietic cell lineage, amoebiasis, and cell adhesion molecules **(Figure 4.8d).** These findings showed transcriptional differences between M1 (I) verses M2 (I) as well as M1 (II) verses M2 (II)

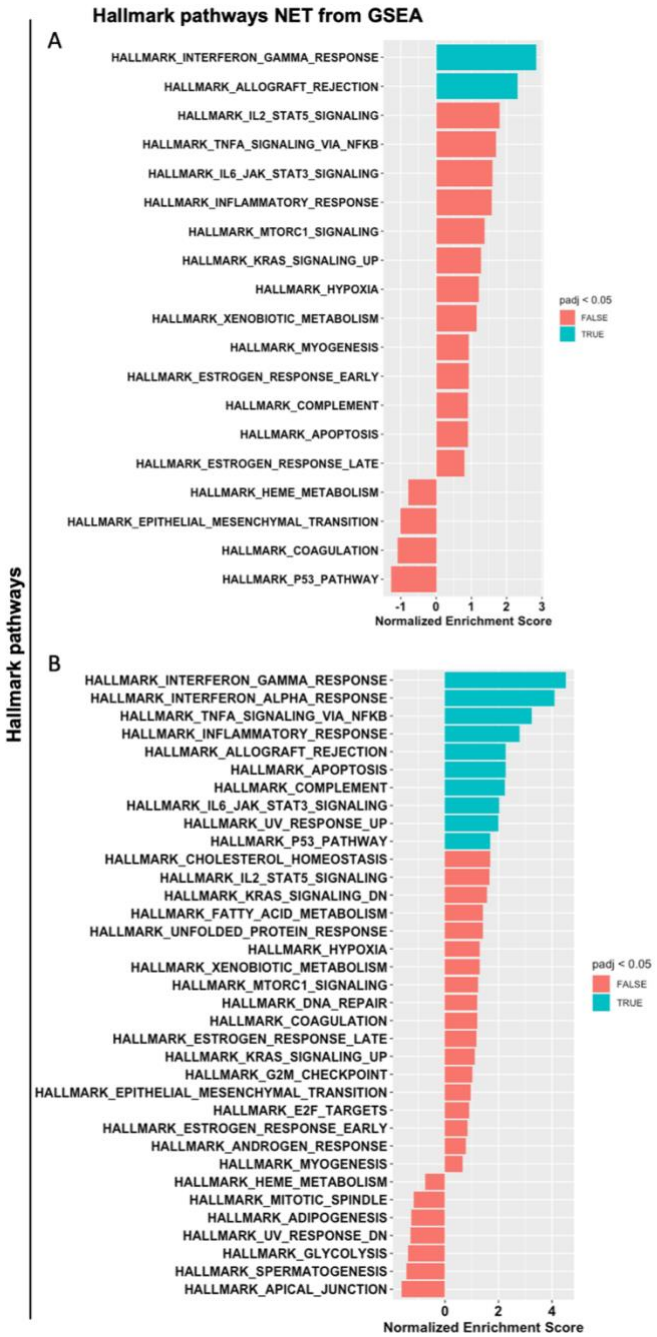

Figure 4.7 Up and downregulated hallmark pathways between M1 (I) and M2 (I) as well as between M1 (II) and M2 (II).

The normalised expression values were used to perform the differential gene expression analysis using DESeq2 analysis. Significantly up or downregulated genes were defined based on the following: (padj <0.05) and (log2 FC=>1.5 or =<-1.5), respectively. The list of genes was ranked according to log2 FC and padj and used as input for enrichment analysis of Hallmark pathways via GSEA. The upregulated hallmark pathways have the highest normalised enrichment score (NES), while the lowest NES is with the downregulated pathways. The green colour (true) is the significant pathway (padj <0.05), while the red colour (false) being for non-significant. **(A)** significant hallmark pathways in **M1 (I) vs. M2 (I)**. (**B)** significant hallmark pathways in **M1 (II) vs. M2 (II)** (n = 7).

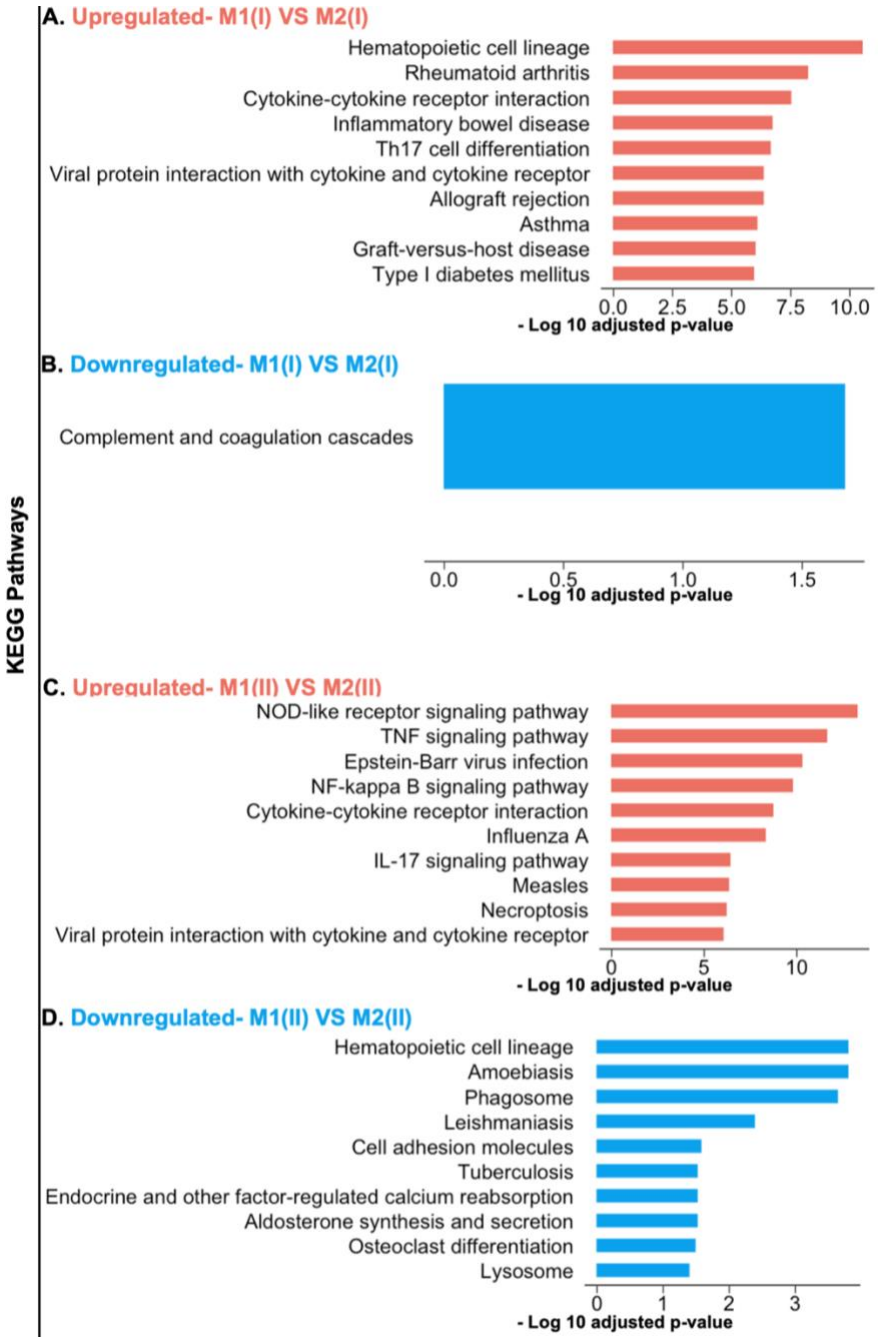

Figure 4.8 Up and downregulated KEGG pathways between M1 (I) and M2 (I) as well as between M1 (II) and M2 (II).

The normalised expression values were used to perform the differential gene expression analysis using DESeq2 analysis. Significantly up or downregulated genes were defined based on the following: (padj <0.05) and (log2 FC=>1.5 or =<-1.5), respectively. **(A)** the upregulated KEGG pathways that are associated with upregulated genes in M1 (I) vs. M2 (I). **(B)** the downregulated KEGG pathways that are associated with upregulated genes in M1 (I) vs. M2 (I). (**C)** the upregulated KEGG pathways that are associated with upregulated genes in M1 (II) vs. M2 (II). **(D)** the downregulated KEGG pathways that are associated with upregulated genes in M1 (II) vs. M2 (II) (n = 7).

4.2.3. Differential gene expression analysis and the corresponding biological pathways across M1 subpopulations

We performed differential expression analysis on M1 subsets of macrophages to phenotype these cells and subsequently investigate the stability of their polarisation states. Initially, we visualised variable genes between three populations of M1 macrophages to have a global view of the differences resulting from sequential stimulation with GM-CSF, followed by LPS and IFN-γ, and finally IL-4 and IL-13 (**Figure 4.1**). Genes associated with pro-inflammatory cytokines and chemokines, such as IL1β and IL12β and CXCL9, CXCL10 and CXCL11, respectively, were highly expressed in M1 (II) as compared to M1 (I) and M1 (III), confirming their activation via LPS and IFN-γ cytokines (**Figure 4.9).** However, when these cells were left without stimulation and then stimulated with IL-4 and IL-13 cytokines for 2 days, a reduction in the expression level of LPS and IFN-γ induced genes and increased expression of Th2 cytokine induced genes such as MAOA, TGM2, and ALOX15 (Martinez et al., 2006, Snodgrass et al., 2021) were observed in M1 (III) as compared to M1 (II) and M1 (I). These findings may indicate a potential continuous change in the polarisation states of M1 in response to different stimuli.

We investigate this observation further by conducting differential expression analysis to identify statistically significant genes between M1 subsets of macrophages. These DEGs were then subjected to downstream analysis, including GSEA and KEGG, to detect their associated biological processes or pathways.

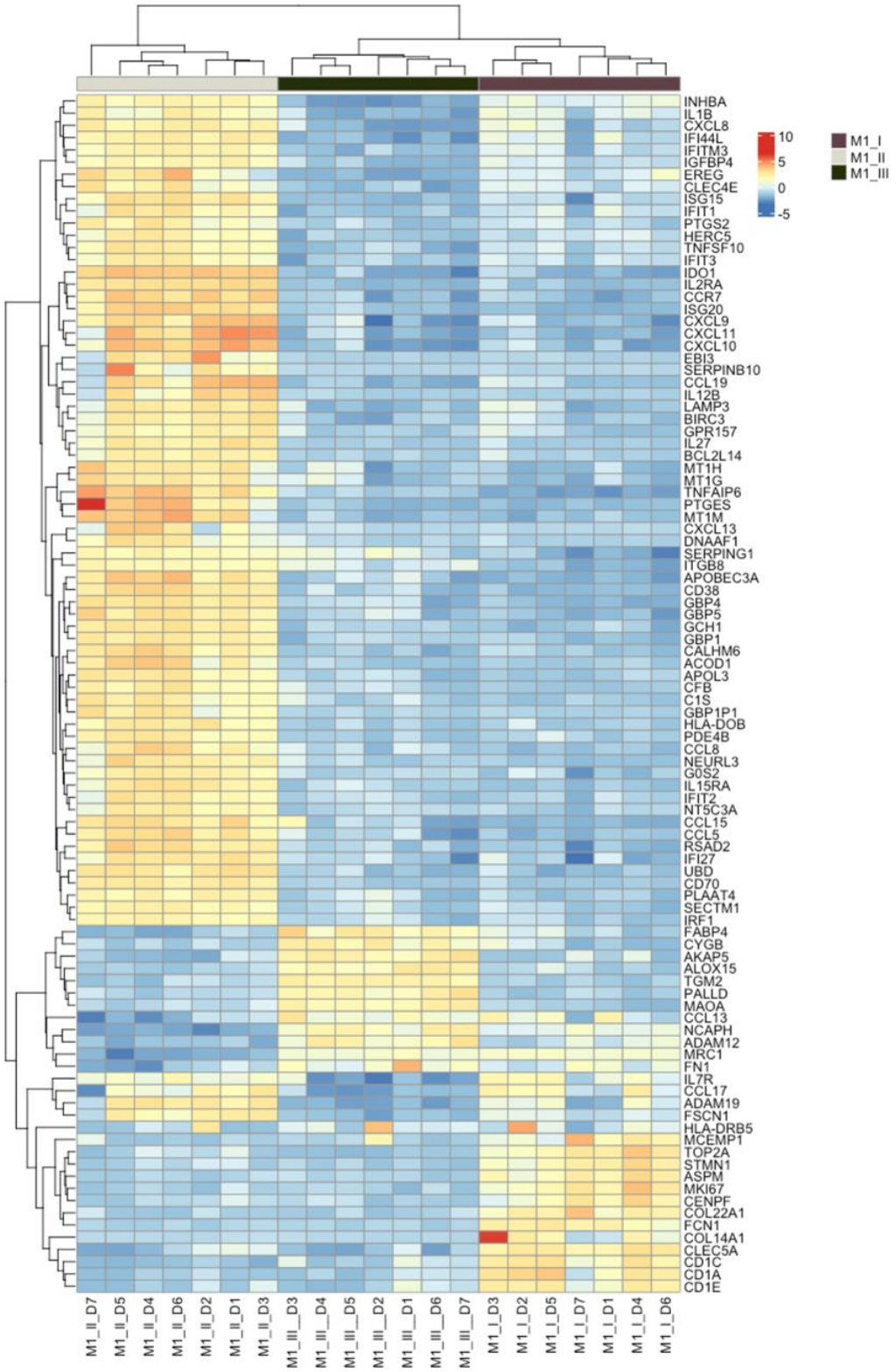

Figure 4.9 Top 100 highly variable genes between M1 (I), M1 (II), and M1 (III). Rlog of raw data was calculated using DESeq2 analysis to identify the top variable genes across M1 (I), M1 (II), and M1 (III) subsets. Heatmap with hierarchical clustering of the 100 highly variable genes across subpopulations (n = 7).

4.2.3.1. Differentially expressed genes and their enrichment analysis between M1 (II) and M1 (I).

To confirm inflammatory activation of M1 (II) by LPS and IFN-γ stimulation, we initially compared M1 (II) versus M1 (I) to identify the significant upregulated and downregulated genes. We define differentially expressed genes as statistically significant up or down regulated genes in our study if they exhibit an adjusted p-value (padj) less than 0.05 and a log2 fold change (log2 FC) equal to or higher than 1.5 or equal less than -1.5, respectively. To gain a biologically meaningful understanding of these differentially expressed genes, we performed downstream analysis, including GSEA and KEGG, using these statistically significant up or down-regulated genes as input. These analyses will provide the potential differences among these subsets, M1 (II) versus M1 (I).

To identify the difference between M1 (I) and M1 (II), the same cells following stimulation with LPS and IFN-γ (**Figure 4.1)**, we visualised the top 50 variable genes among M1 (II) and M1 (I) and found that stimulation with LPS and IFN-γ highly induced inflammation-related genes such as CD38 (Amici et al., 2018), IL12β, CXCL9, CXCL10, and CXCL11 in M1 (II), confirming the efficiency of the stimulation **(Figure 4.10).**

Our differential gene expression analysis found that the number of significant upregulated genes was 822 in M1 (II) following stimulation with LPS and IFN-γ as compared to M1 (I). In M(II), the expression level of genes such as, TNF-alpha-induced protein 6 (TNFAIP6), involved in inflammation (Wisniewski and Vilcek, 2004), and GBP1,4 and 5, which are induced by IFN-γ and have potent antimicrobial activity, are significantly increased (Amici et al., 2017), as shown in **(Figure 4.11).**

Next, DEGs were used to perform downstream analysis, including KEGG and GSEA, to recognise the biological pathways associated with these sets of genes and consequently the influence of LPS and IFNγ stimulation. GSEA analysis demonstrates that hallmark pathways such as the interferon gamma response, TNF-α signalling via NF-κB, and inflammatory responses were significantly upregulated in M1 (II) as compared to M1 (I) (**Figure 4.12).** Similarity, KEGG analysis showed that LPS and NF-γ stimulation significantly upregulate, viral infection, TNF signalling, and NOD-like receptor signalling pathways, suggesting that M1 (II) exhibited pro-inflammatory properties **(Figure 4.13).**

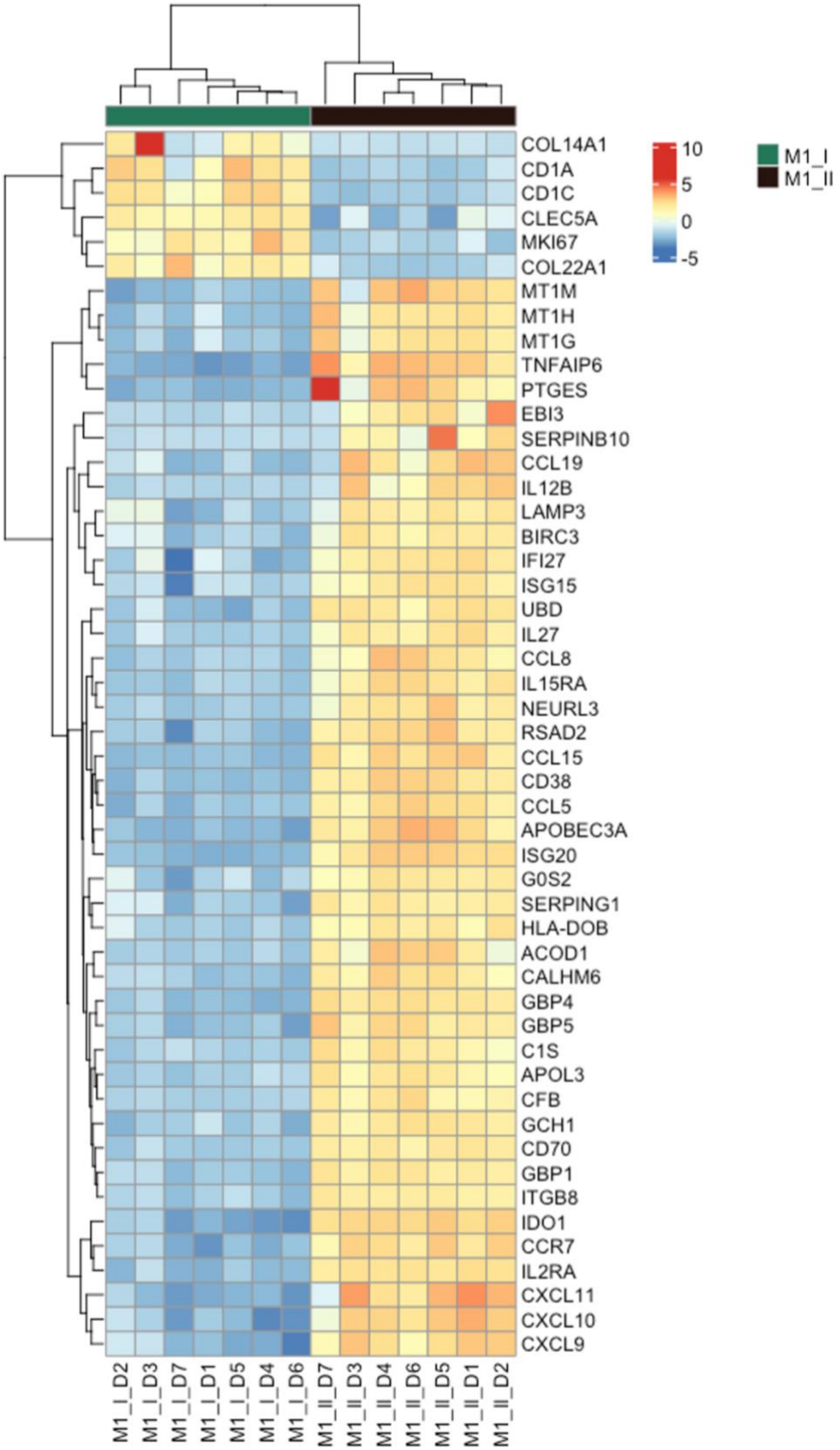

Figure 4.10 Top 100 highly variable genes between M1 (I) and M1 (II).
Rlog of raw data was calculated using DESeq2 analysis to identify the top variable genes between M1 (I), and M1 (II) subsets. Heatmap with hierarchical clustering of the 100 highly variable genes across subpopulations (n = 7).

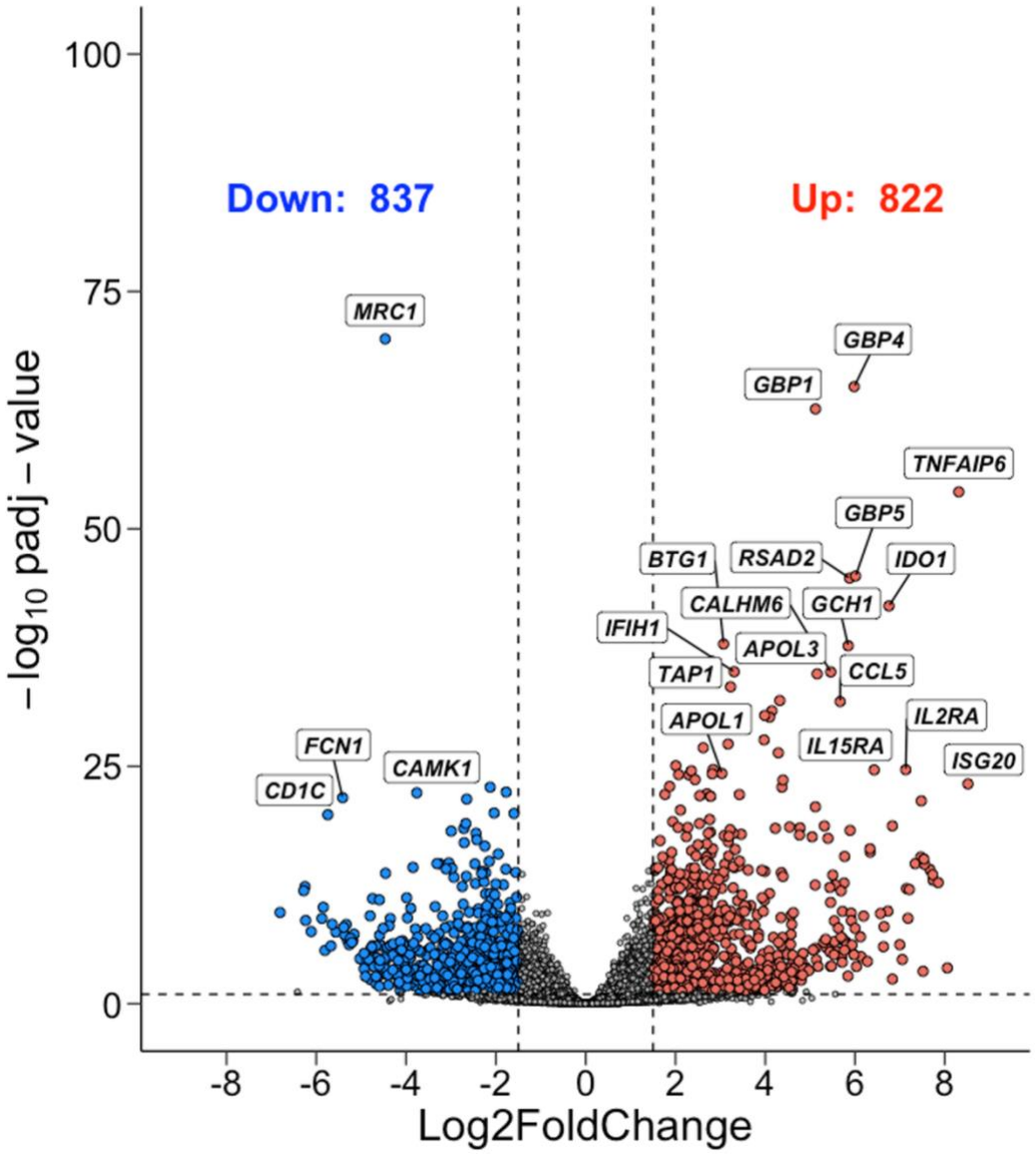

Figure 4.11 Differentially expressed genes between M1 (I) and M1 (II).
The normalised expression values were used to perform the differential gene expression analysis using DESeq2 analysis. Significantly up or downregulated genes were defined based on the following: (padj <0.05) and (log2 FC=>1.5 or =<-1.5), respectively. Volcano plot of upregulated genes in M1 (II) versus M1 (I), depicted in red (**822**), and downregulated genes in M1 (I), depicted in blue (**837**). (n = 7).

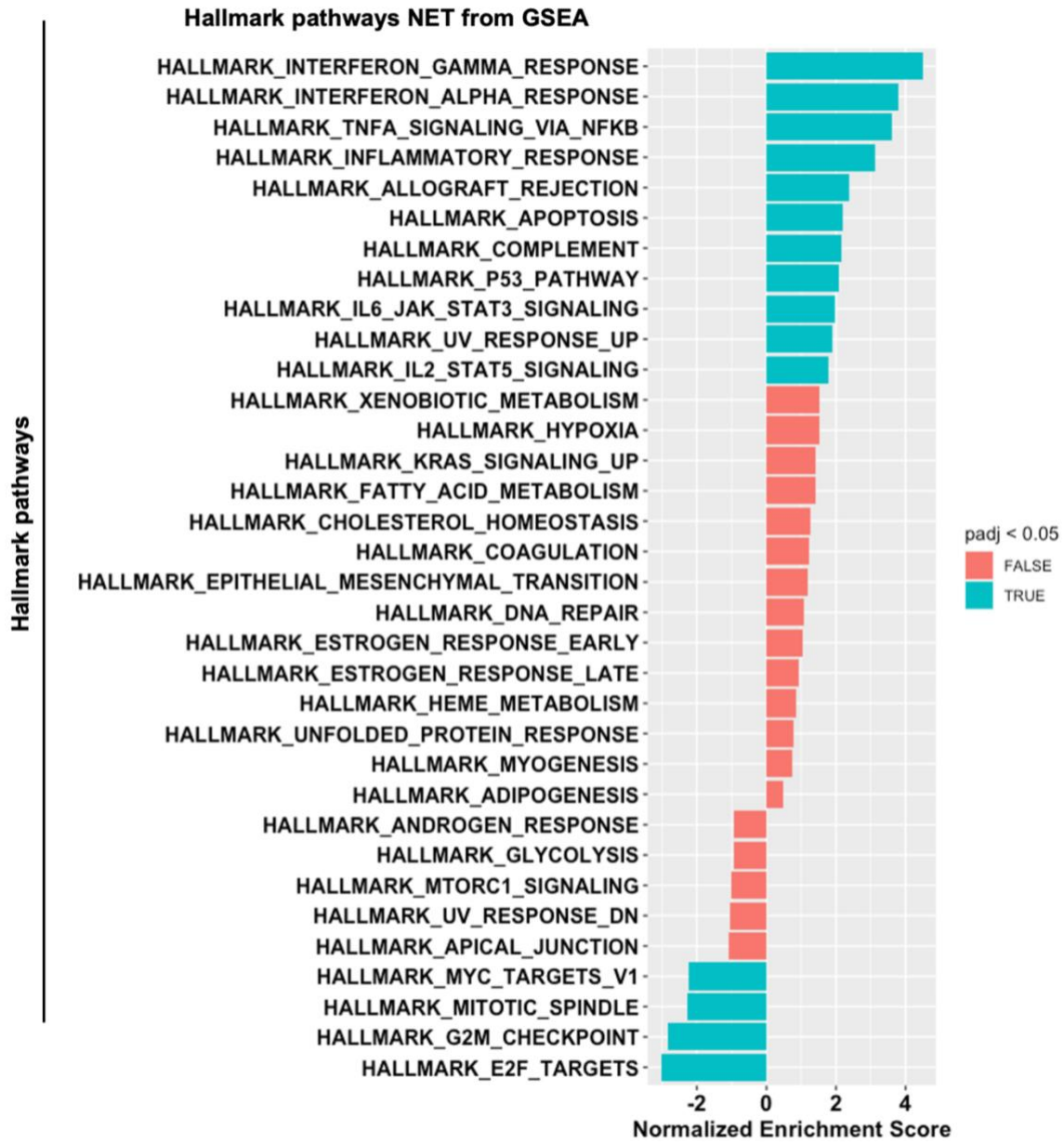

Figure 4.12 Up and downregulated hallmark pathways between M1 (II) and M1 (I).

The normalised expression values were used to perform the differential gene expression analysis using DESeq2 analysis. Significantly up or downregulated genes were defined based on the following: (padj <0.05) and (log2 FC=>1.5 or =<-1.5), respectively. The list of genes was ranked according to log2 FC and padj and used as input for enrichment analysis of Hallmark pathways via GSEA. The upregulated hallmark pathways have the highest normalised enrichment score (NES), while the lowest NES is with the downregulated pathways. The green colour (true) is the significant pathway (padj <0.05), while the red colour (false) being for non-significant. Significant hallmark pathways in **M1 (II) vs. M1 (I)**. (n = 7).

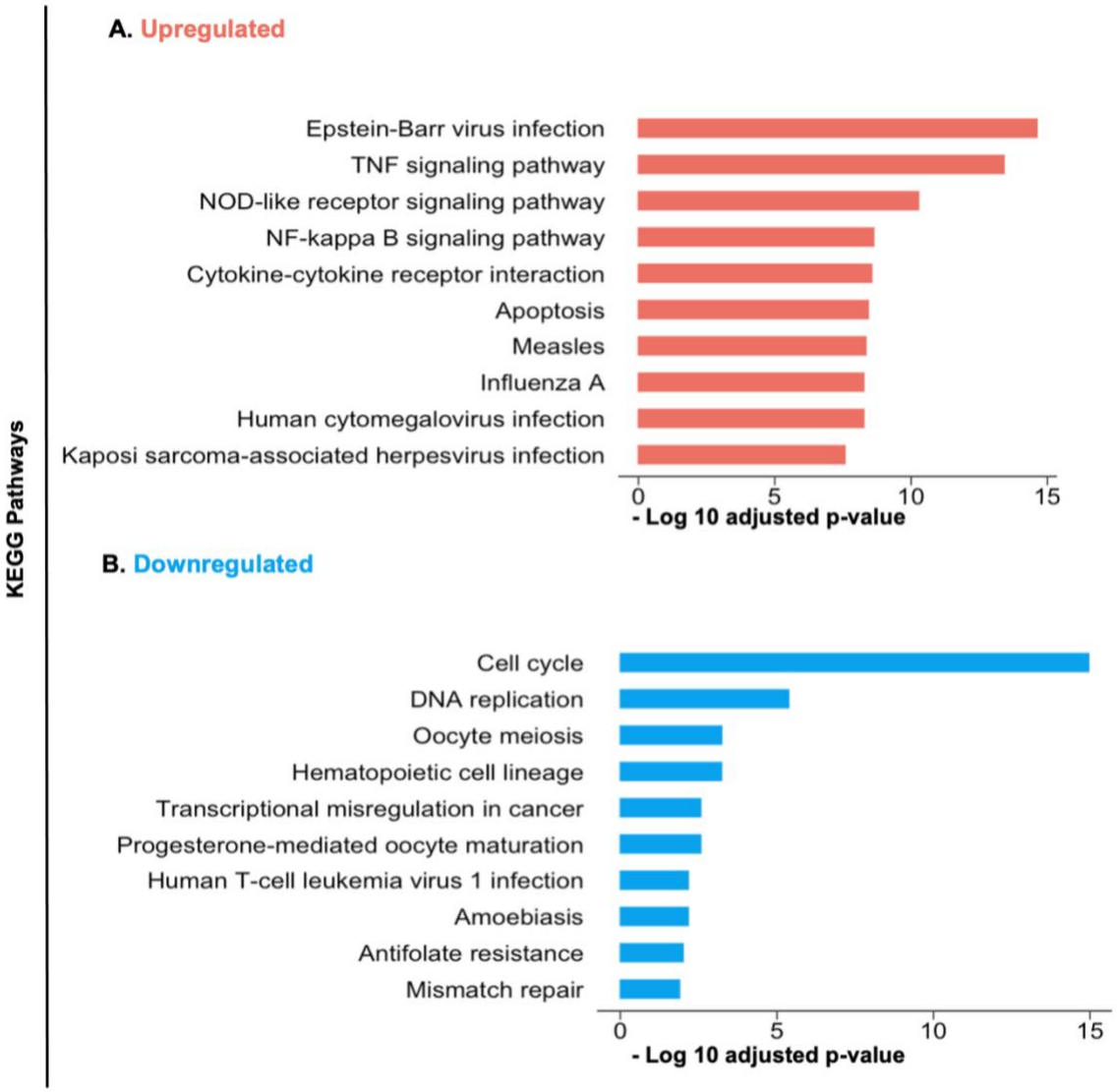

Figure 4.13 Up and downregulated KEGG pathways between M1 (II) and M1 (II).
The normalised expression values were used to perform the differential gene expression analysis using DESeq2 analysis. Significantly up or downregulated genes were defined based on the following: (padj <0.05) and (log2 FC=>1.5 or =<-1.5), respectively. **(A)** the upregulated KEGG pathways that are associated with upregulated genes in M1 (II) vs. M1 (I). **(B)** the downregulated KEGG pathways that are associated with upregulated genes in M1 (II) vs. M1 (I). (n = 7).

4.2.3.2. Differentially expressed genes and their enrichment analysis between M1 (III) and M1 (II).

Upon confirming the pro-inflammatory property of M1 (II) as compared to M1 (I), we sought to determine whether the polarisation state of these cells towards M1 was persistent in response to T-helper type 2 (Th2) cytokines, IL-4 and IL-13. Thus, we maintained M1 (II) in cytokine-free media for 6 days, followed by stimulation with IL-4 and IL-13 for 2 days, as shown in our experiment design. It is worth mentioning that the potential alterations in the polarisation states of M1 (III) are not exclusively attributed to T-helper type 2 (Th2) cytokine stimulation but also to the resting period in cytokine-free media. However, this combined effect still informs whether the polarisation states of macrophages are maintained or not.

Global distinctions among the M1 (III) and M1 (II) subsets were assessed by detecting the top 50 variable genes **(Figure 4.10).** We found that genes that exhibited a higher level of expression in M1 (II) versus M1 (I), including *CD38*, *IL12β*, *CXCL9*, *CXCL10*, and *CXCL11*, demonstrated a lower expression level in M1 (III) as compared to M1 (II), as shown in **Figure 4.14**.

Likewise, differential gene expression analysis in M1 (III) verses M1 (II) showed that several genes were significantly downregulated, such as *GBP1*, *GBP4* and *TNFAIP6*. Conversely, Th2 induced genes, including *MRC1* and *MAOA*, statistically downregulated in M1 (II), were found to be upregulated in M1 (III), as shown in **Figure 4.15.** Taken together, these findings indicated an anti-inflammatory or healing influence of IL-4 and IL-13 cytokines in M1 (III).

To determine the biological relevance of these changes in DEGs, enrichment analysis of these genes for the GSEA and KEGG pathways was performed. GSEA analysis

showed that the upregulated pathways in M1 (II), such as the interferon gamma response, TNFα signalling via NF-κB, and the inflammatory response, were significantly downregulated in M1 (III) as compared to M1 (II), as shown in **Figure 4.16**. In addition, heme metabolism and adipogenesis were significantly upregulated in M1 (III) compared to M1 (II). In line with this finding, KEGG findings showed that upregulated pathways in M1 (II), such as viral infection, the TNF signalling pathway, the NOD-like receptor, and Toll-like receptor signalling pathways, were downregulated in M1 (III) as compared to M1 (II) (**Figure 4.17).** Biological processes involved in phagocytosis and tissue homeostasis in the polarisation of macrophages towards M2, such as the lysosome, phagosome, and fatty acid metabolism pathways, were upregulated in M1 (III). M2 macrophages are characterised as having a potent phagocytic function to engulf apoptotic cells where phagosome and lysosome activity are involved (Roszer, 2015, Hirayama et al., 2017).

The aim of this chapter is to determine whether the polarisation states of our generated M1 and M2 macrophages are maintained or not. The current part of our study showed that maturation of blood monocytes by GM-CSF to produce M1 that was later fully activated by LPS and IFN-γ exhibited a pro-inflammatory transcriptome that seems to not be maintained as these upregulated transcripts and pathways are diminished following stimulation with IL-4 and IL-13.

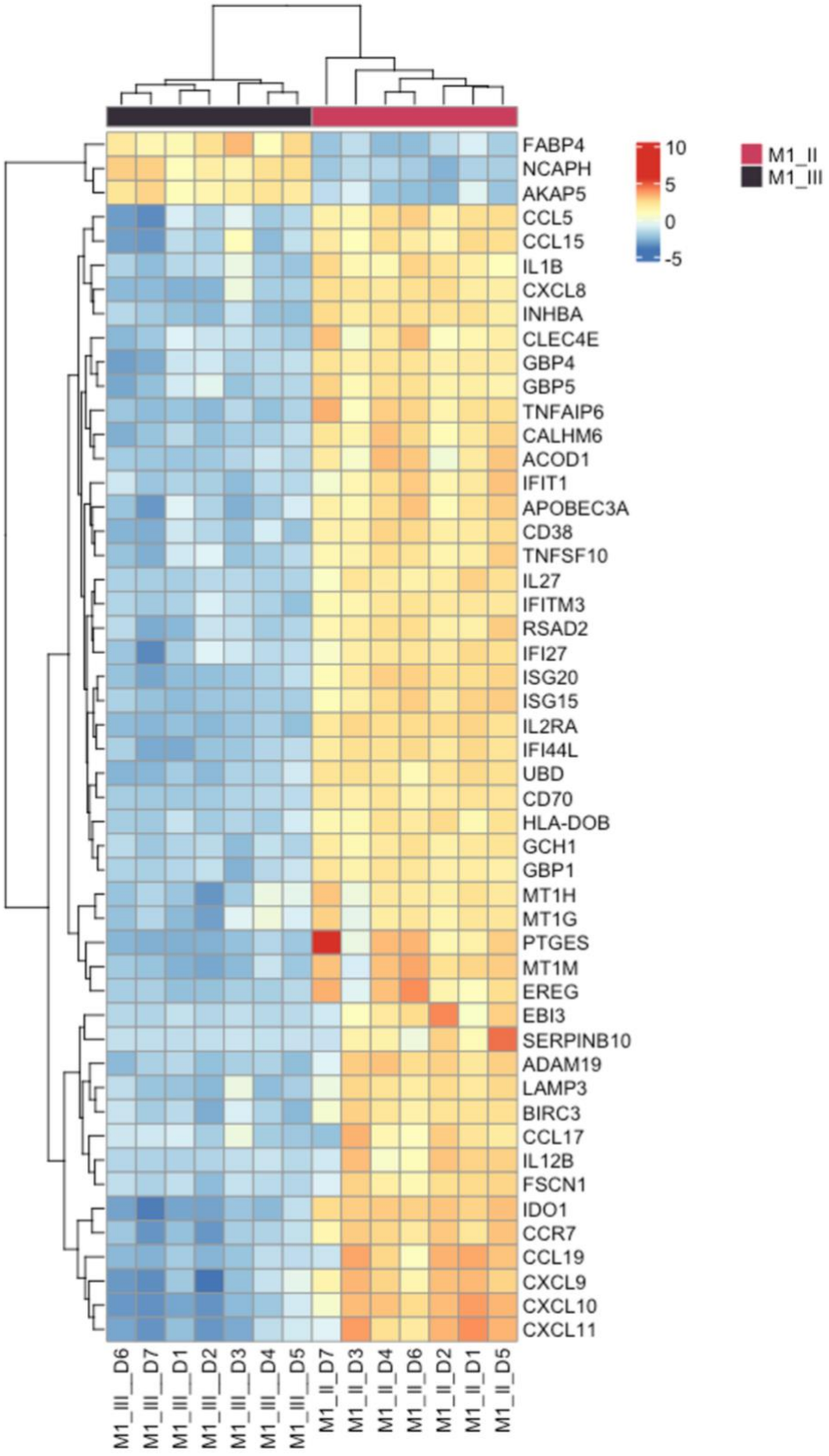

Figure 4.14 Top 100 highly variable genes between M1 (III) and M1 (II).
Rlog of raw data was calculated using DESeq2 analysis to identify the top variable genes between M1 (III), and M1 (II) subsets. Heatmap with hierarchical clustering of the 100 highly variable genes across subpopulations (n = 7).

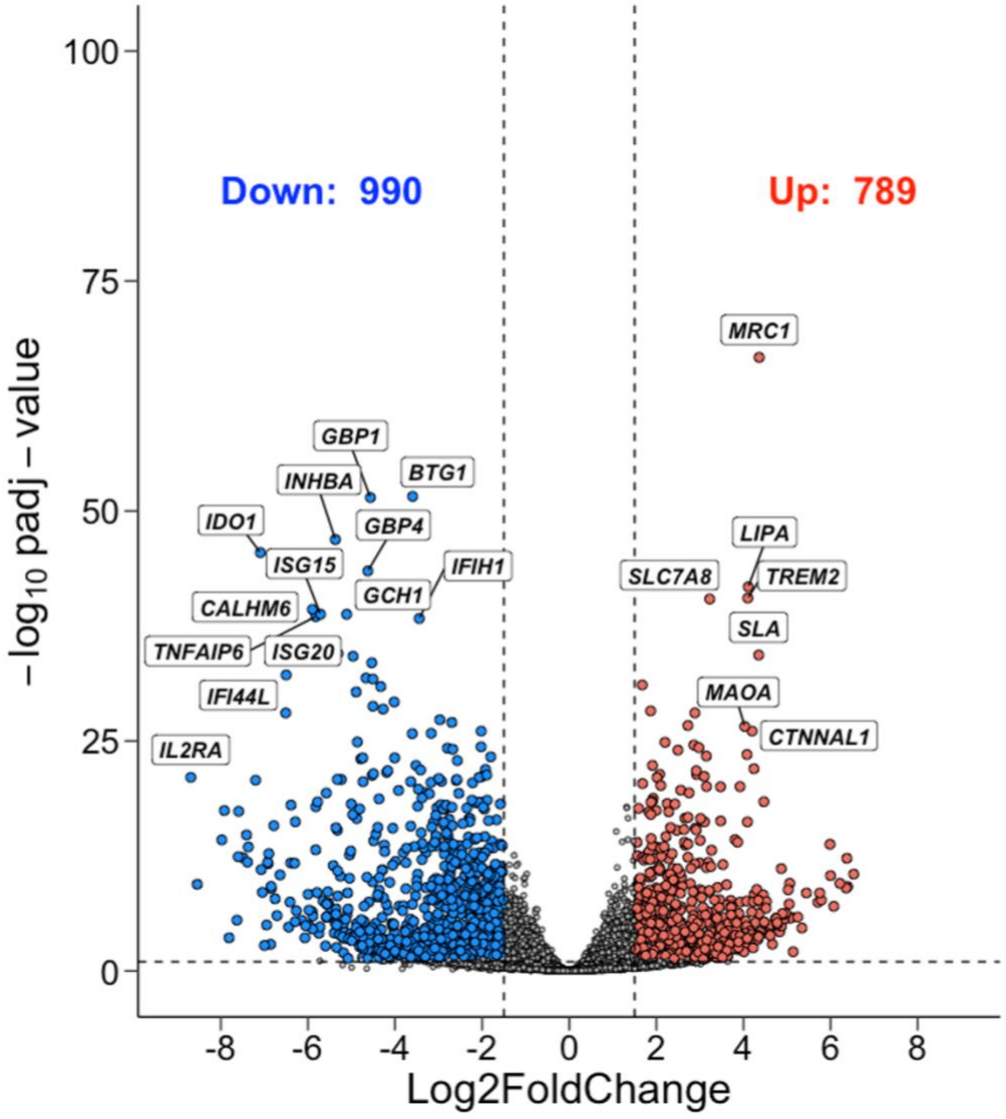

Figure 4.15 Differentially expressed genes between M1 (III) and M1 (II).
The normalised expression values were used to perform the differential gene expression analysis using DESeq2 analysis. Significantly up or downregulated genes were defined based on the following: (padj <0.05) and (log2 FC=>1.5 or =<-1.5), respectively. Volcano plot of upregulated genes in M1 (III) versus M1 (I), depicted in red (**789)**, and downregulated genes in M1 (III), depicted in blue (**990**). (n = 7).

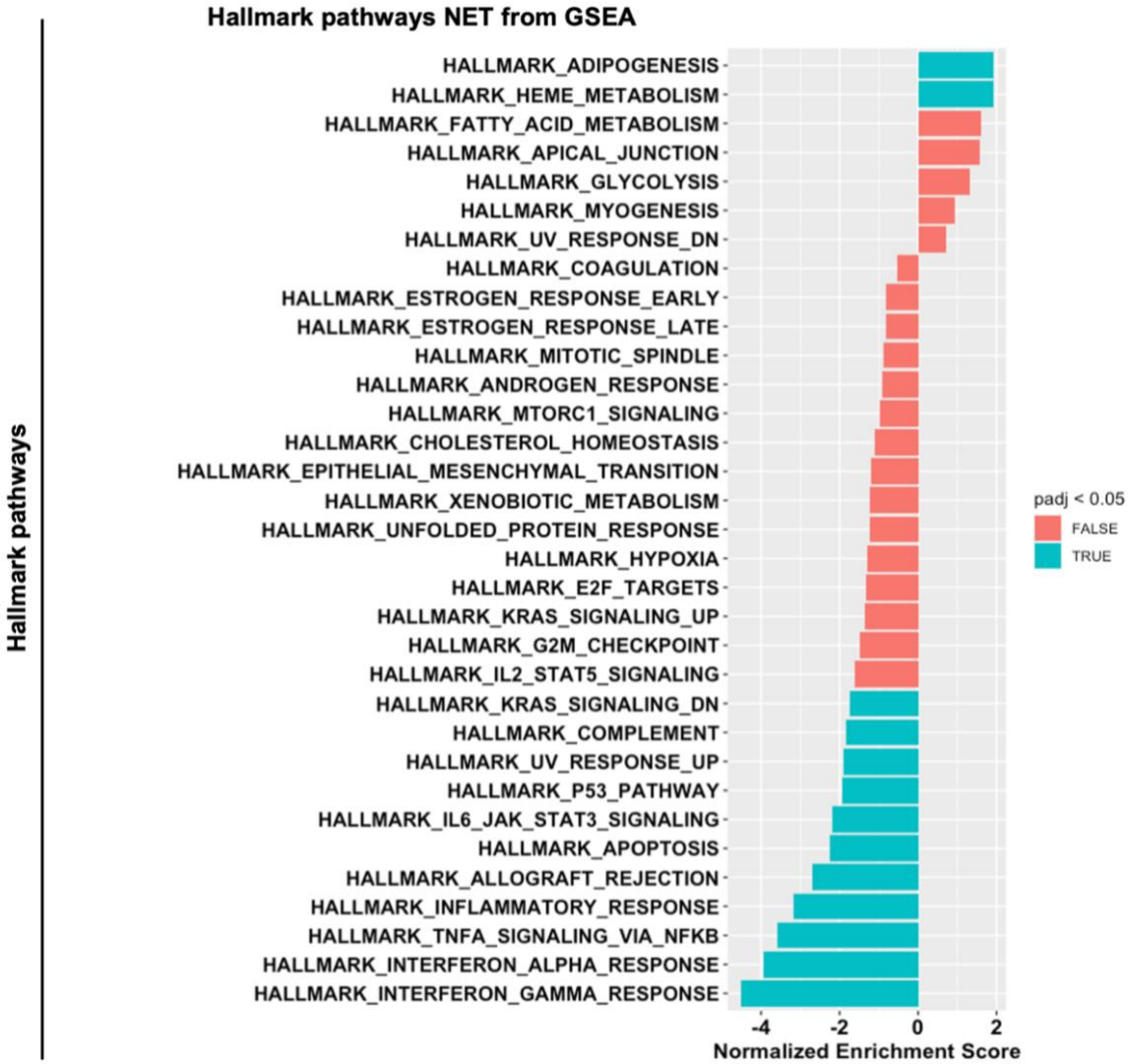

Figure 4.16 Up and downregulated hallmark pathways between M1 (III) and M1 (II).

The normalised expression values were used to perform the differential gene expression analysis using DESeq2 analysis. Significantly up or downregulated genes were defined based on the following: (padj <0.05) and (log2 FC=>1.5 or =<-1.5), respectively. The list of genes was ranked according to log2 FC and padj and used as input for enrichment analysis of Hallmark pathways via GSEA. The upregulated hallmark pathways have the highest normalised enrichment score (NES), while the lowest NES is with the downregulated pathways. The green colour (true) is the significant pathway (padj <0.05), while the red colour (false) being for non-significant. Significant hallmark pathways in **M1 (III) vs. M1 (II)**. (n = 7).

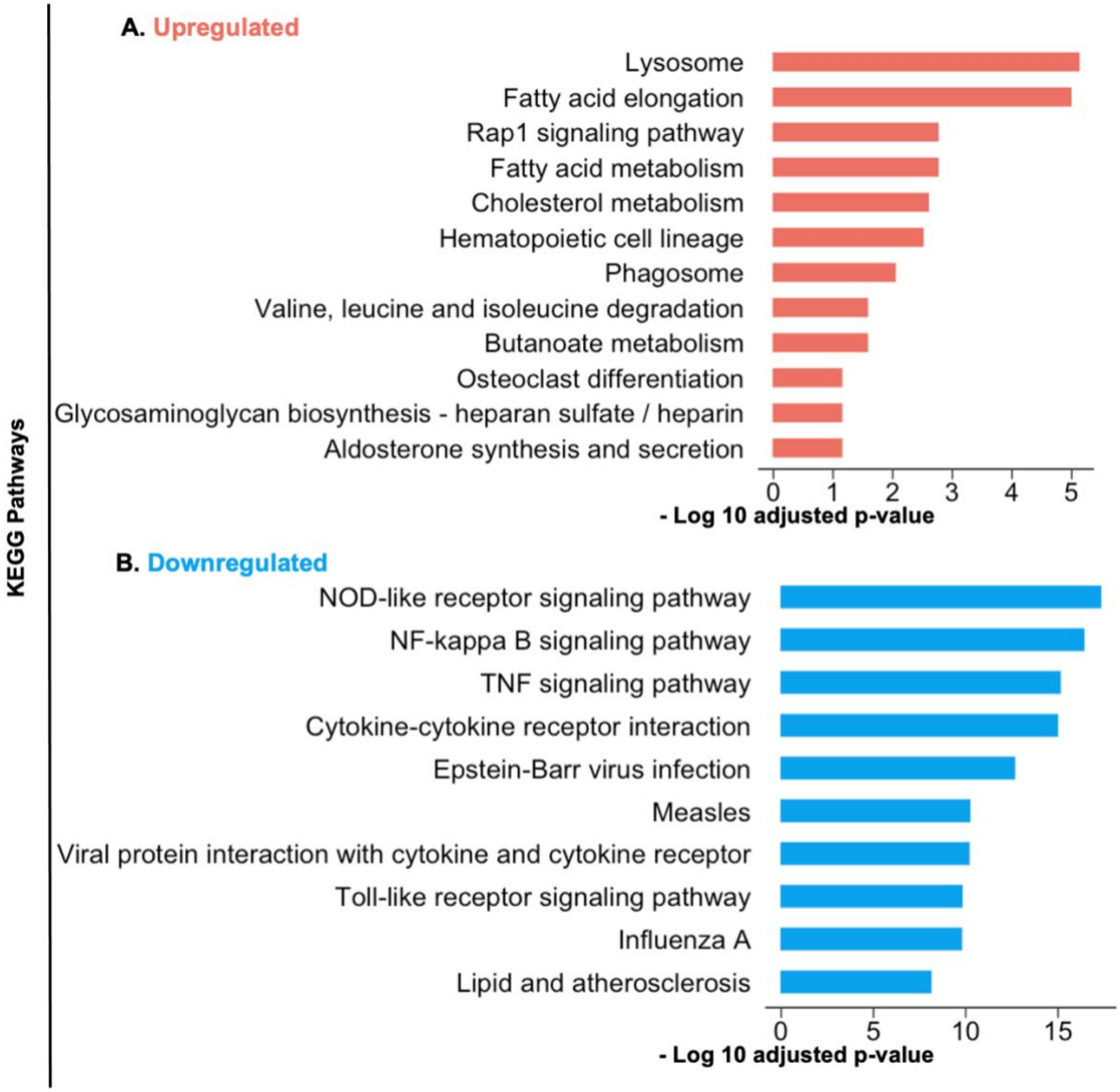

Figure 4.17 Up and downregulated KEGG pathways between M1 (III) and M1 (II). The normalised expression values were used to perform the differential gene expression analysis using DESeq2 analysis. Significantly up or downregulated genes were defined based on the following: (padj <0.05) and (log2 FC=>1.5 or =<-1.5), respectively. **(A)** the upregulated KEGG pathways that are associated with upregulated genes in M1 (III) vs. M1 (II). **(B)** the downregulated KEGG pathways that are associated with upregulated genes in M1 (III) vs. M1 (II). (n = 7).

4.2.4. Differential gene expression analysis and the corresponding biological pathways across M2 subpopulations

Findings from the previous sections indicated that the LPS and IFN-γ -induced pro-inflammatory features in M1 (II) are lost, and anti-inflammatory features are upregulated when subjected to an anti-inflammatory or Th2 environment, indicating the instability of the polarisation states of M1 subsets. Here, we further investigated the polarisation states of M-CSF derived M2 subsets. We cultured isolated monocytes with M-CSF for 6 days, M2 (I), and then stimulated them for 2 days with IL-4 and IL-13 cytokines to produce fully activated M2 (II), as described in **Figure 4.1**. These cells, M2 (II), were maintained without stimulation for 6 days and then subjected to a pro-inflammatory environment by stimulating them with LPS and IFN-γ cytokines. We use RNAseq analysis to identify the transcriptional differences among subsets of M2 macrophages, including M2 (I), M2 (II), and M2 (II).

A heatmap with hierarchical clustering of the top 100 highly variable genes across three subsets of M2 was used to provide a global view of the transcriptional differences of three populations (**Figure 4.18)**. As shown in the heatmap of highly variable genes, M2 gene expression such as *MRC1*, *CD163*, *CCL13*, *CCL18*, *CCL22*, *CCL23*, *CCL26* and *ALOX15* (Martinez et al., 2006) was variably higher in IL-4 and IL-13-stimulated M2 (II), suggesting the acquisition of anti-inflammatory properties and confirmation of IL-4 and IL-13 activation. However, their expression levels in M2 (III) were suppressed following stimulation with LPS and IFN-γ cytokines. Induction of pro-inflammatory related genes was also observed in M2 (III) (**Figure 4.18)**. It is worth noting that the reduction in M2 marker genes in M2 (III) does not mean completely downregulating their expression, particularly *CCL18*, *CCL22*, *CCL26*, and *FN1*, as shown in **Figure 4.18**.

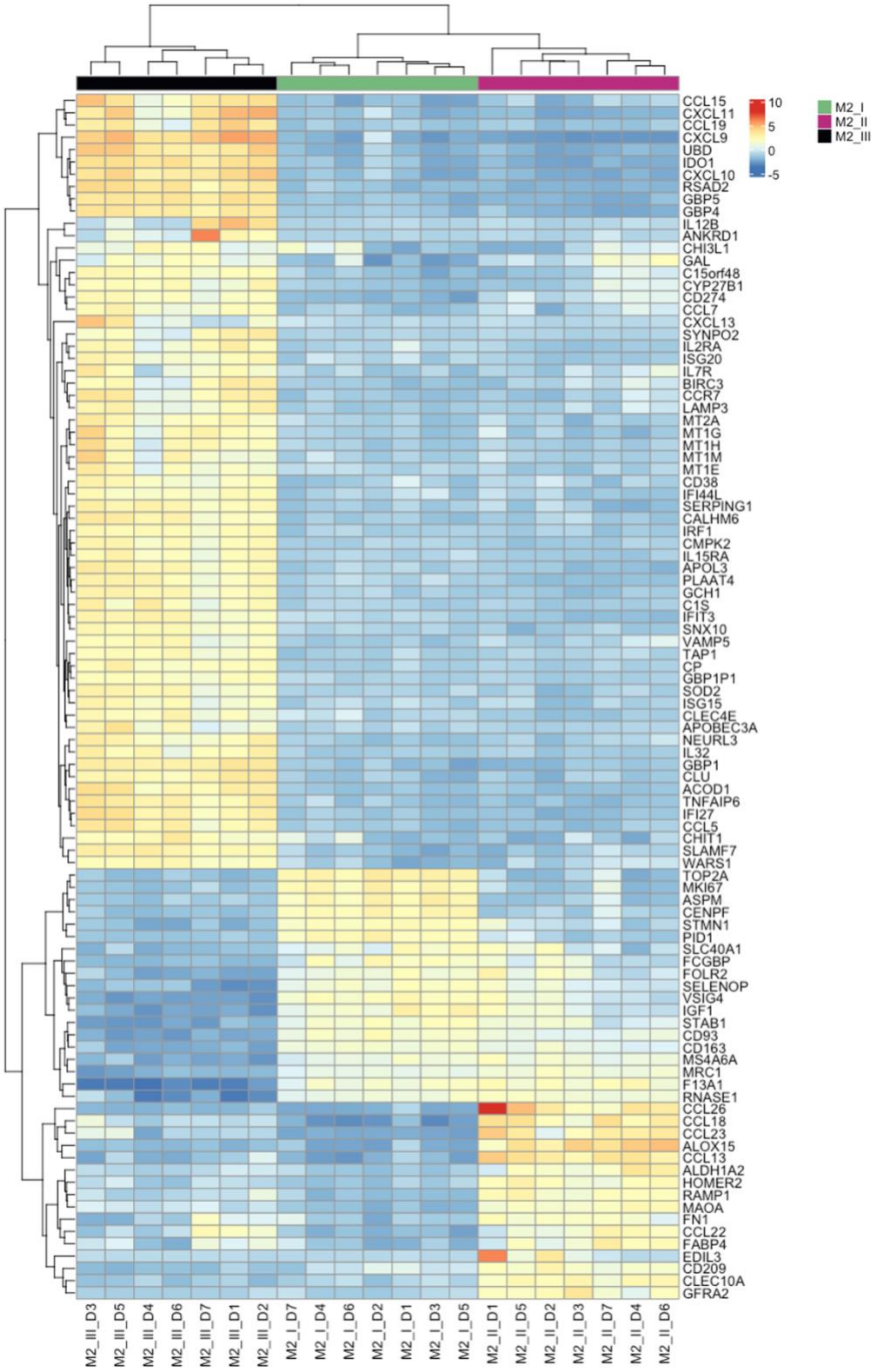

Figure 4.18 Top 100 highly variable genes between M2 (I), M2 (II), and M2 (III). Rlog of raw data was calculated using DESeq2 analysis to identify the top variable genes across M2 (I), M2 (II), and M2 (III) subsets. Heatmap with hierarchical clustering of the 100 highly variable genes across subpopulations (n = 7).

4.2.4.1. Differentially expressed genes and their enrichment analysis between M2 (II) and M2 (I).

We further investigate the transcriptional differences between M2 (II) and M2 (I) to identify DEG and consequently confirm that M2 (II) demonstrates anti-inflammatory properties following stimulation with IL-4 and IL-13 cytokines. It was shown that wound healing and tissue remodelling related genes, such as *CCL26*, *CCL23*, transglutaminase 2 (*TGM2*), *ALOX15*, *CCL18*, and transforming growth factor (*TGF*), demonstrate a higher expression level in M2 (II) than in M2 (I) macrophages, confirming the activation (Martinez et al., 2006, Mantovani et al., 2004, Wynn and Vannella, 2016), as shown in **Figure 4.19**.

Next, we conducted differential expression analysis and found that 298 genes were downregulated, while 279 were upregulated, such as *CCL22*, *TGM2*, *ALOX12*, *CCL18*, and *MAOA* in M2 (II) relative to M2 (I) macrophages, as shown in **Figure 4.20**, confirming the IL-4 and IL-13 stimulation. The number of DEGs, both down and up regulated, in M2 (II) relative to M2 (I) is less than that in M1 (II) relative to M1 (I), where more than 1500 DEGs were altered following LPS and IFN-γ (**Figure** 4.7**)**, suggesting the strong activating influence of LPS and IFN-γ and the more homeostatic role of IL-4 and IL-13.

To explore the biological significance of altered DEG in M2 (II), we performed the GSEA for hallmark pathways and found allograft rejection, *IL2,* Signal Transducer and Activator of Transcription 5 (*STAT5*) signalling, and hypoxia, most of which could be relevant to M2 macrophages **(Figure 4.21),** (Raggi et al., 2017, Jones et al., 2020, Tan et al., 2022).

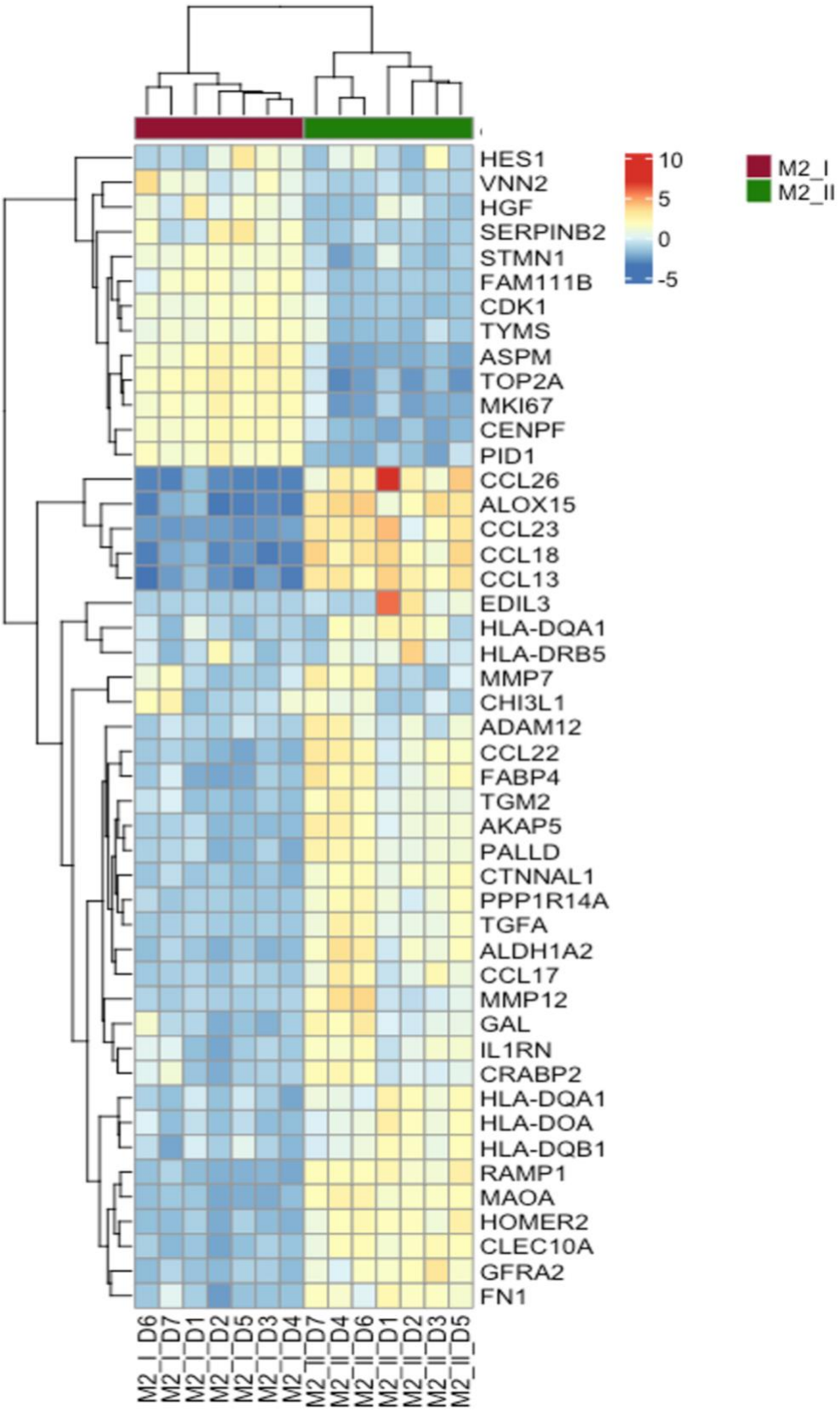

Figure 4.19 Top 100 highly variable genes between M2 (I) and M2 (II).
Rlog of raw data was calculated using DESeq2 analysis to identify the top variable genes between M2 (I), and M2 (II) subsets. Heatmap with hierarchical clustering of the 100 highly variable genes across subpopulations (n = 7).

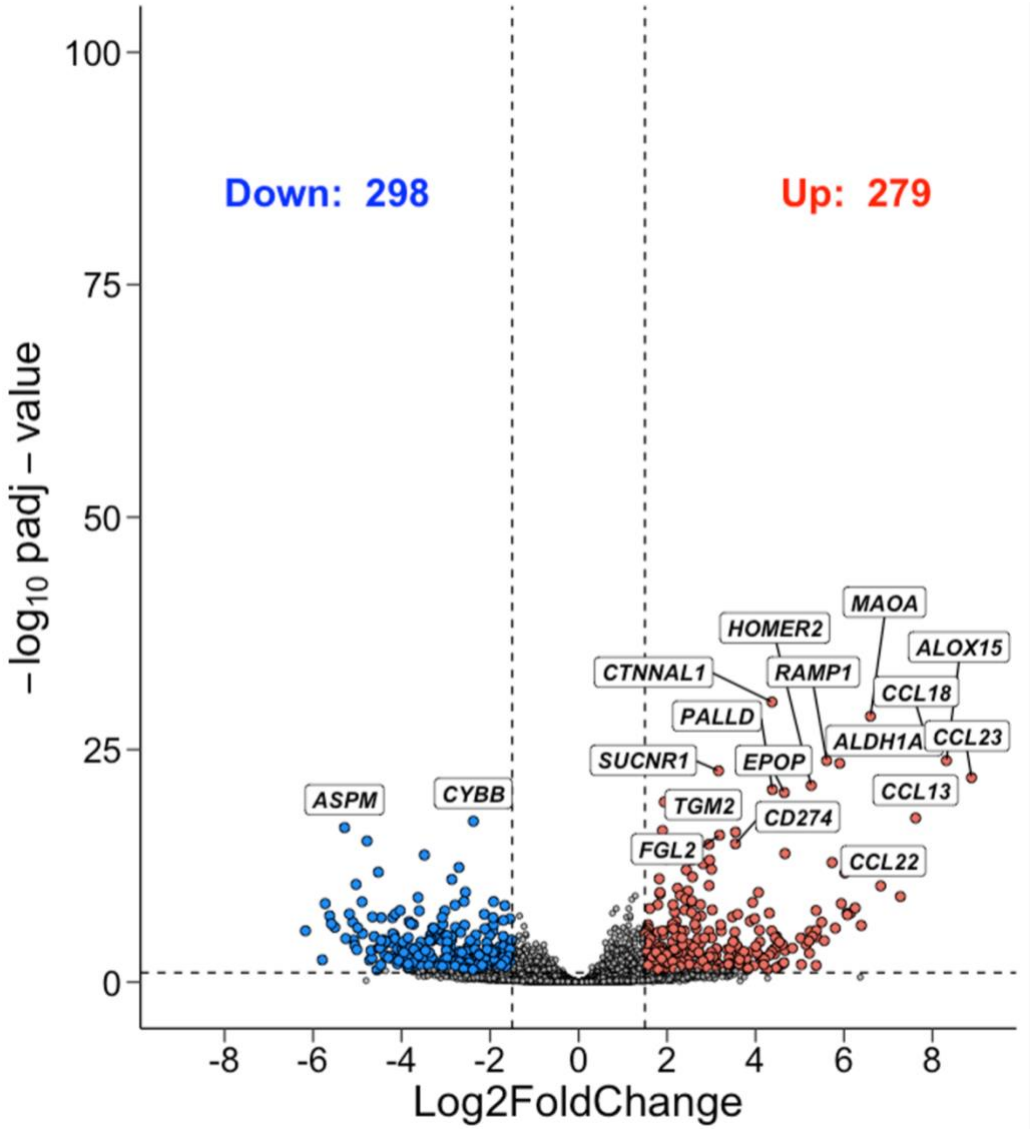

Figure 4.20 Differentially expressed genes between M2 (II) and M2 (I).
The normalised expression values were used to perform the differential gene expression analysis using DESeq2 analysis. Significantly up or downregulated genes were defined based on the following: (padj <0.05) and (log2 FC=>1.5 or =<-1.5), respectively. Volcano plot of upregulated genes in M2 (II) versus M2 (I), depicted in red (**279)**, and downregulated genes in M2 (II), depicted in blue (**298)**. (n = 7).

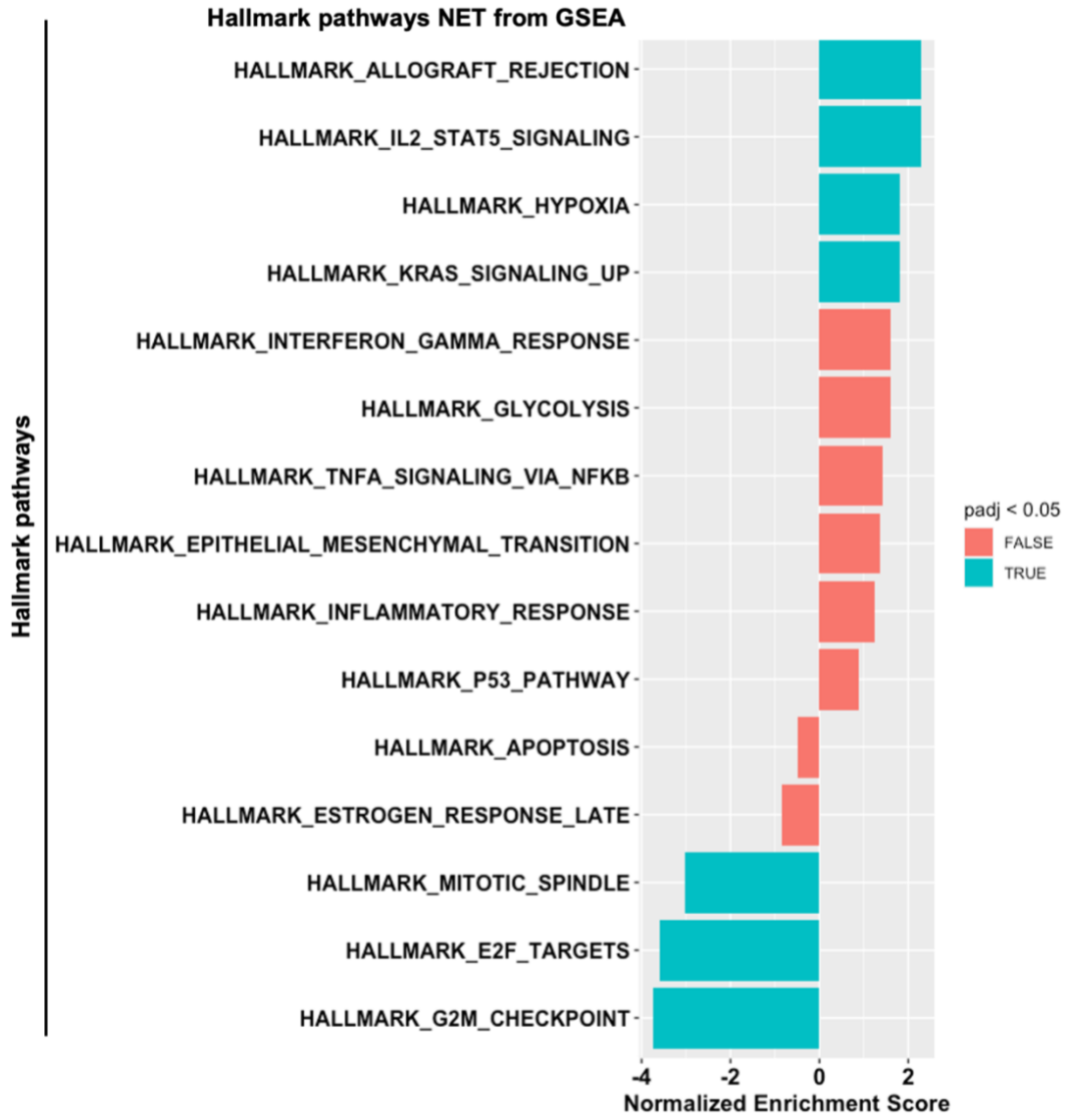

Figure 4.21 Up and downregulated hallmark pathways between M2 (II) and M2 (I).

The normalised expression values were used to perform the differential gene expression analysis using DESeq2 analysis. Significantly up or downregulated genes were defined based on the following: (padj <0.05) and (log2 FC=>1.5 or =<-1.5), respectively. The list of genes was ranked according to log2 FC and padj and used as input for enrichment analysis of Hallmark pathways via GSEA. The upregulated hallmark pathways have the highest normalised enrichment score (NES), while the lowest NES is with the downregulated pathways. The green colour (true) is the significant pathway (padj <0.05), while the red colour (false) being for non-significant. Significant hallmark pathways in **M2 (II) vs. M2 (I)**. (n = 7).

We further conducted the enrichment analysis of the significantly upregulated and downregulated genes for KEGG pathways. The KEGG analysis showed that upregulated genes in M2 (II) are associated with hematopoietic cell lineage, asthma, and allograft rejection, while the cell cycle was the top downregulated pathway (**Figure 4.22)**. These findings are supported by Th2 macrophages involvement in allergic responses such as asthma (Abdelaziz et al., 2020). Taken together, these findings indicated that IL-4 and IL-13 produce an activated M2 (II) subset that significantly upregulates genes linked to the M2 phenotype.

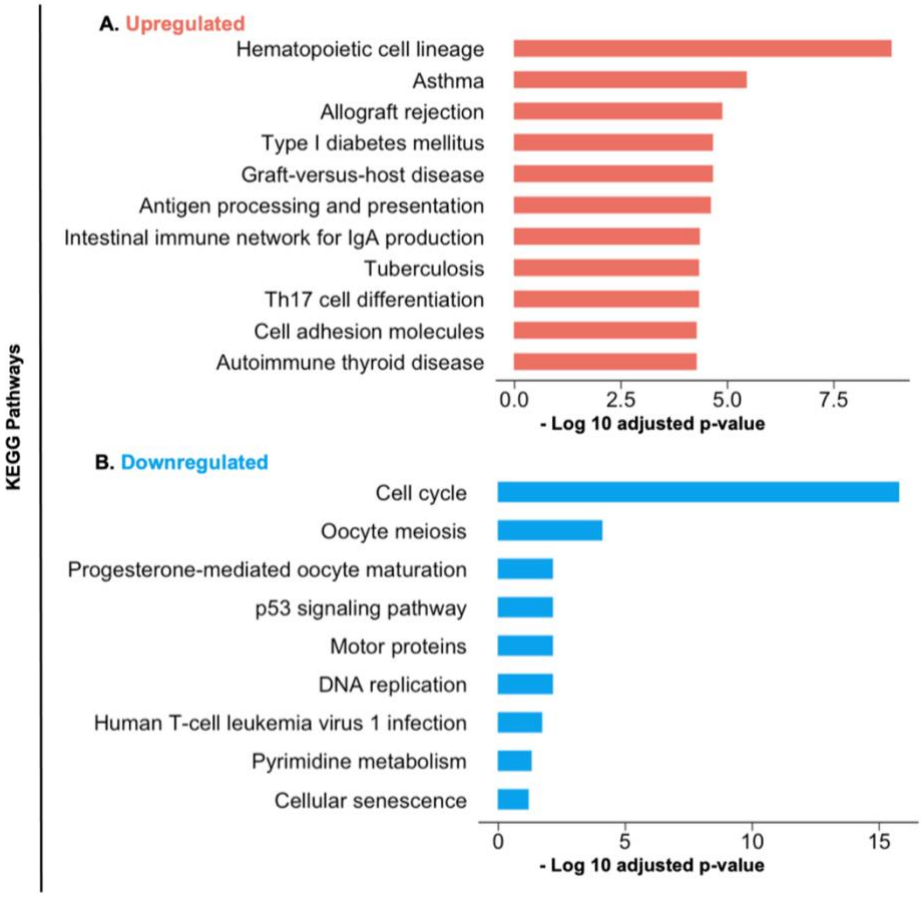

Figure 4.22 Up and downregulated KEGG pathways between M2 (II) and M2 (I). The normalised expression values were used to perform the differential gene expression analysis using DESeq2 analysis. Significantly up or downregulated genes were defined based on the following: (padj <0.05) and (log2 FC=>1.5 or =<-1.5), respectively. **(A)** the upregulated KEGG pathways that are associated with upregulated genes in M2 (II) vs. M2 (I). **(B)** the downregulated KEGG pathways that are associated with upregulated genes in M2 (II) vs. M2 (I). (n = 7).

4.2.4.2. Differentially expressed genes and their enrichment analysis between M2 (III) and M2 (II).

As with M1 (II), to determine the reversibility of the M1 polarisation state, we stimulated M2 (II) with opposing pro-inflammatory cytokines, LPS and IFN-γ, to produce M2 (III) macrophages. Like M1 (III), the potential alterations in the polarisation states of M2 (III) are not exclusively attributed to T pro-inflammatory cytokine stimulation but also to the resting period in cytokine-free media. The heatmap of the top 50 variable genes showed that LPS and IFN-γ induced downregulation of IL-4 and IL-13-induced genes, such as *CCL26*, *CCL23*, *ALOX12*, and *CCL18*, in M2 (III) relative to M2 (II) macrophages **(Figure 4.23)**. LPS and IFN-γ induced genes, such as *IL12β*, *CXCL9*, *CXCL10*, and *CXCL11*, exhibited a higher expression level in M2 (III) as compared to M2 (II), as described in **Figure 4.23**. It is noticeable that the level of IL12β gene expression of some donors in M2 (III) was comparable to M2 (II), which may indicate the impact of cell origin on response to stimulus.

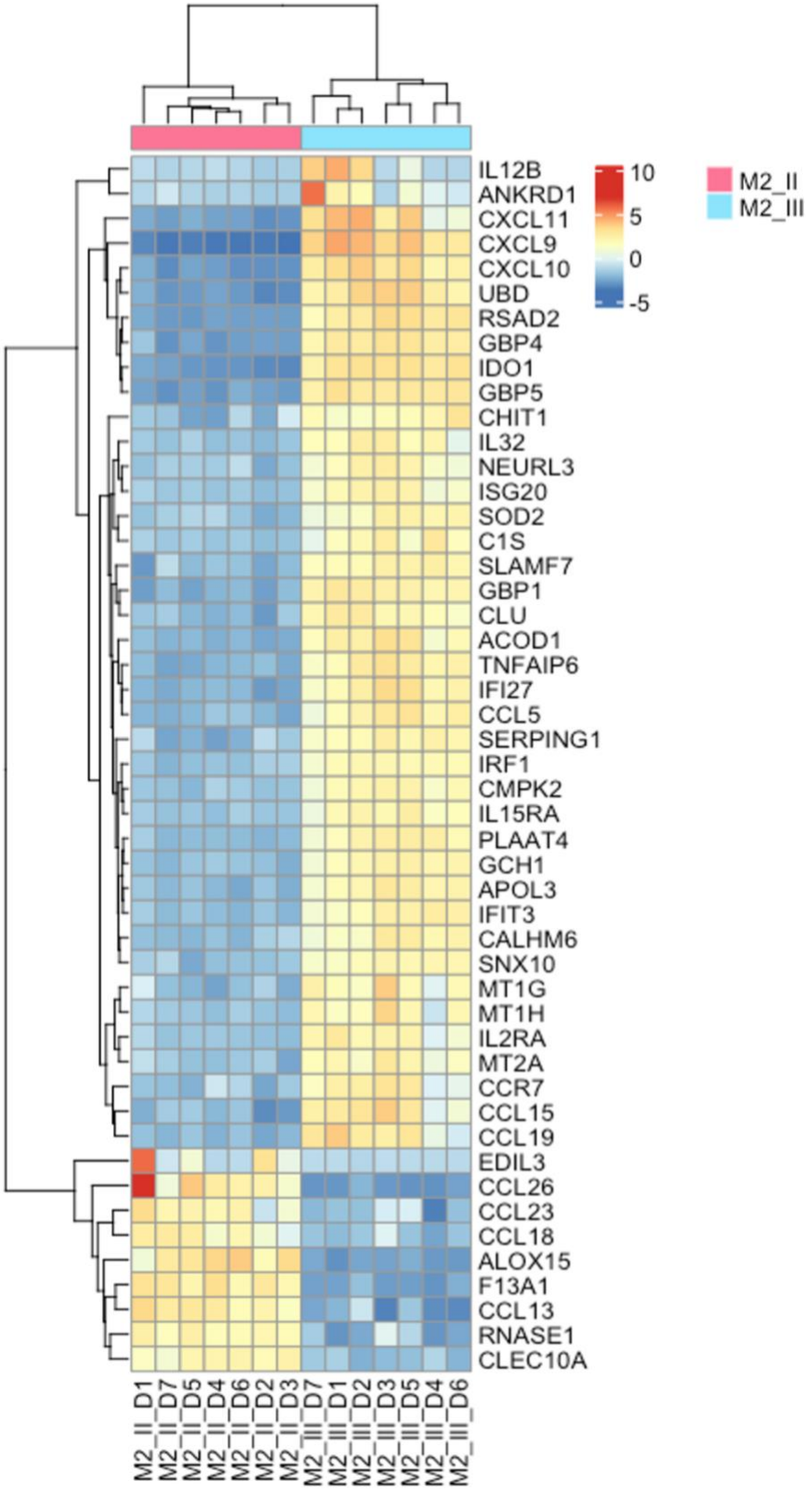

Figure 4.23 Top 100 highly variable genes between M2 (II) and M2 (III).
Rlog of raw data was calculated using DESeq2 analysis to identify the top variable genes between M2 (II), and M2 (III) subsets. Heatmap with hierarchical clustering of the 100 highly variable genes across subpopulations (n = 7).

In response to opposing stimulation, 797 genes, including proinflammatory related genes, were significantly induced in M2 (III), whereas genes that were significantly upregulated in M2 (II), MAOA, and ALOX15 were significantly downregulated in M2 (III) as compared to M2 (II) **(Figure 4.24)**.

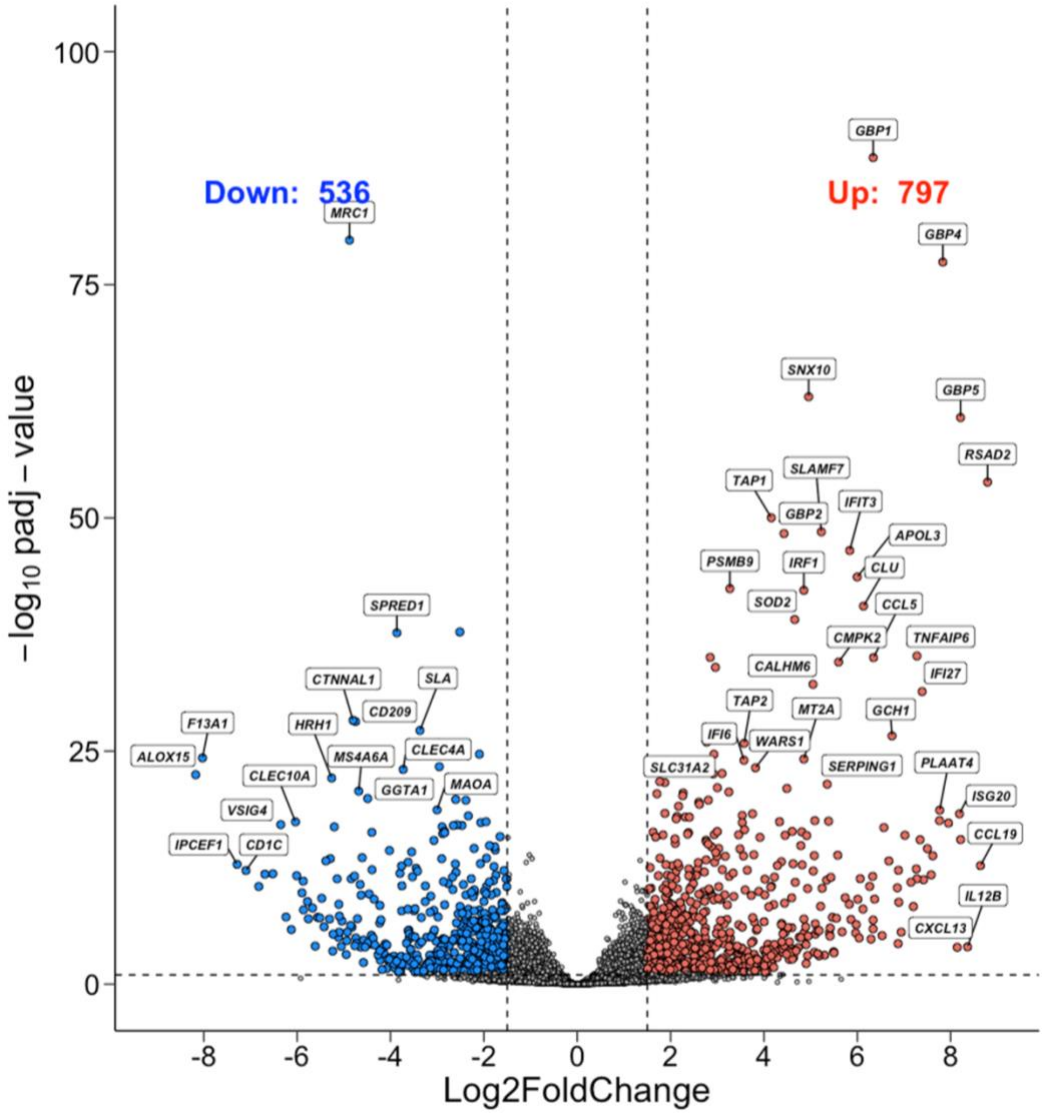

Figure 4.24 Differentially expressed genes between M2 (III) and M2 (II).
The normalised expression values were used to perform the differential gene expression analysis using DESeq2 analysis. Significantly up or downregulated genes were defined based on the following: (padj <0.05) and (log2 FC=>1.5 or =<-1.5), respectively. Volcano plot of upregulated genes in M2 (III) versus M2 (II), depicted in red (**797**), and downregulated genes in M2 (III), depicted in blue (**536**). (n = 7).

We subjected these DEGs to enrichment analysis for hallmark pathways and found that LPS and IFN-γ treatment significantly upregulated hallmark interferon gamma response, interferon alpha response and inflammatory response, as shown in **Figure 4.25**. Furthermore, the up and the down regulated genes were subjected to KEGG pathway analysis **Figure 4.26.**

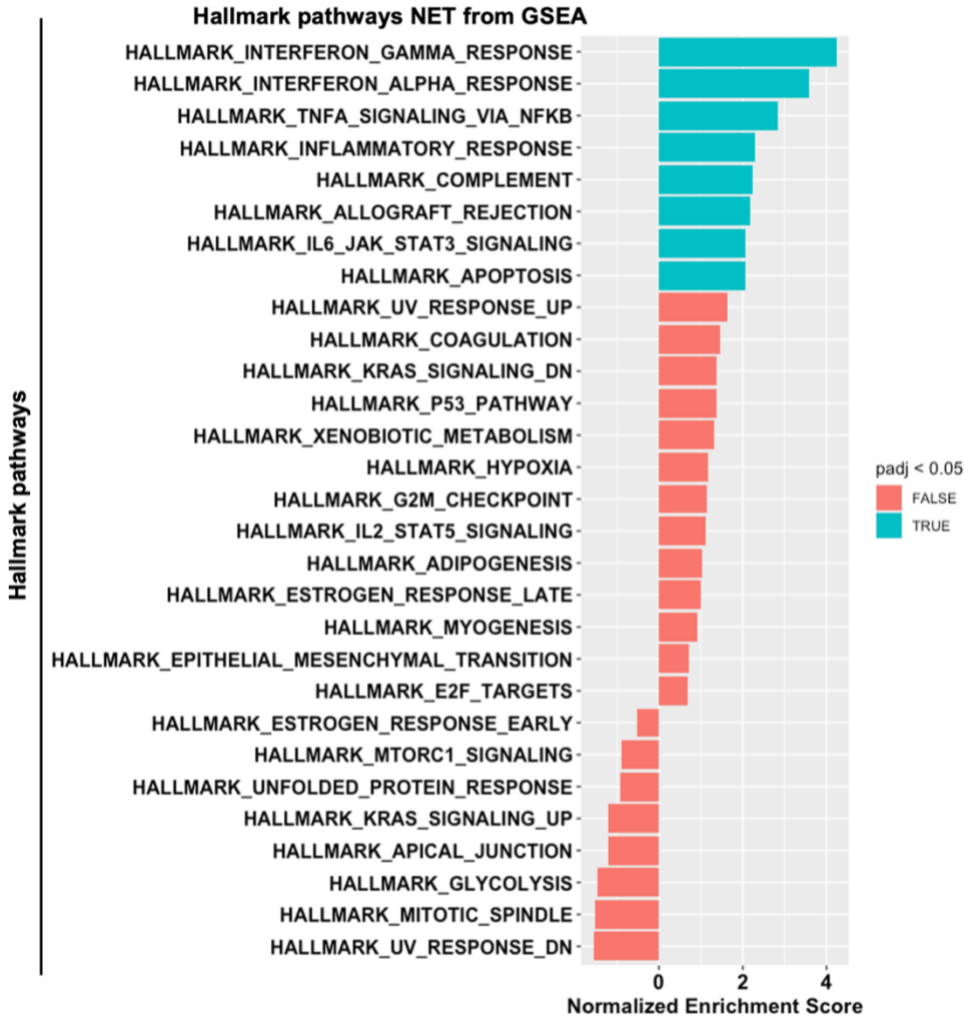

Figure 4.25 Up and downregulated hallmark pathways between M2 (III) and M2 (I). The normalised expression values were used to perform the differential gene expression analysis using DESeq2 analysis. Significantly up or downregulated genes were defined based on the following: (padj <0.05) and (log2 FC=>1.5 or =<-1.5), respectively. The list of genes was ranked according to log2 FC and padj and used as input for enrichment analysis of Hallmark pathways via GSEA. The upregulated hallmark pathways have the highest normalised enrichment score (NES), while the lowest NES is with the downregulated pathways. The green colour (true) is the significant pathway (padj <0.05), while the red colour (false) being for non-significant. Significant hallmark pathways in **M2 (III) vs. M2 (I)**. (n = 7).

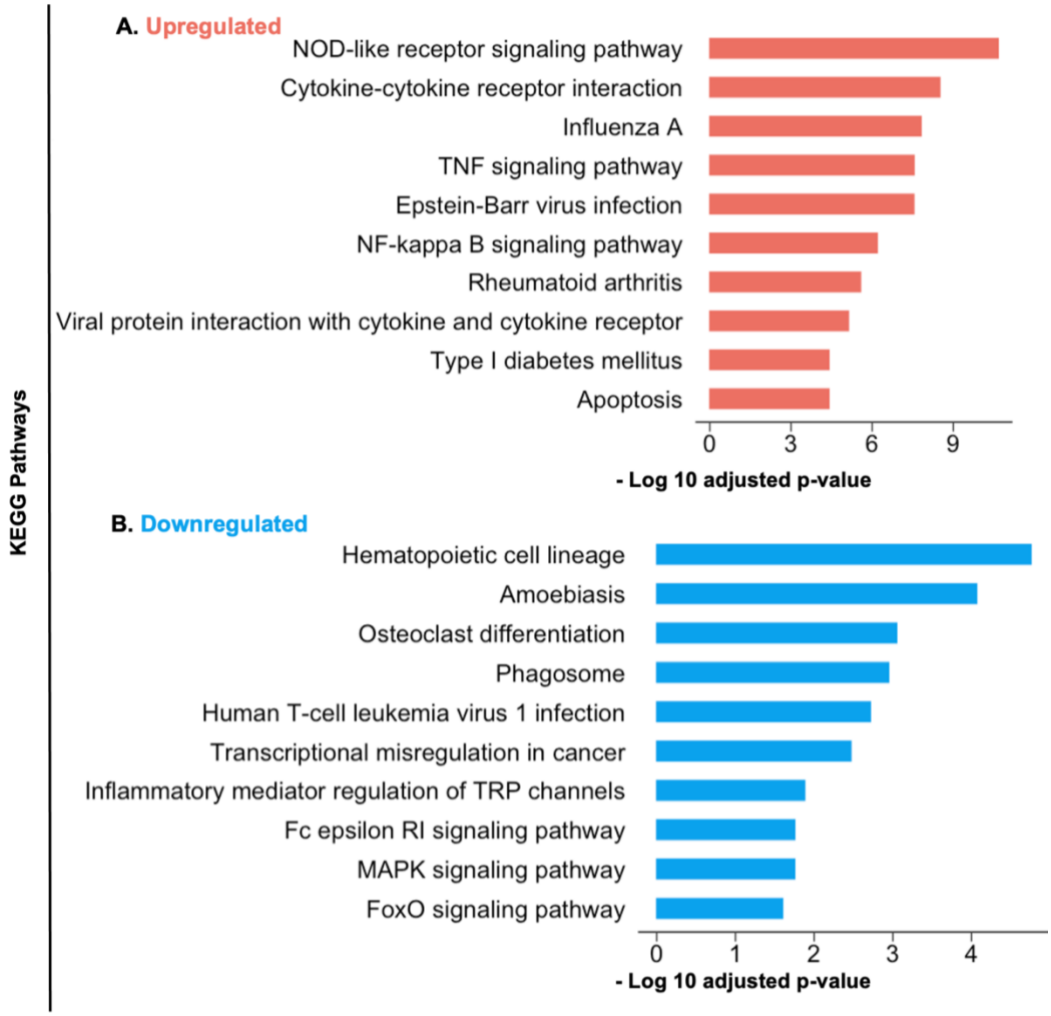

Figure 4.26 Up and downregulated KEGG pathways between M2 (III) and M2 (II). The normalised expression values were used to perform the differential gene expression analysis using DESeq2 analysis. Significantly up or downregulated genes were defined based on the following: (padj <0.05) and (log2 FC=>1.5 or =<-1.5), respectively. **(A)** the upregulated KEGG pathways that are associated with upregulated genes in M2 (II) vs. M2 (I). **(B)** the downregulated KEGG pathways that are associated with upregulated genes in M2 (III) vs. M2 (II). (n = 7).

Taken together, these findings indicated that the anti-inflammatory properties of IL-4 and IL-13 stimulated M2 (II) macrophages are changed towards M1 polarisation following LPS and IFN-γ stimulation, suggesting the instability of the polarisation state of M2 macrophages.

4.2.5. Transcriptional differences between M1 (III) macrophages and M2 (II) macrophages stimulated with IL-4 and IL-13

We then determine whether the resultant M1 (III) showed distinctively anti-inflammatory properties compared to M2 (II). Thus, we visualised the top 100 variable genes between them. We found that M1 (III) demonstrated a lower expression level of M2 associated genes, including *CD163*, *IGF1*, *CCL26*, *ALOX15*, *CCL23*, *CCL18*, and *CCL13*, but not *CCL22* or *TGM2*, when compared to M2 (II) (**Figure 4.27)**. Furthermore, M1 expression genes such as Interferon Alpha Inducible Protein (*IFI*)27 and Clusterin (*CLU*) showed a higher expression in M1 (III) as compared to M2 (II) (**Figure 4.27)**.

We also conducted the differential gene expression analysis for M1 (III) and M2 (II) to identify the DEGs and consequently significant up and downregulated pathways. M1 (III), macrophages demonstrated upregulation of 267 genes, while 300 genes were downregulated when compared to M2 (II), as shown in **Figure 4.28**. Consistent with most variable genes, we found that some of the M2 expression genes, such as *IGF1*, *CCL26*, *CD93*, and *CCL23*, were significantly downregulated in M1 (III), while some of the LPS and IFN-γ induced genes, including *GBP* (4 and 5), *IFI27*, and Interferon-induced protein with tetratricopeptide repeats 3 (*IFIT3*), and others M1-associated genes, such as Radical S-adenosyl methionine domain-containing protein 2 (*RSAD2*) (Chin and Cresswell, 2001)and serpin family G member 1 (*SERPING1*), were significantly upregulated in M1 (III) relative to M2 (II), **Figure 4.28.** We subjected these 567 genes to GSEA for hallmark pathways and found that significant upregulation of interferon gamma and alpha pathways was observed in M1 (III) relative to M2 (II), whereas no significant downregulation was detected (**Figure 4.29).** Like GSEA, only one KEGG pathway, named mineral absorption, was statistically induced in M1 (III) as

compared to M2 (II), while no downregulated pathway was detected. These findings indicated that although opposing stimulation (IL-4 and IL-13) of M1 (III) showed significantly transcriptional differences towards the M2-like phenotype in M1 (III) as compared to M1 (II), these M1 (III) populations still showed a distinctive profile (upregulated interferon response) as compared to our original M2 phenotype, M2 (II). This could be attributed to the GM-CSF differentiation of monocytes towards M1 (I), where they also exhibited significant induction of the interferon gamma response relative to M2 (I), as shown in **Figure 4.7a**. This could also suggest the heterogeneity of macrophages and challenge the concept of the M1 and M2 dichotomies.

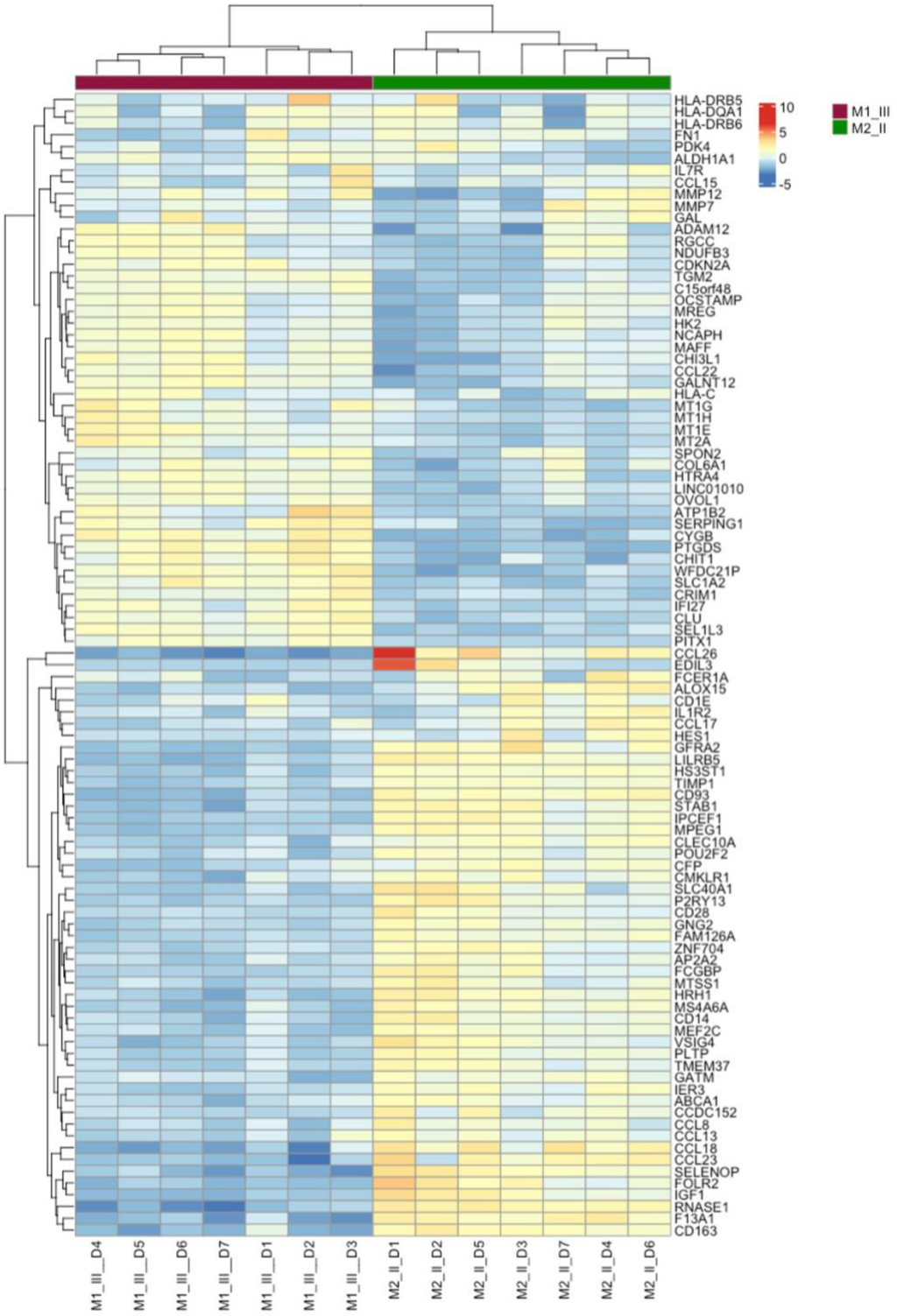

Figure 4.27 Top 100 highly variable genes between M1 (III) and M1 (III).
Rlog of raw data was calculated using DESeq2 analysis to identify the top variable genes between M2 (II), and M1 (III) subsets. Heatmap with hierarchical clustering of the 100 highly variable genes across subpopulations (n = 7).

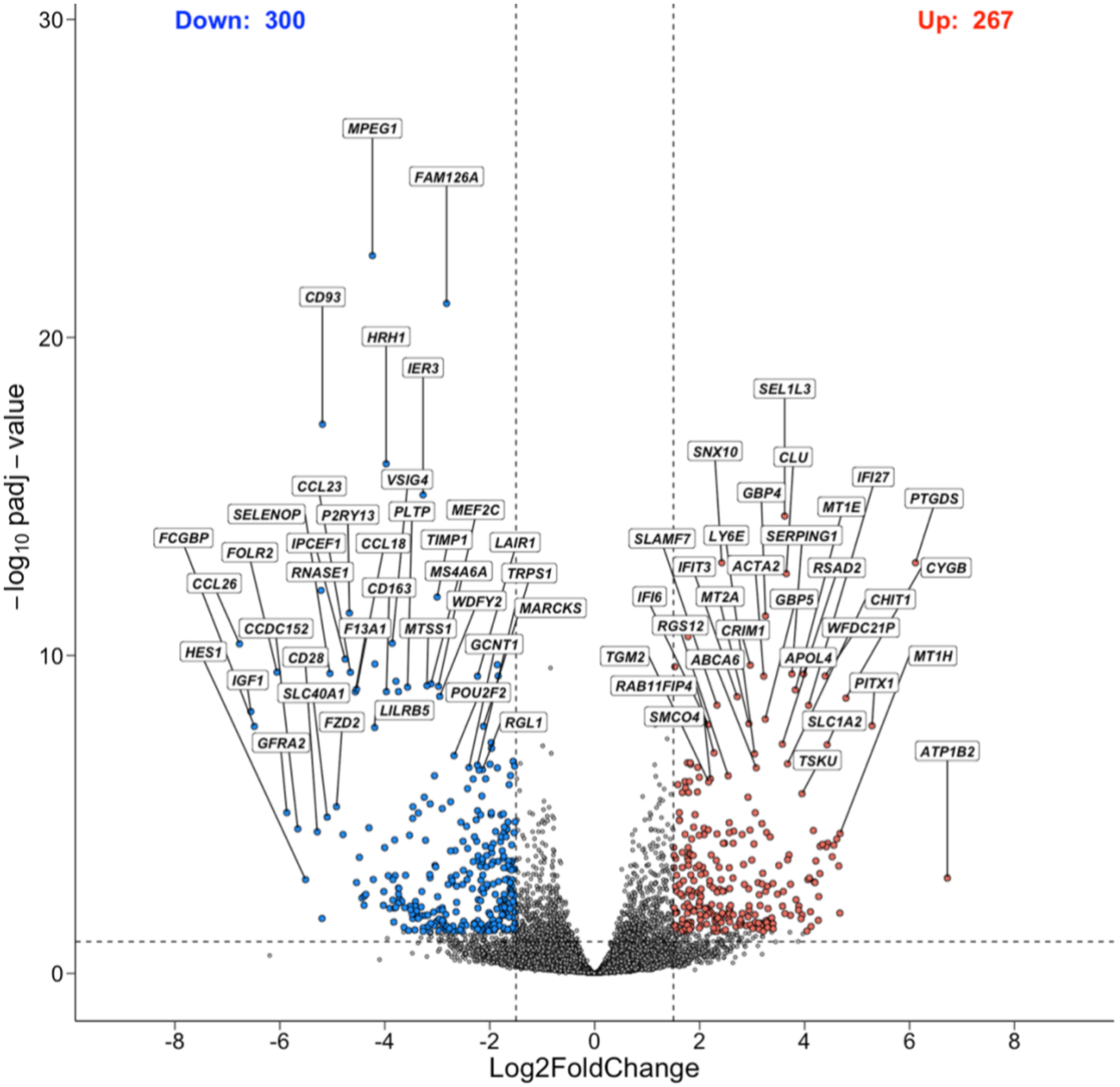

Figure 4.28 Differentially expressed genes between M1 (III) and M2 (II).
The normalised expression values were used to perform the differential gene expression analysis using DESeq2 analysis. Significantly up or downregulated genes were defined based on the following: (padj <0.05) and (log2 FC=>1.5 or =<-1.5), respectively. Volcano plot of upregulated genes in M1 (III) versus M2 (II), depicted in red (**267)**, and downregulated genes in M1 (III), depicted in blue (**300**). (n = 7).

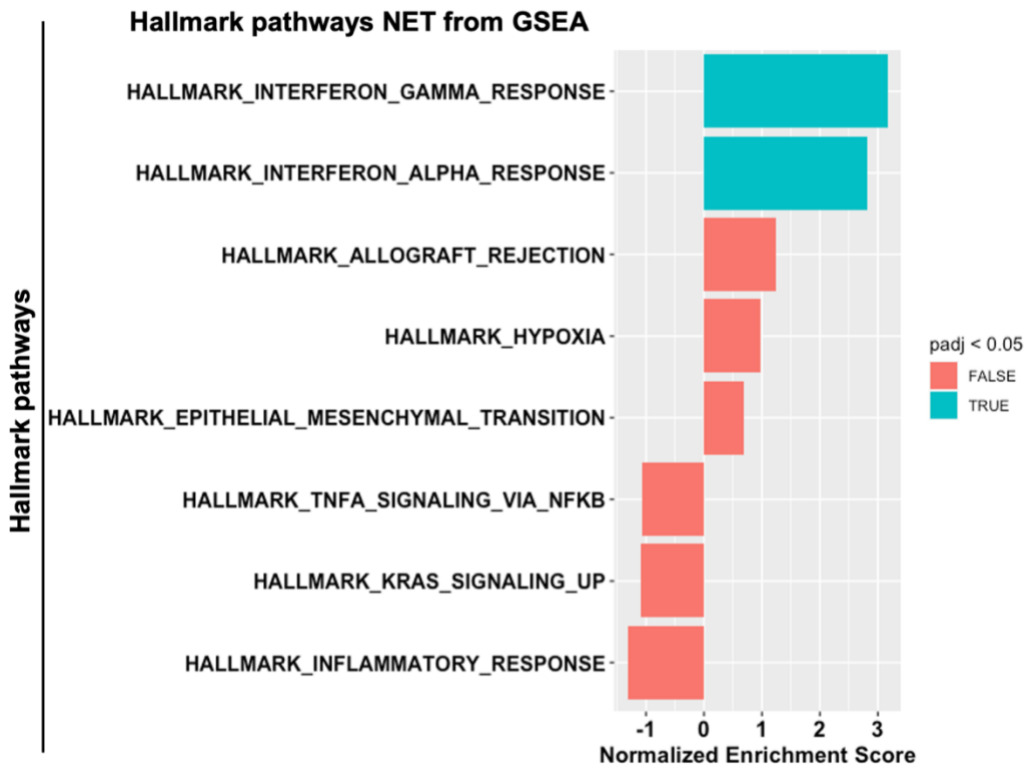

Figure 4.29 Up and downregulated hallmark pathways between M1 (III) and M2 (II).

The normalised expression values were used to perform the differential gene expression analysis using DESeq2 analysis. Significantly up or downregulated genes were defined based on the following: (padj <0.05) and (log2 FC=>1.5 or =<-1.5), respectively. The list of genes was ranked according to log2 FC and padj and used as input for enrichment analysis of Hallmark pathways via GSEA. The upregulated hallmark pathways have the highest normalised enrichment score (NES), while the lowest NES is with the downregulated pathways. The green colour (true) is the significant pathway (padj <0.05), while the red colour (false) being for non-significant. Significant hallmark pathways in **M1 (III) vs. M2 (II)**. (n = 7).

4.2.6. Transcriptional differences between M2 (III) macrophages and M1 (II) macrophages stimulated with LPS and IFN-γ

We also investigated transcriptional differences among LPS and IFN-γ stimulated M2 (III) and the original LPS and IFN-γ stimulated M1 (II) and found that the top 100 variable genes showed slight similarity of gene expression level, as shown **Figure 4.30.** In addition, the gene expression analysis identified total of 385 DEGs, of which 215 were upregulated, such as CD36, while 143 were downregulated **(Figure 4.31)**.

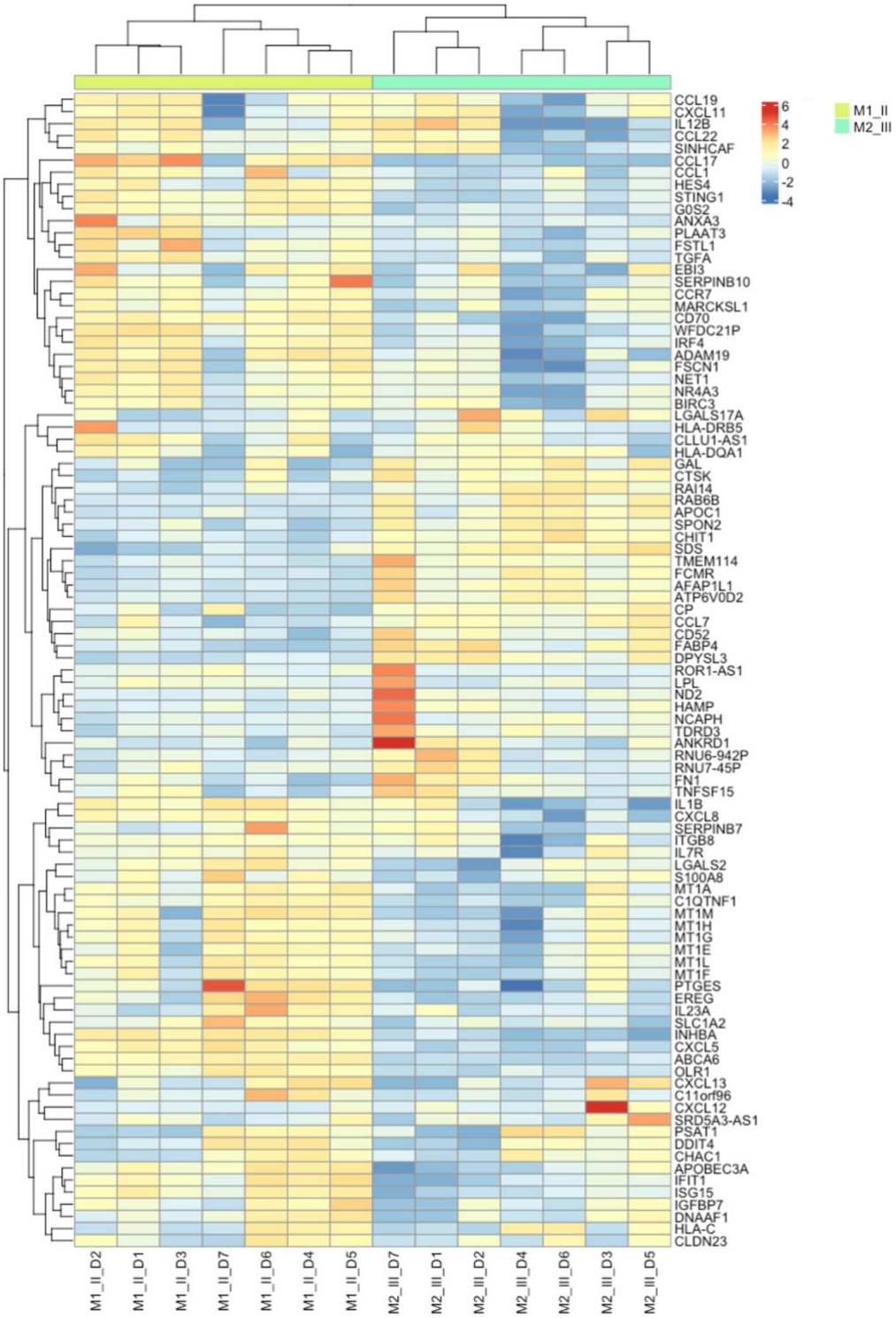

Figure 4.30 Top 100 highly variable genes between M2 (III) and M1 (II).
Rlog of raw data was calculated using DESeq2 analysis to identify the top variable genes between M2 (III), and M1III) subsets. Heatmap with hierarchical clustering of the 100 highly variable genes across subpopulations (n = 7).

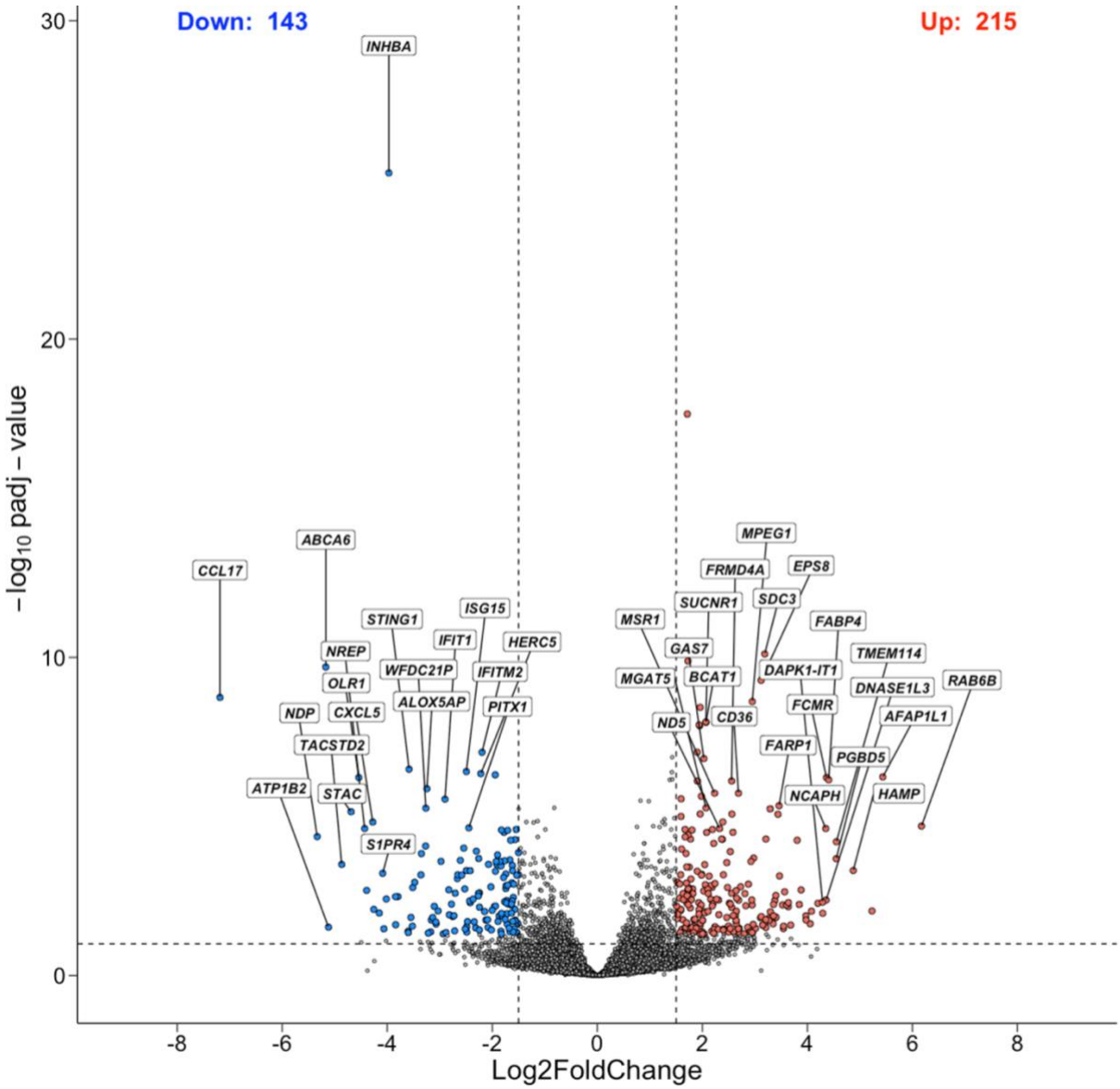

Figure 4.31 Differentially expressed genes between M2 (III) and M1 (II).
The normalised expression values were used to perform the differential gene expression analysis using DESeq2 analysis. Significantly up or downregulated genes were defined based on the following: (padj <0.05) and (log2 FC=>1.5 or =<-1.5), respectively. Volcano plot of upregulated genes in M2 (III) versus M1 (II), depicted in red (**215)**, and downregulated genes in M2 (III), depicted in blue (**143**). (n = 7).

Next, we subjected these DEGs to downstream analysis and found only two significantly downregulated hallmark pathways, including inflammatory and interferon gamma responses, were detected (**Figure 4.32a).** Unlike GSEA, upregulation pathways, such as PPAR signalling, and lysosome pathways were observed **(Figure 4. 32b).** Some of whose genes, including *CD36*, Lysosomal Acid Lipase (*LIPA*), and

Fatty Acid-Binding Protein 4 (*FABP4*), are associated with these pathways. Taken together, these findings indicated that repolarised M2 (III) towards the M1-like phenotype still showed slight transcriptional variation. This could indicate the effect of the types of growth factors, including GM-CSF and M-CSF, that use macrophage differentiation. In addition, this observation indicated the high plasticity of macrophages, where they exhibited a combination of M1 and M2-like phenotypes.

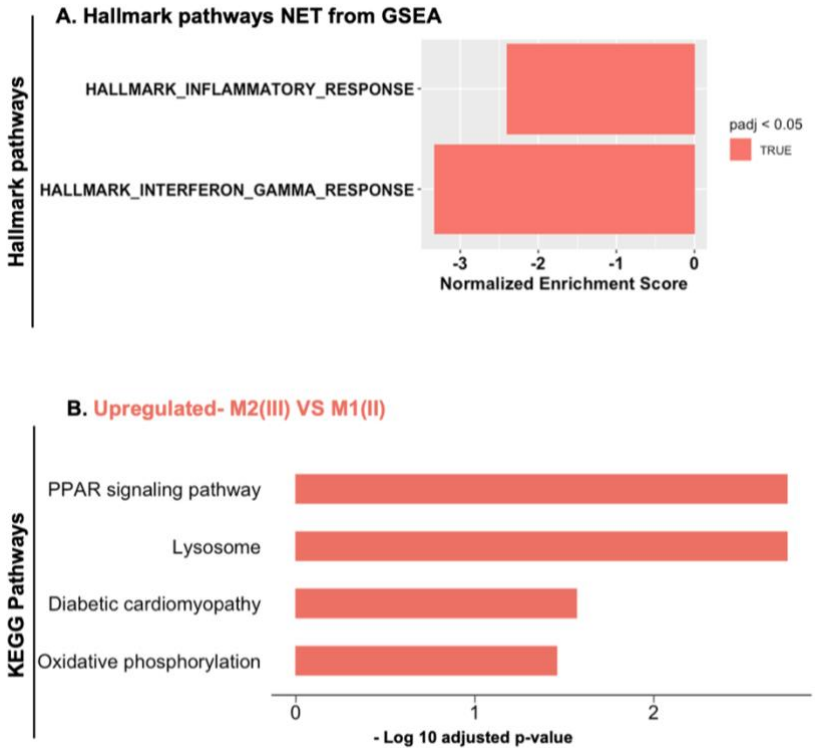

Figure 4.32 Up and downregulated hallmark and KEGG pathways between M2 (III) and M1 (II).

The normalised expression values were used to perform the differential gene expression analysis using DESeq2 analysis. Significantly up or downregulated genes were defined based on the following: (padj <0.05) and (log2 FC=>1.5 or =<-1.5), respectively. The list of genes was ranked according to log2 FC and padj and used as input for enrichment analysis of Hallmark pathways via GSEA. The upregulated hallmark pathways have the highest normalised enrichment score (NES), while the lowest NES is with the downregulated pathways. **(A)** the red colour (true) is the significant pathway (padj <0.05). (**B)** the downregulated KEGG pathways that are associated with downregulated genes in M2 (III) vs. M (II). (n = 7). Significant hallmark pathways and KEGG pathways in **M2 (III) vs. M1 (II)** (n = 7).

4.3. Discussion

The activation state of macrophages plays a critical role during the wound healing response. Therefore, we designed a model to generate different subsets of human M1 and M2 macrophages to investigate the stability of their polarisation states before delivering them to the ocular surface for the prevention of corneal scarring. We found that GM-CSF derived M1 (I) and M-CSF derived M2 (I) exhibited distinctive transcriptional features. M1 (I) exhibited more of the M1 phenotype, while M2 (I) demonstrated anti-inflammatory properties. Stimulation of M1 (I) and M2 (I) with respective pro- and anti-inflammatory agents, including LPS and IFN-γ, or IL-4 and IL-13, resulted in improvement of their respective properties. However, the enhanced pro- or anti-inflammatory features in M1 (II) and M2 (II), respectively, were reversibly altered when they were exposed to opposing cytokines, indicating the instability of their polarisation states. Furthermore, we found that these resultant M1 (III) and M2 (III) exhibited a transcriptional difference as compared to the original M1 (II) and M2 (II), illustrating their capability to acquire a mix of M1 and M2 phenotypes. Although our investigation into the transcriptional profiles of the macrophage subsets demonstrated distinct phenotypic characteristics and reversible polarisation states, functional assays, such as phagocytosis would have provided a more comprehensive characterisation of these macrophage subsets. This would represent a limitation of the current study.

In conclusion, these findings could conclude that we should be careful about the idea of macrophage-based therapy to prevent corneal fibrosis. Although these findings were performed in an *in vitro* study, there are several mediators involved that had a substantial impact on macrophages. For example, two animal models of acute kidney

injury and experimental Autoimmune Encephalomyelitis (EAE) using ex vivo polarised M2 macrophage transplantation demonstrated positive effects, including inhibiting inflammatory responses and consequently improving the outcomes of diseases (Chu et al., 2021, Mao et al., 2020).

PCA results demonstrated global variation of gene expression values for our generated M1 and M2 subsets and showed that LPS and IFN-γ stimulated cells exhibited the majority variance (52%), where they clustered together. This is consistent with the microarray results that showed that LPS and IFN-γ stimulated M1 originated from M-CSF differentiation are associated with most variance,90%, while IL-4 stimulated M2, and GM-CSF and M-CSF derived M0 clustered nearly together(Martinez et al., 2006, Beyer et al., 2012). This may indicate that GM-CSF is not as potent a pro-inflammatory inducer as LPS and IFN-γ.

Our findings showed potential transcriptional differences between GM-CSF and M-CSF derived macrophages, where more than 700 DEGs were detected among M1 (I), such as *MM12*, *INHBA*, *CCL17* and *CD1C*, and M2 (I), including *CD93*, *LGMN*, *IGF1*, *MAFB* and *ITSN1*. Pathway analyses showed that M1 (I) derived from GM-CSF exhibited inflammatory properties as compared to M-CSF derived M2 (I). In accordance with our findings, several studies investigated the phenotype or transcriptional profile of these cells using microarray, RNAseq, or M1 and M2 specific maker approaches. They found that differentiation of human monocytes into macrophages using GM-CSF or M-CSF produced M1 like macrophages with high production of proinflammatory cytokines, such as IL12 and TNF-α, following LPS treatment, or M2 like macrophages with a high level of IL-10 following LPS treatment, respectively (Beyer et al., 2012, Lacey et al., 2012, Verreck et al., 2004, Hashimoto et

al., 1999, Sierra-Filardi et al., 2014, Waldo et al., 2008). These cells also exhibited a distinct transcriptome, where M1 like macrophages expressed highly specific genes, such as *INHBA* and *CCL17*, whereas M2 like macrophages included *CD93*, *LGMN*, *MAFB*, and *ITSN1*. A significantly induced gene in M1 (I), *INHBA*, encodes a component of activin A known as inhibin βA. This activin A was found to impair the anti-inflammatory properties of M2 like macrophages, such as IL-10 production, and reduce the expression of M2 markers, such as *MAFB*. Blockage by the activin Aby antibody diminished its effect on M2 like macrophages (Sierra-Filardi et al., 2011). However, *MAFB*, a transcription factor, consistent with our finding, was found to be expressed highly in human M-CSF derived M2 macrophages, and IL-4 stimulated M2, and its transfection in mouse macrophages drove towards M2 and suppressed the expression of the M1 marker (Kim, 2017). Consistent with our pathway analysis of the inflammatory features of M1 (I) derived from GM-CSF compered M-CSF derived M2 (I), a study found that GM-CSF derived macrophages likely resemble the transcriptional profile of macrophages from synovial fluid from rheumatoid arthritis patients other than M-CSF derived macrophages (Soler Palacios et al., 2015).

Although stimulation of pro-inflammatory M1 (II) with IL-4 and IL-13 cytokines to produce M1 (III) suppressed upregulated LPS and IFN-γ induced genes and functional pathways, these M1 (III) derived from GM-CSF still exhibit slightly different gene expression when compared with their compartment in M-CSF derived M2 (II) or original M2 (II), as shown in **Figures 4.26, 27, and 28**. For example, IL-4 and IL-13 induced genes, including *CCL26*, *IGF*, *CCL18*, *CD163*, and *FOLR2*, were still downregulated. Indeed, LPS and IFN-γ induced genes, such as *GBP4*, *SLAMF7*, (Beyer et al., 2012) and *SERPING1*, and functional pathways, including the IFN-γ response, are still significantly upregulated. This observation was also noticed to a

lesser extent when M2 (III) was compared with the original M1 (II) derived from GM-CSF (**Figure 4.29, 30, and 31**). For example, *CCL17* expression, which is significantly upregulated in GM-CSF derived M1 (I) relative to M-CSF derived M2 (I), was found to be not significantly induced by LPS and IFN-γ stimulation while suppressed by IL-4 and IL-13 stimulation in our GM-CSF derived M1 subpopulations. However, the opposite was *CCL17* expression, which was induced by IL-4 and IL-13 stimulation in the M-CSF derived M2 subpopulation while suppressed by LPS and IFN-γ stimulation. In agreement with this, it was found that the level of released *CCL17* was higher in M1 derived from GM-CSF, and no significant enhancements were noted for further stimulation with LPS and IFN-γ. Conversely, M2 derived M-CSF produced a negligible level of *CCL17*, while further stimulation with IL-4 significantly enhanced *CCL17* at a level comparable to M1 macrophages (Buchacher et al., 2015). This observation of different responses could be attributed to the impact of cytokines used for the differentiation of monocytes into macrophages. GM-CSF derived M1 and M-CSF derived M2 were initially polarised to M2 using IL-4, TGF-β, and IL10, resulting in upregulation of M2 maker genes such as *CD206* and *IL1R2* in both, and *VEGF-*α in M1 and *CCL14* in M2 (Mia et al., 2014). Following LPS and IFN-γ stimulation for 4 hours, upregulated M2 makers were maintained in M2 but not in M1, indeed, this challenging upregulated IL-10 expression in M2.

Thus, the differentiating growth factors could have implications for the response of these cells to another stimuli. Similarly, a study investigated the responses of human GM-CSF and M-CSF derived M1 and M2, respectively, to anti-inflammatory mediators including Prostaglandin E2 (PGE2) and Adenosine (Ado). Following LPS stimulation, M1 and M2 were exposed to regulatory molecules, and it was found that M-CSF was more responsive to these molecules, where they exhibited pro-healing and

angiogenesis properties, while GM-CSF failed to respond to these molecules and they displayed a persistent inflammatory phenotype (Hamidzadeh et al., 2020). This observation was because differentiating GM-CSF failed to upregulate the receptors for these regulatory molecules. The relevance of this study in the context of our project is that which cells would be beneficial in promoting the removal of infection and the resolution of inflammation, followed by the regulation of the profibrotic process. Thus, further study would be beneficial to assess which CSF derived macrophages are more responsive to regulatory meditators for fibrosis.

qPCR results from the previous chapter showed that either well-known M1 markers (*GBP5*, *SERPING1*, *CXCL9*, and *CXCL10*) or M2 markers *MRC1*, *CCL17*, *TGM2*, and *CD163*) were distinctly discriminated between M1 (I) and M2 (I), with *CCL17* and *CD163*, expressed on M1 (I) and M2 (I), respectively, in line with our current findings. We aimed to enhance their pro- and anti-inflammatory properties for our proposed cell-based therapy for the prevention of corneal scarring. Our current findings showed that polarisation of M1 (I) with LPS and IFN-γ profoundly enhanced their proinflammatory features, as revealed by upregulation of gene encoded inflammatory cytokines, chemokines, transcriptional factors and mediators, which were enriched in defence immune responses and inflammation pathways (**Figure4.5, 6, 7, 8 and 9**). In agreement with our findings, stimulation of GM-CSF derived M1 with IFN-γ for 24 hours significantly induced expression of *CCR7*, and *IL12-*β, but also *CXCL10*, in M-CSF derived M2, using qPCR (Kittan et al., 2013). Similar findings were found using RNAseq, where GM-CSF differentiation for 3 days, followed by IFN-γ stimulating for another 3 days was found to induce *CCL5*, Apolipoprotein L3 (*APOL3*), *IL1-*β, and *GBP1* (Beyer et al., 2012). These upregulated inflammatory related genes in M1 (II) were associated with inflammatory immune responses such as

Interferon_Gamma_responses, TNF signalling, and apoptosis pathways. Consistent with this, Derlindati et al. (2015) found that LPS and IFN-γ stimulation for M-CSF derived cells upregulated apoptosis and inflammation pathways.

On the other hand, stimulation of M-CSF derived M2 with IL-4 and IL-13 was found to potentiate their anti-inflammatory properties by upregulating anti-inflammatory and tissue repair related genes, *ALOX15*, *CCL23*, *MAOA*, *CCL26*, *CCL18*, *IGF*, and *TGM2*, similar to the findings of Martinez et al. (2006) when M-CSF derived human macrophages were stimulated with only IL-4 for 18h. These DEGs were found to be associated with type 2 responses, such as *ALOX15*, *MRC1*, *CCL17*, and *CCL22*, which were significantly upregulated in M-CSF derived M2 following IL-4 and IL-13 stimulation (Gerrick et al., 2018, Spiller et al., 2016). Similarity, a recent study found that M-CSF derived M2 stimulated with IL-4 significantly upregulated *MRC1* expression, and *CCL13*, *CCL17*, and *CCL18* production (Hickman et al., 2023).

Regarding stability of polarisation states of our generated macrophages, we found that polarisation of M1 (II) towards M2, M1 (III), using IL-4 and IL-13, suppresses LPS and IFN-γ upregulated genes as well as the inflammation related pathways, as shown in **Figure 4.10, 11, 12, and 13**), Indeed, expression of M2 markers, such as *MCR1*, *LIPA*, *TREM2* (Turnbull et al., 2006), *FABP4* (Boss et al., 2015), *ALOX15*, and *TGM2* was upregulated. Levels of *CCL26*, *CCL18*, and *CCL23* were still downregulated in M1 (III) (**Figure 4.4**). Indeed, these M1 (III) cells exhibited transcriptional differences, which is in agreement with a study by O'Brien and Spiller (2022) who found that exposing human monocyte derived macrophages to LPS and IFN-γ activation prior to IL-4 polarisation resulted in M2 like macrophages that differed from IL-4 stimulated M2 that was directly stimulated with IL-4. Like M1, M2 (II), stimulation with LPS and IFN-γ

resulted in the upregulation of most inflammation related genes and pathways as well as the downregulation of anti-inflammatory related genes. Taken together, these findings may indicate that repolarised macrophages undergo changes to adapt to the stimuli, but they are still different from the original macrophages. We showed this when we compared repolarised macrophages with their originals, where they still had a distinct transcriptional profile and consequently different functions.

A future study on these different subsets of macrophages, when exposed to gellan fluid gel, using next generation sequencing technologies such as RNA seq, would provide insights into the effects of this delivery platform on the transcriptional characteristics of the proposed therapeutic cells. This would enhance our understanding of the biocompatibility of the gellan fluid gel.

In conclusion, it would be worth investigating the polarisation state further in vivo model of microbial keratitis, as there is a diversity of mediators that would have impacts on the mechanism of macrophages polarisation states.

Chapter 5. Validation of RNA sequencing results of pro-inflammatory M1 and pro -healing M2 macrophages using qPCR and Luminex Techniques

5.1. Background

In the previous chapter, we designed a model to characterise our generated subsets of M1 and M2 macrophages and simultaneously assess the persistence and reversibility of their polarisation states in response to opposing cytokines using the RNA sequencing technique **(Figure 4.1)**. We found that GM-CSF derived M1 (I) and M-CSF derived M2 (I) exhibited distinctive transcriptional features. Stimulation of M1 (I) and M2 (I) with the respective pro- and anti-inflammatory signals LPS and IFN-γ, or IL-4 and IL-13, enhanced the features of M1 or M2, respectively. However, the enhanced pro- or anti-inflammatory features in M1 (II) and M2 (II), respectively, were reversibly altered when exposed to opposing cytokines, suggesting their instable states and their capability to respond to the surrounding environment.

However, it is recommended to validate the RNAseq results by qPCR using independent biological replicates to confirm the biological findings (Fang and Cui, 2011). Thus, qPCR of randomly selected genes from the top 50 variable genes across M1 (I), (II), and (III) and M2 (I), (II), and (III) was employed to validate our RNAseq findings. These genes are *IL12β, PTGES, CCL22, MKI67, and IGF1*. Additionally, we also employed a Luminex assay to measure the level of pro-inflammatory and anti-inflammatory molecules, including IL-1β, IL-4, IL-8, Il-10, IL-12p70, IL-13, TNF-α, CCL5, MMP7, PDGF-BB, TGF-β1, and VEGF, from the same biological replicates of RNAseq experiments. This to further validate the protein-coding gene expression level for the corresponding protein secreted.

Inflammatory cytokines and chemokines, including IL-1β, IL-8, IL-12, TNF-α, and MMP7, are secreted by macrophages upon exposure to Th1 cytokines or LPS (Arango Duque and Descoteaux, 2014, Burke, 2004), and to release a range of molecules

with pro-healing properties, such as IL-4, IL-13, IL-10, PDGF-BB, TGF-β1, and VEGF-A, during the wound healing response (Pouliot et al., 2005, Tarique et al., 2015, Barrientos et al., 2008, Arango Duque and Descoteaux, 2014). **Table 5.1** shows the main activities of the assessed molecules in the current chapter.

Thus, the aim of the current chapters is to validate our RNAseq results of three subpopulations of each M1 and M2 macrophages using qPCR and Luminex assay.

Table 5.1

Molecules	Immunological Function
IL-1β	Key pro-inflammatory cytokine involved in immune responses to infection or injury, where it can activate immune cells such as lymphocytes, cause fever contributing in clearance of infection, and induce cell death programme and acute phase reactants (Boraschi, 2022).
IL-8	A chemokine involved in neutrophil and basophil recruitment and angiogenesis(Justiz Vaillant and Qurie, 2023).
IL-12	A key cytokine in the differentiation of Th1 and activation of T cells and NK cells to produce IFN-γ (Justiz Vaillant and Qurie, 2023).
TNFα	A key regulator cytokine of the inflammatory response to infection and injury by promotion of inflammation, induction of fever, apoptosis and acute phase reactants (Kearney et al., 2015, Jang et al., 2021, Arango Duque and Descoteaux, 2014).

CCL5	A pro-inflammatory chemokine mainly involved in the recruitment of T cells and innate immune cells, such as eosinophils, to infected or injured areas (Arango Duque and Descoteaux, 2014).
MMP7	A proteolytic enzyme, Matrilysin, involved in inflammation by the release of TNF-α from the macrophage surface and tissue remodelling by the degradation of ECM components such as Elastin (Parks et al., 2004, Haro et al., 2000).
IL-4	A cytokine involved in differentiation of Th2 and B cells, in response to parasitic infection and allergy, and inhibition of Th1 by suppression of IL-12 (Opal and DePalo, 2000). Involved in the wound healing process by the development of pro-healing M2 macrophages and collagen production(Allen, 2023).
IL-13	Like IL-4, an anti-inflammatory cytokine involved in healing by promotion of M2 macrophages and ECM remodelling (Allen, 2023).
IL-10	An anti-inflammatory cytokine involved in the suppression of pro-inflammatory IL-12 and the antigen-presenting function of Th1 and macrophages (Opal and DePalo, 2000, Justiz Vaillant and Qurie, 2023).
TGF-β1	An anti-inflammatory growth factor involved in suppression of inflammatory responses of immune cells, induction of Treg cells, and wound healing by promotion of cell differentiation and proliferation of fibroblasts (Arango Duque and Descoteaux, 2014, Midgley et al., 2013). It is a key contributor to pathological fibrosis by activating the key effector cells involved in the fibrotic response (Frangogiannis, 2020).

PDGF-BB	A growth factor involved in wound healing and tissue repair by promoting the recruitment of immune cells such as macrophages, the production of TGF-β, VEGF, and IGF-1, contributing to reepithelialisation and remodelling (Barrientos et al., 2008).
VEGF	Like PDGF-BB, a growth factor that has a potent role during the wound healing by promoting blood vessel formation, tissue remodelling and angiogenesis (Barrientos et al., 2008).

5.2. Results

5.2.1. qPCR analysis to assess the expression of randomly set gene - IL12β, PTGES, MKI67, CCL22, CCL26 and IGF1.

To validate the RNAseq expression values, qPCR was employed to independently assess the expression of randomly selected genes from the top 50 variable genes between the 6 subsets of M1 and M2 from the RNAseq results. We selected genes associated with the inflammatory response, *IL12β,* and *PTGES* or a type two response, *CCL22, CCL26 and IGF1*. *IL12β and PTGES* encoded a component of IL-12 cytokine called p40 and an enzyme involved in the formation of PGE2, respectively (Ma et al., 2015, Mosca et al., 2007). *MKI67* was selected as it highly expressed on both M1 (I) and M2 (I). *MKI67* gene encodes a protein ki-67, which is a marker for cellular proliferation (Scholzen and Gerdes, 2000). *CCL22* gene encodes CCL22 chemokine involved in NK and cell trafficking and Th2 responses through its receptor CCR4, while *CCL26* encodes CCL26 involved in recruitment of eosinophils and basophils through its receptor, CCR3 (Korobova et al., 2023, Stubbs et al., 2010).

IGF1 gene encodes Insulin-like growth factor (IGF1) that is involved in tissue regeneration (Tonkin et al., 2015).

For this propose, we generated M1 (I), (II) and (III) and M2 (I), (II) and (III), as shown in the methods chapter (**Figure 2.3)**. Subsequently, primer design and RNA isolation of these cells was performed for qPCR experiment to quantify the expression level of these genes. A comparison of the qPCR results versus the RNAseq results showed compatible patterns of gene expression. qPCR analysis showed that LPS and IFN-γ induced *IL12β and PTGES* genes in M1 (II) and M2 (III) showed a similar pattern of upregulation when compared to RNAseq results, (**Figure 5.1, A and B)**. Similarly, MKI*67* gene expression was consistent in M1 (I) and M2 (I) compared to RNAseq data (**Figure 5.1, C)**. IL-4 and IL-13 induced *CCL22* gene expression in M1 (III) and M2 (II), similar to RNAseq results (**Figure 5.2, A).** In M2 (I) and M2 (II), comparable induction of *IGF1* was observed, consistent with findings obtained from RNAseq (**Figure 5.2, C)**. The only IL-4 and IL-13 induced gene that showed an incompatible pattern is *CCL26* gene with M2 stimulation inducing a rise in RNAseq which is not matched by qPCR (**Figure 5.2, B).** This may be attributed to many reasons, for example, the normalised method in RNAseq analysis considered all the induced genes while only one gene, UBC was used for normalisation in qPCR (Aguiar et al., 2023). Secondly, biological variation and a higher number of biological replicates in RNAseq may be responsible. However, in general these qPCR findings are consistent with RNAseq results, indicating the reliability of our RNAseq data.

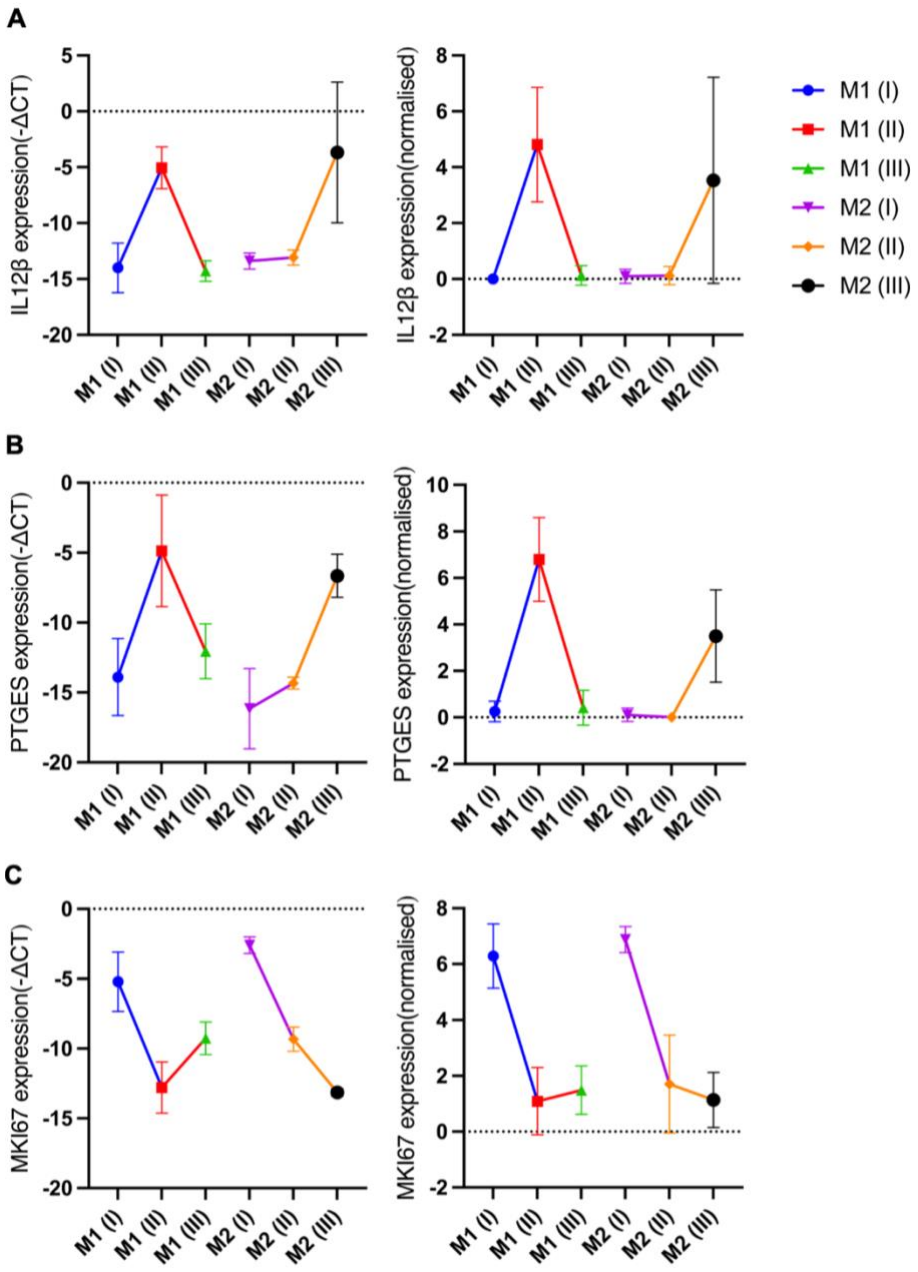

Figure 5.1 Validation of RNAseq results via qPCR: assessing the expression level of genes related to inflammatory responses.

Expression of randomly selected genes from the top 50 variable genes from RNAseq data that are associated with inflammation were independently detected using qPCR. RNA of six subpopulations of macrophages from three independent biological samples were used to perform qPCR analysis. The -dCT values (gene – a normaliser (UBC)) of each gene were plotted as mean with SD (left) to indicate expression level. While RNAseq results of each gene from seven samples were plotted as mean with SD of log2 normalised counts (right). (A) presents *ILβ gene* qPCR (left) and RNAseq(right). (B) presents *PTGES gene* qPCR (lift) and RNAseq(right). (C) presents *MKI67 gene* qPCR (left) and RNAseq(right).

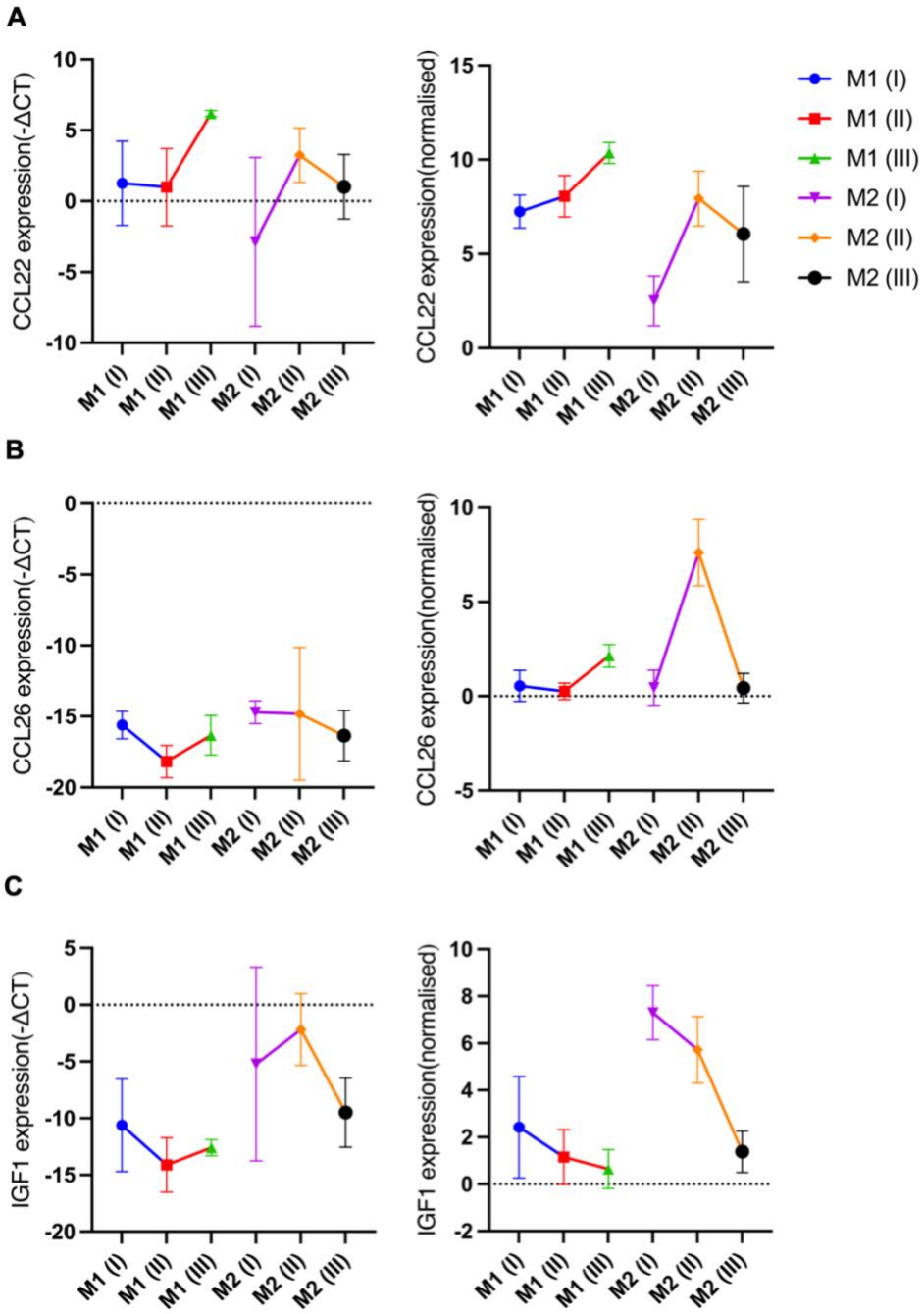

Figure 5.2 Validation of RNAseq results via qPCR: assessing the expression level of genes related to type two immune response.

Expression of randomly certain genes from the top 50 variable genes from RNAseq data that associated with healing process were independently detected using qPCR. RNA of six subpopulations of macrophages from three independent biological samples were used to perform qPCR analysis. The -dCT values (gene – a normaliser (UBC)) of each gene were plotted as mean with SD (left) to indicate expression level. While RNAseq results of each gene from seven samples were plotted as mean with SD of log2 normalised counts (right). (A) presents *CCL22 gene* qPCR (left) and RNAseq(right). (B) presents *CCL26 gene* qPCR (lift) and RNAseq(right). (C) presents *IGF1 gene* qPCR (left) and RNAseq(right).

5.2.2. Measurement of M1 subset production for pro-and anti-inflammatory or pro-healing molecules.

M1 (I), M1 (II) and M1 (III) were generated and subjected to different stimulations to determine their secretion of either anti-inflammatory or proinflammatory meditators, as shown in Figure 5.3, A. The Luminex results revealed that M1 (I) released a noticeable level of these pro-inflammatory molecules, including IL-1β, IL-8, TNFα, CCL5, but not IL-12p70 (**Figure 5.3, B)**. The level of these meditators clearly enhanced following pro-inflammatory stimulation with LPS and IFN-γ in M1 (II) but was not statistically significant. Conversely, anti-inflammatory stimulation with IL-4 and IL-13 led to significant suppression in most of these molecules, apart from IL-12p70, and MMP7 which were not statistically significant (**Figure 5.3, B)**.

Conversely, the Luminex findings of the anti-inflammatory or pro-healing secretion in three subsets of M1 revealed that M1 (I) released a detectable range of anti-inflammatory molecules such as IL-10, PDGF-BB, TGF-β1 but not VEGF-A, IL-4 or IL-13 (**Figure 5.4**). Upon pro-inflammatory stimulation, a noticeably continuous increase in IL-10 secretion was observed in M1 (II), while PDGF-BB, and TGF-β1 production was reduced in M1 (II) when compared with M1 (I) and M1 (III) (**Figure 5.4**). Indeed, production of TGFβ-1 seems to be comparable among M1 subsets. Low levels of IL-4 and IL-13 were detected in M1 (II) relative to M1 (I). Conversely, anti-inflammatory stimulation resulted in a significant reduction in IL-10 levels in M1 (II) as compared to M1 (III), while PDGF-BB level was increased in M1 (III) relative to M1 (I) and M1 (II), though this increase was not significant (**Figure 5.4**). Although an increased TGF-β1 level was observed following anti-inflammatory stimulation in M1 (III), M1 (I) is still a higher producer as compared to M1 (II) and M1 (III). M1 (II) significantly produced IL-

4 and IL-13 when compared to M1 (I) and M1 (II), while VEGF-A production was not detected in any of M1 subsets (**Figure 5.4**). This significant production of IL-4 and IL-13 upon IL-4 and IL-13 stimulation could be attributed to the remaining IL-4 and IL-13. The gene expression of each corresponding cytokine is shown in supplementary **Table S**1.

Taken together, these findings demonstrated that the transcriptional changes of M1 subsets, identified by RNAseq analysis, in response pro-and anti-inflammatory stimulation are generally consistent at the protein level.

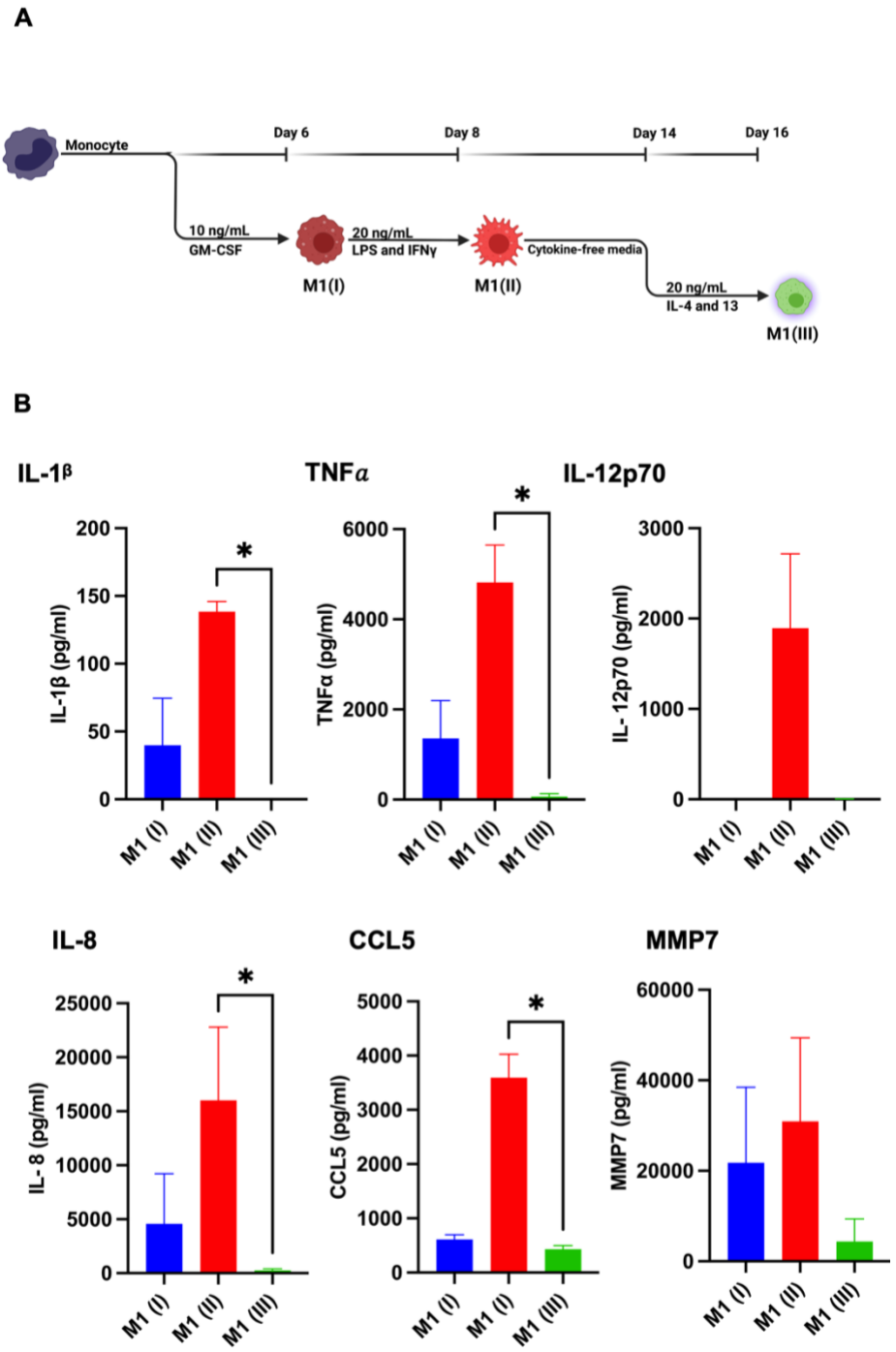

Figure 5.3 Validation of RNAseq results via Luminex: assessing the inflammatory related molecules level in M1 subsets.

The level of inflammatory molecules in three biological replicates from the RNAseq samples were detected using Luminex assay. Supernatants of three M1 subpopulations of macrophages that are generated and treated as described in **(A)** were used to perform the Luminex assay. **(B)** The concentration (pg/ml) of each molecule, including IL-1β, TNFα, IL-12p70, IL-8, CCL5 and MMP7, were plotted as mean with SD. GraphPad prism was utilised for statistical analysis, and significance was assessed via one-way ANOVA with Dunn's multiple comparisons. (* $p<0.05$), (n=3).

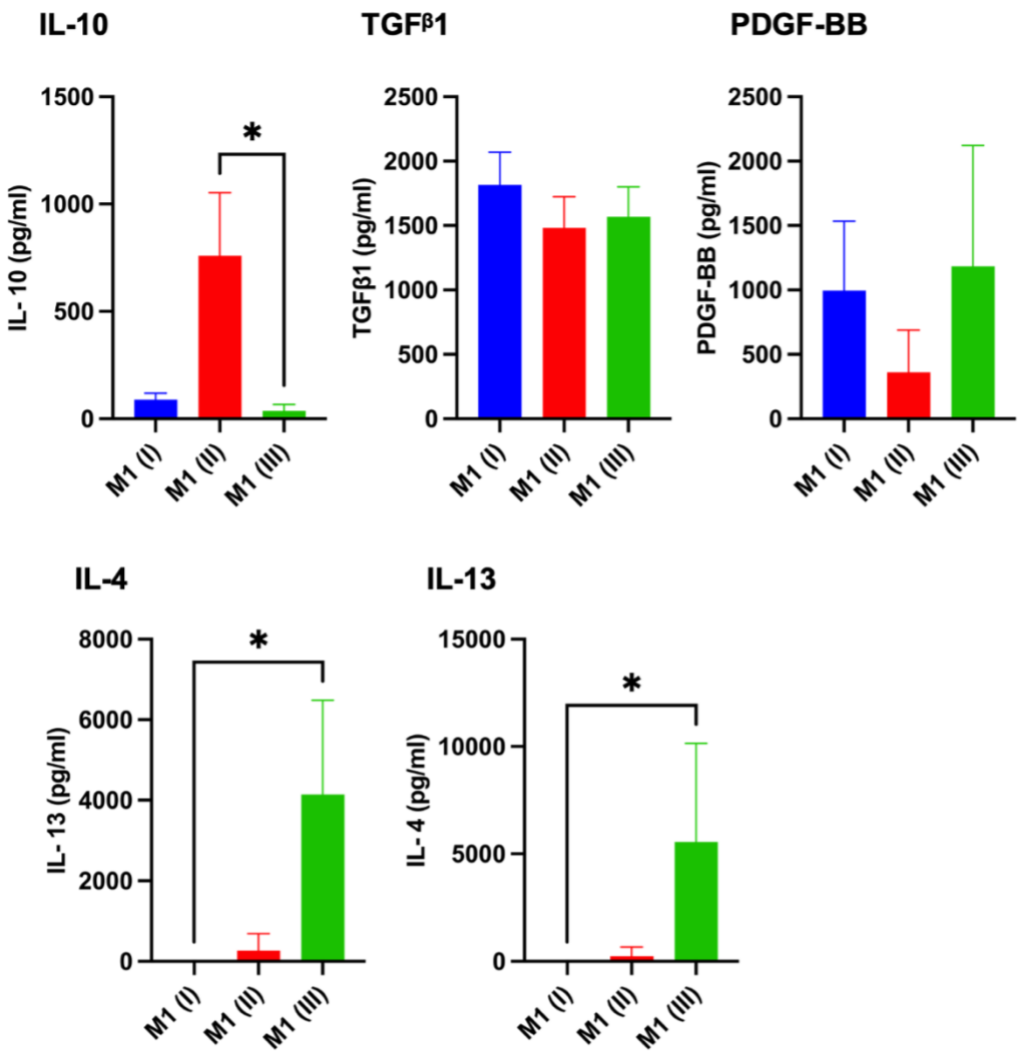

Figure 5.4 Validation of RNAseq results via Luminex: assessing the anti-inflammatory or pro-healing related molecules level in M1 subsets.

The level of anti-inflammatory or pro-healing molecules in three biological replicates from the RNAseq samples were detected using Luminex assay. Supernatants of three M1 subpopulations of macrophages that are generated and treated as described in **(5.3, A)** were used to perform the Luminex assay. **(B)** The concentration (pg/ml) of each molecule, including IL-10, TGFβ1, PDGF-BB, IL-4, and IL-13, were plotted as mean with SD. GraphPad prism was utilised for statistical analysis, and significance was assessed via one-way ANOVA with Dunn's multiple comparisons. (* $p<0.05$), (n=3).

5.2.3. Measurement of M2 subset production for pro-and anti-inflammatory or pro-healing molecules.

As described in **Figure 5.5, A**, three subsets of M2 were formed and exposed to different stimulations to measure their secretion of either anti-inflammatory or pro-inflammatory meditators. The Luminex results revealed that M2 (I) released low levels of IL-1β, TNF-α, IL-8, and MMP7, while CCL5, and IL-12p70 were not detected (**Figure 5.5, B)**. The level of these meditators decreased in response to anti-inflammatory stimulation, IL-4 and IL-13, in M2 (II), (**Figure 5.5, B)**. Conversely, upon pro-inflammatory stimulation with LPS and IFN-γ, M2 (III) exhibited higher secretion of these molecules compared to M2 (I) and M2 (II). However, the only statistically significant change was observed for IL-12p70 (**Figure 5.5, B)**.

In contrast, the anti-inflammatory or pro-healing molecule production in three subsets of M2 revealed that M2 (I) released detectable ranges of IL-10, PDGF-BB, TGF-β1 and VEGF-A, while IL-4 and IL-13 were not detected (**Figure 5.6)**. Similar, to M1, levels of TGFβ-1 production were observed in all M2 subsets. IL-4 and IL-13 production was only seen in M2 (II), (**Figure 5.6)**. This higher production of IL-4 and IL-13 upon IL-4 and IL-13 stimulation could be attributed to the remaining IL-4 and IL-13.

Pro-inflammatory stimulation with LPS and IFN-γ, increased levels of IL-10, PDGF-BB, TGF-β1and VEGF-A, in M2 (III) relative to M2 (II) and M2 (I), with undetectable levels of IL-4 and IL-13 (**Figure 5.6)**. However, the observed alterations in molecule levels across M2 subsets were not statistically significant, which could be due to the use of only three biological replicates, limiting statistical power of our experiments. The gene expression of each corresponding cytokine is shown in supplementary **Table S2**.

Overall, although our findings showed certain trends in the molecule levels across M2 subsets, it is worth mentioning that we should be cautious about these alterations due to the insufficient power of our experiments.

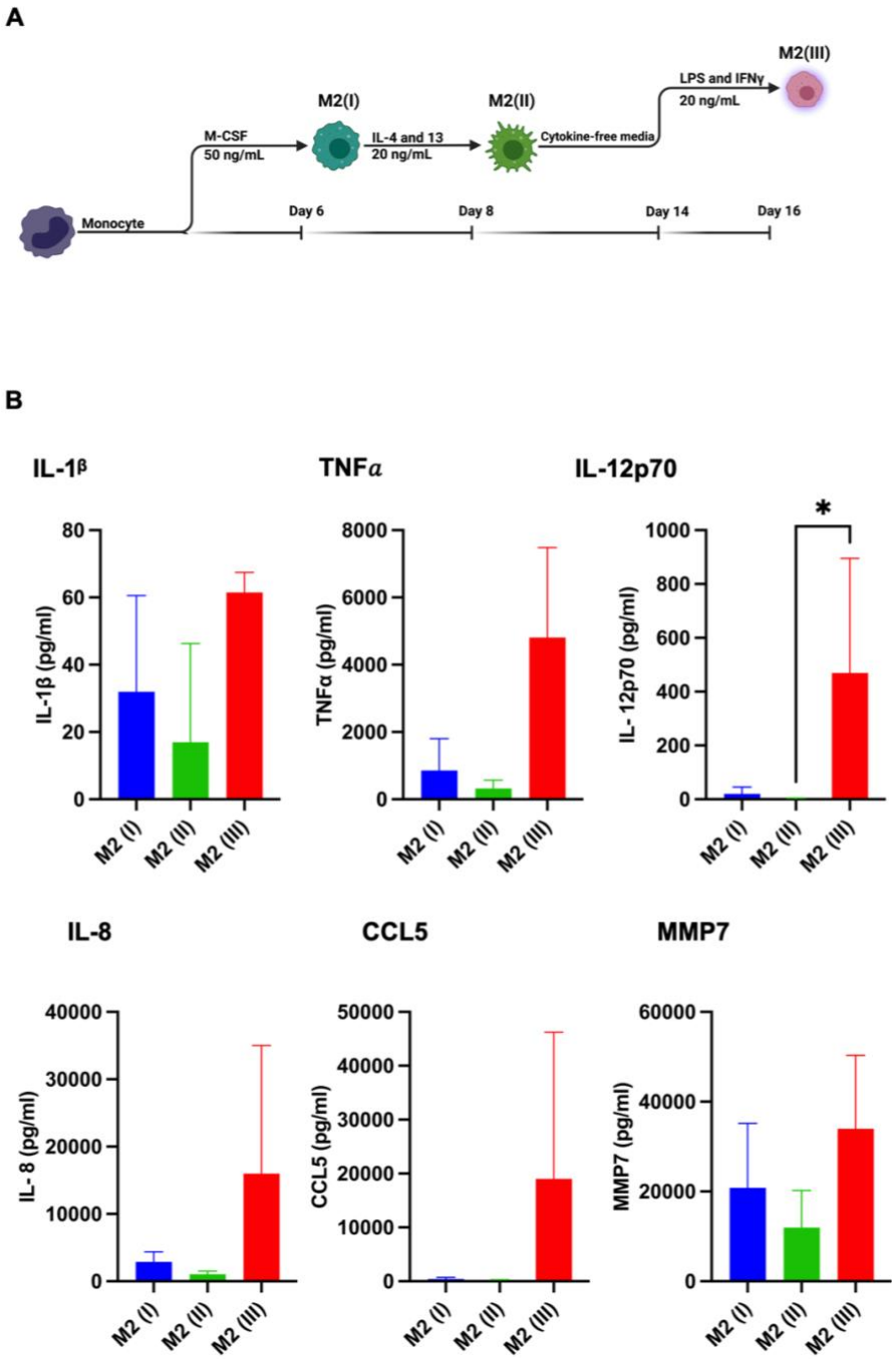

Figure 5.5 Validation of RNAseq results via Luminex: assessing the inflammatory related molecules level in M2 subsets.

The level of inflammatory molecules in three biological replicates from the RNAseq samples were detected using Luminex assay. Supernatants of three M2 subpopulations of macrophages that are generated and treated as described in **(A)** were used to perform the Luminex assay. **(B)** The concentration (pg/ml) of each molecule, including IL-1β, TNFα, IL-12p70, IL-8, CCL5, and MMP7, were plotted as mean with SD. GraphPad prism was utilised for statistical analysis, and significance was assessed via one-way ANOVA with Dunn's multiple comparisons. (* $p<0.05$), (n=3).

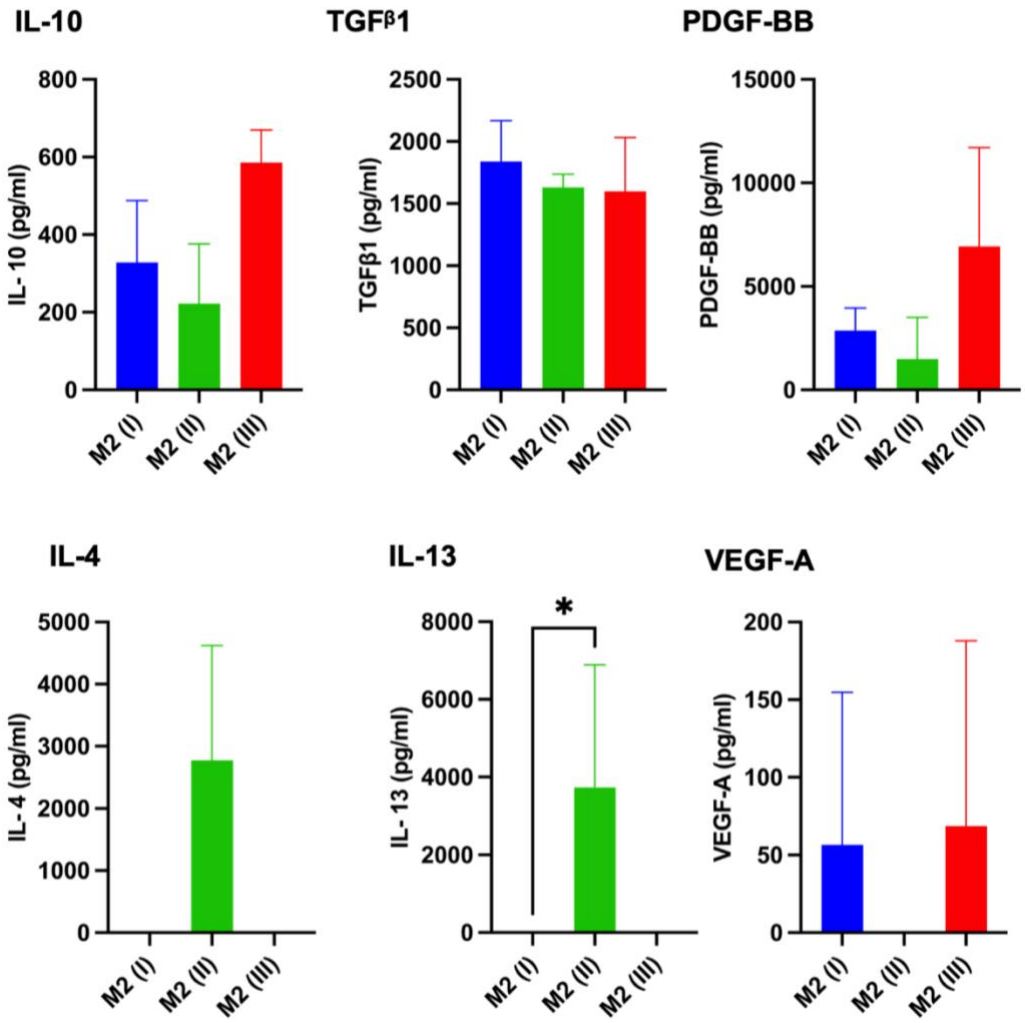

Figure 5.6 Validation of RNAseq results via Luminex: assessing the anti-inflammatory or pro-healing related molecules level in M2 subsets.

The level of anti-inflammatory or pro-healing molecules in three biological replicates from the RNAseq samples were detected using Luminex assay. Supernatants of three M2 subpopulations of macrophages that are generated and treated as described in (**5.5, A**) were used to perform the Luminex assay. (B) The concentration (pg/ml) of each molecule, including IL-10, TGFβ1, PDGF-BB, IL-4, and IL-13, were plotted as mean with SD. GraphPad prism was utilised for statistical analysis, and significance was assessed via one-way ANOVA with Dunn's multiple comparisons. (* $p<0.05$), (n=3).

5.3. Discussion

To validate the RNAseq data of six subpopulations of M1 and M2 macrophages, qPCR and Luminex were used to measure the mRNA and protein levels of selected genes and molecules. qPCR showed compatible patterns of gene expression for *IL12β, PTGES, and MKI67,* or *CCL22, CCL26 and IGF1.* (**Figure 5.1** and **5.2)**. Although, at the protein level, the production of cytokines, chemokines, and growth factors appears to change in response to sequential stimulations, some of these changes were not statistically significant, particularly in the M2 subpopulation (**Figures 5.5 and 5.6**). These observations suggest that there might be instability in the polarisation states of M1 and M2 subpopulations. However, caution should be considered when interpreting these results in M2 subsets. Thus, increasing the number of biological replicates would enhance the power of our experiment and would confirm our findings.

Consistency in results between RNAseq and qPCR methods was observed in a study by Everaert et al. (2017) who found the RNAseq results highly correlated with that in qPCR. Additionally, upregulated expression of *IL12β,* in our qPCR results in response to LPS and IFNγ treatment and high induction of *CCL22*, *CCL26* and *IGF1* associated with IL-4 and IL-13 treatment is supported by a study by Martinez et al. (2006) who generated LPS and IFN-γ stimulated M1 and IL-4 stimulated M2 from M-CSF derived macrophages.

The suppression of pro-inflammatory molecules in response to IL-4 and IL-13 stimuli in both M1 and M2 subsets supports their identification as IFN-γ antagonists and found to decrease macrophage production of IL-1 and TNF-α (Gordon, 2003).

The observed increase in PDGF-BB production in IL-4 and IL-13 stimulated M1 (III) is in line with a study by Scott et al. (2021) who phenotyped different subsets of cord blood monocyte- derived M1 and M2 macrophages and assessed their polarisation stability to use them for regenerative intervention. In contradiction with our findings in M2 (II), IL-4 and IL-13 produced significantly higher levels of PDGF-BB, while its production was suppressed by LPS and IFN-γ stimulation. Moreover, levels of VEGF-A secretion, undetectable in our M1 subsets, were increased in response to LPS and IFN-γ. Conversely, they found that IL-4 and IL-13 activated M2 produced high levels of VEGF-A following LPS and IFN-γ stimulation, consistent with our results in M2 (III) (Scott et al., 2021). The contrary findings could be attributed to several factors. For example, cord blood monocytes were used in their study to produce macrophage subpopulations, whereas our M1 and M2 are originated from monocytes in adult peripheral blood. Jiang et al. (2004) transcriptionally profiled circulating monocytes and cord blood monocytes using microarray technology. Circulating monocytes exhibited distinctive transcription in response to LPS stimulation as compared to neonatal monocytes. For example, significantly increased expression of pro-inflammatory cytokines and chemokines, including IL-1β, IL-8 and CCL5, was observed in circulating relative to neonatal monocytes. Secondly, a study examining the impact of LPS and IFN-γ, IL-4 and IL-10 treatments on the cytokine production of human monocyte-derived macrophages found that the time points of stimulation significantly impacted the level of cytokine secretion. Production of IL-10 and TGFβ-1 peaked at day 3, whereas in our studies, the time point of the cytokine production was on day 2. Undetectable VEGF-A in our M1 subsets could be explained by its peak level was at 6 days(Unuvar Purcu et al., 2022).

Elevated IL10 production by macrophages following LPS and IFNγ stimulation, M1 (II) and M2 (III), is consistent with findings of other studies and the regulatory response of macrophages to secrete IL-10 to relieve the potent inflammatory environment (Smith et al., 1998, Iyer et al., 2010). Thus, anti-inflammatory effects of IL-4 and IL-13 may result in the downregulation of these regulatory mechanisms. Consistent with this concept, our results showed that IL-10 production was not induced by IL-4 and IL-13 stimulation.

We showed that M1 (I) and M2 (I) and their corresponding subsets M1 (II) and M1 (III) or M2 (II) and M2 (III), respectively, secreted elevated amount of TGFβ-1, which was in line with a study by Vogel et al. (2014) who investigated the impact of several maturating factors, including M-CSF, GM-CSF, and human serum on phenotype and cytokine production of monocyte derived macrophages. They found M-CSF and GM-CSF derived macrophages exposed to stimulation with either LPS and IFN-γ or IL-4 produced a higher level of TGFβ-1 with no significant difference among these subsets of macrophages. This could explain the similar level of TGFβ-1 among our M1 and M2 subsets.

The findings of our *in vitro* experiment to assess the maintenance of the polarisation states for monocyte-derived macrophages showed instabilities in subpopulations as determined by transcriptional and partially by protein production. However, these results are limited by the use of circulating monocyte derived macrophages that can infiltrate the injured or inflamed tissue, but do not include tissue resident macrophages. Moreover, our experimental approach does not consider the *in vivo* setting including interaction with surrounding cells and the ECM, which circulating monocytes would encounter when entering an inflamed site. Recent data has shown that the tissue

environment was found to directly affect macrophage phenotypes in ovarian cancer metastasis, leading to a poor prognosis for the disease. Healthy monocytes co-cultured with decellularised ECM from patient tissue resulted in macrophages that exhibited a similar transcriptional profile of tumor associated macrophages in ovarian cancer (Puttock et al., 2023).

It is worth mentioning that validating these observed alterations in the transcriptome and secretome by assessing phagocytic and efferocytotic functions, will significantly enhance our understanding of the stability of polarisation states of macrophage. Therefore, it should be acknowledged that the assessment of these effector functions in M1 and M2 subpopulations is a major limitation of the current study.

In conclusion, we have shown that *in vitro* generated M1 and M2 macrophages change their phenotype in response to sequential stimulation at both mRNA and partially at protein levels emphasizing the cautious use of these cells in the prevention of corneal scarring from microbial keratitis.

Chapter 6. General discussion

6.1. General discussion

6.1.1. A novel treatment

Ocular opacity still occupies the leading cause of blindness throughout the globe (Flaxman et al., 2017), with a recent estimate demonstrating that more than five million people suffer from vision impairment due to corneal scarring (Wang et al., 2023a). Corneal transplantation is an effective treatment; however, its limited availability still represents a significant challenge(World Health Organization, 2019).

Thus, studies to develop a novel treatment to prevent corneal scarring are required. Recent studies have reported gene therapy to prevent the scar formation which showed promising results at *in vitro* and *in vivo* level, yet no efficient response was seen in clinical studies. (Yang et al., 2023). As rapidly clearing infection and reducing inflammation to limit damage in affected cornea are crucial for regenerative corneal repair, this project focuses on developing a novel treatment using multiple molecules released rather than one at a time using subsets of M1 and M2 macrophages. However, it is essential to determine whether the activation states of the implanted macrophages will be maintained within the context of the affected cornea. Therefore, we initially aimed to investigate the stability of macrophage polarisation states *in vitro*. These macrophage-derived molecules, including anti-microbial peptides (Zhang et al., 2021), growth factors, and anti-inflammatory mediators, aid re-epithelialisation, while minimising fibrotic signalling cascades to aid 'scarless' healing of the ocular surface and the preservation of sight. The requirement of macrophages for regenerative responses in tissue is increasingly evident, for example, by a recent study of lens regeneration in newts. Compared to the non-injected group, macrophage ablation by clodronate liposome injection at the early or late phase of the healing response

following lentectomy resulted in chronic inflammation and fibrosis and the absence of lens regeneration. External application of fibroblast growth factor 2 that can be produced by macrophages onto the eye of the ablated group enhanced the growth of iris pigment epithelial cells and ultimately improved generative repair (Tsissios et al., 2023).

There are two novel findings from this study. One is that embedding in gellan gel does not alter the phenotype of polarised macrophages with the exception of CD163, which may be lost on retrieving cells from the gel. In proposed in vivo studies macrophages would be “released” onto the corneal surface as the gel becomes fluid due to natural shear stress. Secondly, with regards to macrophage polarisation this is one of the first studies challenge cells with a third cytokine incubation as opposed to a single challenge. This would mimic our proposed in vivo study where cells would be polarised in vitro to M1 (II) or M2 (II) then transferred to inflamed corneas where the environment may mimic (M1 (III) or M2 (III) conditions. That these cells remain plastic in these environments suggests that this protocol requires further investigation. It is possible that the in vitro conditions to generate M1 (III) and M2 (III) are too strong, and a more nuanced environment may be present in the inflamed cornea at different times. Only *in vivo* studies could answer that question.

6.1.2. Gellan fluid gel as a delivery system

Despite the significant number of studies into novel therapies for corneal scarring, the effective delivery of these treatments to the ocular surface still poses a significant challenge, due to nasolacrimal drainage and eye blinking which can wipe the treatment and decrease its retention. We used gellan fluid gel as delivery platform for our macrophage-based therapy that promote the sustained release of multiple molecules

on the ocular surface and enhance their retention. Gellan fluid gel is characterised by its ability to behave as liquid when subjected to motion and then recover to a solid form when the movement is eliminated. This unique property is attributed to applying shear force during the gelation process, which, unlike topical gel, creates a microstructure, leading to this property. The concentration and type of biopolymer, cross-linking agents, and magnitude of applied force during gel preparation are key factors in determining this property (Norton et al., 1999). This unique feature of gellan fluid gel makes it an ideal vehicle for delivering cells to the ocular surface. Thus, it can easily flow from the eye drop onto the surface of the eye and then recover to a solid layer that increases the bioavailability and resists quick removal, ultimately increasing the bioavailability.

Recent reports emphasise the significant limitations of current treatment for eye surface diseases. These limitations include decreased retention of treatment and bioavailability, and their consequently increased frequent application of treatment, and inadequate lubricating properties, consequently leading to increased stress on the eye surface. Consistent with our study, recent reports advocate for the use of fluid gel as a delivery platform for the treatment of ocular surface diseases to overcome these limitations of the current treatments (Grover et al., 2022, Zheng et al., 2023). Our findings that showed the biocompatibility of gellan fluid gel supports its usage as a delivery platform to other molecules or other cell-based therapy. Additionally, our findings may indicate that the gellan fluid gel does not alter the phenotype of M1 and M2.

Hill et al. (2018) applied gellan fluid gel with decorin on the surface of the cornea of mice in a model of bacterial keratitis. They concluded that a resorbable and optical

clear dressing is created that facilitated continued release of decorin on cornea and prevented the formation of corneal scar and also suggested feasibility to be eye drop. Interestingly, without of the addition of decorin, the fluid gel alone appeared to generate a microenvironment that promotes scar free wound healing, as seen by a decrease in corneal opacity and signs of scar formation (Hill et al., 2018). Consistent with our study, Chouhan et al. (2019) assessed the biocompatibility, release of active agents, optical clarity, and retention of gellan fluid gel. Decorin capsulated in gellan fluid gel continues to release over 3 hours, a desired feature for therapeutic agent. Using human corneal fibroblast *in vitro* culture, the viability of these cells for a period of 12 days was not affected by gellan fluid gel. Additionally, the light transmission rate of gellan fluid gel in the eyes of a rat model *in vivo* remained more than 90% for a period of one month, suggesting stable transparency of the gellan fluid gel. In the rat model, the retention of gellan fluid gel was significantly increased as compared to PBS, where 50 μm of gellan fluid gel were detected after about 2h of applying 1000 μm of gellan fluid gel to a corneal rat. The use of gellan fluid gel as a spray delivery platform for autologous cell transfer for the treatment of burned skin demonstrated promising outcomes. It showed effective spreading properties and had higher retention after application when compared to the clinically available saline solution. It has no effect on the viability of the seeded human dermal fibroblasts in vitro for a period of 7 days as well as post spraying (Ter Horst et al., 2019).

Although our findings indicated that the gellan fluid gel does not alter the phenotype of M1 and M2 macrophages at the mRNA level, flow cytometry importantly showed a significant reduction in CD163 expression in M2 macrophages following gellan fluid gel application. However, this reduction could potentially be attributed to CD163 shedding. Some studies have shown the promising outcomes of fluid gel-based

delivery of cell therapy and therapeutic agents. Its usage in the form of hydrogel (no shear force) as a carrier system for drug and cell therapy has provided promising results, as reviewed by Das and Giri (2020). A recent study, for example, used gellan gum-based hydrogel to deliver corneal endothelial cells to rabbits in vitro. Gellan gum-based hydrogel has promoted their proliferation and has no effect on their viability(Seo et al., 2023).

The topical carrier systems of ophthalmic drugs, for example, are dry eye drops, intraocular injections, and contact lenses, which can be associated with limitations such as inadequate retention and bioavailability, the risk of microbial keratitis (contact lenses), and visual distortion (Grover et al., 2022, Shahrizan et al., 2022). Consequently, these limitations reduce the efficacy of treatment, patient compliance, and ultimately corneal scarring and blindness. Thus, the properties of gellan fluid gel, including biocompatibility, transparency, and its physical liquid-solid transition, would establish it as an ideal platform for carrying drugs onto the ocular surface.

In conclusion, we demonstrated the biocompatibility of gellan fluid gel as an ophthalmic delivery platform, not only for our macrophage-based therapy but potentially for a variety of ocular surface diseases. However, the assessment of the effector functions of implanted macrophages and their behaviour needs to be investigated in an in vivo model to fully confirm its applicability. Unfortunately, due to the COVID-19 pandemic, this part of the work was not possible.

6.1.3. Simulation of depolarisation

In this project, we were able to effectively generate different subsets of M1 and M2 macrophages from peripheral human monocytes, which exhibited a gene/protein

expression profile consistent with either pro-inflammatory or anti-inflammatory properties, respectively.

We showed that the polarisation states of macrophages are reversible and that both pro-inflammatory and anti-inflammatory features can be exhibited by macrophages dependent on the microenvironment. The stability of polarised macrophages has been assessed by several studies. Most of these studies showed that macrophages change their phenotype in response to secondary stimulation. However, these phenotypic changes may not necessarily lead to complete depolarisation towards the original phenotype but may exhibit mixed features of both phenotypes.

The reversibility of activation states in *ex vivo* experiments was observed by a study that found isolated M2 arginase 1 (ARG1+), resistin-like molecule α (RELM-α+), and chitinase-like 3 (Ym1+) macrophages from a mouse model of chronic parasitic infection associated Th2 response. *Ex vivo* stimulation of these M2 with LPS and IFN-γ resulted in enhanced microbiocidal effects of these cells, such as increased production of nitric oxide (NO) and suppressed expression of RELM-α and Ym1. However, they found these cells failed to induce IL-12 secretion, which is critical for Th1 responses (Mylonas et al., 2009).

A second study found that switching stimuli in monocyte-derived macrophages resulted in changing their phenotype as determined by common markers. In this study IFN-γ or IL-4 were bound to scaffolds to mimic a short release microenvironment. Switching macrophages to different scaffolds led to changes in genes, proteins and markers consistent with altered polarisation (Spiller et al., 2015).

We found that IL-4 and IL-13 stimulation appeared to result in higher levels of PDGF-BB in M1 (III) compared to LPS and IFN-γ-stimulated M1 (II), which might suggest an anti-inflammatory effect of IL-4 and IL-13. Conversely, LPS and IFN-γ stimulation tended to increase PDGF-BB levels in M2 (III) compared to other M2 subsets. This observation could imply that macrophages exhibit a mix of M1 and M2 features, rather than fitting neatly into one category. However, it is worth noting that these observed changes in molecule levels were not statistically significant, likely due to the limited number of biological replicates in our study. Therefore, these findings should be interpreted with caution because they do not indicate sufficient evidence of this effect.

The findings of instable states of our polarised macrophages in our model could emphasise the implication of prior either pro- or anti-inflammatory activation on subsequent activation of macrophages, which has resulted in distinctive macrophage phenotypes (O'Brien and Spiller, 2022, Czimmerer et al., 2022).

A study examined the phenotypic changes of human monocyte-derived macrophages during a normal inflammatory response using an *in vitro* model, recapitulating the subsequent stages of the inflammation process. Initially, monocytes were subjected to CCL2 stimulation, followed by pro-inflammatory stimulation with LPS, TNF-α, and IFN-γ. To mimic the resolution phase of inflammation, monocytes were stimulated with IL-10 and TGF-β. Using RNAseq, these cells exhibited the transcriptional features of M1 macrophages in response to pro-inflammatory stimulation and then acquired the M2 phenotype in response to anti-inflammatory stimulation, suggesting the instability of the activation states of these cells. However, these cells were subjected to pro-inflammatory molecules instead of anti-inflammatory stimulation to mimic chronic inflammation. These cells exhibited both transcriptional features of M1 and M2

macrophages (Italiani et al., 2020). However, the complex mechanism that underlies the dynamic change in phenotype in response to the surrounding stimuli is still not well understood (Guilliams and Svedberg, 2021, Katkar and Ghosh, 2023).

Regarding to our proposed therapy in the current project, our findings showed the instable states of the polarised M1 and M2 macrophages. This result necessitates caution when using these cells in the treatment of corneal fibrosis from microbial keratitis. According to our results, the microenvironment of the infected cornea would regulate the polarisation states of administrated macrophages. For example, the pro-inflammatory microenvironment may either shift M2 macrophages towards a pro-inflammatory state or sustain the activity of pro-inflammatory macrophages, which may lead to undesirable outcomes. However, there are many factors related to our delivery platform and the nature of the ocular surface that could affect macrophage polarisation, including whether gellan fluid gel would enable cells to migrate to the cornea. Macrophages would be released onto the inflamed cornea *in vivo* as the gel is dispersed via the mechanical effects of eye blinking and tear production. This would be future work testing our proposed therapy using a mouse model of microbial keratitis(Hill et al., 2018).

6.2. Limitations of the study

Our project investigated the applicability of using gellan fluid gel as a delivery system to apply a novel macrophages-based therapy onto the injured cornea to promote scar free healing and ultimately prevention of blindness. The biocompatible assessment of the gellan fluid gel and the investigation of stability of polarisation states of macrophages of human macrophages were carried out *in vitro* using monocyte derived macrophages from healthy donors provided from NHS Blood and Transplant

Birmingham centre. As stated, due to constraints of COVID were able to access samples from a few patients. Moreover, using blood samples from different donors without knowledge of their gender, age, and underlying health conditions may have introduced a level of variability in the findings of our investigation. The availability of details about the donors would decrease the level of variability resulting from these factors.

Secondly, while we were able to investigate the effect of fluid gel on the phenotype or polarisation states of M1 and M2 macrophages, we were not able to investigate the effect of the gellan fluid gel on encapsulated macrophage activities, including their migration and sustained release of their cytokines. This was because the mechanical force exerted by the eyelid will be significantly involved in the release of either the macrophages or their products. It was not possible to apply such force *in vitro*. To address this, we planned to apply gellan fluid gel containing macrophage subsets labelled tomato red fluorescent on the injured cornea of Cx3cr1-gfp mice, in which resident monocyte derived cells in the eye are GFP+ fluorescent green (Zinkernagel et al., 2010). Macrophage migration, phenotype and function would have been analysed in this model. We planned to use this keratitis model in collaboration with Dr. Jose Hombrebueno, University of Birmingham, to apply macrophage-based therapy, however, development of the model in our BMSU was severely affected by its closure due to the COVID-19 pandemic. Moreover, as stated human donor blood samples were not available during the pandemic and therefore when newly available finishing the in vitro part of the project took precedence.

Thirdly, we used sequential stimulation of combinations of cytokines *in vitro* to mimic the cytokine environment of corneal healing response from microbial keratitis. Direct

application of combination of cytokines, such as LPS and IFNγ, on macrophages would not necessarily reflect what happens during corneal wound healing process following microbial keratitis. For example, the presence of LPS and IFNγ molecules in the patient cornea is less likely because treatment of patients with antibiotic and anti-inflammatory agents in eyedrops are effective in infection clearance and resolution of inflammation.

Moreover, the interaction of applied macrophages with surrounding cells and the ECM may produce different results and only an animal model would enable the effect of the entire microenvironment on macrophage polarisation and corneal healing response to be assessed.

6.3. Future work

We showed that gellan fluid gel is a biocompatible material and did not exert any effects on M1 and M2 macrophage polarisation states. Thus, it has potential applicability as a delivery system for M1 and M2 macrophages into the cornea. Future work would investigate an approach that generates macrophages that have the capacity to maintain a specific polarisation state. This would enable macrophage delivered by gellan fluid gel on the cornea to modulate its cornea microenvironment towards pro-healing and anti-scarring repones.

One recently reported feasible approach are engineered macrophages, identified as macrophage Chimeric Antigen Receptor (CAR). The concept of these CAR macrophages is inspired by CAR T cells, which, incorporating variable regions of antibody with a costimulatory CD3ζ domain of the T-cell receptor to enhance the anticancer activity of T cells to kill cancer cells, showed efficient anticancer activity in the management of blood cancer (Mitra et al., 2023). A recent study by Lei et al. (2024) developed pluripotent stem cells derived CAR macrophages with proinflammatory

properties (second generation) that have enhanced anticancer activity to destroy tumour cells in solid cancer. The second-generation CAR M1 macrophages were engineered to have an intracellular domain of TLR4 for the induction of proinflammatory responses and a CD3ζ domain for the promotion of phagocytic function to enhance their antitumor effect. CAR M1 exhibited proinflammatory responses such as the production of IL12 and TNF and antitumor function both *in vitro* and *in vivo* (Lei et al., 2024). Such a type of engineered CAR macrophages would be able to resist and modulate the cornea microenvironment towards regenerative corneal wound healing and eventual preservation of sight.

A second approach would be to deliver autologous blood monocytes via gellan fluid gel into the inflamed cornea. Monocytes are a diverse population that may be categorised into three types, as described in Chapter 1. A study examining the function of infiltrating monocytes in a mouse model of myocardial infraction found that two different subpopulations traffic to affected site in a sequential manner and display different functions. Early recruited monocytes exhibited phagocytic and inflammatory responses, while pro-healing reparative activity was demonstrated by the later recruited monocytes (Nahrendorf et al., 2007). The benefit of using monocyte-based therapy is that it applies immediately to the infected cornea, promoting the clearance of the infection. Sequentially, a pro-healing subset of monocytes would be applied to induce the resolution of inflammation and the repair process.

In conclusion, we have shown that gellan gel is a potential delivery system for cell or drug-based therapies for scarring corneal conditions. The type of cell delivered and the required timing for effectiveness needs to be developed.

Chapter 7. Supplementary

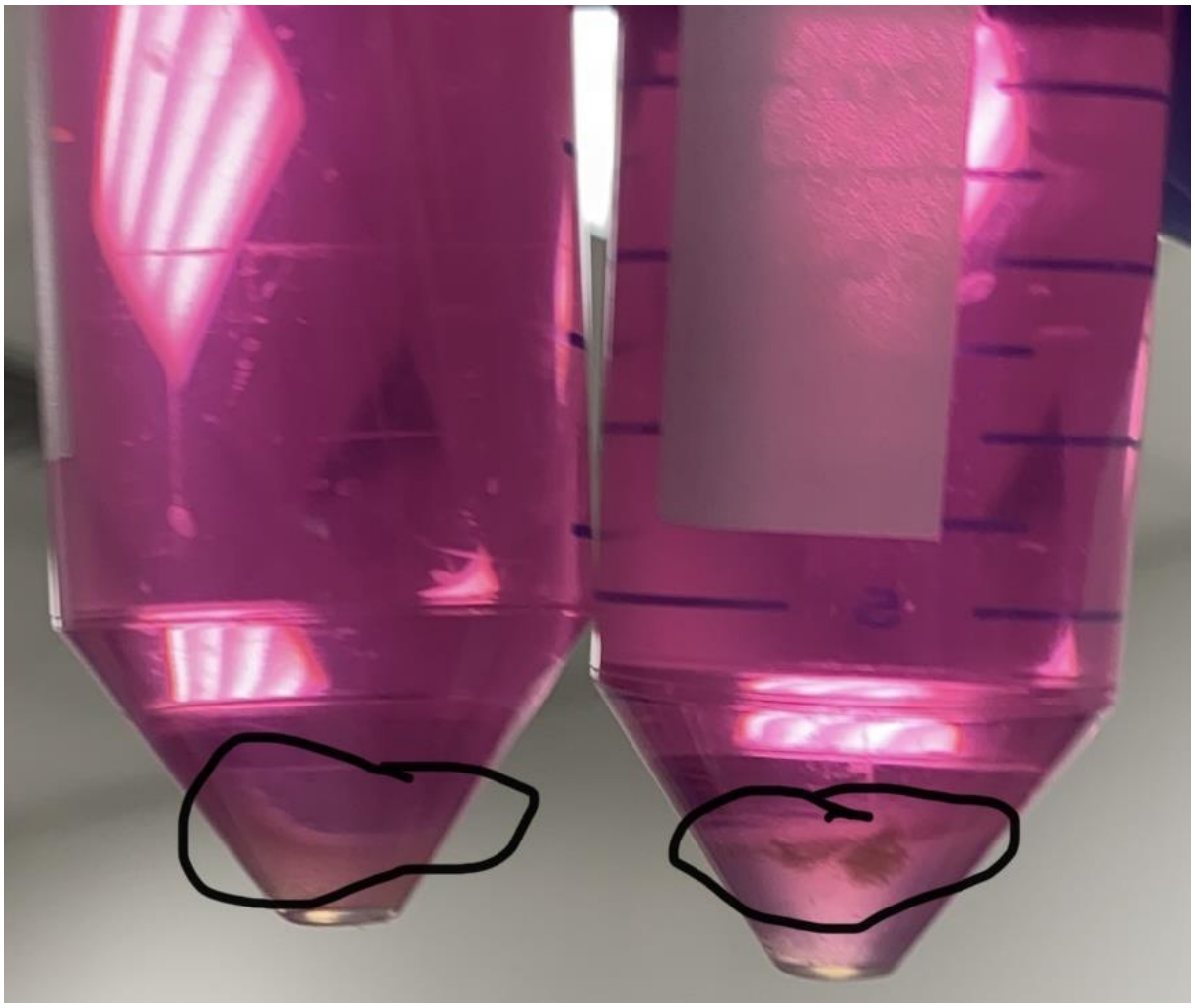

(Figure S1). Showed the cells that were stuck in the upper layer of the gel

Table S1.

	Protein concentration (pg/mL)			Gene expression (Log2 of normalised count)		
SYMBOL	**M1 (I)**	**M1 (II)**	**M1 (III)**	**M1 (I)**	**M1 (II)**	**M1 (III)**
CCL5	610.71	3595.62	432.53	4.29	9.82	4.64
IL1B	39.87	138.36	0.00	4.39	6.51	1.46
IL12B	0.27	1894.78	1.23	0.00	4.81	0.13
IL4	0.00	246.32	5554.53	0.00	0.00	0.00
IL13	0.00	272.42	4141.63	0.22	0.00	0.00
TGFB1	1816.46	1482.20	1567.24	4.45	3.04	4.11
TNF	1355.89	4818.55	67.59	2.87	4.03	1.05
IL8	4567.94	16008.45	260.26	4.15	7.73	1.89
VEGFA	0.00	0.00	0.00	2.23	4.14	1.86
PDGFB	994.16	361.11	1184.41	1.01	2.20	3.39
MMP7	21789.31	30901.19	4366.74	4.51	5.64	3.89
IL10	89.27	759.56	36.75	0.71	0.30	1.57

Table S2

	Protein concentration (pg/mL)			Gene expression (Log2 of normalised count)		
SYMBOL	**M2 (I)**	**M2 (II)**	**M2 (III)**	**M2 (I)**	**M2 (II)**	**M2 (III)**
CCL5	453.40	273.24	19028.64	2.94	2.73	8.75
IL1B	32.00	16.94	61.45	2.13	1.08	3.14
IL12B	20.13	1.79	469.52	0.09	0.12	3.53
IL4	0.00	2774.93	0.00	0.00	0.00	0.00
IL13	0.00	3727.93	1.47	0.00	0.00	0.00
TGFB1	1837.84	1630.50	1598.34	4.37	4.37	3.97
TNF	855.29	320.98	4809.12	0.65	1.86	4.13
IL8	2883.89	1031.61	15994.52	2.59	1.77	5.57
VEGFA	56.64	0.00	68.80	1.89	1.83	4.20
PDGFB	2863.10	1489.47	6937.48	2.74	3.66	3.42
MMP7	20808.13	11982.42	33973.51	2.33	3.46	4.98
IL10	328.42	222.31	585.36	2.41	1.85	0.74

Chapter 8. References

ABDELAZIZ, M. H., ABDELWAHAB, S. F., WAN, J., CAI, W., HUIXUAN, W., JIANJUN, C., KUMAR, K. D., VASUDEVAN, A., SADEK, A., SU, Z., WANG, S. & XU, H. 2020. Alternatively activated macrophages; a double-edged sword in allergic asthma. *J Transl Med,* 18**,** 58.

ABDELFATTAH, N. S., AMGAD, M. & ZAYED, A. A. 2016. Host immune cellular reactions in corneal neovascularization. *Int J Ophthalmol,* 9**,** 625-33.

ACHUTHAN, A., COOK, A. D., LEE, M. C., SALEH, R., KHIEW, H. W., CHANG, M. W., LOUIS, C., FLEETWOOD, A. J., LACEY, D. C., CHRISTENSEN, A. D., FRYE, A. T., LAM, P. Y., KUSANO, H., NOMURA, K., STEINER, N., FORSTER, I., NUTT, S. L., OLSHANSKY, M., TURNER, S. J. & HAMILTON, J. A. 2016. Granulocyte macrophage colony-stimulating factor induces CCL17 production via IRF4 to mediate inflammation. *J Clin Invest,* 126**,** 3453-66.

AGUIAR, V. R. C., CASTELLI, E. C., SINGLE, R. M., BASHIROVA, A., RAMSURAN, V., KULKARNI, S., AUGUSTO, D. G., MARTIN, M. P., GUTIERREZ-ARCELUS, M., CARRINGTON, M. & MEYER, D. 2023. Comparison between qPCR and RNA-seq reveals challenges of quantifying HLA expression. *Immunogenetics,* 75**,** 249-262.

AKAGAWA, K. S., KOMURO, I., KANAZAWA, H., YAMAZAKI, T., MOCHIDA, K. & KISHI, F. 2006. Functional heterogeneity of colony-stimulating factor-induced human monocyte-derived macrophages. *Respirology,* 11 Suppl**,** S32-6.

AL-GHAMDI, A. S. 2019. Adults visual impairment and blindness–An overview of prevalence and causes in Saudi Arabia. *Saudi Journal of Ophthalmology,* 33**,** 374-381.

ALLEN, J. E. 2023. IL-4 and IL-13: Regulators and Effectors of Wound Repair. *Annu Rev Immunol,* 41**,** 229-254.

AMBARUS, C. A., KRAUSZ, S., VAN EIJK, M., HAMANN, J., RADSTAKE, T. R., REEDQUIST, K. A., TAK, P. P. & BAETEN, D. L. 2012. Systematic validation of specific phenotypic markers for in vitro polarized human macrophages. *J Immunol Methods,* 375**,** 196-206.

AMICI, S. A., DONG, J. & GUERAU-DE-ARELLANO, M. 2017. Molecular Mechanisms Modulating the Phenotype of Macrophages and Microglia. *Front Immunol,* 8**,** 1520.

AMICI, S. A., YOUNG, N. A., NARVAEZ-MIRANDA, J., JABLONSKI, K. A., ARCOS, J., ROSAS, L., PAPENFUSS, T. L., TORRELLES, J. B., JARJOUR, W. N. & GUERAU-DE-ARELLANO, M. 2018. CD38 Is Robustly Induced in Human Macrophages and Monocytes in Inflammatory Conditions. *Frontiers in Immunology,* 9.

ARANGO DUQUE, G. & DESCOTEAUX, A. 2014. Macrophage cytokines: involvement in immunity and infectious diseases. *Front Immunol,* 5**,** 491.

ARTAL, P. 2014. Optics of the eye and its impact in vision: a tutorial. *Advances in Optics and Photonics,* 6**,** 340-367.

AUSTIN, A., LIETMAN, T. & ROSE-NUSSBAUMER, J. 2017. Update on the Management of Infectious Keratitis. *Ophthalmology,* 124**,** 1678-1689.

BARRIENTOS, S., STOJADINOVIC, O., GOLINKO, M. S., BREM, H. & TOMIC-CANIC, M. 2008. Growth factors and cytokines in wound healing. *Wound repair and regeneration,* 16**,** 585-601.

BARTAKOVA, A., KUNZEVITZKY, N. J. & GOLDBERG, J. L. 2014. Regenerative Cell Therapy for Corneal Endothelium. *Curr Ophthalmol Rep,* 2**,** 81-90.

BARTIMOTE, C., FOSTER, J. & WATSON, S. 2019. The Spectrum of Microbial Keratitis: An Updated Review. *Open Ophthalmology Journal,* 13**,** 100-130.

BAXTER, E. W., GRAHAM, A. E., RE, N. A., CARR, I. M., ROBINSON, J. I., MACKIE, S. L. & MORGAN, A. W. 2020. Standardized protocols for differentiation of THP-1 cells to macrophages with distinct M(IFNgamma+LPS), M(IL-4) and M(IL-10) phenotypes. *J Immunol Methods,* 478**,** 112721.

BENDER, A. T., OSTENSON, C. L., GIORDANO, D. & BEAVO, J. A. 2004. Differentiation of human monocytes in vitro with granulocyte-macrophage colony-stimulating factor and macrophage colony-stimulating factor produces distinct changes in cGMP phosphodiesterase expression. *Cell Signal,* 16**,** 365-74.

BENHAR, I., LONDON, A. & SCHWARTZ, M. 2012. The privileged immunity of immune privileged organs: the case of the eye. *Front Immunol,* 3**,** 296.

BEYER, M., MALLMANN, M. R., XUE, J., STARATSCHEK-JOX, A., VORHOLT, D., KREBS, W., SOMMER, D., SANDER, J., MERTENS, C., NINO-CASTRO, A., SCHMIDT, S. V. & SCHULTZE, J. L. 2012. High-resolution transcriptome of human macrophages. *PLoS One,* 7**,** e45466.

BHATTACHARJEE, J., DAS, B., MISHRA, A., SAHAY, P. & UPADHYAY, P. 2017. Monocytes isolated by positive and negative magnetic sorting techniques show different molecular characteristics and immunophenotypic behaviour. *F1000Res,* 6**,** 2045.

BOADA-ROMERO, E., MARTINEZ, J., HECKMANN, B. L. & GREEN, D. R. 2020. The clearance of dead cells by efferocytosis. *Nat Rev Mol Cell Biol,* 21**,** 398-414.

BORASCHI, D. 2022. What is IL-1 for? The functions of interleukin-1 across evolution. *Frontiers in Immunology,* 13**,** 872155.

BOSS, M., KEMMERER, M., BRUNE, B. & NAMGALADZE, D. 2015. FABP4 inhibition suppresses PPARgamma activity and VLDL-induced foam cell formation in IL-4-polarized human macrophages. *Atherosclerosis,* 240**,** 424-30.

BOUCHERY, T. & HARRIS, N. 2019. The ins and outs of macrophages in tissue repair. *Immunol Cell Biol,* 97**,** 244-245.

BOYETTE, L. B., MACEDO, C., HADI, K., ELINOFF, B. D., WALTERS, J. T., RAMASWAMI, B., CHALASANI, G., TABOAS, J. M., LAKKIS, F. G. & METES, D. M. 2017. Phenotype, function, and differentiation potential of human monocyte subsets. *PLoS One,* 12**,** e0176460.

BRISSETTE-STORKUS, C. S., REYNOLDS, S. M., LEPISTO, A. J. & HENDRICKS, R. L. 2002. Identification of a novel macrophage population in the normal mouse corneal stroma. *Invest Ophthalmol Vis Sci,* 43**,** 2264-71.

BROCHERIOU, I., MAOUCHE, S., DURAND, H., BRAUNERSREUTHER, V., LE NAOUR, G., GRATCHEV, A., KOSKAS, F., MACH, F., KZHYSHKOWSKA, J. & NINIO, E. 2011.

Antagonistic regulation of macrophage phenotype by M-CSF and GM-CSF: implication in atherosclerosis. *Atherosclerosis,* 214**,** 316-24.

BUCHACHER, T., OHRADANOVA-REPIC, A., STOCKINGER, H., FISCHER, M. B. & WEBER, V. 2015. M2 Polarization of Human Macrophages Favors Survival of the Intracellular Pathogen Chlamydia pneumoniae. *PLoS One,* 10**,** e0143593.

BUKOWIECKI, A., HOS, D., CURSIEFEN, C. & EMING, S. A. 2017. Wound-Healing Studies in Cornea and Skin: Parallels, Differences and Opportunities. *Int J Mol Sci,* 18.

BURKE, B. 2004. The role of matrix metalloproteinase 7 in innate immunity. *Immunobiology,* 209**,** 51-6.

BURTON, M. J. 2009. Corneal blindness: prevention, treatment, rehabilitation. *Community Eye Health,* 22.

CABRERA-AGUAS, M., KHOO, P. & WATSON, S. L. 2022. Infectious keratitis: A review. *Clin Exp Ophthalmol,* 50**,** 543-562.

CALDERON, B., CARRERO, J. A., FERRIS, S. T., SOJKA, D. K., MOORE, L., EPELMAN, S., MURPHY, K. M., YOKOYAMA, W. M., RANDOLPH, G. J. & UNANUE, E. R. 2015. The pancreas anatomy conditions the origin and properties of resident macrophages. *Journal of Experimental Medicine,* 212**,** 1497-1512.

CARLSON, M. 2021. org. Hs. eg. db: Genome wide annotation for Human, R Package.

CATHCART, M. K. & BHATTACHARJEE, A. 2014. Monoamine oxidase A (MAO-A): a signature marker of alternatively activated monocytes/macrophages. *Inflamm Cell Signal,* 1.

CHEN, S., SO, E. C., STROME, S. E. & ZHANG, X. 2015. Impact of Detachment Methods on M2 Macrophage Phenotype and Function. *J Immunol Methods,* 426**,** 56-61.

CHEN, Z., YOU, J., LIU, X., COOPER, S., HODGE, C., SUTTON, G., CROOK, J. M. & WALLACE, G. G. 2018. Biomaterials for corneal bioengineering. *Biomed Mater,* 13**,** 032002.

CHIN, K. C. & CRESSWELL, P. 2001. Viperin (cig5), an IFN-inducible antiviral protein directly induced by human cytomegalovirus. *Proc Natl Acad Sci U S A,* 98**,** 15125-30.

CHINNERY, H. R., HUMPHRIES, T., CLARE, A., DIXON, A. E., HOWES, K., MORAN, C. B., SCOTT, D., ZAKRZEWSKI, M., PEARLMAN, E. & MCMENAMIN, P. G. 2008. Turnover of bone marrow-derived cells in the irradiated mouse cornea. *Immunology,* 125**,** 541-8.

CHINNERY, H. R., MCMENAMIN, P. G. & DANDO, S. J. 2017. Macrophage physiology in the eye. *Pflugers Arch,* 469**,** 501-515.

CHINNERY, H. R., RUITENBERG, M. J., PLANT, G. W., PEARLMAN, E., JUNG, S. & MCMENAMIN, P. G. 2007. The chemokine receptor CX3CR1 mediates homing of MHC class II-positive cells to the normal mouse corneal epithelium. *Invest Ophthalmol Vis Sci,* 48**,** 1568-74.

CHOUHAN, G., MOAKES, R. J. A., ESMAEILI, M., HILL, L. J., DECOGAN, F., HARDWICKE, J., RAUZ, S., LOGAN, A. & GROVER, L. M. 2019. A self-healing hydrogel eye drop for the sustained delivery of decorin to prevent corneal scarring. *Biomaterials,* 210**,** 41-50.

CHU, F., SHI, M., LANG, Y., CHAO, Z., JIN, T., CUI, L. & ZHU, J. 2021. Adoptive transfer of immunomodulatory M2 macrophages suppresses experimental autoimmune encephalomyelitis in C57BL/6 mice via blockading NF-κB pathway. *Clinical & Experimental Immunology,* 204**,** 199-211.

CONESA, A., MADRIGAL, P., TARAZONA, S., GOMEZ-CABRERO, D., CERVERA, A., MCPHERSON, A., SZCZESNIAK, M. W., GAFFNEY, D. J., ELO, L. L., ZHANG, X. & MORTAZAVI, A. 2016. A survey of best practices for RNA-seq data analysis. *Genome Biol,* 17**,** 13.

COOKE, M. E., JONES, S. W., TER HORST, B., MOIEMEN, N., SNOW, M., CHOUHAN, G., HILL, L. J., ESMAELI, M., MOAKES, R. J. A., HOLTON, J., NANDRA, R., WILLIAMS, R. L., SMITH, A. M. & GROVER, L. M. 2018. Structuring of Hydrogels across Multiple Length Scales for Biomedical Applications. *Advanced Materials,* 30.

CRICK, F. 1970. Central dogma of molecular biology. *Nature,* 227**,** 561-3.

CURSIEFEN, C., CHEN, L., BORGES, L. P., JACKSON, D., CAO, J., RADZIEJEWSKI, C., D'AMORE, P. A., DANA, M. R., WIEGAND, S. J. & STREILEIN, J. W. 2004. VEGF-A stimulates lymphangiogenesis and hemangiogenesis in inflammatory neovascularization via macrophage recruitment. *J Clin Invest,* 113**,** 1040-50.

CZIMMERER, Z., HALASZ, L., DANIEL, B., VARGA, Z., BENE, K., DOMOKOS, A., HOEKSEMA, M., SHEN, Z., BERGER, W. K. & CSEH, T. 2022. The epigenetic state of IL-4-polarized macrophages enables inflammatory cistromic expansion and extended synergistic response to TLR ligands. *Immunity,* 55**,** 2006-2026. e6.

DA SILVA, H. B., FONSECA, R., PEREIRA, R. M., CASSADO, A. D., ALVAREZ, J. M. & LIMA, M. R. D. 2015. Splenic macrophage subsets and their function during blood-borne infections. *Frontiers in Immunology,* 6.

DAS, A., SINHA, M., DATTA, S., ABAS, M., CHAFFEE, S., SEN, C. K. & ROY, S. 2015. Monocyte and macrophage plasticity in tissue repair and regeneration. *Am J Pathol,* 185**,** 2596-606.

DAS, M. & GIRI, T. K. 2020. Hydrogels based on gellan gum in cell delivery and drug delivery. *Journal of Drug Delivery Science and Technology,* 56.

DE OLIVEIRA, R. C. & WILSON, S. E. 2020. Fibrocytes, Wound Healing, and Corneal Fibrosis. *Invest Ophthalmol Vis Sci,* 61**,** 28.

DEMPSEY, M. P. & CONRADY, C. D. 2023. The Host-Pathogen Interplay: A Tale of Two Stories within the Cornea and Posterior Segment. *Microorganisms,* 11.

DERLINDATI, E., DEI CAS, A., MONTANINI, B., SPIGONI, V., CURELLA, V., ALDIGERI, R., ARDIGÒ, D., ZAVARONI, I. & BONADONNA, R. C. 2015. Transcriptomic analysis of human polarized macrophages: more than one role of alternative activation? *PloS one,* 10**,** e0119751.

DESHPANDE, D., CHHUGANI, K., CHANG, Y., KARLSBERG, A., LOEFFLER, C., ZHANG, J., MUSZYNSKA, A., MUNTEANU, V., YANG, H., ROTMAN, J., TAO, L., BALLIU, B., TSENG, E., ESKIN, E., ZHAO, F., MOHAMMADI, P., P, P. L. & MANGUL, S. 2023. RNA-seq data science: From raw data to effective interpretation. *Front Genet,* 14**,** 997383.

DI ZAZZO, A., GAUDENZI, D., YIN, J., COASSIN, M., FERNANDES, M., DANA, R. & BONINI, S. 2021. Corneal angiogenic privilege and its failure. *Experimental Eye Research,* 204.

DOLGALEV, I. 2022. msigdbr: MSigDB Gene Sets for Multiple Organisms in a Tidy Data Format.

DONALDSON, P. J., GREY, A. C., MACEO HEILMAN, B., LIM, J. C. & VAGHEFI, E. 2017. The physiological optics of the lens. *Prog Retin Eye Res,* 56**,** e1-e24.

DORAN, A. C., YURDAGUL, A., JR. & TABAS, I. 2020. Efferocytosis in health and disease. *Nat Rev Immunol,* 20**,** 254-267.

DOWNIE, L. E., ZHANG, X., WU, M., KARUNARATNE, S., LOI, J. K., SENTHIL, K., ARSHAD, S., BERTRAM, K., CUNNINGHAM, A. L., CARNT, N., MUELLER, S. N. & CHINNERY, H. R. 2023. Redefining the human corneal immune compartment using dynamic intravital imaging. *Proc Natl Acad Sci U S A,* 120**,** e2217795120.

EBIHARA, N., YAMAGAMI, S., YOKOO, S., AMANO, S. & MURAKAMI, A. 2007. Involvement of C-C chemokine ligand 2-CCR2 interaction in monocyte-lineage cell recruitment of normal human corneal stroma. *J Immunol,* 178**,** 3288-92.

EGRILMEZ, S. & YILDIRIM-THEVENY, S. 2020. Treatment-Resistant Bacterial Keratitis: Challenges and Solutions. *Clin Ophthalmol,* 14**,** 287-297.

ELIGINI, S., FIORELLI, S., TREMOLI, E. & COLLI, S. 2016. Inhibition of transglutaminase 2 reduces efferocytosis in human macrophages: Role of CD14 and SR-AI receptors. *Nutr Metab Cardiovasc Dis,* 26**,** 922-30.

ENOCH, J., MCDONALD, L., JONES, L., JONES, P. R. & CRABB, D. P. 2019. Evaluating Whether Sight Is the Most Valued Sense. *JAMA Ophthalmol,* 137**,** 1317-1320.

EVERAERT, C., LUYPAERT, M., MAAG, J. L. V., CHENG, Q. X., DINGER, M. E., HELLEMANS, J. & MESTDAGH, P. 2017. Benchmarking of RNA-sequencing analysis workflows using whole-transcriptome RT-qPCR expression data. *Sci Rep,* 7**,** 1559.

FAN, X., ZHANG, H., CHENG, Y., JIANG, X., ZHU, J. & JIN, T. 2016. Double Roles of Macrophages in Human Neuroimmune Diseases and Their Animal Models. *Mediators Inflamm,* 2016**,** 8489251.

FANG, Z. & CUI, X. 2011. Design and validation issues in RNA-seq experiments. *Brief Bioinform,* 12**,** 280-7.

FARAHANI, M., PATEL, R. & DWARAKANATHAN, S. 2017. Infectious corneal ulcers. *Dis Mon,* 63**,** 33-37.

FARBER, J. M. 1990. A macrophage mRNA selectively induced by gamma-interferon encodes a member of the platelet factor 4 family of cytokines. *Proc Natl Acad Sci U S A,* 87**,** 5238-42.

FILARDY, A. A., PIRES, D. R., NUNES, M. P., TAKIYA, C. M., FREIRE-DE-LIMA, C. G., RIBEIRO-GOMES, F. L. & DOSREIS, G. A. 2010. Proinflammatory Clearance of Apoptotic Neutrophils Induces an IL-12

IL-10

Regulatory Phenotype in Macrophages. *Journal of Immunology,* 185**,** 2044-2050.

FINOTELLO, F. & DI CAMILLO, B. 2015. Measuring differential gene expression with RNA-seq: challenges and strategies for data analysis. *Brief Funct Genomics,* 14**,** 130-42.

FLAXMAN, S. R., BOURNE, R. R. A., RESNIKOFF, S., ACKLAND, P., BRAITHWAITE, T., CICINELLI, M. V., DAS, A., JONAS, J. B., KEEFFE, J., KEMPEN, J. H., LEASHER, J., LIMBURG, H., NAIDOO, K., PESUDOVS, K., SILVESTER, A., STEVENS, G. A., TAHHAN, N., WONG, T. Y., TAYLOR, H. R. & VISION LOSS EXPERT GROUP OF THE GLOBAL BURDEN OF DISEASE, S. 2017. Global causes of blindness and distance vision impairment 1990-2020: a systematic review and meta-analysis. *Lancet Glob Health,* 5**,** e1221-e1234.

FRANGOGIANNIS, N. 2020. Transforming growth factor-beta in tissue fibrosis. *J Exp Med,* 217**,** e20190103.

FUJIWARA, Y., HIZUKURI, Y., YAMASHIRO, K., MAKITA, N., OHNISHI, K., TAKEYA, M., KOMOHARA, Y. & HAYASHI, Y. 2016. Guanylate-binding protein 5 is a marker of interferon-gamma-induced classically activated macrophages. *Clin Transl Immunology,* 5**,** e111.

FUKUZUMI, M., SHINOMIYA, H., SHIMIZU, Y., OHISHI, F. & UTSUMI, S. 1996. Endotoxin-induced enhancement of glucose influx into murine peritoneal macrophages via GLUT1. *Infection and Immunity,* 64**,** 108-112.

GE, Z., CHEN, Y., MA, L., HU, F. & XIE, L. 2024. Macrophage polarization and its impact on idiopathic pulmonary fibrosis. *Front Immunol,* 15**,** 1444964.

GERRICK, K. Y., GERRICK, E. R., GUPTA, A., WHEELAN, S. J., YEGNASUBRAMANIAN, S. & JAFFEE, E. M. 2018. Transcriptional profiling identifies novel regulators of macrophage polarization. *PLoS One,* 13**,** e0208602.

GINHOUX, F. & GUILLIAMS, M. 2016. Tissue-Resident Macrophage Ontogeny and Homeostasis. *Immunity,* 44**,** 439-449.

GOLDBERG, M. F., FERGUSON, T. A. & PEPOSE, J. S. 1994. Detection of cellular adhesion molecules in inflamed human corneas. *Ophthalmology,* 101**,** 161-8.

GORDON, S. 2003. Alternative activation of macrophages. *Nature reviews immunology,* 3**,** 23-35.

GORDON, S. 2008. Elie Metchnikoff: father of natural immunity. *Eur J Immunol,* 38**,** 3257-64.

GORDON, S. & MARTINEZ, F. O. 2010. Alternative activation of macrophages: mechanism and functions. *Immunity,* 32**,** 593-604.

GOTE, V., SIKDER, S., SICOTTE, J. & PAL, D. 2019. Ocular Drug Delivery: Present Innovations and Future Challenges. *J Pharmacol Exp Ther,* 370**,** 602-624.

GREGORY, C. D. 2000. CD14-dependent clearance of apoptotic cells: relevance to the immune system. *Curr Opin Immunol,* 12**,** 27-34.

GROVER, L. M., MOAKES, R. & RAUZ, S. 2022. Innovations in fluid-gel eye drops for treating disease of the eye: prospects for enhancing drug retention and reducing corneal scarring. *Expert Review of Ophthalmology,* 17**,** 175-181.

GU, Z., EILS, R. & SCHLESNER, M. 2016. Complex heatmaps reveal patterns and correlations in multidimensional genomic data. *Bioinformatics,* 32**,** 2847-2849.

GU, Z., GU, L., EILS, R., SCHLESNER, M. & BRORS, B. 2014. " Circlize" implements and enhances circular visualization in R.

GUILLIAMS, M., MILDNER, A. & YONA, S. 2018. Developmental and Functional Heterogeneity of Monocytes. *Immunity,* 49**,** 595-613.

GUILLIAMS, M. & SVEDBERG, F. R. 2021. Does tissue imprinting restrict macrophage plasticity? *Nature Immunology,* 22**,** 118-127.

GULKA, S. M., LITKE, A. M., DELANEY, K. R. & CHOW, R. L. 2021. Live whole-eye, ex vivo imaging and laser-induced micro injury of the corneal basal epithelium and visualization of resident macrophage responses. *bioRxiv***,** 2021.06. 02.446679.

HADRIAN, K., WILLENBORG, S., BOCK, F., CURSIEFEN, C., EMING, S. A. & HOS, D. 2021. Macrophage-Mediated Tissue Vascularization: Similarities and Differences Between Cornea and Skin. *Frontiers in Immunology,* 12.

HAMIDZADEH, K., BELEW, A. T., EL-SAYED, N. M. & MOSSER, D. M. 2020. The transition of M-CSF-derived human macrophages to a growth-promoting phenotype. *Blood Adv,* 4**,** 5460-5472.

HAMILTON, T. A., ZHAO, C., PAVICIC, P. G., JR. & DATTA, S. 2014. Myeloid colony-stimulating factors as regulators of macrophage polarization. *Front Immunol,* 5**,** 554.

HAMRAH, P., LIU, Y., ZHANG, Q. & DANA, M. R. 2003. The corneal stroma is endowed with a significant number of resident dendritic cells. *Investigative Ophthalmology & Visual Science,* 44**,** 581-589.

HARO, H., CRAWFORD, H. C., FINGLETON, B., SHINOMIYA, K., SPENGLER, D. M. & MATRISIAN, L. M. 2000. Matrix metalloproteinase-7-dependent release of tumor necrosis factor-alpha in a model of herniated disc resorption. *J Clin Invest,* 105**,** 143-50.

HASHIMOTO, S., SUZUKI, T., DONG, H. Y., YAMAZAKI, N. & MATSUSHIMA, K. 1999. Serial analysis of gene expression in human monocytes and macrophages. *Blood,* 94**,** 837-44.

HASSELL, J. R. & BIRK, D. E. 2010. The molecular basis of corneal transparency. *Exp Eye Res,* 91**,** 326-35.

HE, Y., HARA, H. & NUNEZ, G. 2016. Mechanism and Regulation of NLRP3 Inflammasome Activation. *Trends in Biochemical Sciences,* 41**,** 1012-1021.

HERB, M. & SCHRAMM, M. 2021. Functions of ROS in Macrophages and Antimicrobial Immunity. *Antioxidants (Basel),* 10.

HICKMAN, E., SMYTH, T., COBOS-URIBE, C., IMMORMINO, R., REBULI, M. E., MORAN, T., ALEXIS, N. E. & JASPERS, I. 2023. Expanded characterization of in vitro polarized M0, M1, and M2 human monocyte-derived macrophages: Bioenergetic and secreted mediator profiles. *PLoS One,* 18**,** e0279037.

HILL, L. J., MOAKES, R. J. A., VAREECHON, C., BUTT, G., NG, A., BROCK, K., CHOUHAN, G., VINCENT, R. C., ABBONDANTE, S., WILLIAMS, R. L., BARNES, N. M., PEARLMAN, E., WALLACE, G. R., RAUZ, S., LOGAN, A. & GROVER, L. M. 2018. Sustained release of decorin to the surface of the eye enables scarless corneal regeneration. *NPJ Regen Med,* 3**,** 23.

HIRAYAMA, D., IIDA, T. & NAKASE, H. 2017. The Phagocytic Function of Macrophage-Enforcing Innate Immunity and Tissue Homeostasis. *Int J Mol Sci,* 19.

HIRAYAMA, D., IIDA, T. & NAKASE, H. 2018. The Phagocytic Function of Macrophage-Enforcing Innate Immunity and Tissue Homeostasis. *International Journal of Molecular Sciences,* 19.

HOEFFEL, G. & GINHOUX, F. 2018. Fetal monocytes and the origins of tissue-resident macrophages. *Cell Immunol,* 330**,** 5-15.

HORI, J., KUNISHIGE, T. & NAKANO, Y. 2020. Immune Checkpoints Contribute Corneal Immune Privilege: Implications for Dry Eye Associated with Checkpoint Inhibitors. *Int J Mol Sci,* 21.

HORI, J., YAMAGUCHI, T., KEINO, H., HAMRAH, P. & MARUYAMA, K. 2019. Immune privilege in corneal transplantation. *Prog Retin Eye Res,* 72**,** 100758.

HORNSCHUH, M., HAAS, V., WINKEL, P. P., GOKYILDIRIM, M. Y., MULLINS, C. S., WROBEL, I. M., MANTEUFFEL, C. & WIRTHGEN, E. 2022. Negative Magnetic Sorting Preserves the

Functionality of Ex Vivo Cultivated Non-Adherent Human Monocytes. *Biology (Basel),* 11.

HOS, D., BUCHER, F., REGENFUSS, B., DREISOW, M. L., BOCK, F., HEINDL, L. M., EMING, S. A. & CURSIEFEN, C. 2016. IL-10 Indirectly Regulates Corneal Lymphangiogenesis and Resolution of Inflammation via Macrophages. *Am J Pathol,* 186**,** 159-71.

HUME, D. A. 2015. The Many Alternative Faces of Macrophage Activation. *Front Immunol,* 6**,** 370.

HUTMACHER, F. 2019. Why Is There So Much More Research on Vision Than on Any Other Sensory Modality? *Front Psychol,* 10**,** 2246.

HUWAIT, E., AYOUB, M. & KARIM, S. 2022. Investigation of the Molecular Mechanisms Underlying the Antiatherogenic Actions of Kaempferol in Human THP-1 Macrophages. *Int J Mol Sci,* 23.

INGERSOLL, M. A., SPANBROEK, R., LOTTAZ, C., GAUTIER, E. L., FRANKENBERGER, M., HOFFMANN, R., LANG, R., HANIFFA, M., COLLIN, M., TACKE, F., HABENICHT, A. J. R., ZIEGLER-HEITBROCK, L. & RANDOLPH, G. J. 2010. Comparison of gene expression profiles between human and mouse monocyte subsets. *Blood,* 115**,** E10-E19.

ISTOMINE, R., PAVEY, N. & PICCIRILLO, C. A. 2016. Posttranscriptional and Translational Control of Gene Regulation in CD4+ T Cell Subsets. *J Immunol,* 196**,** 533-40.

ITALIANI, P., MOSCA, E., DELLA CAMERA, G., MELILLO, D., MIGLIORINI, P., MILANESI, L. & BORASCHI, D. 2020. Profiling the Course of Resolving vs. Persistent Inflammation in Human Monocytes: The Role of IL-1 Family Molecules. *Front Immunol,* 11**,** 1426.

IYER, S. S., GHAFFARI, A. A. & CHENG, G. 2010. Lipopolysaccharide-mediated IL-10 transcriptional regulation requires sequential induction of type I IFNs and IL-27 in macrophages. *J Immunol,* 185**,** 6599-607.

JAGUIN, M., HOULBERT, N., FARDEL, O. & LECUREUR, V. 2013. Polarization profiles of human M-CSF-generated macrophages and comparison of M1-markers in classically activated macrophages from GM-CSF and M-CSF origin. *Cell Immunol,* 281**,** 51-61.

JAIN, N., MOELLER, J. & VOGEL, V. 2019. Mechanobiology of Macrophages: How Physical Factors Coregulate Macrophage Plasticity and Phagocytosis. *Annual Review of Biomedical Engineering, Vol 21,* 21**,** 267-297.

JAKUBZICK, C., GAUTIER, E. L., GIBBINGS, S. L., SOJKA, D. K., SCHLITZER, A., JOHNSON, T. E., IVANOV, S., DUAN, Q. N., BALA, S., CONDON, T., VAN ROOIJEN, N., GRAINGER, J. R., BELKAID, Y., MA'AYAN, A., RICHES, D. W. H., YOKOYAMA, W. M., GINHOUX, F., HENSON, P. M. & RANDOLPH, G. J. 2013. Minimal Differentiation of Classical Monocytes as They Survey Steady-State Tissues and Transport Antigen to Lymph Nodes. *Immunity,* 39**,** 599-610.

JANG, D. I., LEE, A. H., SHIN, H. Y., SONG, H. R., PARK, J. H., KANG, T. B., LEE, S. R. & YANG, S. H. 2021. The Role of Tumor Necrosis Factor Alpha (TNF-alpha) in Autoimmune Disease and Current TNF-alpha Inhibitors in Therapeutics. *Int J Mol Sci,* 22.

JEGERSCHOLD, C., PAWELZIK, S. C., PURHONEN, P., BHAKAT, P., GHEORGHE, K. R., GYOBU, N., MITSUOKA, K., MORGENSTERN, R., JAKOBSSON, P. J. & HEBERT, H. 2008. Structural basis for induced formation of the inflammatory mediator prostaglandin E2. *Proc Natl Acad Sci U S A,* 105**,** 11110-5.

JIANG, H., VAN DE VEN, C., SATWANI, P., BAXI, L. V. & CAIRO, M. S. 2004. Differential gene expression patterns by oligonucleotide microarray of basal versus lipopolysaccharide-activated monocytes from cord blood versus adult peripheral blood. *J Immunol,* 172**,** 5870-9.

JONES, D. M., READ, K. A. & OESTREICH, K. J. 2020. Dynamic Roles for IL-2-STAT5 Signaling in Effector and Regulatory CD4(+)d T Cell Populations. *Journal of Immunology,* 205**,** 1721-1730.

JUSTIZ VAILLANT, A. A. & QURIE, A. 2023. Interleukin. *StatPearls.* Treasure Island (FL).

KALAIVANI, K. 2021. An Overview on Etiology of Corneal Blindness. *New Frontiers in Medicine and Medical Research Vol. 4***,** 44-52.

KALLURI, R. & WEINBERG, R. A. 2009. The basics of epithelial-mesenchymal transition. *J Clin Invest,* 119**,** 1420-8.

KAMIL, S. & MOHAN, R. R. 2021. Corneal stromal wound healing: Major regulators and therapeutic targets. *Ocul Surf,* 19**,** 290-306.

KATE, A. & BASU, S. 2023. Corneal blindness in the developing world: The role of prevention strategies. *F1000Research,* 12**,** 1309.

KATKAR, G. & GHOSH, P. 2023. Macrophage states: there's a method in the madness. *Trends Immunol,* 44**,** 954-964.

KEARNEY, C. J., CULLEN, S. P., TYNAN, G. A., HENRY, C. M., CLANCY, D., LAVELLE, E. C. & MARTIN, S. J. 2015. Necroptosis suppresses inflammation via termination of TNF- or LPS-induced cytokine and chemokine production. *Cell Death Differ,* 22**,** 1313-27.

KIM, H. 2017. The transcription factor MafB promotes anti-inflammatory M2 polarization and cholesterol efflux in macrophages. *Sci Rep,* 7**,** 7591.

KIM, S. Y. & NAIR, M. G. 2019. Macrophages in wound healing: activation and plasticity. *Immunol Cell Biol,* 97**,** 258-267.

KITTAN, N. A., ALLEN, R. M., DHALIWAL, A., CAVASSANI, K. A., SCHALLER, M., GALLAGHER, K. A., CARSON, W. F. T., MUKHERJEE, S., GREMBECKA, J., CIERPICKI, T., JARAI, G., WESTWICK, J., KUNKEL, S. L. & HOGABOAM, C. M. 2013. Cytokine induced phenotypic and epigenetic signatures are key to establishing specific macrophage phenotypes. *PLoS One,* 8**,** e78045.

KOCH, C. M., CHIU, S. F., AKBARPOUR, M., BHARAT, A., RIDGE, K. M., BARTOM, E. T. & WINTER, D. R. 2018. A Beginner's Guide to Analysis of RNA Sequencing Data. *Am J Respir Cell Mol Biol,* 59**,** 145-157.

KOHYAMA, M., ISE, W., EDELSON, B. T., WILKER, P. R., HILDNER, K., MEJIA, C., FRAZIER, W. A., MURPHY, T. L. & MURPHY, K. M. 2009. Role for Spi-C in the development of red pulp macrophages and splenic iron homeostasis. *Nature,* 457**,** 318-21.

KOROBOVA, Z. R., ARSENTIEVA, N. A. & TOTOLIAN, A. A. 2023. Macrophage-Derived Chemokine MDC/CCL22: An Ambiguous Finding in COVID-19. *Int J Mol Sci,* 24.

KOROTKEVICH, G., SUKHOV, V., BUDIN, N., SHPAK, B., ARTYOMOV, M. N. & SERGUSHICHEV, A. 2016. Fast gene set enrichment analysis. *BioRxiv***,** 060012.

LACEY, D. C., ACHUTHAN, A., FLEETWOOD, A. J., DINH, H., ROINIOTIS, J., SCHOLZ, G. M., CHANG, M. W., BECKMAN, S. K., COOK, A. D. & HAMILTON, J. A. 2012. Defining GM-CSF- and macrophage-CSF-dependent macrophage responses by in vitro models. *J Immunol,* 188**,** 5752-65.

LAI, T. S. & GREENBERG, C. S. 2013. TGM2 and implications for human disease: role of alternative splicing. *Front Biosci (Landmark Ed),* 18**,** 504-19.

LAKHUNDI, S., SIDDIQUI, R. & KHAN, N. A. 2017. Pathogenesis of microbial keratitis. *Microb Pathog,* 104**,** 97-109.

LAMARRE, S., FRASSE, P., ZOUINE, M., LABOURDETTE, D., SAINDERICHIN, E., HU, G., LE BERRE-ANTON, V., BOUZAYEN, M. & MAZA, E. 2018. Optimization of an RNA-Seq Differential Gene Expression Analysis Depending on Biological Replicate Number and Library Size. *Front Plant Sci,* 9**,** 108.

LAMY, R., WOLF, M., BISPO, C., CLAY, S. M., ZHENG, S., WOLFREYS, F., PAN, P. & CHAN, M. F. 2022. Characterization of Recruited Mononuclear Phagocytes following Corneal Chemical Injury. *Int J Mol Sci,* 23.

LAPP, T., ZAHER, S. S., HAAS, C. T., BECKER, D. L., THRASIVOULOU, C., CHAIN, B. M., LARKIN, D. F. & NOURSADEGHI, M. 2015. Identification of Therapeutic Targets of Inflammatory Monocyte Recruitment to Modulate the Allogeneic Injury to Donor Cornea. *Invest Ophthalmol Vis Sci,* 56**,** 7250-9.

LARI, R., FLEETWOOD, A. J., KITCHENER, P. D., COOK, A. D., PAVASOVIC, D., HERTZOG, P. J. & HAMILTON, J. A. 2007. Macrophage lineage phenotypes and osteoclastogenesis--complexity in the control by GM-CSF and TGF-beta. *Bone,* 40**,** 323-36.

LASSANCE, L., MARINO, G. K., MEDEIROS, C. S., THANGAVADIVEL, S. & WILSON, S. E. 2018. Fibrocyte migration, differentiation and apoptosis during the corneal wound healing response to injury. *Exp Eye Res,* 170**,** 177-187.

LEE, E. Y., LEE, Z. H. & SONG, Y. W. 2009. CXCL10 and autoimmune diseases. *Autoimmun Rev,* 8**,** 379-83.

LEI, A., YU, H., LU, S., LU, H., DING, X., TAN, T., ZHANG, H., ZHU, M., TIAN, L., WANG, X., SU, S., XUE, D., ZHANG, S., ZHAO, W., CHEN, Y., XIE, W., ZHANG, L., ZHU, Y., ZHAO, J., JIANG, W., CHURCH, G., CHAN, F. K., GAO, Z. & ZHANG, J. 2024. A second-generation M1-polarized CAR macrophage with antitumor efficacy. *Nat Immunol,* 25**,** 102-116.

LESCOAT, A., BALLERIE, A., AUGAGNEUR, Y., MORZADEC, C., VERNHET, L., FARDEL, O., JEGO, P., JOUNEAU, S. & LECUREUR, V. 2018. Distinct Properties of Human M-CSF and GM-CSF Monocyte-Derived Macrophages to Simulate Pathological Lung Conditions In Vitro: Application to Systemic and Inflammatory Disorders with Pulmonary Involvement. *Int J Mol Sci,* 19.

LESEIGNEUR, C., LE-BURY, P., PIZARRO-CERDA, J. & DUSSURGET, O. 2020. Emerging Evasion Mechanisms of Macrophage Defenses by Pathogenic Bacteria. *Front Cell Infect Microbiol,* 10**,** 577559.

LI, C., WANG, Y., LI, Y., YU, Q., JIN, X., WANG, X., JIA, A., HU, Y., HAN, L., WANG, J., YANG, H., YAN, D., BI, Y. & LIU, G. 2018a. HIF1alpha-dependent glycolysis promotes macrophage functional activities in protecting against bacterial and fungal infection. *Sci Rep,* 8**,** 3603.

LI, R., SERRANO, J. C., XING, H., LEE, T. A., AZIZGOLSHANI, H., ZAMAN, M. & KAMM, R. D. 2018b. Interstitial flow promotes macrophage polarization toward an M2 phenotype. *Mol Biol Cell,* 29**,** 1927-1940.

LI, Y., JEONG, J. & SONG, W. 2022. Molecular Characteristics and Distribution of Adult Human Corneal Immune Cell Types. *Front Immunol,* 13**,** 798346.

LIS-LOPEZ, L., BAUSET, C., SECO-CERVERA, M. & COSIN-ROGER, J. 2021. Is the Macrophage Phenotype Determinant for Fibrosis Development? *Biomedicines,* 9.

LIU, J. & LI, Z. 2021. Resident Innate Immune Cells in the Cornea. *Front Immunol,* 12**,** 620284.

LIU, J., WU, M., HE, J., XIAO, C., XUE, Y., FU, T., LIN, C., DONG, D. & LI, Z. 2018. Antibiotic-Induced Dysbiosis of Gut Microbiota Impairs Corneal Nerve Regeneration by Affecting CCR2-Negative Macrophage Distribution. *Am J Pathol,* 188**,** 2786-2799.

LIU, J., XUE, Y., DONG, D., XIAO, C., LIN, C., WANG, H., SONG, F., FU, T., WANG, Z., CHEN, J., PAN, H., LI, Y., CAI, D. & LI, Z. 2017. CCR2(-) and CCR2(+) corneal macrophages exhibit distinct characteristics and balance inflammatory responses after epithelial abrasion. *Mucosal Immunol,* 10**,** 1145-1159.

LJUBIMOV, A. V. & SAGHIZADEH, M. 2015. Progress in corneal wound healing. *Prog Retin Eye Res,* 49**,** 17-45.

LOVE, M. I., HUBER, W. & ANDERS, S. 2014. Moderated estimation of fold change and dispersion for RNA-seq data with DESeq2. *Genome biology,* 15**,** 1-21.

LOW, L., FUENTES-UTRILLA, P., HODSON, J., O'NEIL, J. D., ROSSITER, A. E., BEGUM, G., SULEIMAN, K., MURRAY, P. I., WALLACE, G. R., LOMAN, N. J., RAUZ, S., WEST MIDLANDS COLLABORATIVE OPHTHALMOLOGY NETWORK FOR CLINICAL, E. & RESEARCH BY, T. 2021. Evaluation of full-length nanopore 16S sequencing for detection of pathogens in microbial keratitis. *PeerJ,* 9**,** e10778.

LOW, L., NAKAMICHI, K., AKILESWARAN, L., LEE, C. S., LEE, A. Y., MOUSSA, G., MURRAY, P. I., WALLACE, G. R., VAN GELDER, R. N., RAUZ, S., WEST MIDLANDS COLLABORATIVE OPHTHALMOLOGY NETWORK FOR CLINICAL, E. & RESEARCH BY, T. 2022. Deep Metagenomic Sequencing for Endophthalmitis Pathogen Detection Using a Nanopore Platform. *Am J Ophthalmol,* 242**,** 243-251.

LUKIC, A., LARSSEN, P., FAULAND, A., SAMUELSSON, B., WHEELOCK, C. E., GABRIELSSON, S. & RADMARK, O. 2017. GM-CSF- and M-CSF-primed macrophages present similar resolving but distinct inflammatory lipid mediator signatures. *FASEB J,* 31**,** 4370-4381.

LUO, C., ZHAO, J., CHEN, M. & XU, H. 2018. The expression of C1 inhibitor (C1INH) in macrophages is upregulated by retinal pigment epithelial cells - implication in subretinal immune privilege in the aging eye. *Aging (Albany NY),* 10**,** 1380-1389.

MA, X., YAN, W., ZHENG, H., DU, Q., ZHANG, L., BAN, Y., LI, N. & WEI, F. 2015. Regulation of IL-10 and IL-12 production and function in macrophages and dendritic cells. *F1000Res,* 4.

MAHARANA, P. K., NAWAZ, S., SINGHAL, D., JHANJI, V., AGARWAL, T., SHARMA, N. & VAJPAYEE, R. B. 2019. Causes and Management Outcomes of Acquired Corneal Opacity in a Preschool Age (0-5 Years) Group: A Hospital-Based Study. *Cornea,* 38**,** 868-872.

MAHIDA, R. Y., SCOTT, A., PAREKH, D., LUGG, S. T., BELCHAMBER, K. B. R., HARDY, R. S., MATTHAY, M. A., NAIDU, B. & THICKETT, D. R. 2021. Assessment of Alveolar Macrophage Dysfunction Using an in vitro Model of Acute Respiratory Distress Syndrome. *Front Med (Lausanne),* 8**,** 737859.

MANTOVANI, A., SICA, A., SOZZANI, S., ALLAVENA, P., VECCHI, A. & LOCATI, M. 2004. The chemokine system in diverse forms of macrophage activation and polarization. *Trends Immunol,* 25**,** 677-86.

MAO, R., WANG, C., ZHANG, F., ZHAO, M., LIU, S., LIAO, G., LI, L., CHEN, Y., CHENG, J. & LIU, J. 2020. Peritoneal M2 macrophage transplantation as a potential cell therapy for enhancing renal repair in acute kidney injury. *Journal of cellular and molecular medicine,* 24**,** 3314-3327.

MARTINEZ, F. O. & GORDON, S. 2014. The M1 and M2 paradigm of macrophage activation: time for reassessment. *F1000Prime Rep,* 6**,** 13.

MARTINEZ, F. O., GORDON, S., LOCATI, M. & MANTOVANI, A. 2006. Transcriptional profiling of the human monocyte-to-macrophage differentiation and polarization: New molecules and patterns of gene expression. *Journal of Immunology,* 177**,** 7303-7311.

MARTINEZ, F. O., HELMING, L., MILDE, R., VARIN, A., MELGERT, B. N., DRAIJER, C., THOMAS, B., FABBRI, M., CRAWSHAW, A., HO, L. P., TEN HACKEN, N. H., COBOS JIMENEZ, V., KOOTSTRA, N. A., HAMANN, J., GREAVES, D. R., LOCATI, M., MANTOVANI, A. & GORDON, S. 2013. Genetic programs expressed in resting and IL-4 alternatively activated mouse and human macrophages: similarities and differences. *Blood,* 121**,** e57-69.

MARUYAMA, K., NAKAZAWA, T., CURSIEFEN, C., MARUYAMA, Y., VAN ROOIJEN, N., D'AMORE, P. A. & KINOSHITA, S. 2012. The Maintenance of Lymphatic Vessels in the Cornea Is Dependent on the Presence of Macrophages. *Investigative Ophthalmology & Visual Science,* 53**,** 3145-3153.

MASS, E., NIMMERJAHN, F., KIERDORF, K. & SCHLITZER, A. 2023. Tissue-specific macrophages: how they develop and choreograph tissue biology. *Nature Reviews Immunology*.

MATHEWS, P. M., LINDSLEY, K., ALDAVE, A. J. & AKPEK, E. K. 2018. Etiology of Global Corneal Blindness and Current Practices of Corneal Transplantation: A Focused Review. *Cornea,* 37**,** 1198-1203.

MCDERMOTT, A. M., PEREZ, V., HUANG, A. J., PFLUGFELDER, S. C., STERN, M. E., BAUDOUIN, C., BEUERMAN, R. W., BURNS, A. R., CALDER, V. L. & CALONGE, M. 2005. Pathways of corneal and ocular surface inflammation: a perspective from the cullen symposium. *The ocular surface,* 3**,** S-131-S-138.

MCMENAMIN, P. G., CREWE, J., MORRISON, S. & HOLT, P. G. 1994. Immunomorphologic studies of macrophages and MHC class II-positive dendritic cells in the iris and ciliary body of the rat, mouse, and human eye. *Invest Ophthalmol Vis Sci,* 35**,** 3234-50.

MCWHORTER, F. Y., WANG, T., NGUYEN, P., CHUNG, T. & LIU, W. F. 2013. Modulation of macrophage phenotype by cell shape. *Proc Natl Acad Sci U S A,* 110**,** 17253-8.

MEDAWAR, P. B. 1948. Immunity to Homologous Grafted Skin .3. The Fate of Skin Homografts Transplanted to the Brain, to Subcutaneous Tissue, and to the Anterior Chamber of the Eye. *British Journal of Experimental Pathology,* 29**,** 58-&.

MEDEIROS, C. S., MARINO, G. K., SANTHIAGO, M. R. & WILSON, S. E. 2018. The Corneal Basement Membranes and Stromal Fibrosis. *Invest Ophthalmol Vis Sci,* 59**,** 4044-4053.

MEDRANO-BOSCH, M., SIMON-CODINA, B., JIMENEZ, W., EDELMAN, E. R. & MELGAR-LESMES, P. 2023. Monocyte-endothelial cell interactions in vascular and tissue remodeling. *Front Immunol,* 14**,** 1196033.

MEEK, K. M. & KNUPP, C. 2015. Corneal structure and transparency. *Prog Retin Eye Res,* 49**,** 1-16.

MEHROTRA, P. & RAVICHANDRAN, K. S. 2022. Drugging the efferocytosis process: concepts and opportunities. *Nat Rev Drug Discov,* 21**,** 601-620.

MENKO, A. S., WALKER, J. L. & STEPP, M. A. 2019. Fibrosis: Shared Lessons From the Lens and Cornea. *Anat Rec (Hoboken)*.

METZEMAEKERS, M., VANHEULE, V., JANSSENS, R., STRUYF, S. & PROOST, P. 2018. Overview of the Mechanisms that May Contribute to the Non-Redundant Activities of Interferon-Inducible CXC Chemokine Receptor 3 Ligands. *Frontiers in Immunology,* 8.

MIA, S., WARNECKE, A., ZHANG, X. M., MALMSTRÖM, V. & HARRIS, R. A. 2014. An optimized protocol for human M2 macrophages using M-CSF and IL-4/IL-10/TGF-β yields a dominant immunosuppressive phenotype. *Scandinavian journal of immunology,* 79**,** 305-314.

MIDGLEY, A. C., ROGERS, M., HALLETT, M. B., CLAYTON, A., BOWEN, T., PHILLIPS, A. O. & STEADMAN, R. 2013. Transforming growth factor-β1 (TGF-β1)-stimulated fibroblast to myofibroblast differentiation is mediated by hyaluronan (HA)-facilitated epidermal growth factor receptor (EGFR) and CD44 co-localization in lipid rafts. *Journal of Biological Chemistry,* 288**,** 14824-14838.

MILLS, C. D., KINCAID, K., ALT, J. M., HEILMAN, M. J. & HILL, A. M. 2000. M-1/M-2 macrophages and the Th1/Th2 paradigm. *J Immunol,* 164**,** 6166-73.

MITRA, A., BARUA, A., HUANG, L., GANGULY, S., FENG, Q. & HE, B. 2023. From bench to bedside: the history and progress of CAR T cell therapy. *Front Immunol,* 14**,** 1188049.

MOBARAKI, M., ABBASI, R., OMIDIAN VANDCHALI, S., GHAFFARI, M., MOZTARZADEH, F. & MOZAFARI, M. 2019. Corneal Repair and Regeneration: Current Concepts and Future Directions. *Front Bioeng Biotechnol,* 7**,** 135.

MOLL, P., ANTE, M., SEITZ, A. & REDA, T. 2014. QuantSeq 3' mRNA sequencing for RNA quantification. Nature Publishing Group US New York.

MOLLER, H. J. 2012. Soluble CD163. *Scand J Clin Lab Invest,* 72**,** 1-13.

MORRIS, E. R., NISHINARI, K. & RINAUDO, M. 2012. Gelation of gellan - A review. *Food Hydrocolloids,* 28**,** 373-411.

MOSCA, M., POLENTARUTTI, N., MANGANO, G., APICELLA, C., DONI, A., MANCINI, F., DE BORTOLI, M., COLETTA, I., POLENZANI, L., SANTONI, G., SIRONI, M., VECCHI, A. & MANTOVANI, A. 2007. Regulation of the microsomal prostaglandin E synthase-1 in polarized mononuclear phagocytes and its constitutive expression in neutrophils. *J Leukoc Biol,* 82**,** 320-6.

MOSSER, D. M. & EDWARDS, J. P. 2008. Exploring the full spectrum of macrophage activation. *Nat Rev Immunol,* 8**,** 958-69.

MURRAY, P. J. 2017. Macrophage Polarization. *Annu Rev Physiol,* 79**,** 541-566.

MURRAY, P. J. & WYNN, T. A. 2011. Protective and pathogenic functions of macrophage subsets. *Nat Rev Immunol,* 11**,** 723-37.

MYLONAS, K. J., NAIR, M. G., PRIETO-LAFUENTE, L., PAAPE, D. & ALLEN, J. E. 2009. Alternatively Activated Macrophages Elicited by Helminth Infection Can Be Reprogrammed to Enable Microbial Killing. *Journal of Immunology,* 182**,** 3084-3094.

NAHRENDORF, M., SWIRSKI, F. K., AIKAWA, E., STANGENBERG, L., WURDINGER, T., FIGUEIREDO, J. L., LIBBY, P., WEISSLEDER, R. & PITTET, M. J. 2007. The healing myocardium sequentially mobilizes two monocyte subsets with divergent and complementary functions. *J Exp Med,* 204**,** 3037-47.

NARIMATSU, A., HATTORI, T., KOIKE, N., TAJIMA, K., NAKAGAWA, H., YAMAKAWA, N., USUI, Y., KUMAKURA, S., MATSUMOTO, T. & GOTO, H. 2019. Corneal lymphangiogenesis ameliorates corneal inflammation and edema in late stage of bacterial keratitis. *Sci Rep,* 9**,** 2984.

NEGI, A., SHUKLA, A., JAISWAR, A., SHRINET, J. & JASROTIA, R. S. 2022. Applications and challenges of microarray and RNA-sequencing. *Bioinformatics***,** 91-103.

NERI, S., MARIANI, E., MENEGHETTI, A., CATTINI, L. & FACCHINI, A. 2001. Calcein-acetyoxymethyl cytotoxicity assay: Standardization of a method allowing additional analyses on recovered effector cells and supernatants. *Clinical and Diagnostic Laboratory Immunology,* 8**,** 1131-1135.

NEU, C., SEDLAG, A., BAYER, C., FORSTER, S., CRAUWELS, P., NIESS, J. H., VAN ZANDBERGEN, G., FRASCAROLI, G. & RIEDEL, C. U. 2013. CD14-dependent monocyte isolation enhances phagocytosis of listeria monocytogenes by proinflammatory, GM-CSF-derived macrophages. *PLoS One,* 8**,** e66898.

NGUYEN, V. & LEE, G. A. 2019. Management of microbial keratitis in general practice. *Australian Journal of General Practice,* 48**,** 516-519.

NIEDERKORN, J. Y. 2011. Cornea: Window to Ocular Immunology. *Curr Immunol Rev,* 7**,** 328-335.

NIELSEN, M. C., ANDERSEN, M. N. & MOLLER, H. J. 2019. Monocyte isolation techniques significantly impact the phenotype of both isolated monocytes and derived macrophages in vitro. *Immunology*.

NIELSEN, M. C., HVIDBJERG GANTZEL, R., CLARIA, J., TREBICKA, J., MOLLER, H. J. & GRONBAEK, H. 2020. Macrophage Activation Markers, CD163 and CD206, in Acute-on-Chronic Liver Failure. *Cells,* 9.

NORTON, I. T., JARVIS, D. A. & FOSTER, T. J. 1999. A molecular model for the formation and properties of fluid gels. *Int J Biol Macromol,* 26**,** 255-61.

O'BRIEN, E. M. & SPILLER, K. L. 2022. Pro-inflammatory polarization primes Macrophages to transition into a distinct M2-like phenotype in response to IL-4. *Journal of leukocyte biology,* 111**,** 989-1000.

OPAL, S. M. & DEPALO, V. A. 2000. Anti-inflammatory cytokines. *Chest,* 117**,** 1162-1172.

OSHLACK, A., ROBINSON, M. D. & YOUNG, M. D. 2010. From RNA-seq reads to differential expression results. *Genome Biol,* 11**,** 220.

PAGÈS, H., CARLSON, M., FALCON, S. & LI, N. 2021. AnnotationDbi: Manipulation of SQLite-based annotations in Bioconductor. *R package version,* 1.

PANT, S. R., BHATTA, R. C., BHATTA, S. & SAPKOTA, Y. 2022. Prevalence and causes of blindness and visual impairment in Sudur paschim Province of Nepal. *medRxiv***,** 2022.11. 24.22282704.

PARKS, W. C., WILSON, C. L. & LÓPEZ-BOADO, Y. S. 2004. Matrix metalloproteinases as modulators of inflammation and innate immunity. *Nature Reviews Immunology,* 4**,** 617-629.

PESCOSOLIDO, N., BARBATO, A., PASCARELLA, A., GIANNOTTI, R., GENZANO, M. & NEBBIOSO, M. 2014. Role of Protease-Inhibitors in Ocular Diseases. *Molecules,* 19**,** 20557-20569.

POULIOT, P., TURMEL, V., GELINAS, E., LAVIOLETTE, M. & BISSONNETTE, E. Y. 2005. Interleukin-4 production by human alveolar macrophages. *Clin Exp Allergy,* 35**,** 804-10.

PRICE, J. V. & VANCE, R. E. 2014. The macrophage paradox. *Immunity,* 41**,** 685-93.

PUTTOCK, E. H., TYLER, E. J., MANNI, M., MANIATI, E., BUTTERWORTH, C., RAMOS, M. B., PEERANI, E., HIRANI, P., GAUTHIER, V., LIU, Y., MANISCALCO, G., RAJEEVE, V., CUTILLAS, P., TREVISAN, C., POZZOBON, M., LOCKLEY, M., RASTRICK, J., LAEUBLI, H., WHITE, A. & PEARCE, O. M. T. 2023. Extracellular matrix educates an immunoregulatory tumor macrophage phenotype found in ovarian cancer metastasis. *Nature Communications,* 14.

QAZI, Y. & HAMRAH, P. 2013. Corneal Allograft Rejection: Immunopathogenesis to Therapeutics. *J Clin Cell Immunol,* 2013.

RAGGI, F., PELASSA, S., PIEROBON, D., PENCO, F., GATTORNO, M., NOVELLI, F., EVA, A., VARESIO, L., GIOVARELLI, M. & BOSCO, M. C. 2017. Regulation of Human Macrophage M1-M2 Polarization Balance by Hypoxia and the Triggering Receptor Expressed on Myeloid Cells-1. *Frontiers in Immunology,* 8.

RALPH, R. A. 2000. Tetracyclines and the treatment of corneal stromal ulceration: a review. *Cornea,* 19**,** 274-7.

RAMACHANDRAN, P., PELLICORO, A., VERNON, M. A., BOULTER, L., AUCOTT, R. L., ALI, A., HARTLAND, S. N., SNOWDON, V. K., CAPPON, A., GORDON-WALKER, T. T., WILLIAMS, M. J., DUNBAR, D. R., MANNING, J. R., VAN ROOIJEN, N., FALLOWFIELD, J. A., FORBES, S. J. & IREDALE, J. P. 2012. Differential Ly-6C expression identifies the recruited macrophage phenotype, which orchestrates the regression of murine liver fibrosis. *Proceedings of the National Academy of Sciences of the United States of America,* 109**,** E3186-E3195.

REBE, C., RAVENEAU, M., CHEVRIAUX, A., LAKOMY, D., SBERNA, A. L., COSTA, A., BESSEDE, G., ATHIAS, A., STEINMETZ, E., LOBACCARO, J. M., ALVES, G., MENICACCI, A., VACHENC, S., SOLARY, E., GAMBERT, P. & MASSON, D. 2009. Induction of transglutaminase 2 by a liver X receptor/retinoic acid receptor alpha pathway increases the clearance of apoptotic cells by human macrophages. *Circ Res,* 105**,** 393-401.

ROSZER, T. 2015. Understanding the Mysterious M2 Macrophage through Activation Markers and Effector Mechanisms. *Mediators Inflamm,* 2015**,** 816460.

ROY, O., LECLERC, V. B., BOURGET, J. M., THERIAULT, M. & PROULX, S. 2015. Understanding the process of corneal endothelial morphological change in vitro. *Invest Ophthalmol Vis Sci,* 56**,** 1228-37.

SAMANIEGO, R., PALACIOS, B. S., DOMIGUEZ-SOTO, A., VIDAL, C., SALAS, A., MATSUYAMA, T., SANCHEZ-TORRES, C., DE LA TORRE, I., MIRANDA-CARUS, M. E., SANCHEZ-MATEOS, P. & PUIG-KROGER, A. 2014. Macrophage uptake and accumulation of folates are

polarization-dependent in vitro and in vivo and are regulated by activin A. *J Leukoc Biol,* 95**,** 797-808.

SCHLOTZER-SCHREHARDT, U., BACHMANN, B. O., LAASER, K., CURSIEFEN, C. & KRUSE, F. E. 2011. Characterization of the cleavage plane in DESCemet's membrane endothelial keratoplasty. *Ophthalmology,* 118**,** 1950-7.

SCHOLZEN, T. & GERDES, J. 2000. The Ki-67 protein: from the known and the unknown. *J Cell Physiol,* 182**,** 311-22.

SCHULZ, D., SEVERIN, Y., ZANOTELLI, V. R. T. & BODENMILLER, B. 2019. In-Depth Characterization of Monocyte-Derived Macrophages using a Mass Cytometry-Based Phagocytosis Assay. *Sci Rep,* 9**,** 1925.

SCOTT, C. L. & GUILLIAMS, M. 2018. The role of Kupffer cells in hepatic iron and lipid metabolism. *J Hepatol,* 69**,** 1197-1199.

SCOTT, R. A., KIICK, K. L. & AKINS, R. E. 2021. Substrate stiffness directs the phenotype and polarization state of cord blood derived macrophages. *Acta Biomater,* 122**,** 220-235.

SEO, J. S., TUMURSUKH, N. E., CHOI, J. H., SONG, Y., JEON, G., KIM, N. E., KIM, S. J., KIM, N., SONG, J. E. & KHANG, G. 2023. Modified gellan gum-based hydrogel with enhanced mechanical properties for application as a cell carrier for cornea endothelial cells. *International Journal of Biological Macromolecules,* 236.

SEYED-RAZAVI, Y., CHINNERY, H. R. & MCMENAMIN, P. G. 2014. A novel association between resident tissue macrophages and nerves in the peripheral stroma of the murine cornea. *Invest Ophthalmol Vis Sci,* 55**,** 1313-20.

SHAHRIZAN, M. S. M., ABD AZIZ, Z. H. & KATAS, H. 2022. Fluid gels: A systematic review towards their application in pharmaceutical dosage forms and drug delivery systems. *Journal of Drug Delivery Science and Technology,* 67.

SHAO, H., SCOTT, S. G., NAKATA, C., HAMAD, A. R. & CHAKRAVARTI, S. 2013. Extracellular matrix protein lumican promotes clearance and resolution of Pseudomonas aeruginosa keratitis in a mouse model. *PLoS One,* 8**,** e54765.

SHAPOURI-MOGHADDAM, A., MOHAMMADIAN, S., VAZINI, H., TAGHADOSI, M., ESMAEILI, S. A., MARDANI, F., SEIFI, B., MOHAMMADI, A., AFSHARI, J. T. & SAHEBKAR, A. 2018. Macrophage plasticity, polarization, and function in health and disease. *J Cell Physiol,* 233**,** 6425-6440.

SHU, D. Y. & LOVICU, F. J. 2017. Myofibroblast transdifferentiation: The dark force in ocular wound healing and fibrosis. *Prog Retin Eye Res,* 60**,** 44-65.

SIEBURTH, D., JABS, E. W., WARRINGTON, J. A., LI, X., LASOTA, J., LAFORGIA, S., KELLEHER, K., HUEBNER, K., WASMUTH, J. J. & WOLF, S. F. 1992. Assignment of genes encoding a unique cytokine (IL12) composed of two unrelated subunits to chromosomes 3 and 5. *Genomics,* 14**,** 59-62.

SIERRA-FILARDI, E., NIETO, C., DOMINGUEZ-SOTO, A., BARROSO, R., SANCHEZ-MATEOS, P., PUIG-KROGER, A., LOPEZ-BRAVO, M., JOVEN, J., ARDAVIN, C., RODRIGUEZ-FERNANDEZ, J. L., SANCHEZ-TORRES, C., MELLADO, M. & CORBI, A. L. 2014. CCL2 shapes macrophage polarization by GM-CSF and M-CSF: identification of CCL2/CCR2-dependent gene expression profile. *J Immunol,* 192**,** 3858-67.

SIERRA-FILARDI, E., PUIG-KROGER, A., BLANCO, F. J., NIETO, C., BRAGADO, R., PALOMERO, M. I., BERNABEU, C., VEGA, M. A. & CORBI, A. L. 2011. Activin A skews macrophage polarization by promoting a proinflammatory phenotype and inhibiting the acquisition of anti-inflammatory macrophage markers. *Blood,* 117**,** 5092-101.

SLOWIKOWSKI, K. 2020. ggrepel: Automatically position non-overlapping text labels with 'ggplot2'. *R package version 0.8,* 2.

SMIGIEL, K. S. & PARKS, W. C. 2018. Macrophages, Wound Healing, and Fibrosis: Recent Insights. *Curr Rheumatol Rep,* 20**,** 17.

SMITH, W., FELDMANN, M. & LONDEI, M. 1998. Human macrophages induced in vitro by macrophage colony-stimulating factor are deficient in IL-12 production. *Eur J Immunol,* 28**,** 2498-507.

SNIBSON, G. R., GREAVES, J. L., SOPER, N. D. W., TIFFANY, J. M., WILSON, C. G. & BRON, A. J. 1992. Ocular Surface Residence Times of Artificial Tear Solutions. *Cornea,* 11**,** 288-293.

SNODGRASS, R. G., BENATZY, Y., SCHMID, T., NAMGALADZE, D., MAINKA, M., SCHEBB, N. H., LUTJOHANN, D. & BRUNE, B. 2021. Efferocytosis potentiates the expression of arachidonate 15-lipoxygenase (ALOX15) in alternatively activated human macrophages through LXR activation. *Cell Death Differ,* 28**,** 1301-1316.

SNYDER, R. J., LANTIS, J., KIRSNER, R. S., SHAH, V., MOLYNEAUX, M. & CARTER, M. J. 2016. Macrophages: A review of their role in wound healing and their therapeutic use. *Wound Repair and Regeneration,* 24**,** 613-629.

SOLER PALACIOS, B., ESTRADA-CAPETILLO, L., IZQUIERDO, E., CRIADO, G., NIETO, C., MUNICIO, C., GONZALEZ-ALVARO, I., SANCHEZ-MATEOS, P., PABLOS, J. L., CORBI, A. L. & PUIG-KROGER, A. 2015. Macrophages from the synovium of active rheumatoid arthritis exhibit an activin A-dependent pro-inflammatory profile. *J Pathol,* 235**,** 515-26.

SPILLER, K. L., NASSIRI, S., WITHEREL, C. E., ANFANG, R. R., NG, J., NAKAZAWA, K. R., YU, T. & VUNJAK-NOVAKOVIC, G. 2015. Sequential delivery of immunomodulatory cytokines to facilitate the M1-to-M2 transition of macrophages and enhance vascularization of bone scaffolds. *Biomaterials,* 37**,** 194-207.

SPILLER, K. L., WRONA, E. A., ROMERO-TORRES, S., PALLOTTA, I., GRANEY, P. L., WITHEREL, C. E., PANICKER, L. M., FELDMAN, R. A., URBANSKA, A. M. & SANTAMBROGIO, L. 2016. Differential gene expression in human, murine, and cell line-derived macrophages upon polarization. *Experimental cell research,* 347**,** 1-13.

SRIDHAR, M. S. 2018. Anatomy of cornea and ocular surface. *Indian J Ophthalmol,* 66**,** 190-194.

STEIN, M., KESHAV, S., HARRIS, N. & GORDON, S. 1992. Interleukin 4 potently enhances murine macrophage mannose receptor activity: a marker of alternative immunologic macrophage activation. *J Exp Med,* 176**,** 287-92.

STEINBAUGH, M. J., PANTANO, L., KIRCHNER, R. D., BARRERA, V., CHAPMAN, B. A., PIPER, M. E., MISTRY, M., KHETANI, R. S., RUTHERFORD, K. D. & HOFMANN, O. 2017. bcbioRNASeq: R package for bcbio RNA-seq analysis. *F1000Research,* 6**,** 1976.

STRIZOVA, Z., BENESOVA, I., BARTOLINI, R., NOVYSEDLAK, R., CECRDLOVA, E., FOLEY, L. K. & STRIZ, I. 2023. M1/M2 macrophages and their overlaps - myth or reality? *Clin Sci (Lond),* 137**,** 1067-1093.

STUBBS, V. E., POWER, C. & PATEL, K. D. 2010. Regulation of eotaxin-3/CCL26 expression in human monocytic cells. *Immunology,* 130**,** 74-82.

STUNAULT, M. I., BORIES, G., GUINAMARD, R. R. & IVANOV, S. 2018. Metabolism Plays a Key Role during Macrophage Activation. *Mediators Inflamm,* 2018**,** 2426138.

TAM, A. L., CÔTÉ, E., SALDANHA, M., LICHTINGER, A. & SLOMOVIC, A. R. 2017. Bacterial keratitis in Toronto: a 16-year review of the microorganisms isolated and the resistance patterns observed. *Cornea,* 36**,** 1528-1534.

TAN, L., GUO, Y. A., FENG, C., HOU, Y. X., XIE, X. B. & ZHAO, Y. 2022. The Dual Regulatory Roles of Macrophages in Acute Allogeneic Organ Graft Rejection. *Engineering,* 10**,** 21-29.

TARIQUE, A. A., LOGAN, J., THOMAS, E., HOLT, P. G., SLY, P. D. & FANTINO, E. 2015. Phenotypic, functional, and plasticity features of classical and alternatively activated human macrophages. *Am J Respir Cell Mol Biol,* 53**,** 676-88.

TEDESCO, S., DE MAJO, F., KIM, J., TRENTI, A., TREVISI, L., FADINI, G. P., BOLEGO, C., ZANDSTRA, P. W., CIGNARELLA, A. & VITIELLO, L. 2018. Convenience versus Biological Significance: Are PMA-Differentiated THP-1 Cells a Reliable Substitute for Blood-Derived Macrophages When Studying in Vitro Polarization? *Front Pharmacol,* 9**,** 71.

TER HORST, B., MOAKES, R. J. A., CHOUHAN, G., WILLIAMS, R. L., MOIEMEN, N. S. & GROVER, L. M. 2019. A gellan-based fluid gel carrier to enhance topical spray delivery. *Acta Biomater,* 89**,** 166-179.

THOMAS, P. A. & GERALDINE, P. 2007. Infectious keratitis. *Curr Opin Infect Dis,* 20**,** 129-41.

TIDKE, S. C. & TIDAKE, P. 2022. A Review of Corneal Blindness: Causes and Management. *Cureus,* 14**,** e30097.

TING, D. S. J., HO, C. S., DESHMUKH, R., SAID, D. G. & DUA, H. S. 2021. Infectious keratitis: an update on epidemiology, causative microorganisms, risk factors, and antimicrobial resistance. *Eye (Lond),* 35**,** 1084-1101.

TING, D. S. J., SETTLE, C., MORGAN, S. J., BAYLIS, O. & GHOSH, S. 2018. A 10-year analysis of microbiological profiles of microbial keratitis: the North East England Study. *Eye,* 32**,** 1416-1417.

TONKIN, J., TEMMERMAN, L., SAMPSON, R. D., GALLEGO-COLON, E., BARBERI, L., BILBAO, D., SCHNEIDER, M. D., MUSARO, A. & ROSENTHAL, N. 2015. Monocyte/Macrophage-derived IGF-1 Orchestrates Murine Skeletal Muscle Regeneration and Modulates Autocrine Polarization. *Mol Ther,* 23**,** 1189-1200.

TORRICELLI, A. A., SANTHANAM, A., WU, J., SINGH, V. & WILSON, S. E. 2016. The corneal fibrosis response to epithelial-stromal injury. *Exp Eye Res,* 142**,** 110-8.

TORRICELLI, A. A., SINGH, V., SANTHIAGO, M. R. & WILSON, S. E. 2013. The corneal epithelial basement membrane: structure, function, and disease. *Invest Ophthalmol Vis Sci,* 54**,** 6390-400.

TORRICELLI, A. A. & WILSON, S. E. 2014. Cellular and extracellular matrix modulation of corneal stromal opacity. *Exp Eye Res,* 129**,** 151-60.

TRAN, T. M., DUONG, H., BONNET, C., KASHANCHI, A., BUCKSHEY, A. & ALDAVE, A. J. 2020. Corneal Blindness in Asia: A Systematic Review and Meta-Analysis to Identify Challenges and Opportunities. *Cornea,* 39**,** 1196-1205.

TSISSIOS, G., SALLESE, A., PEREZ-ESTRADA, J. R., TANGEMAN, J. A., CHEN, W., SMUCKER, B., RATVASKY, S. C., GRAJALES-ESQUIVE, E. L., MARTINEZ, A., VISSER, K. J., ARAUS, A. J., WANG, H., SIMON, A., YUN, M. H. & RIO-TSONIS, K. D. 2023. Macrophages modulate fibrosis during newt lens regeneration. *Res Sq*.

TUCEY, T. M., VERMA, J., HARRISON, P. F., SNELGROVE, S. L., LO, T. L., SCHERER, A. K., BARUGAHARE, A. A., POWELL, D. R., WHEELER, R. T., HICKEY, M. J., BEILHARZ, T. H., NADERER, T. & TRAVEN, A. 2018. Glucose Homeostasis Is Important for Immune Cell Viability during Candida Challenge and Host Survival of Systemic Fungal Infection. *Cell Metab,* 27**,** 988-1006 e7.

TURNBULL, I. R., GILFILLAN, S., CELLA, M., AOSHI, T., MILLER, M., PICCIO, L., HERNANDEZ, M. & COLONNA, M. 2006. Cutting edge: TREM-2 attenuates macrophage activation. *Journal of Immunology,* 177**,** 3520-3524.

UCHIYAMA, M., SHIMIZU, A., MASUDA, Y., NAGASAKA, S., FUKUDA, Y. & TAKAHASHI, H. 2013. An ophthalmic solution of a peroxisome proliferator-activated receptor gamma agonist prevents corneal inflammation in a rat alkali burn model. *Mol Vis,* 19**,** 2135-50.

UDALOVA, I. A., MANTOVANI, A. & FELDMANN, M. 2016. Macrophage heterogeneity in the context of rheumatoid arthritis. *Nature Reviews Rheumatology,* 12**,** 472-485.

UNG, L., BISPO, P. J. M., SHANBHAG, S. S., GILMORE, M. S. & CHODOSH, J. 2019. The persistent dilemma of microbial keratitis: Global burden, diagnosis, and antimicrobial resistance. *Surv Ophthalmol,* 64**,** 255-271.

UNG, L. & CHODOSH, J. 2021. Foundational concepts in the biology of bacterial keratitis. *Exp Eye Res,* 209**,** 108647.

UNUVAR PURCU, D., KORKMAZ, A., GUNALP, S., HELVACI, D. G., ERDAL, Y., DOGAN, Y., SUNER, A., WINGENDER, G. & SAG, D. 2022. Effect of stimulation time on the expression of human macrophage polarization markers. *PLoS One,* 17**,** e0265196.

VAN DEN BOSSCHE, J., BAARDMAN, J., OTTO, NATASJA A., VAN DER VELDEN, S., NEELE, ANNETTE E., VAN DEN BERG, SUSAN M., LUQUE-MARTIN, R., CHEN, H.-J., BOSHUIZEN, MARIEKE C. S., AHMED, M., HOEKSEMA, MARTEN A., DE VOS, ALEX F. & DE WINTHER, MENNO P. J. 2016. Mitochondrial Dysfunction Prevents Repolarization of Inflammatory Macrophages. *Cell Rep,* 17**,** 684-696.

VAN LOOKEREN CAMPAGNE, M., WIESMANN, C. & BROWN, E. J. 2007. Macrophage complement receptors and pathogen clearance. *Cell Microbiol,* 9**,** 2095-102.

VERRECK, F. A., DE BOER, T., LANGENBERG, D. M., HOEVE, M. A., KRAMER, M., VAISBERG, E., KASTELEIN, R., KOLK, A., DE WAAL-MALEFYT, R. & OTTENHOFF, T. H. 2004. Human IL-23-producing type 1 macrophages promote but IL-10-producing type 2 macrophages subvert immunity to (myco)bacteria. *Proc Natl Acad Sci U S A,* 101**,** 4560-5.

VERRECK, F. A., DE BOER, T., LANGENBERG, D. M., VAN DER ZANDEN, L. & OTTENHOFF, T. H. 2006. Phenotypic and functional profiling of human proinflammatory type-1 and anti-inflammatory type-2 macrophages in response to microbial antigens and IFN-gamma- and CD40L-mediated costimulation. *J Leukoc Biol,* 79**,** 285-93.

VIOLA, A., MUNARI, F., SANCHEZ-RODRIGUEZ, R., SCOLARO, T. & CASTEGNA, A. 2019. The Metabolic Signature of Macrophage Responses. *Front Immunol,* 10**,** 1462.

VOGEL, D. Y., GLIM, J. E., STAVENUITER, A. W., BREUR, M., HEIJNEN, P., AMOR, S., DIJKSTRA, C. D. & BEELEN, R. H. 2014. Human macrophage polarization in vitro: maturation and activation methods compared. *Immunobiology,* 219**,** 695-703.

WALDO, S. W., LI, Y., BUONO, C., ZHAO, B., BILLINGS, E. M., CHANG, J. & KRUTH, H. S. 2008. Heterogeneity of human macrophages in culture and in atherosclerotic plaques. *Am J Pathol,* 172**,** 1112-26.

WANG, E. Y., KONG, X., WOLLE, M., GASQUET, N., SSEKASANVU, J., MARIOTTI, S. P., BOURNE, R., TAYLOR, H., RESNIKOFF, S. & WEST, S. 2023a. Global Trends in Blindness and Vision Impairment Resulting from Corneal Opacity 1984-2020: A Meta-analysis. *Ophthalmology,* 130**,** 863-871.

WANG, H., ZHANG, Y., LI, Z., WANG, T. & LIU, P. 2014. Prevalence and causes of corneal blindness. *Clin Exp Ophthalmol,* 42**,** 249-53.

WANG, L. X., ZHANG, S. X., WU, H. J., RONG, X. L. & GUO, J. 2019a. M2b macrophage polarization and its roles in diseases. *J Leukoc Biol,* 106**,** 345-358.

WANG, X., WANG, T., LAM, E., ALVAREZ, D. & SUN, Y. 2023b. Ocular Vascular Diseases: From Retinal Immune Privilege to Inflammation. *Int J Mol Sci,* 24.

WANG, Z., GERSTEIN, M. & SNYDER, M. 2009. RNA-Seq: a revolutionary tool for transcriptomics. *Nat Rev Genet,* 10**,** 57-63.

WANG, Z., KOENIG, A. L., LAVINE, K. J. & APTE, R. S. 2019b. Macrophage Plasticity and Function in the Eye and Heart. *Trends Immunol,* 40**,** 825-841.

WATTS, C. 1997. Capture and processing of exogenous antigens for presentation on MHC molecules. *Annu Rev Immunol,* 15**,** 821-50.

WELP, A., WOODBURY, R. B., MCCOY, M. A., TEUTSCH, S. M., NATIONAL ACADEMIES OF SCIENCES, E. & MEDICINE 2016. The impact of vision loss. *Making eye health a population health imperative: vision for tomorrow.* National Academies Press (US).

WELS, M., ROELS, D., RAEMDONCK, K., DE SMEDT, S. C. & SAUVAGE, F. 2021. Challenges and strategies for the delivery of biologics to the cornea. *J Control Release,* 333**,** 560-578.

WENG, L., FUNDERBURGH, J. L., KHANDAKER, I., GEARY, M. L., YANG, T., BASU, R., FUNDERBURGH, M. L., DU, Y. & YAM, G. H.-F. 2020. The anti-scarring effect of corneal stromal stem cell therapy is mediated by transforming growth factor β3. *Eye and Vision,* 7.

WENG, S. Y., WANG, X., VIJAYAN, S., TANG, Y., KIM, Y. O., PADBERG, K., REGEN, T., MOLOKANOVA, O., CHEN, T., BOPP, T., SCHILD, H., BROMBACHER, F., CROSBY, J. R., MCCALEB, M. L., WAISMAN, A., BOCKAMP, E. & SCHUPPAN, D. 2018. IL-4 Receptor Alpha Signaling through Macrophages Differentially Regulates Liver Fibrosis Progression and Reversal. *EBioMedicine,* 29**,** 92-103.

WEST-MAYS, J. A. & DWIVEDI, D. J. 2006. The keratocyte: corneal stromal cell with variable repair phenotypes. *Int J Biochem Cell Biol,* 38**,** 1625-31.

WICKHAM, H., CHANG, W. & WICKHAM, M. H. 2016. Package 'ggplot2'. *Create elegant data visualisations using the grammar of graphics. Version,* 2**,** 1-189.

WIECZOREK, M., ABUALROUS, E. T., STICHT, J., ALVARO-BENITO, M., STOLZENBERG, S., NOE, F. & FREUND, C. 2017. Major Histocompatibility Complex (MHC) Class I and MHC Class II Proteins: Conformational Plasticity in Antigen Presentation. *Front Immunol,* 8**,** 292.

WIEGHOFER, P., HAGEMEYER, N., SANKOWSKI, R., SCHLECHT, A., STASZEWSKI, O., AMANN, L., GRUBER, M., KOCH, J., HAUSMANN, A., ZHANG, P., BONEVA, S., MASUDA, T., HILGENDORF, I., GOLDMANN, T., BOTTCHER, C., PRILLER, J., ROSSI, F. M., LANGE, C. & PRINZ, M. 2021. Mapping the origin and fate of myeloid cells in distinct compartments of the eye by single-cell profiling. *EMBO J,* 40**,** e105123.

WILKINSON, H. N. & HARDMAN, M. J. 2020. Wound healing: cellular mechanisms and pathological outcomes. *Open Biol,* 10**,** 200223.

WILLENBORG, S., INJARABIAN, L. & EMING, S. A. 2022. Role of Macrophages in Wound Healing. *Cold Spring Harb Perspect Biol,* 14.

WILSON, S. E. 2020a. Bowman's layer in the cornea- structure and function and regeneration. *Exp Eye Res,* 195**,** 108033.

WILSON, S. E. 2020b. Corneal myofibroblasts and fibrosis. *Exp Eye Res,* 201**,** 108272.

WILSON, S. E., SAMPAIO, L. P., SHIJU, T. M., HILGERT, G. S. L. & DE OLIVEIRA, R. C. 2022. Corneal Opacity: Cell Biological Determinants of the Transition From Transparency to Transient Haze to Scarring Fibrosis, and Resolution, After Injury. *Invest Ophthalmol Vis Sci,* 63**,** 22.

WISNIEWSKI, H. G. & VILCEK, J. 2004. Cytokine-induced gene expression at the crossroads of innate immunity, inflammation and fertility: TSG-6 and PTX3/TSG-14. *Cytokine Growth Factor Rev,* 15**,** 129-46.

WOLF, A. A., YANEZ, A., BARMAN, P. K. & GOODRIDGE, H. S. 2019a. The Ontogeny of Monocyte Subsets. *Front Immunol,* 10**,** 1642.

WOLF, J. B. 2013. Principles of transcriptome analysis and gene expression quantification: an RNA-seq tutorial. *Molecular ecology resources,* 13**,** 559-572.

WOLF, M., CLAY, S. M., ZHENG, S., PAN, P. & CHAN, M. F. 2019b. MMP12 Inhibits Corneal Neovascularization and Inflammation through Regulation of CCL2. *Sci Rep,* 9**,** 11579.

WORLD HEALTH ORGANISATION (WHO). 2023. *Blindness and vision impairment* [Online]. WHO. Available: https://www.who.int/news-room/fact-sheets/detail/blindness-and-visual-impairment [Accessed 02 November 2023].

WORLD HEALTH ORGANIZATION 2019. World report on vision. Geneva: World Health Organization; 2019. *CC BY-NC-SA 3.0 IGO.*

WU, M., LIU, J., LI, F., HUANG, S., HE, J., XUE, Y., FU, T., FENG, S. & LI, Z. 2020. Antibiotic-induced dysbiosis of gut microbiota impairs corneal development in postnatal mice by affecting CCR2 negative macrophage distribution. *Mucosal Immunol,* 13**,** 47-63.

WU, T., HU, E., XU, S., CHEN, M., GUO, P., DAI, Z., FENG, T., ZHOU, L., TANG, W. & ZHAN, L. 2021. clusterProfiler 4.0: A universal enrichment tool for interpreting omics data. *The innovation,* 2.

WU, Z., ZHANG, Z., LEI, Z. & LEI, P. 2019. CD14: Biology and role in the pathogenesis of disease. *Cytokine Growth Factor Rev,* 48**,** 24-31.

WYNN, T. A. & VANNELLA, K. M. 2016. Macrophages in Tissue Repair, Regeneration, and Fibrosis. *Immunity,* 44**,** 450-462.

XU, H., CHEN, M., REID, D. M. & FORRESTER, J. V. 2007. LYVE-1-positive macrophages are present in normal murine eyes. *Invest Ophthalmol Vis Sci,* 48**,** 2162-71.

XU, J., CHEN, P., LUAN, X., YUAN, X., WEI, S., LI, Y., GUO, C., WU, X. & DI, G. 2022. The NLRP3 Activation in Infiltrating Macrophages Contributes to Corneal Fibrosis by Inducing TGF-beta1 Expression in the Corneal Epithelium. *Invest Ophthalmol Vis Sci,* 63**,** 15.

XU, W., ZHAO, X., DAHA, M. R. & VAN KOOTEN, C. 2013. Reversible differentiation of pro- and anti-inflammatory macrophages. *Mol Immunol,* 53**,** 179-86.

YAM, G. H. F., RIAU, A. K., FUNDERBURGH, M. L., MEHTA, J. S. & JHANJI, V. 2020. Keratocyte biology. *Exp Eye Res,* 196**,** 108062.

YAMAGAMI, S., EBIHARA, N., USUI, T., YOKOO, S. & AMANO, S. 2006. Bone marrow-derived cells in normal human corneal stroma. *Arch Ophthalmol,* 124**,** 62-9.

YAMAGAMI, S., HAMRAH, P., MIYAMOTO, K., MIYAZAKI, D., DEKARIS, I., DAWSON, T., LU, B., GERARD, C. & DANA, M. R. 2005. CCR5 chemokine receptor mediates recruitment of MHC class II-positive Langerhans cells in the mouse corneal epithelium. *Invest Ophthalmol Vis Sci,* 46**,** 1201-7.

YANG, A. Y., CHOW, J. & LIU, J. 2018. Corneal Innervation and Sensation: The Eye and Beyond. *Yale J Biol Med,* 91**,** 13-21.

YANG, G. N., ROBERTS, P. K., GARDNER-RUSSELL, J., SHAH, M. H., COUPER, T. A., ZHU, Z., POLLOCK, G. A., DUSTING, G. J. & DANIELL, M. 2023. From bench to clinic: Emerging therapies for corneal scarring. *Pharmacol Ther,* 242**,** 108349.

YANG, J. Y., ZHANG, L. X., YU, C. J., YANG, X. F. & WANG, H. 2014. Monocyte and macrophage differentiation: circulation inflammatory monocyte as biomarker for inflammatory diseases. *Biomarker Research,* 2.

YAO, Y., XU, X. H. & JIN, L. 2019. Macrophage Polarization in Physiological and Pathological Pregnancy. *Front Immunol,* 10**,** 792.

YILMAZ, M., DEMIR, E., FIRATLI, Y., FIRATLI, E. & GURSOY, U. K. 2022. Tissue Levels of CD80, CD163 and CD206 and Their Ratios in Periodontal and Peri-Implant Health and Disease. *Current Issues in Molecular Biology,* 44**,** 4704-4713.

ZANONI, I. & GRANUCCI, F. 2013. Role of CD14 in host protection against infections and in metabolism regulation. *Front Cell Infect Microbiol,* 3**,** 32.

ZHANG, Q. Y., YAN, Z. B., MENG, Y. M., HONG, X. Y., SHAO, G., MA, J. J., CHENG, X. R., LIU, J., KANG, J. & FU, C. Y. 2021. Antimicrobial peptides: mechanism of action, activity and clinical potential. *Mil Med Res,* 8**,** 48.

ZHANG, S., LIU, Y., ZHANG, X., ZHU, D., QI, X., CAO, X., FANG, Y., CHE, Y., HAN, Z. C., HE, Z. X., HAN, Z. & LI, Z. 2018. Prostaglandin E2 hydrogel improves cutaneous wound healing via M2 macrophages polarization. *Theranostics,* 8**,** 5348-5361.

ZHAO, J., ANDREEV, I. & SILVA, H. M. 2024. Resident tissue macrophages: Key coordinators of tissue homeostasis beyond immunity. *Sci Immunol,* 9**,** eadd1967.

ZHENG, L., HAN, Y., YE, E., ZHU, Q., LOH, X. J., LI, Z. & LI, C. 2023. Recent Advances in Ocular Therapy by Hydrogel Biomaterials. *World Scientific Annual Review of Functional Materials,* 1**,** 2230002.

ZHU, X., HONG, J. & ZHOU, X. 2023. Biological Immune Mechanism of Retina. *Front Biosci (Landmark Ed),* 28**,** 363.

ZINKERNAGEL, M. S., PETITJEAN, C., FLEMING, P., CHINNERY, H. R., CONSTABLE, I. J., MCMENAMIN, P. G. & DEGLI-ESPOSTI, M. A. 2010. In Vivo Imaging of Ocular MCMV Infection. *Investigative Ophthalmology & Visual Science,* 51**,** 369-374.

ZUNDLER, S. & NEURATH, M. F. 2015. Interleukin-12: Functional activities and implications for disease. *Cytokine Growth Factor Rev,* 26**,** 559-68.